

RESEARCH ARTICLE | AUGUST 30 2023

Roadmap on ferroelectric hafnia- and zirconia-based materials and devices

José P. B. Silva ; Ruben Alcala ; Uygar E. Avci ; Nick Barrett ; Laura Bégon-Lours ; Mattias Borg ; Seungyong Byun ; Sou-Chi Chang ; Sang-Wook Cheong ; Duk-Hyun Choe ; Jean Coignus ; Veeresh Deshpande ; Athanasios Dimoulas ; Catherine Dubourdieu ; Ignasi Fina ; Hiroshi Funakubo ; Laurent Grenouillet ; Alexei Gruverman ; Jinseong Heo ; Michael Hoffmann ; H. Alex Hsain ; Fei-Ting Huang ; Cheol Seong Hwang ; Jorge Íñiguez ; Jacob L. Jones ; Ilya V. Karpov ; Alfred Kersch ; Taegyu Kwon ; Suzanne Lancaster ; Maximilian Lederer ; Younghwan Lee ; Patrick D. Lomenzo ; Lane W. Martin ; Simon Martin ; Shinji Migita ; Thomas Mikolajick ; Beatriz Noheda ; Min Hyuk Park ; Karin M. Rabe ; Sayeef Salahuddin ; Florencio Sánchez ; Konrad Seidel ; Takao Shimizu ; Takahisa Shiraishi ; Stefan Slesazeck ; Akira Toriumi ; Hiroshi Uchida ; Bertrand Vilquin ; Xianghan Xu ; Kun Hee Ye ; Uwe Schroeder 



APL Mater 11, 089201 (2023)

<https://doi.org/10.1063/5.0148068>

CrossMark

View
OnlineExport
Citation

AMERICAN ELEMENTS
THE ADVANCED MATERIALS MANUFACTURER 

sapphire windows	Nd:YAG	yttrium iron garnet	glassy carbon	beam splitters	fused quartz	additive manufacturing
spintronics	raman substrates	zeolites	III-IV semiconductors	gallium lump	copper nanoparticles	organometallics
silver nanoparticles	perovskites	epitaxial crystal growth	cerium oxide polishing powder	europlum phosphors	photronics	infrared dyes
MOICVD	beta-barium borate	cerium	surface functionalized nanoparticles	He	transparent ceramics	CIGS
rare earth metals	quantum dots	Li	Al	C	cermet	nanodispersions
osmium	scintillation Ce:YAG	Ca	Si	N	MBE grade materials	thin film
refractory metals	laser crystals	Sc	P	O	OLED lighting	solar energy
anodized aluminum nitobate	InAs wafers	Ti	Ge	F	ceramic	nanoparticles
perovskite crystals	MOFs	V	As	Ne	nanodispersions	thin film
ZnS	AuNPs	Cr	Se	Cl	MBE grade materials	thin film
CdTe		Mn	Te	Ar	OLED lighting	solar energy
		Fe	W	I	ceramic	nanoparticles
		Co	Ru	Xe	transparent ceramics	CIGS
		Ni	Pd		cermet	nanodispersions
		Cu	Ag		MBE grade materials	thin film
		Zn	Cd		OLED lighting	solar energy
		Ga	As		ceramic	nanoparticles
		Ge	Se		nanodispersions	thin film
		As	Sb		MBE grade materials	thin film
		Se	Yb		OLED lighting	solar energy
					ceramic	nanoparticles
					nanodispersions	thin film
					MBE grade materials	thin film
					OLED lighting	solar energy
					ceramic	nanoparticles
					nanodispersions	thin film
					MBE grade materials	thin film
					OLED lighting	solar energy
					ceramic	nanoparticles
					nanodispersions	thin film
					MBE grade materials	thin film
					OLED lighting	solar energy
					ceramic	nanoparticles
					nanodispersions	thin film
					MBE grade materials	thin film
					OLED lighting	solar energy
					ceramic	nanoparticles
					nanodispersions	thin film
					MBE grade materials	thin film
					OLED lighting	solar energy
					ceramic	nanoparticles
					nanodispersions	thin film
					MBE grade materials	thin film
					OLED lighting	solar energy
					ceramic	nanoparticles
					nanodispersions	thin film
					MBE grade materials	thin film
					OLED lighting	solar energy
					ceramic	nanoparticles
					nanodispersions	thin film
					MBE grade materials	thin film
					OLED lighting	solar energy
					ceramic	nanoparticles
					nanodispersions	thin film
					MBE grade materials	thin film
					OLED lighting	solar energy
					ceramic	nanoparticles
					nanodispersions	thin film
					MBE grade materials	thin film
					OLED lighting	solar energy
					ceramic	nanoparticles
					nanodispersions	thin film
					MBE grade materials	thin film
					OLED lighting	solar energy
					ceramic	nanoparticles
					nanodispersions	thin film
					MBE grade materials	thin film
					OLED lighting	solar energy
					ceramic	nanoparticles
					nanodispersions	thin film
					MBE grade materials	thin film
					OLED lighting	solar energy
					ceramic	nanoparticles
					nanodispersions	thin film
					MBE grade materials	thin film
					OLED lighting	solar energy
					ceramic	nanoparticles
					nanodispersions	thin film
					MBE grade materials	thin film
					OLED lighting	solar energy
					ceramic	nanoparticles
					nanodispersions	thin film
					MBE grade materials	thin film
					OLED lighting	solar energy
					ceramic	nanoparticles
					nanodispersions	thin film
					MBE grade materials	thin film
					OLED lighting	solar energy
					ceramic	nanoparticles
					nanodispersions	thin film
					MBE grade materials	thin film
					OLED lighting	solar energy
					ceramic	nanoparticles
					nanodispersions	thin film
					MBE grade materials	thin film
					OLED lighting	solar energy
					ceramic	nanoparticles
					nanodispersions	thin film
					MBE grade materials	thin film
					OLED lighting	solar energy
					ceramic	nanoparticles
					nanodispersions	thin film
					MBE grade materials	thin film
					OLED lighting	solar energy
					ceramic	nanoparticles
					nanodispersions	thin film
					MBE grade materials	thin film
					OLED lighting	solar energy
					ceramic	nanoparticles
					nanodispersions	thin film
					MBE grade materials	thin film
					OLED lighting	solar energy
					ceramic	nanoparticles
					nanodispersions	thin film
					MBE grade materials	thin film
					OLED lighting	solar energy
					ceramic	nanoparticles
					nanodispersions	thin film
					MBE grade materials	thin film
					OLED lighting	solar energy
					ceramic	nanoparticles
					nanodispersions	thin film
					MBE grade materials	thin film
					OLED lighting	solar energy
					ceramic	nanoparticles
					nanodispersions	thin film
					MBE grade materials	thin film
					OLED lighting	solar energy
					ceramic	nanoparticles
					nanodispersions	thin film
					MBE grade materials	thin film
					OLED lighting	solar energy
					ceramic	nanoparticles
					nanodispersions	thin film
					MBE grade materials	thin film
					OLED lighting	solar energy
					ceramic	nanoparticles
					nanodispersions	thin film
					MBE grade materials	thin film
					OLED lighting	solar energy
					ceramic	nanoparticles
					nanodispersions	thin film
					MBE grade materials	thin film
					OLED lighting	solar energy
					ceramic	nanoparticles
					nanodispersions	thin film
					MBE grade materials	thin film
					OLED lighting	solar energy
					ceramic	nanoparticles
					nanodispersions	thin film
					MBE grade materials	thin film
					OLED lighting	solar energy
					ceramic	nanoparticles
					nanodispersions	thin film
					MBE grade materials	thin film
					OLED lighting	solar energy
					ceramic	nanoparticles
					nanodispersions	thin film
					MBE grade materials	thin film
					OLED lighting	solar energy
					ceramic	nanoparticles
					nanodispersions	thin film
					MBE grade materials	thin film
					OLED lighting	solar energy
					ceramic	nanoparticles
					nanodispersions	thin film
					MBE grade materials	thin film
					OLED lighting	solar energy
					ceramic	nanoparticles
					nanodispersions	thin film
					MBE grade materials	thin film
					OLED lighting	solar energy
					ceramic	nanoparticles
					nanodispersions	thin film
					MBE grade materials	thin film
					OLED lighting	solar energy
					ceramic	nanoparticles
					nanodispersions	thin film
					MBE grade materials	thin film
					OLED lighting	solar energy
					ceramic	nanoparticles
					nanodispersions	thin film
					MBE grade materials	thin film
					OLED lighting	solar energy
					ceramic	nanoparticles
					nanodispersions	thin film
					MBE grade materials	thin film
					OLED lighting	solar energy
					ceramic	nanoparticles
					nanodispersions	thin film
					MBE grade materials	thin film
					OLED lighting	solar energy
					ceramic	nanoparticles
					nanodispersions	thin film
					MBE grade materials	thin film
					OLED lighting	solar energy
					ceramic	nanoparticles
					nanodispersions	thin film
					MBE grade materials	thin film
					OLED lighting	solar energy
					ceramic	nanoparticles
					nanodispersions	thin film
					MBE grade materials	thin film
					OLED lighting	solar energy
					ceramic	nanoparticles
					nanodispersions	thin film
					MBE grade materials	thin film
					OLED lighting	solar energy
					ceramic	nanoparticles
					nanodispersions	thin film
					MBE grade materials	thin film</td

Roadmap on ferroelectric hafnia- and zirconia-based materials and devices

Cite as: APL Mater. 11, 089201 (2023); doi: 10.1063/5.0148068

Submitted: 28 February 2023 • Accepted: 27 July 2023 •

Published Online: 30 August 2023



View Online



Export Citation



CrossMark

José P. B. Silva^{1,2} Ruben Alcalá³ Uygar E. Avci⁴ Nick Barrett,⁵ Laura Bégon-Lours,⁶ Mattias Borg^{7,8} Seungyong Byun⁹ Sou-Chi Chang,⁴ Sang-Wook Cheong,¹⁰ Duk-Hyun Choe,¹¹ Jean Coignus,¹² Veeresh Deshpande,¹³ Athanasios Dimoulas,¹⁴ Catherine Dubourdieu^{13,15} Ignasi Fina,¹⁶ Hiroshi Funakubo,¹⁷ Laurent Grenouillet,¹² Alexei Gruverman,¹⁸ Jinseong Heo,¹¹ Michael Hoffmann,¹⁹ H. Alex Hsain,²⁰ Fei-Ting Huang,¹⁰ Cheol Seong Hwang,⁹ Jorge Íñiguez^{21,22} Jacob L. Jones,²⁰ Ilya V. Karpov,⁴ Alfred Kersch,²³ Taegyu Kwon,⁹ Suzanne Lancaster,³ Maximilian Lederer,²⁴ Younghwan Lee^{20,25} Patrick D. Lomenzo,³ Lane W. Martin^{26,27} Simon Martin,¹² Shinji Migita,²⁸ Thomas Mikolajick^{3,29} Beatriz Noheda,³⁰ Min Hyuk Park^{9,25} Karin M. Rabe,³¹ Sayeef Salahuddin^{27,32} Florencio Sánchez,¹⁶ Konrad Seidel,²⁴ Takao Shimizu,³³ Takahisa Shiraishi³⁴ Stefan Slesazeck,³ Akira Toriumi,³⁵ Hiroshi Uchida,³⁶ Bertrand Vilquin,³⁷ Xianghan Xu,³⁸ Kun Hee Ye^{9,39} and Uwe Schroeder^{3,a}

For affiliations, please see the end of the Reference section

ABSTRACT

Ferroelectric hafnium and zirconium oxides have undergone rapid scientific development over the last decade, pushing them to the forefront of ultralow-power electronic systems. Maximizing the potential application in memory devices or supercapacitors of these materials requires a combined effort by the scientific community to address technical limitations, which still hinder their application. Besides their favorable intrinsic material properties, HfO_2 – ZrO_2 materials face challenges regarding their endurance, retention, wake-up effect, and high switching voltages. In this Roadmap, we intend to combine the expertise of chemistry, physics, material, and device engineers from leading experts in the ferroelectrics research community to set the direction of travel for these binary ferroelectric oxides. Here, we present a comprehensive overview of the current state of the art and offer readers an informed perspective of where this field is heading, what challenges need to be addressed, and possible applications and prospects for further development.

© 2023 Author(s). All article content, except where otherwise noted, is licensed under a Creative Commons Attribution (CC BY) license (<http://creativecommons.org/licenses/by/4.0/>). <https://doi.org/10.1063/5.0148068>

TABLE OF CONTENTS

I.	INTRODUCTION	3	3.	Advances required to meet the challenges	7
II.	THE FIELD OF EMERGENT FERROELECTRICS	4	4.	Concluding remarks	8
A.	Status	4	5.	Acknowledgments	8
B.	Current and future challenges	4	B.	Ferroelectricity	8
C.	Advances required to meet these challenges	5	1.	Status	8
D.	Concluding remarks	6	2.	Current and future challenges	8
III.	FUNDAMENTAL MATERIALS PROPERTIES	6	3.	Advances in science and engineering	9
A.	Simulation	6	to meet these challenges	9	
1.	Status	6	4.	Concluding remarks	9
2.	Current and future challenges	6	C.	Piezoelectricity	9
			1.	Status	9
			2.	Current and future challenges	10

3.	Advances in science and engineering to meet these challenges	10	1.	Status	27
4.	Concluding remarks	11	2.	Current and future challenges	28
5.	Acknowledgments	11	3.	Concluding remarks	29
D.	Pyroelectricity	11	F.	Molecular beam epitaxy	29
1.	Status	11	1.	Status	29
2.	Current and future challenges	12	2.	Current and future challenges	30
3.	Advances in science and engineering to meet these challenges	12	3.	Advances in science and engineering to meet these challenges	30
4.	Concluding remarks	13	4.	Concluding remarks	32
5.	Acknowledgments	13	VI.	CHARACTERIZATION AND PROPERTIES	32
E.	Negative capacitance	13	A.	Dopants	32
1.	Status	13	1.	Status	32
2.	Current and future challenges	14	2.	Current and future challenges	33
3.	Advances in science and engineering to meet these challenges	14	3.	Advances in science and engineering to meet these challenges	33
4.	Concluding remarks	14	4.	Concluding remarks	34
F.	Domain walls	15	5.	Acknowledgments	34
1.	Status	15	B.	Defect engineering	34
2.	Current and future challenges	15	1.	Status	34
3.	Domain wall dynamics	15	2.	Current and future challenges	34
4.	Advances in science and engineering to meet these challenges	16	3.	Advances in science and engineering to meet these challenges	35
5.	Concluding remarks	17	4.	Concluding remarks	36
IV.	BULK GROWTH	17	C.	Interface engineering	36
A.	Status	17	1.	Status	36
B.	Current and future challenges	17	2.	Current and future challenges	37
C.	Advances in science and engineering to meet these challenges	18	3.	Advances in science and engineering to meet these challenges	37
D.	Concluding remarks	19	4.	Concluding remarks	37
E.	Acknowledgments	19	5.	Acknowledgments	38
V.	THIN FILM GROWTH	20	D.	Electrodes optimization	38
A.	Metal-organic chemical vapor deposition	20	1.	Status	38
1.	Status	20	2.	Current and future challenges	38
2.	Current and future challenges	20	3.	Advances in science and engineering to meet these challenges	38
3.	Concluding remarks	21	4.	Concluding remarks	39
B.	Chemical solution deposition	21	E.	Laminated structures	39
1.	Status	21	1.	Status	39
2.	Current and future challenges	21	2.	Current and future challenges	39
3.	Advances in science and engineering to meet these challenges	22	3.	Advances in science and engineering to meet these challenges	40
4.	Concluding remarks	22	4.	Concluding remarks	40
C.	Pulsed laser deposition	22	F.	Thickness scaling	40
1.	Status	22	1.	Status	40
2.	Current and future challenges	23	2.	Current and future challenges	41
3.	Advances in science and engineering to meet these challenges	24	3.	Advances in science and engineering to meet these challenges	41
4.	Concluding remarks	24	4.	Concluding remarks	42
5.	Acknowledgments	24	VII.	DEVICES	42
D.	Atomic layer deposition	24	A.	Ferroelectric random access memories	42
1.	Status	24	1.	Status	42
2.	Current and future challenges	25	2.	Current and future challenges	42
3.	Advances in science and engineering to meet these challenges	27	3.	Advances in science and engineering to meet these challenges	43
4.	Concluding remarks	27	4.	Concluding remarks	43
5.	Acknowledgments	27	5.	Acknowledgments	43
E.	Sputtering	27	B.	Ferroelectric field-effect transistors	43

1.	Status	43	Author Contributions	59
2.	Current and future challenges	44	DATA AVAILABILITY	60
3.	Advances in science and engineering to meet these challenges	44	REFERENCES	60
C.	Ferroelectric tunnel junctions	45		
1.	Status	45		
2.	Current and future challenges	45		
3.	Advances in science and engineering to meet these challenges	45		
4.	Concluding remarks	46		
5.	Acknowledgments	46		
D.	Energy storage capacitors	46		
1.	Status	46		
2.	Current and future challenges	46		
3.	Advances in science and engineering to meet these challenges	47		
4.	Concluding remarks	48		
5.	Acknowledgments	48		
E.	Beyond memory application and neuromorphic	48		
1.	Status	48		
2.	Current and future challenges	49		
3.	Advances in science and engineering to meet the challenges	49		
4.	Concluding remarks	50		
VIII.	OVERARCHING CHALLENGES	50		
A.	Measurement protocol	50		
1.	Status	50		
2.	Current and future challenges	51		
3.	Advances in science and engineering to meet these challenges	52		
4.	Concluding remarks	52		
5.	Acknowledgments	52		
B.	Switching voltages/retention	52		
1.	Status	52		
2.	Current and future challenges	53		
3.	Advances in science and engineering to meet these challenges	53		
4.	Concluding remarks	53		
C.	Endurance	53		
1.	Status	53		
2.	Current and future challenges	54		
3.	Advances in science and engineering to meet these challenges	54		
4.	Concluding remarks	55		
5.	Acknowledgments	55		
IX.	COMMERCIAL MARKET OPPORTUNITIES			
	IN NON-VOLATILE MEMORIES	55		
A.	Status	55		
B.	Current and future challenges	56		
C.	Advances in science and engineering to meet the challenges	56		
D.	Concluding remarks	57		
X.	INDUSTRY PROSPECTIVE	57		
XI.	CONCLUSIONS AND OUTLOOK	58		
	AUTHOR DECLARATIONS	59		
	Conflict of Interest	59		

I. INTRODUCTION

Uwe Schroeder and José P. B. Silva

In the last decade, ferroelectric (FE) hafnium (HfO_2) and zirconium (ZrO_2) oxides have been intensively investigated, and tremendous progress has been made. Non-FE HfO_2 has been typically used in the mass production of complementary metal-oxide semiconductors (CMOSs) as a high-permittivity (k) gate insulator in high-performance field-effect transistors (FETs). The discovery of ferroelectricity in 2006, five years before the first publication about the FE properties of Si-doped HfO_2 thin films, has revolutionized the research in the field both from the fundamental and from the application point of view. These surprising results were originally unexpected because fluorite crystal structures have well-established phase diagrams, and they do not show any polar phase that is thermodynamically stable under normal fabrication conditions. Yet, the FE phase in HfO_2 - and ZrO_2 -based materials is accepted as the metastable orthorhombic (o) oIII phases (space group: $\text{Pca}2_1$) and the polar rhombohedral (r) phase (space group: $\text{R}3m$). Devices based on FE HfO_2 - and ZrO_2 -based materials could greatly benefit from the CMOS compatibility and potentially disentangle the energy efficiency problem of scaled semiconductor technology.

For these reasons, researchers have significantly increased their understanding of the material class, concerning, for example, the requirements to stabilize those FE phases or by exploring a large number of causes such as doping, oxygen vacancies, surface energy, and stress to enhance the FE properties. Interestingly, the success of this original high-performance material rejuvenated the search by theoreticians and experimentalists to look beyond and explore further promising applications. Over the past 10 years, their applications have grown from FE capacitors, transistors, and tunnel junctions for non-volatile memory applications to negative capacitance, logic-in-memory, neuromorphic computing, supercapacitors, and pyroelectric- or piezoelectric-based applications.

In this Roadmap, we overview important research aspects concerning FE HfO_2 - and ZrO_2 -based materials. In Sec. II, we discuss the emergent field of FEs, while in Sec. III, we address some fundamental properties and the specific features of this material class. In Secs. IV and V, we cover aspects of bulk and thin film fabrication. The growth of single crystals has been demonstrated, while the fabrication of these materials films has been improved considerably over the last few years. Nevertheless, further improvement of the growth conditions is still an important research field, and the processing of FE HfO_2 - and ZrO_2 -based thin films from chemical methods up to physical ones needs further investigation. The characterization and properties (see Sec. VI) have been significantly improved since the first report in 2011. Different strategies, such as doping, defect engineering, interface engineering, electrode optimization, and the formation of laminated structures, have been

TABLE I. Comparison of different operation parameters for various volatile and non-volatile memory device examples.^{1–7}

	Volatile		Non-volatile (FeRAM)		
Structure	6T (SRAM) ³	1T1C (DRAM) ⁴	1T1C ^{5,6}	1T1C ^{7,8}	1T1C ¹
Minimum write voltage (V)	~1.1	~1.1	2.0	2.5	0.6
Write latency (ns)	<1	<20	16	4	20
Retention	...	32–64 ms	>10 ³ min @ 85 °C	>10 ² min @ 85 °C	Not reported
Endurance (cycles)	>10 ¹⁵	>10 ¹⁵	>10 ¹⁵	>10 ⁷	Not reported
Array size	4 MB (L1)	16 Gbit	64 kbit	16 kbit	8 Gbit

intensively investigated. However, several details of the underlying physical mechanisms are still not completely understood. In Sec. VII, we outline the current status and future challenges of different devices that are currently being investigated with the use of FE HfO₂- and ZrO₂-based thin films. The major challenges and aspects that need to be considered and improved for broader applicability of these materials are addressed in Sec. VIII. Currently, the correct and precise measurement of FE HfO₂- and ZrO₂-based devices is still an issue. In addition, the need to fade the wake-up effect in order to improve reproducibility is still highly demanded. Another major challenge that remains to be solved is the possibility to decrease the switching voltages of these devices. Even though there has been significant progress, the device retention and endurance still need to be improved. Finally, we include a perspective on commercial market opportunities in non-volatile memories (Sec. IX) and an industry perspective (Sec. X) where these materials can play a crucial role.

Regardless of these challenges concerning understanding materials properties and device physics, there has been tremendous progress on these materials, and there is no FE material in recent years that attracted such high interest for ultralow-power electronic systems (Sec. VII, Table I).

In this Roadmap, we overview the current status of the research of FE HfO₂- and ZrO₂-based materials and indicate promising directions for future research efforts.

II. THE FIELD OF EMERGENT FERROELECTRICS

Lane W. Martin

A. Status

While the 100th anniversary of the discovery of ferroelectricity has come and gone, the field of stands poised to enter a new era driven, in part, by the discovery of new classes of FE materials and a renewed interest in their application.⁹ As it was in the middle of the last century, challenges of the day are bringing about fundamental and applied advances to meet these challenges.

The term “emergent ferroelectrics” captures the surprise that has accompanied the discovery of ferroelectricity and exotic phenomena in novel materials and heterostructures and points to a challenge. While properties such as piezoelectricity and pyroelectricity are directly related to material symmetry,¹⁰ ferroelectricity has

an empirical definition—polar materials that exhibit two or more orientational states in the absence of an electric field, which can be switched from one to another with an electric field. As such, identifying FEs relies on our (in)ability to both synthesize and characterize materials in a way that supports this function. The advances in synthesis and characterization that will be reviewed later have unleashed new worlds of phenomena. Even in traditional perovskite (ABO₃) FEs, our ability to heterostructure materials with atomic-scale control has begotten unexpected polar structures, including vortices, skyrmions, merons, and more [Fig. 1(a)].^{11–13} Simultaneously, research studies have been predicting and in some cases experimentally demonstrating ferroelectricity in novel materials, such as 2D van der Waals layered materials [e.g., transition metal dichalcogenides, group IV monochalcogenides, metal triphosphates, layered perovskites, layered nitrides, and indium selenide (In₂Se₃)] [Fig. 1(b)]^{14–16} and wurtzite-structured materials (e.g., Al_{1-x}Sc_xN, Al_{1-x}B_xN, and Zn_{1-x}Mg_xO).^{17,18}

While these observations have been highly touted, perhaps no other single area in the field has caught the attention of scientists and engineers alike in the last decade than the study of HfO₂- and ZrO₂-based compounds [Fig. 1(c)].^{20,21} The observation of the FE response in such materials has opened a more straightforward door for direct integration of FE properties into CMOS processes (something more challenging with traditional perovskite FEs). The report of ferroelectricity in these materials was not, however, immediately embraced across the community. This skepticism likely arose from the same challenges hinted at before concerning the definition of ferroelectricity. The community was fresh off of an explosion of work on multiferroics in which the combination of new materials, characterization techniques, and the expansion of researchers to fields outside of FEs led to numerous questionable reports of ferroelectricity [culminating in the (in)famous report of FE bananas].²² Just a few years later, reports of ferroelectricity, seemingly non-polar materials, such as HfO₂-based systems, quickly drew questions from a (perhaps, rightly) conservative community. While it took a few years to convince the world that these observations were not just artifacts from defects or charge trapping, this careful approach has laid a robust foundation for what has been done in the last half-decade.

B. Current and future challenges

First, while advances in computational/theoretical predictions, synthesis, and characterization have been critical in advancing this field, they also open new challenges. For example, the rapid

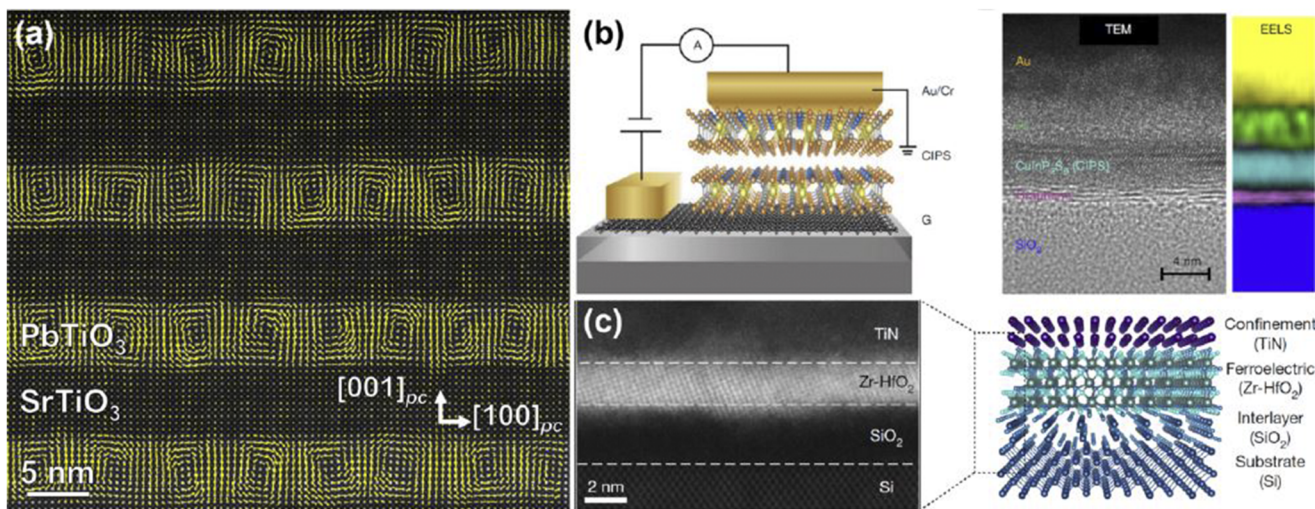


FIG. 1. (a) Cross-sectional, atomic-resolution scanning transmission electron microscopy (scanning-TEM) polarization-map of polar vortices in $(\text{PbTiO}_3)_n/(\text{SrTiO}_3)_n$ superlattices. Adapted from Ref. 13. (b) Schematic (left) and cross-sectional TEM image (right) of a CuInP_2S_6 (CIPS) device structure. Adapted from Ref. 16. (c) Cross-sectional scanning-TEM image of ultrathin $\text{Hf}_{0.8}\text{Zr}_{0.2}\text{O}_2$ heterostructures (left) and a schematic illustration of the same (right). Adapted from Ref. 19.

expansion of predicted candidate FEs means that experimentalists struggle to realize the “diamonds in the rough.” This is exacerbated by challenges in producing these chemically diverse systems, in addressing their stability for study, and in rationalizing their (sometimes) exotic behavior (thus raising the question if these are truly novel phenomena or simple artifacts of the measurement process on new materials). At the same time, there is a trend to push the limits of materials in terms of size (thickness and lateral scaling), time (how fast can a material switch), energy (what is the minimum voltage/energy for actuation), and susceptibilities (how responsive can the material be). These are important questions for materials that are increasingly transitioning from “next-generation” to “this-generation.” The challenge is balancing fundamental science studies and engineering applications—there is probably little argument that real progress in both will require the support of the other.

In HfO_2 - and ZrO_2 -based materials, this competition between fundamental and engineering efforts has been at play for much of the last decade. Melding these approaches has enabled rapid progress in some areas, while other topics remain open. First and foremost, a full understanding of the mechanism for stabilizing the metastable FE phase remains a matter of discussion. While there is more widespread agreement on the different structures that can and have been observed, the reasons why are more varied (from surface/volume-energy, to doping, to strain, to defects, to kinetic arguments, and more). Especially to those new to the community, the fast-moving and wide-ranging discussion can seem incongruent and contradictory. This is further complicated by disparate approaches to studying these materials (e.g., polycrystalline vs single-crystalline films, thick vs thin films, different synthesis methods, and different electrodes), which can make the narrative overwhelming. Even in the face of this lack of clarity, some are (rightly) pushing forward to try to improve the overall

performance. (Effectively saying, “I don’t care how it works, as long as it does.”) Such efforts have clarified some points (e.g., the role of defects in the wake-up process), while others remain to be fully addressed (e.g., routes to reduce the coercive voltage, improve reliability, assure retention, and reduce fatigue and imprint). These materials also present exotic new effects—including robust polarization in ultrathin (<10 nm) films and inverse size effects¹⁹ (which are potentially explained by exotic lattice dynamics)²³—which are important observations but remain to be fully fleshed out. Finally, looking at the utilization of these materials, while considerable effort has been put into the exploration of these materials for application in logic and memory, the question arises as to the suitability of these materials for the wider range of FE applications and devices.

C. Advances required to meet these challenges

A number of themes begin to arise that could show the community how to address these challenges. First is to embrace the unique perspectives and approaches of fundamental and engineering sciences. Continued collaboration between academia and industry and coordinated efforts to share the most important questions with one another will accelerate real solutions. Second, as the introduction of new materials welcomes a wider swatch of science and engineering to the interesting (and often complex) world of FEs, the community should be sure to embrace (and remind themselves of) the lessons from work on thin-film FE devices at the end of the last century as well as lessons from thin-film epitaxy in more traditional FEs. While the materials might be different, the challenges might be the same. Much has been learned about how to address interfaces, alleviate imprint and fatigue, and study defects and how to subtly manipulate polarization processes. Third, welcoming input from other (perhaps less obvious) communities. For example, as there is

growing consensus that oxygen vacancies play an important role in mediating the stabilization of the desired phases in the HfO_2 -based systems, exploring the work of those in the solid-oxide electrochemistry world could provide new ways of assessing and confirming understanding. Simultaneously (and this is happening already), the community needs to tap into a wider array of measurement approaches (e.g., state-of-the-art microscopes, synchrotron-based structural and spectroscopic approaches, and *in-operando* studies). Among such areas, there is an urgent need in the realm of the science of material growth. Introducing new metrologies to study the growth of these materials (*in situ* during the process) and working toward real-time feedback could be critical for them really becoming viable in industry. Finally, focused attention on addressing deficiencies in the materials. For example, in the HfO_2 - and ZrO_2 -based systems, despite the ability to make ultra-thin films, the coercive voltage remains a challenge. If, for example, the coercive field (E_c) is 2000 kV/cm for even a film that is just 5 nm thick, we would require a voltage of at least 1 V to switch the material. Current goals are to drive switching voltages down to just 0.1 V—an improvement of 10 \times from where we are today. Addressing these challenges is a key part of the future of these materials.

D. Concluding remarks

All in all, it is an exciting time to be working on FEs. The urgency with which these materials are being discovered and considered for an array of applications provides a renewed energy. At the same time, we must maintain a keen awareness that no single material or class of materials is likely to address the diversity of applications that call for FEs. In other words, there is no “cure-all” solution to what ails us. There are, as there always has been, every growing and changing need for functional materials in information technology, communications, healthcare, national security, energy efficiency, and beyond. “Emergent ferroelectrics” are poised to play a critical role in addressing some of these challenges. The diversification of materials begets a diversification of opportunities to really change how things are done in many areas. Our role as scientists and engineers is to make those connections and find the right approaches to address these societal challenges.

III. FUNDAMENTAL MATERIALS PROPERTIES

A. Simulation

Karin M. Rabe, Alfred Kersch, and Jorge Iñiguez

1. Status

Simulations play an increasingly important role in understanding and guiding experimental work on complex functional materials, particularly FEs and related compounds. Computations of total energy can be used to explore the structural energy landscape and identify candidate metastable phases. Quantitative predictions of the crystal structure parameters, phonons, elastic constants, polarization, and related properties, such as piezoelectricity and pyroelectricity, can be used to identify the phases in experimental bulk and thin films. Computations of minimum barrier paths connecting different structures, domain wall energetics and motion, defect

energetics, and diffusion can assist in understanding electric field switching.

Initial simulation studies of HfO_2 and ZrO_2 ^{24,25} covered the structural properties and free energy of the polar *o-Pca*₂ phase (standard FE phase) and the possible occurrence of competing polar *o-Pmn*₂₁, *r-R3*,^{24–27} and other phases. The metastable, tetragonal (*t*) *P4*₂/*nmc* state plays a special role as its comparatively large entropy enables first-order temperature-induced phase transitions from the polar phase.²⁸ The *t*-phase has more favorable energy in ZrO_2 than in HfO_2 ,²⁹ which is a major reason for the relatively easy formation of $\text{Hf}_x\text{Zr}_{1-x}\text{O}_2$ (HZO). A second polar phase has been experimentally detected, which could be *r-R3* or *R3m*²⁷ or even *o-Pmn*₂₁,²⁶ the signature XRD peak of these phases being similar. An overview of the lowest energy structures can be found in Fig. 2.

In single crystalline HfO_2 and ZrO_2 , the calculated free energy of the polar *Pca*₂ phase is above the monoclinic (*m*) *P2*₁/*c* ground state. Favorable conditions for the thermodynamic stability of poly- or monocrystalline polar *Pca*₂ investigated in simulation include the following: (i) the film is very thin or polycrystalline with grains smaller than a few nanometers,³⁰ (ii) there are favorable elastic boundary conditions,³¹ (iii) the crystallization is far from thermal equilibrium,³² (iv) there is intrinsic doping by oxygen defects,³³ and (v) there is extrinsic doping with a suitable dopant on the level of a few percent,^{34–36} possibly inhomogeneously distributed.³⁷ Si, La, Y, and Al have been identified as the most favorable dopants. HZO is an important example where doping alone does not seem sufficient to stabilize a polar ground state. Nevertheless, under the described circumstances, polar *Pca*₂ is energetically sufficiently stable, and its formation is favored, but the dynamic phase stabilization mechanism remains to be elucidated.

The piezoelectric constants of HfO_2 and ZrO_2 were calculated to be relatively small³⁸ and unusually negative, which is explained by the chemical bonds of the polar oxygens.³⁹ Interestingly, large and positive electro-strain effects were also found, and it is under discussion whether they indicate an alternative switching pathway^{40–42} or a competing field-induced phase transformation from a remaining *t*-phase fraction.⁴³ The pyroelectric constants are also unusual because the primary and secondary pyroelectric coefficients add up and become attractively large; the effect is enhanced close to the polymorphic phase boundary.^{38,44}

2. Current and future challenges

Phonon calculations for the cubic fluorite structure²⁴ show that there is no unstable polar mode, suggesting that this system should be considered as an improper ferroelectric. Moreover, the formation of the polar phase from the *t-P4*₂/*nmc* polymorph and the polarization reversal require multiple phonons^{25,45,46} resulting from anharmonic couplings, which complicate the understanding of ferroelectricity in fluorites compared to perovskites. In addition, Lee *et al.*²³ suggested that the marginal dispersion of phonon bands in the tetragonal state should have a strong influence on the switching dynamics, which may be dominated by nucleation with very slow growth.

The phonons are an initial indicator of minimum energy paths connecting the metastable phases. In addition to the standard pathway for polarization reversal,²⁴ alternative pathways have been systematically searched⁴⁷ as they may play a role in FE switching. Several approaches to the reversal have been explored

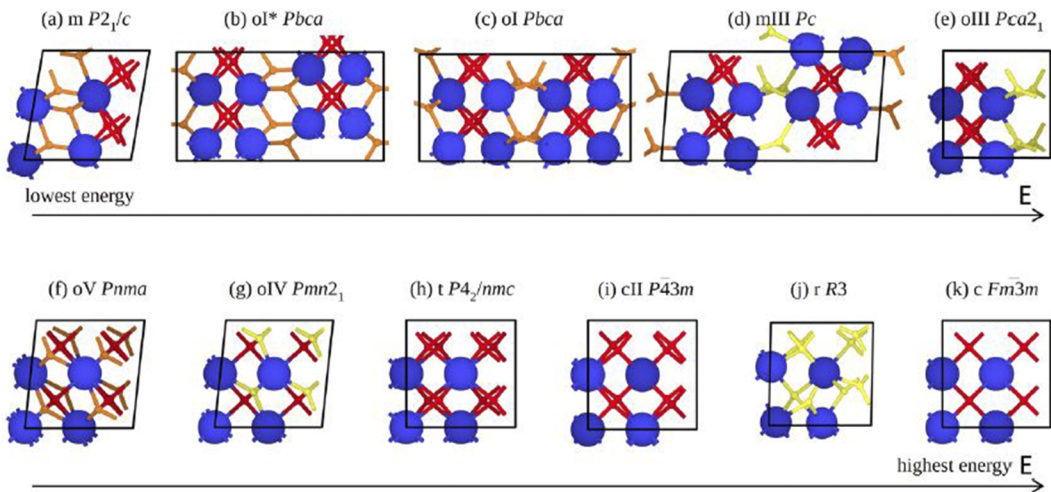


FIG. 2. (a)–(k) Crystal phases with the increasing total energy. Nonpolar oxygen (red), polar oxygen (yellow), and polar oxygen compensated within the crystal (orange). Adapted from Ref. 29. (f) and (g) The 24- and 12-atomic pseudocubic cells and the 12- and 6-atom orthorhombic unit cells are contained in a 45° rotated cuboid with half the area in the plane.

in simulations, but no unambiguous model has been found yet. (i) The Kolmogorov–Avrami–Ishibashi (KAI) model⁴⁸ successfully describes the kinetics of FE switching in single-crystal perovskites. The model is characterized by lateral growth or shrinkage of pre-existing domains of opposite polarity. The critical interfacial energy and barrier parameters for domain motion were calculated, and either low interfacial energy with a very high barrier^{23,49} or a low barrier but very high interfacial energy⁵⁰ was determined. Not all possible configurations have been investigated yet. (ii) In the Nucleation-Limited Switching (NLS) model,⁴⁸ a nucleus with opposite polarization is randomly generated in the polarized domain by thermal activation and grows inexorably when the critical size is exceeded. The critical parameter to be studied in the simulation is the interfacial energy, most simply of 180° domain walls, rather than mobility, since nucleation is limiting. The experimental results from Ref. 51 are in favor of the NLS model. (iii) According to the Landau–Khalatnikov (LK) model,⁴⁸ there are independent crystal-like domains (grains or crystallites) within a grain in which the switching is homogeneous so that only the minimum energy barrier between initial and final homogeneous polarization states is the relevant parameter. Here, it is immediately observed that the predicted E_c is almost an order of magnitude too large as compared to experiments.^{25,52} In addition to the FE domain wall (DW), the interfaces and their energies between the *t*-phase and the polar phase were also calculated⁵³ since they are important for the formation of the polar phase from the tetragonal state and for the antiferroelectric field-induced phase transformation.

3. Advances required to meet the challenges

The simulation of basic material properties is well developed, but the functionals used in the first-principles calculations have not yet been systematically validated for HfO_2 and ZrO_2 . For example,

the calculated kinetic barriers significantly depend on the chosen functional, and experiments are needed to validate the predictions. Hybrid functionals provide accurate results for electronic defect levels⁵⁴ but have yet to be systematically applied with realistic, sufficiently large supercells. First-principles theory suggests that the polar phase can be viewed as generated from the cubic fluorite structure through the coupling of multiple phonon modes^{25,45,46} and that FE polarization has an improper character. However, experimentally, a sharp permittivity peak has been observed during the temperature-controlled transition from the polar to the tetragonal phase,²⁸ which is typical for the proper behavior. This suggests that the known theoretical multimode expansion corresponding to the $T = 0$ K limit is not suitable to describe the experiments; therefore, molecular dynamics studies based on either first-principles or using machine-learned potentials are needed. These approaches may also elucidate the field-induced transition from the tetragonal to the polar state, which may allow us to obtain giant piezoelectric and pyroelectric effects.

The systematic development and application of machine-learned potentials also offer hope in other important areas. Some potentials of this kind have already been developed for HfO_2 ⁵⁵ and ZrO_2 ,^{44,56} but not yet for doped or defective materials. They are critical for studying polarization reversal, domain nucleation, and growth. More realistic potentials (capable of accounting for chemical bond breaking and formation) will be crucial to study the thickness dependence of the polar phase in thin films or the mechanisms for polar phase stabilization in grains. Combined with kinetic Monte Carlo techniques, these potentials—and potentially other simplified models, such as cluster expansion approaches⁵⁷—will eventually enable us to study the behavior of extrinsic defects and fatigue and wake-up mechanisms. Finally, simple phase field models have been developed to address HfO_2 - and ZrO_2 -related materials and discuss their electrical behavior in devices (e.g., in the context of negative

capacitance studies^{58,59}). However, given the polymorphic nature of these materials and the non-standard nature of their ferroelectricity, the applicability of simple Ginzburg–Landau potentials is questionable and further work is needed to derive appropriate and reliable continuum models.

4. Concluding remarks

The discovery of ferroelectricity in HfO_2 and related compounds has brought new challenges to the theory and simulation of FEs, as well as a sense of urgency for methodological innovation. HfO_2 offers unquestionable and (among FEs) unparalleled technological promise. However, it is still controversial whether and how HfO_2 deviates from the standard model of FEs in the soft mode property, which is best represented by perovskite oxides. Thus, HfO_2 forces us to rethink our theories and simulation approaches to ferroelectricity, to revisit assumptions that would otherwise seem obvious, and to keep an open mind for new possibilities. Many distinctive properties of HfO_2 FEs, including structural, electromechanical, and dopant-related behaviors, have already been captured by first-principles simulations, while others, including phase formation, dynamics of polarization reversal, and extrinsic contributions, have so far eluded a good understanding. As discussed in this piece, new first-principles-based approaches, such as machine-learned potentials and kinetic simulations, are needed to tackle these challenges. The experience so far suggests many exciting discoveries ahead. The journey has just begun.

5. Acknowledgments

J.Í. acknowledges the support from the Luxembourg National Research Fund through Grant No. INTER/NWO/20/15079143/TRICOLOR.

B. Ferroelectricity

Cheol Seong Hwang, Seungyong Byun, and Kun Hee Ye

1. Status

When Böscke *et al.* first reported the FE properties from the Si-doped HfO_2 film having the TiN electrodes in 2011,⁶⁰ the FE community encountered difficulties in accepting the finding due to several reasons. First, the doped- HfO_2 film has already been in mass-production as the high- k gate dielectric layer in high-performance CMOS devices, where the FE-hysteresis is detrimental. Second, HfO_2 (isostructural ZrO_2 , too) is a well-studied material with an established phase diagram where no polar phase is reported.²¹ Third, the FE phase evolution is critically dependent on not only the material parameters and process variables but also film thickness, which significantly complicates the identification of the critical parameters, such as remanent polarization (P_r) and E_c .²¹ However, the intense and collaborative research worldwide during the past decade convinced the community of the robustness of the FE performance of the doped HfO_2 films, including the $(\text{Hf}, \text{Zr})\text{O}_2$, which offers from a dielectric (Hf-rich) to FE (~5:5) to antiferroelectric (AFE) (Zr-rich) performances. In addition, the well-established contamination control protocols in the mass production line, due to the

already matured production of the high- k CMOS devices, facilitate the acceptance of the material in the semiconductor industry at an unprecedented pace.

It is now well accepted that the FE properties of fluorite-structured HfO_2 -based materials are ascribed to the $o\text{-}Pca2_1$ structure. However, it differs from conventional perovskite-structured FE materials, such as $\text{Pb}(\text{Zr}, \text{Ti})\text{O}_3$ (PZT), in that the former has a non-centrosymmetric distribution of oxygen ions, whereas the latter has a non-centrosymmetric distribution of cations (Ti, Zr). The origins of the specific atomic configuration of the unit cell structure in these materials have been recently understood from the density functional theory (DFT) for phonon calculation. It shows that the high symmetry cubic phase (space group: $Fm\text{-}3m$) has an imaginary frequency phonon mode at the Brillouin zone boundary. This phonon mode induces the antiparallel displacement of oxygen ions to cause a transition into a t -phase (space group: $P4_2/nmc$).⁶¹ The FE o -phase can be formed via the splitting of the phonon modes of the t -phase into the zone center mode (parallel movement of all oxygen ions along the $+z$ direction) and the zone boundary antipolar mode (antiparallel movement of the half of the oxygen ions along $\pm z$ directions, respectively). Due to the coupling of the two phonon modes, FE $o\text{-}\text{HfO}_2$ has a structure in which a non-polar spacer layer and a FE layer are repeated. Because of the presence of the spacer layer, it shows different domain properties from the perovskite FEs, which is induced from the only zone center soft phonon mode. Such a two-layer structure, parallel to the spontaneous polarization (P_s) direction (c axis), reduces the elastic and electrostatic interaction between the neighboring unit cells, decreasing the 180° domain wall (DW) energy to even a negative value. This feature may decrease the DW thickness to the sub-monolayer level. However, it should not be overlooked that many other types of DWs with much higher DW energy have been experimentally observed.⁶² More detailed discussions on the DW configuration are given in another section (Choe and Heo).

2. Current and future challenges

Actually, the FE domain structure with a unit-cell thickness corresponds to the AFE $Pbca$ structure, so it cannot represent the macroscopically observed FE property of HfO_2 . Interestingly, the recent DFT calculations show that the AFE $Pbca$ structure has a lower free energy than the FE $Pca2_1$ structure.²³ As discussed in detail in another section, the formation of the FE- HfO_2 phase is dominantly controlled by kinetic factors rather than the thermodynamic driving force, such as the energy barrier between the tetragonal phase and orthorhombic phases.²¹ Therefore, an energetically favorable AFE $Pbca$ structure, in addition to the thickness-dependent phase stability of different phases (AFE $Pbca$ or field-induced FE $P4_2/nmc$ $< \sim 5$ nm; dielectric $P2_1/c$ $> \sim 20$ nm), complicates the practical fabrication of the high-performance metal–ferroelectric–metal (MFM) capacitor structure. The most feasible FE performance is generally achieved at a thickness of ~ 10 nm, in which FE $Pca2_1$ remained intact even under the absence of the field due to the high barrier for the transition from FE $Pca2_1$ to AFE $Pbca$. In addition, the stability of AFE $Pbca$ over the FE $Pca2_1$ phase renders the fatigue behavior²¹ (reduction of P_r with the increasing switching cycle number) different from the conventional perovskite FE materials, where the production of oxygen

vacancies and accompanying domain pinning constitutes the primary mechanism. The electrical cycling provides the FE *Pca2*₁ phase with the energy to overcome the barrier to recover AFE *Pbca* without generating additional oxygen vacancies. In this case, the fatigued film could be rejuvenated to the FE phase by applying a slightly higher poling voltage without increasing the leakage current.⁶³ In addition, the most commonly adopted TiN electrode almost always involves non-FE interfacial layers. All these factors render practically achieving the theoretical P_r value ($\sim 51 \mu\text{C}/\text{cm}^2$)⁴¹ challenging. Nonetheless, optimizing the process variables, such as annealing temperature, time, and cooling rate; changing the electrode from conventional TiN to W;⁶⁴ and adopting interfacial layers, such as HfON, have significantly improved the achievable P_r of a technically viable polycrystalline film from ~ 15 to $> 35 \mu\text{C}/\text{cm}^2$.^{10,65}

In this regard, the growth of the FE-phase-pure epitaxial film must be a crucial task to prove the intrinsic FE performance of the films. This task has been challenging because aligning the [001] P_s direction to the out-of-plane direction has been hampered even on the lattice-matched Y-stabilized ZrO₂ single crystal substrate, which might be ascribed to the intricate kinetic process of the FE phase formation during cooling.⁶⁶ However, recent work demonstrates that the careful control of the growth condition and cooling step can deposit a phase-pure epitaxial 5% Y-doped HfO₂ film on a LaSrMnO/SrTiO₃ substrate, alleviating the rhombohedral distortion.⁶⁷ Interestingly, the (111)-oriented Y-doped HfO₂ film grown on a (001)-oriented substrate had a maximum P_r value of $\sim 50 \mu\text{C}/\text{cm}^2$, demonstrating that the P_s value along the (001) direction was close to the theoretical value.

3. Advances in science and engineering to meet these challenges

These findings indicate that the robust ferroelectricity of doped-HfO₂ films is now well-proven in both polycrystalline and epitaxial films. Nevertheless, the interwound influences of the process/material variables and film thickness effects, especially for thinner (< 10 nm) films, pose significant challenges in fabricating nanoscale electronic devices. For example, to manufacture the ferroelectric random-access memory (FeRAM) or ferroelectric field-effect transistors (FeFETs) with dimensions comparable to the state-of-the-art dynamic random-access memory (DRAM) and NAND flash memory, the film thickness must be < 5 nm. Therefore, the recent report on the FeRAM cell fabrication with an ~ 17 nm-design rule DRAM capacitor structure with the standard TiN electrode¹ is notable. Even though the 4–6 nm-thick (Hf, Zr)O₂ films showed distorted polarization–voltage curves, the thinner film had an even better charge response to the given short voltage pulses. Furthermore, adopting the production-worthy atomic layer deposition (ALD) process demonstrated the already well-established fabrication process of these relatively new materials in the CMOS line.

In academia, researchers attempted to explore the lower limit of the film thickness retaining the FE performances.^{68,69} Although several reports argued even sub-nm thickness (only one unit cell thickness) films showed robust FE properties, the direct structural and electrical evidence is still being debated.

In addition, the progress in the scanning TEM with the spherical aberration correction (Cs-STEM) provided the community with more direct imaging of the oxygen ion positions within the unit cell,

which has been challenging in conventional HRTEM.⁶³ Still, the data availability is limited due to the highly limited imaging conditions and grain orientation issues in the polycrystalline film.⁶³

4. Concluding remarks

In summary, the recent advances in the experimental and theoretical works for the doped FE HfO₂ materials (bulk, epitaxial and polycrystalline films) proved the robustness of ferroelectricity in these materials. The CMOS fabrication line-friendly material properties accelerate their active adoption in the semiconductor field at an unseen pace. It is exciting to expect the commercialization of mainstream semiconductor devices, not niche markets, using ferroelectric material after its finding ~ 100 years ago.

C. Piezoelectricity

Alexei Gruverman and Jorge Íñiguez

1. Status

HfO₂-based FEs are one of the most actively studied groups of materials due to their vast range of fundamentally captivating and technologically alluring properties, making them extremely appealing for the development of electronic devices based on switchable spontaneous polarization.²¹ Most of the studies of HfO₂-based FEs have so far focused on the mechanism of the stabilization of their polar phase; their unusual scaling properties, which seemingly defy detrimental depolarizing effects; and the interplay between the intrinsic and extrinsic factors determining the static and dynamic polarization behavior. In comparison, relatively little attention has been given to hafnia's piezoelectric properties. Although these materials exhibit weaker piezoelectricity in comparison with perovskite FEs—typical values for the measured piezo-coefficients are in the range of several pm/V—their response is comparable to that of AlN-based films, which makes them a viable alternative for application in electromechanical devices, such as sensors, resonators, and transducers. However, probably, the most intriguing aspect of the piezoelectric behavior of HfO₂ is its high sensitivity to a variety of parameters, including film thickness, fabrication methods, doping, and electric field cycling, which opens a possibility of tuning the electromechanical functionality of these materials.^{70,71}

First-principles calculations converge on the negative longitudinal piezoelectricity response of the *o*-phase of HfO₂,^{39,72} whereby a compression along the polar axis results in an enhanced polarization. At the atomic level, this feature is attributed to the chemical coordination of the active oxygen atoms³⁹ (Fig. 3): upon mechanical strain, the length of the Hf–O bond aligned with the polar direction is preserved via the shift of the oxygen ion. This shift results in a polarization increase/decrease upon compressive/tensile strain, yielding a negative longitudinal piezoresponse. In contrast, there are considerable disparities in the experimental reports on the magnitude and sign of piezoelectric coefficients of HfO₂, which still has not received an adequate explanation. For example, piezoelectric strain measurements carried out in 20 nm-thick Si:HfO₂ films reveal a relatively strong (17.8 pm/V) positive d_{33} coefficient, which decreases dramatically to negligible values upon ac cycling.⁷³

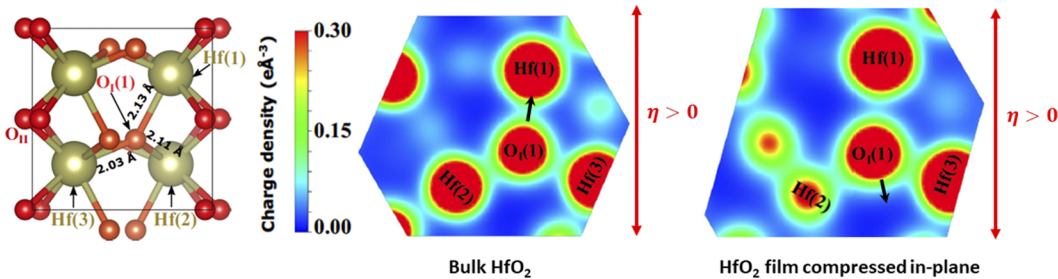


FIG. 3. Left panel: Structure of the ferroelectric phase of bulk hafnia. The Hf–O bond distances involving the polar-active oxygen “O₁(1)” are indicated. Center and right panels: Electronic charge density around oxygen O₁(1), which controls the piezoresponse in both bulk HfO₂ (center) and an epitaxially compressed film (right). If we stretch the material along the polarization direction ($\eta > 0$ along the vertical), the active oxygen moves (black arrow) to preserve the length of the chemical bonds most affected by the strain. Thus, the vertical Hf(1)–O bond dominates the response in the bulk compound; in the compressed film, this link is broken, and the bonds with Hf(2) and Hf(3) prevail (adapted from Ref. 39).

On the other hand, piezoresponse force microscopy studies yield negative longitudinal d_{33} piezocoefficients in relatively thin La:HfO₂ films (<30 nm), while in much thicker La:HfO₂ films (>50 nm), piezoelectricity is found to be positive.⁷⁴ Notably, thin and thick La:HfO₂ films had different electrodes (TiN and Pt, respectively) and were fabricated by using different methods [ALD and chemical solution deposition (CSD), respectively].⁷⁰ Moreover, the coexistence of regions with positive and negative d_{33} in the same La:HfO₂ capacitors has been reported,⁷⁰ which hints at the tuning of the d_{33} sign upon electrical cycling.

2. Current and future challenges

a. Experiment. Experimental studies of piezoelectricity in HfO₂ are based on the use of macroscopic testing techniques [double beam laser interferometer (DBLI), synchrotron XRD] and local probe methods piezoelectric force microscopy (PFM). While the macroscopic methods are more straightforward in that they directly measure the field-induced strain, they are not informative enough when it comes to understanding the tunability of the piezoelectric properties. In this regard, the PFM-based approach has an advantage as it allows for differentiation between the polar and non-polar phases by evaluating the local piezoresponse at the level of a single grain (several nanometers), as well as monitoring its evolution upon electrical cycling or annealing. On the other hand, interpretation of the PFM signal is not easy since it can be beset by various artifacts, such as electrostatic effects, electrochemical reactions, thermal effects, and complex cantilever dynamics.^{75,76} Even more challenging are the measurements in the resonance-enhanced mode developed to circumvent the issue of a low signal-to-noise ratio in materials with a weak piezoelectric response, where the cantilever is driven near its contact resonance. In this case, the PFM signal, which contains information about the d_{33} sign, strongly depends on the driving frequency relative to the resonance. Verification of a true sign of d_{33} requires reliable, artifact-free measurements of the PFM phase signal and careful selection of the measurement conditions⁷⁰ and should be further corroborated by the local probe quasi-static strain measurements. To date, there are very few systematic studies of the effect of confinement, chemical doping, or electrical cycling on the sign of the piezoresponse in the hafnia ferroelectric family. As a result, there is still a lack of understanding of

the mechanism for what seems to be a unique opportunity to tune piezoelectricity in these materials.

b. Theory. As regards theory and simulation, HfO₂-based FEs pose singular challenges. These compounds present many polymorphs that constitute robust (meta)stable phases separated by relatively high energy barriers. In such conditions, even the identification of a reference paraelectric structure becomes non-trivial, and so does the elucidation of polarization switching paths. The *t*-polymorph is usually taken as the centrosymmetric phase associated with the usual *o*-FE state, and based on this choice, ferroelectricity is interpreted as having an improper nature.⁴⁵ However, if the *t*-polymorph were, indeed, the experimentally relevant high-symmetry phase, one would expect to find four different polarization domains in the samples, something that has not been observed. On a related note, it has been recently emphasized that in HfO₂-like FEs, calculation of the spontaneous polarization itself is not trivial as it relies on an underlying assumption about the switching path between the positive and negative polarization states:⁴⁰ the usual choice of path—through the *t*-centrosymmetric phase—ultimately leads to a negative longitudinal piezoresponse. However, there exists at least one competing switching path^{40,41} that involves a different polarization assignment (i.e., the state usually interpreted as having a positive polarization would now have a negative one) and leads to a positive longitudinal piezoresponse. In other words, although the atomistic mechanisms controlling the piezoresponse³⁹ stay the same regardless of the switching path, the sign of d_{33} may vary. It remains to be seen which switching path is experimentally relevant or whether it may even be possible to deterministically control the path for intrinsic polarization switching. Other exotic theoretical predictions, such as the dependence of the d_{33} sign on mechanical constraints,³⁹ seem to be more directly related to the experimental conditions and could be tested in the near future.

3. Advances in science and engineering to meet these challenges

Recent years witnessed significant progress in the enhancement of the piezoelectric properties of FEs via domain engineering, controlling structural instability, and redistribution of mobile

ionic species.^{77,78} In HfO_2 -based FEs, structural transformations induced by electrical field cycling are strongly coupled to their electromechanical behavior. Sophisticated processing methods, structural phase engineering, stoichiometry control, and advanced techniques for macroscopic/nanoscopy electromechanical testing provide a foundation for designing HfO_2 -based materials with tunable piezoelectric properties, opening a possibility for their utilization in a variety of nanoelectromechanical devices. Fabrication of thick (hundreds of nanometers) HfO_2 films by CSD⁷⁹ is particularly beneficial for electromechanical applications as they provide a larger mechanical strain. Recent reports on the giant enhancement of piezoelectricity by field-induced rearrangement of oxygen vacancies in centrosymmetric materials⁷⁷ and the favorable effect of oxygen deficiency on the ferroelectricity in HfO_2 are indicative of the viability of this approach for better understanding and control of the tunable piezoelectric activity of HfO_2 . Availability of the macroscopic (DLBI) and nanoscopic techniques (PFM) sensitive to the electromechanical strain provides a set of necessary tools for testing piezoelectricity over a broad scale range and establishing a correlation between the global (device-level) and local piezoelectric behavior.

From a theoretical perspective, understanding piezoelectricity in HfO_2 FEs requires first-principles modeling of all relevant polar and non-polar polymorphs—and the paths connecting them—as a function of composition. This kind of knowledge is particularly relevant for addressing the piezoelectric properties of HfO_2 because of the basic problem of how to interpret the measured spontaneous polarization, which, in turn, is related to the uncertainty about the switching path. The effective-Hamiltonian and second-principles approaches that have been so successful to study FE perovskite oxides^{80,81} do not seem suitable here. Among many difficulties, let us mention the question of whether a suitable reference state can be defined or not,⁴² and the challenge of treating multiple switching paths—Involving the formation and breaking of bonds—within such perturbative formalisms. Instead, other force fields^{82–84} and machine-learned models appear to be the methods of choice. Recent publication of machine-learned potentials for HfO_2 is excellent news.⁵⁵

4. Concluding remarks

Addressing the full complexity of the HfO_2 -based FE compounds associated with different phases, domain configurations, vacancies, grains, and interfaces will be a major test for the approaches mentioned above, both experimental and theoretical. In particular, oxygen vacancies are known to play an important role in the measured electric properties of these compounds, and the piezoresponse cannot be expected to be an exception. The predicted multiplicity of polarization switching paths, which implies an easy migration of oxygens from cell to cell, suggests a critical role of these *extrinsic* contributions and should become a major focus of attention. A combination of local probe and electron microscopy studies with structural characterization along with electrical and electromechanical testing is required to achieve a deeper understanding of the physical mechanism behind the observed high variability of the piezoresponse and to provide a physical foundation for tailoring the piezoelectric properties of the HfO_2 -based FEs. Bridging the gap between theory and experiment, particularly by addressing the extrinsic factors in the calculations, is very challenging, but its

successful implementation will facilitate much faster progress. Ultimately, the difficulties that HfO_2 FEs pose are also one of their main appeals: never had we seen a FE compound with so many possibilities for experimental control of the piezoelectric properties, from a mechanical reversal of the sign of the piezoresponse without even having to switch the polarization³⁹ to tuning of the piezoelectric behavior by selecting the polarization switching path.⁴⁰ This is a challenge worth taking.

5. Acknowledgments

J.Í. acknowledges the support from the Luxembourg National Research Fund through Grant No. INTER/NWO/20/15079143/TRICOLOR.

D. Pyroelectricity

Patrick D. Lomenzo

1. Status

Pyroelectric films are extensively used in infrared (IR) detectors for a wide range of applications, such as gas detection (CO , CO_2 , CH_4 , and C_3H_8), flame detectors, motion and gesture detection, and thermal imagers. Pyroelectrics also receive increasing interest for energy harvesting and electrocaloric cooling applications. Perovskite single-crystal LiTaO_3 or PZT materials are frequently employed in infrared detectors due to their large pyroelectric coefficients (p). The pyroelectric coefficient is comparatively smaller in HfO_2 - and ZrO_2 -based pyroelectric films, yet the CMOS compatibility, environmentally sustainable chemistry, and the relative ease of fabrication are attractive for fluorite-based hafnia and zirconia IR detector development.

HfO_2 - and ZrO_2 -based FEs are pyroelectric active materials due to the existence of the polar Pca_2 *o*-crystal structure.³⁸ Since the FE dipole in this crystal phase is temperature dependent, a temperature change in FE HfO_2 or ZrO_2 can lead to the modulation of surface charge and voltage potential at the device terminals (primary pyroelectric effect). The generation of a pyroelectric voltage or current will only occur in these FEs after being polarized by the application of an electric field of sufficient strength or if the films are grown with a preferred out-of-plane dipole orientation.^{85,86}

FE doped HfO_2 and $\text{Hf}_{1-x}\text{Zr}_x\text{O}_2$ most frequently exhibit a polycrystalline structure, which leads to a pyroelectric coefficient that is proportional to P_r and, therefore, highly dependent on the electrical history of the device, such as wake-up cycling or poling field strength.^{86,87} Wake-up causes a simultaneous increase in P_r and p in doped- HfO_2 and HZO FEs.^{85,87} A wide variety of dopants that induce ferroelectricity in HfO_2 , including La, Gd, Al, Si, and Sr, have exhibited comparable pyroelectric performance that generally depends on the product of ϵ_r and P_r .^{88,89} Pyroelectric coefficients with a magnitude between 20 and $90 \mu\text{C m}^{-2} \text{K}^{-1}$ in FE doped- HfO_2 and HZO films are most commonly reported in planar devices.^{38,85–89} Larger pyroelectric coefficients exceeding $-100 \mu\text{C m}^{-2} \text{K}^{-1}$ have been reported for Si-doped films near a morphotropic phase boundary.^{90,91} A plot of p vs P_r is shown in Fig. 4(a). The giant pyroelectric effect, which involves a much larger temperature range and irreversible phase transitions, has been indirectly

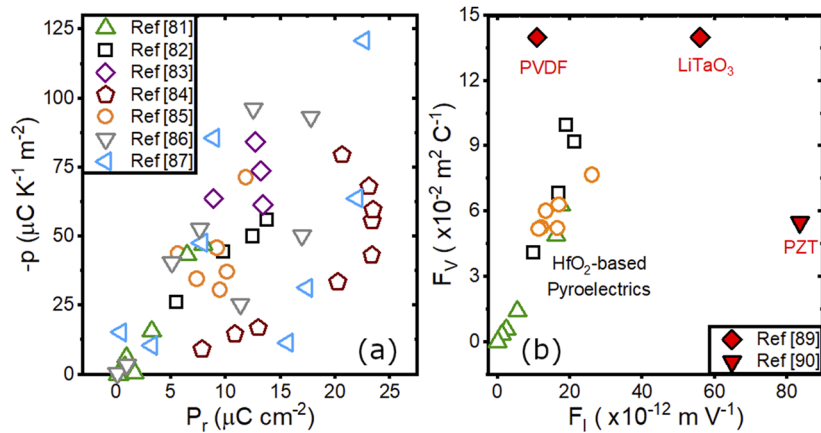


FIG. 4. (a) Pyroelectric coefficients (p) vs remanent polarization (P_r) for various types of FE HfO₂-based thin films. (b) Voltage sensitivity vs current sensitivity figures of merit of HfO₂-based pyroelectrics compared with other materials. The pyroelectric coefficient in HfO₂ is typically proportional to the product of $\epsilon_r P_r$, though proximity to a phase transition may enhance p further.

calculated with a magnitude of up to $-1300 \mu\text{C m}^{-2} \text{ K}^{-1}$ in Si-doped HfO₂.⁹² Voltage responsivity (F_v) and current responsivity (F_1) are common material figures of merit for pyroelectric detectors that are used to assess the maximum output voltage and output current, respectively. Figure 4(b) shows HfO₂-based pyroelectric figures of merit for voltage and current sensitivity. These figures of merit are smaller compared to other pyroelectric materials, such as polyvinylidene difluoride (PVDF), LiTaO₃, and lead zirconate titanate (PZT).^{93,94}

2. Current and future challenges

Polycrystalline FE HfO₂- and ZrO₂-based films are frequently formed with coexisting crystal phases that can be influenced by the film deposition conditions, film thickness, annealing temperature, type of incorporated dopant, and dopant concentration.^{38,85-92,95} Nonpolar phases, such as the *t*-*P4₂/nmc* phase ($k \sim 40$) and the *P2₁/c* *m*-phase ($k \sim 18$), can coexist with the polar *Pca2₁* *o*-phase ($k \sim 30$) in polycrystalline FE films. The presence of *m*- and/or *t*-phases is generally undesirable for pyroelectric films because of the resulting lower P_r of the FE fluorite structured films, which can decrease the pyroelectric coefficient. However, the morphotropic phase boundary between the *o*-phase and *t*-phase enhances the pyroelectric coefficient, and the slight co-presence of the *t*-phase can, in this case, be beneficial, especially if wake-up cycling is performed to facilitate an irreversible tetragonal-to-orthorhombic phase transition.

The *m*-phase is particularly harmful for pyroelectric devices since its low relative permittivity can establish large depolarization fields and lower the effective permittivity of the FE film, adversely affecting the pyroelectric coefficient. The annealing temperature and doping concentration can impact the formation of the *m*-phase,^{85,88} but the *m*-phase problematically exhibits a strong film thickness dependence. The monoclinic phase has been widely observed to grow as the film thickness is increased beyond 15 nm in atomic layer deposited FE doped HfO₂ and Hf_{0.5}Zr_{0.5}O₂.⁸⁶ Thicker pyroelectric films can improve the output voltage of pyroelectric sensors, which

simplifies the sensing circuits. The growth of the monoclinic phase with increasing film thickness is problematic from this point of view. The increase in grain size and decrease in in-plane tensile stress with growing film thickness make the *m*-phase more energetically favorable than the *o*- and *t*-phases, thus creating challenging conditions to manufacture thicker FE HfO₂-based films with best-in-class pyroelectric performance.

One method to inhibit the formation of the *m*-phase is to interrupt the crystalline structure of the FE films by incorporating a 0.5–1 nm amorphous oxide layer in films thicker than 10 nm. This technique was successfully demonstrated for Si-doped HfO₂ with Al₂O₃ interlayers where a total film thickness of 50 nm was grown without the formation of the monoclinic phase, and a pyroelectric coefficient of $62 \mu\text{C m}^{-2} \text{ K}^{-1}$ was reported.⁸⁷ The interlayer approach to fabricate thicker pyroelectric films is not necessarily flawless, however, since the pyroelectric coefficient decreased from 84 to $62 \mu\text{C m}^{-2} \text{ K}^{-1}$ when increasing the Al₂O₃ interlayer Si-doped HfO₂ film thickness from 20 to 50 nm. New methods to further increase the pyroelectric coefficient, film thickness, and loss tangent would benefit pyroelectric applications, such as infrared sensors.

3. Advances in science and engineering to meet these challenges

Key advantages FE HfO₂-based pyroelectrics have over other pyroelectric materials are its CMOS compatibility and the mature deposition capabilities available for thin films. Three-dimensional trench capacitors have been demonstrated with FE HfO₂-based pyroelectric materials.^{96,97} These trench capacitors greatly increase the effective pyroelectric coefficient when compared to planar capacitors. Moreover, a CMOS-compatible integrated infrared sensor with doped HfO₂ has been demonstrated comparing planar and trench capacitor pyroelectric performances.⁹⁷ In that work, trench capacitors magnified the effective area and the responsivity by a factor of 15 compared to the planar pyroelectric HfO₂-based infrared detectors. However, the authors observed that the trench

capacitors increased the electrical capacitance and noise, preventing the sought-after improvement in the signal-to-noise ratio compared to the planar devices.⁹⁷ Moreover, the geometry of trench capacitors might preclude some pyroelectric applications, such as thermal array imagers, since incident radiation may not be uniformly sensed from the environment compared to planar thermal pixels. Reducing the loss tangent and increasing the FE HfO_2 film thickness without degrading the pyroelectric coefficient are required to improve infrared sensors developed from fluorite pyroelectrics.

Laminate structures, superlattices, refinements in processing, and doping strategies should facilitate incremental improvements in the pyroelectric performance of FE HfO_2 thin films. In particular, optimization of the FE films for pyroelectric applications will require (i) minimization of the m -phase, (ii) high P_r , (iii) improvements in film deposition processing, and (iv) a suitable poling technique to achieve optimal pyroelectric performance. CSD is a good candidate to realize much thicker FE HfO_2 - and ZrO_2 -based films for improved infrared sensor characteristics. Pyroelectric measurements on epitaxial films could also give further material insights since polycrystalline effects can be excluded. Pre-poling or self-poled FE capacitors through the fabrication process would be preferable for production processes of infrared sensors.

Pyroelectric energy harvesting devices that take advantage of the giant pyroelectric effect on FE HfO_2 and ZrO_2 films have been predicted to be very promising based on indirect calculations,⁹² but direct measurements are needed to better assess the material performance for energy harvesters. Furthermore, pyroelectric-based energy harvesters with trench capacitor geometries could aid in improving the active pyroelectric volume that can scavenge thermal energy. Future investigations into HfO_2 - and ZrO_2 -based films that employ direct measurements of the giant pyroelectric effect near the orthorhombic-to-tetragonal phase transition at or above room temperature would help to shed light on how the proximity of the phase transition might advance energy harvester. The development of nanostructures and evaluating the role of substrate clamping effects would also aid in better assessing primary and secondary pyroelectric coefficients, the latter of which arises from the piezoelectric effect and thermal expansion.⁹⁸

4. Concluding remarks

FE HfO_2 - and ZrO_2 -based films show very promising pyroelectric properties for infrared sensing, energy harvesting, and electrocaloric cooling applications. Although this fluorite structured material system lags behind in some infrared sensor performance metrics with best-in-class materials, such as LiTaO_3 and PZT, research on HfO_2 - and ZrO_2 -based FE materials has only exceeded the one-decade mark at the time of writing. With further advances in processing and film development, it remains to be seen if FE HfO_2 and ZrO_2 materials can close the performance gap in infrared sensing devices compared to leading commercial materials.

Phase transitions or films near the morphological phase boundary could be further exploited in a wide variety of doped HfO_2 and ZrO_2 films to achieve enhanced pyroelectric and giant pyroelectric effects. Direct measurements of the giant pyroelectric effect through phase transitions will help to reveal this material system's full

potential for pyroelectric energy harvesting devices. In conclusion, there remain many opportunities to both discover and optimize more pyroelectric properties in these fluorite-structured ferroelectrics.

5. Acknowledgments

P.L. was funded by the German Research Foundation (DFG)—Project Nos. 430054035 and 433647091.

E. Negative capacitance

Michael Hoffmann

1. Status

Negative capacitance (NC) occurs when the charge on a capacitor changes oppositely to the voltage across it, which can be caused by various physical phenomena in different materials and structures.⁹⁹ In 1976, Landauer first proposed that FEs should exhibit NC due to their polarization instability,¹⁰⁰ but experimental evidence only started to appear some 30 years later.¹⁰¹ Importantly, there are two different types of NC, which must be distinguished: transient and stabilized NC. While transient NC can occur during hysteretic polarization switching in FEs, NC can be stabilized by an external positive capacitance to achieve hysteresis-free behavior. In 2008, Salahuddin and Datta proposed that stabilized NC could be used to amplify the voltage in nanoscale transistors, thus overcoming the fundamental limit of the subthreshold swing (SS) of 60 mV/decade at room temperature.¹⁰² However, the first experimental NC results were obtained in epitaxial perovskite FEs, which are not compatible with standard semiconductor manufacturing.^{103,104}

From the integration point of view, fluorite-structure FEs based on HfO_2 and ZrO_2 are ideal for NC applications since they are scalable and can be easily integrated into advanced semiconductor devices.^{105,106} The first direct measurement of transient NC in fluorite-structure MFM capacitors was reported in 2016.¹⁰⁷ Since then, stabilized NC has been demonstrated in pulsed electrical measurements of FE/dielectric and AFE/dielectric capacitors using relatively thick films (~10 nm) and large voltages (>5 V).^{58,108,109} It has been proposed that NC in such heterostructure capacitors could enable higher energy storage density and efficiency in electrostatic supercapacitors.¹¹⁰ However, the origin of these experimental NC effects observed in fluorite-structure ferroelectric capacitors has been debated. For example, it has been argued that parasitic circuit components could result in similar transient NC behavior as observed in MFM capacitors.¹¹¹ It was also suggested that the charge boost in FE/dielectric capacitors might be explained by ferroelectric imprint and reverse switching from a vortex-like domain structure.¹¹²

Furthermore, there have been many reports of transistors with fluorite-structure gate oxides, which exhibit below 60 mV/decade SS under certain measurement conditions.¹¹³ However, the vast majority of these claimed “NC transistors” seem to exhibit a transient NC effect with substantial hysteresis, which limits their potential for applications.^{105,114–116} Unambiguous reports of NC transistors with hysteresis-free sub-60 mV/decade SS are still elusive so far. Nevertheless, it has been shown that ultrathin (<3 nm) fluorite-structure

gate oxides can lead to improved performance of scaled transistors compared to regular amorphous HfO_2 , even when the SS is still larger than 60 mV/decade at room temperature.¹⁰⁶ Recently, it has been shown that 2 nm thick $\text{HfO}_2/\text{ZrO}_2/\text{HfO}_2$ (HZH) superlattices with mixed FE/AFE order can reduce the equivalent oxide thickness (EOT) of advanced transistors down to 6.5 Å, lower than the physical thickness of the SiO_2 interfacial layer.⁶⁹ These promising results suggest that the HZH layer can be stabilized in an NC state, thus achieving lower overall EOT without degrading the transistor performance and reliability.

2. Current and future challenges

To enable NC transistors based on fluorite-structure (anti)ferroelectric oxides with even lower EOT and SS values, several critical challenges must be overcome. While some of these challenges are related to our limited understanding of NC and the basic material properties of fluorite-structure oxides, others stem from the need for a practical NC device design and FE material integration.^{105,117} While the microscopic origin of NC is relatively well understood in model systems, such as epitaxial perovskite FEs,^{103,104,118} it is less clear in fluorite-structure (anti)ferroelectrics so far.

For example, fluorite-structure (anti)ferroelectric thin films are typically polycrystalline with complex domain topologies as well as mixed FE and non-FE grains of various sizes and orientations,¹¹⁹ which makes the microscopic imaging of the domain and grain structure challenging. Charge trapping effects can play an important role due to the presence of defects at interfaces and grain boundaries.¹⁰⁵ This complicates the development of more accurate NC models for fluorite-structure oxides, which need to take at least the domain and grain structure into account.^{120,121} From a theoretical point of view, the basic anisotropy and domain coupling constants, as well as the domain wall mobilities, are still not well established. So far, these critical values for NC device simulation are typically fitted to experimental data. Without realistic estimates for these values, it is challenging to understand the microscopic origin of NC in fluorite-structure oxides^{121,122} and to assess the theoretical limits of NC devices based on these materials.

For the development of nanoscale NC transistors, the gate oxide should ideally be as thin as 2 nm. While fluorite-structure (anti)ferroelectrics in this thickness range tend to become more textured when grown on silicon by ALD, they still show substantial spatial inhomogeneity, in part, due to their *t/o*-phase mixture.^{19,69,123} This presents a challenge for ultimately scaled NC transistors, which might exhibit larger device-to-device variability due to the polycrystalline nature of the gate oxide, which in conventional devices is amorphous. While there are currently no experimental data to support this, variability might also be exacerbated for scaled 3D NC transistors, such as FinFETs or nanosheet FETs. One major challenge in achieving hysteresis-free sub-60 mV/decade SS in NC transistors seems to be the large change in the quantum capacitance of the semiconductor channel with gate voltage.¹²⁴ Furthermore, the need for a thin SiO_2 interfacial layer in silicon-based devices might “absorb” most of the NC benefit, leading to an overall positive capacitance of the gate stack and, thus, SS larger than 60 mV/decade.⁶⁹

3. Advances in science and engineering to meet these challenges

In recent years, substantial progress has been made on both the demonstration and understanding of NC effects in fluorite-structure (anti)ferroelectrics.¹²⁵ On the theory side, multi-domain and even multi-grain numerical models have been developed, which are able to reproduce experimental NC data.^{120–122} Furthermore, first-principles calculations have revealed some of the unique domain wall properties of fluorite-structure ferroelectrics,^{49,50,126} which are crucial to better understand the microscopic origin of NC. In particular, the importance of topological domain walls⁵⁰ might explain the qualitative differences of NC behavior observed in thicker (anti)ferroelectric/dielectric capacitor structures^{58,108,109} compared to ultrathin mixed-phase films.⁶⁹ Uncovering the relationship between topological domain wall dynamics and NC in fluorite-structure oxides is a promising topic for future research. High-resolution transmission electron microscopy (HRTEM) techniques could help to directly image such domain wall structures¹²⁷ in devices with macroscopic NC behavior. In principle, HRTEM combined with *in situ* voltage biasing could directly reveal such domain wall movement.¹²⁸

A significant recent advance in experimental NC devices was the demonstration of stable NC in ultrathin HZH gate oxides, resulting in a low EOT without interfacial layer scavenging.⁶⁹ After demonstrations on 90 nm gate length n-type transistors, further experiments with even shorter channels and p-type devices will be important for CMOS applications. Variability and reliability of ultimately scaled NC transistors should be investigated. As mentioned before, more theoretical insights into how to tune NC in these mixed-phase ultrathin films will be helpful to reduce the EOT further by optimizing the FE and interfacial SiO_2 layers.¹²⁹ Furthermore, it seems promising to investigate other channel materials besides silicon, where SiO_2 interfacial layers might not be necessary or which can be operated in the quantum capacitance limit.¹²⁴ Future research should also investigate 2D and 3D electrostatic effects due to the multi-domain nature of the FE layer and how these influence the quantum confinement in the semiconductor channel.

Beyond nanoscale transistors, other promising applications for NC include energy storage¹¹⁰ as well as actuators and sensors.¹³⁰ From a more basic research point of view, experiments on NC could also give new insights into the fundamental switching mechanism of (anti)ferroelectric fluorite-structure oxides,^{109,122} which is still not fully understood.^{50,51,131} Additionally, combining NC with other solid-state physics phenomena, such as high-temperature superconductivity,¹³² could enable entirely new applications for fluorite-structure FEs.

4. Concluding remarks

NC in fluorite-structure (anti)ferroelectric oxides is a promising phenomenon, especially for applications in nanoscale transistors as well as fundamental physical material investigations. NC experiments could give new insights into the FE-switching behavior of fluorite-structure FEs. Recent progress in the experimental demonstration of stabilized NC in ultrathin fluorite-structure oxides is encouraging for future transistor applications. However, more microscopic insights, from both theory and experiment, are needed to fully understand the physical origin of NC in fluorite-structure

oxides and to optimize the NC device design. In particular, the role of topological domain walls and the mixed-phase microstructure needs further investigation. For nanoscale transistor applications, further reduction of the EOT and SS is needed through material and device optimization with the help of multi-domain modeling. Beyond transistors, NC seems promising, e.g., for energy storage applications. Finally, investigating NC in combination with other solid-state phenomena, such as quantum confinement or superconductivity, could enable entirely new applications.

F. Domain walls

Duk-Hyun Choe and Jinseong Heo

1. Status

Although infinitely large FE crystals prefer a single-domain state, in principle, real FE crystals are usually divided into multiple domains of different polarities. Such domains can occur spontaneously (for example, owing to defects and/or finite-size effects), and they can also be formed and engineered by the application of external fields. The boundaries separating these domains are called FE DWs. FE DWs not only play a central role in polarization switching, but they can lead to many emergent phenomena, including charged DW, DW conduction, and exotic topological textures (vortices, skyrmions, and merons).^{11,133} Therefore, understanding their structure, topology, and motion is of both fundamental and technological importance. In HfO₂-based FEs, work on intrinsic properties of DWs and the mechanism of their dynamics is still in its infancy. This section briefly reviews the field of DW physics in HfO₂-based FEs and provides an outlook based on the current and future challenges.

2. Current and future challenges

A number of interesting DWs can exist in HfO₂-based FEs. Several types of DW structures in the common *o*-(*Pca*₂₁) phase of FE HfO₂ were identified using scanning transmission electron microscopy (STEM) analysis. Grimley *et al.* reported the first reliable observation of 90° DWs in ALD-grown Gd:HfO₂.¹¹⁹ Kiguchi *et al.* introduced and identified several types of atomically sharp 180° and 90° DWs as well as tilted DWs in epitaxial Y:HfO₂.⁶² Both studies, however, could not identify the exact sign of the domain polarizations. Using atomic-resolution STEM, Cheng *et al.* were able to distinguish the direction of the polarization in a mixture of *Pca*₂₁ and *Pbca* phases of Zr:HfO₂,⁶³ in which their phase boundary bears structural resemblance to the 180° DWs. Interestingly, a recent study by Zhou *et al.* identified a charged 90° DW having a tail-to-tail domain structure in Zr:HfO₂,¹³⁴ which could affect the wake-up behavior in the polarization hysteresis depending on the orientation of the DW. The first systematical categorization of DWs in HfO₂ was done by Ding *et al.* based on first-principles calculations.⁴⁹ They established ten basic types of 180° and 90° DWs by considering the orientation and lattice vectors of the unit cell of the *Pca*₂₁ phase of HfO₂. It should be noted that the DW energy of the most stable 180° DW is calculated to be negative,^{23,49} suggesting a possible preference of anti-polar domains even in an infinitely large, pristine HfO₂ crystal. Moreover, the domains separated by such DWs have

shown to persist its polarization at the ultimate scale, i.e., a half-unit cell width (~2.5 Å).^{23,49} Lee *et al.* attributed these striking differences from traditional perovskite FEs to the intrinsic flat phonon bands in HfO₂.²³ On the other hand, Choe *et al.* revealed a class of topological DWs in HfO₂ that is characterized by the relative quasi-chirality and the parity of the number of half-unit cells between the neighboring domains.⁵⁰ The term topological is used due to the requirement of *global* structural changes for transitions between different topological classes of DWs, while transitions within the same class only require *local* structural changes near the DW. This has opened up new possibilities in the search of DWs not only in the *Pca*₂₁ phase but also in inter-phase boundaries between *t*-(*P4*₂/*nmc*), *o*-(*Pca*₂₁), and *m*-(*P2*₁/*c*) phases, which are often present in experiments.^{62,119} Zhao *et al.* further expanded the family of the topological DWs into 93 irreducible configurations based on the lattice mode analysis.¹²⁶

3. Domain wall dynamics

Theoretical studies suggest that DW dynamics and the polarization switching mechanism in HfO₂-based FEs can be markedly different from those in perovskite FEs. In particular, the energy barrier for the DW motion in HfO₂ via the most stable 180° DW is calculated to be more than an order of magnitude higher than its perovskite counterparts.^{23,49} Lee *et al.* pointed out that the polar domains in HfO₂ can be independently switchable (or nucleated) down to the ultimate limit,²³ with a high energy barrier that is similar to that of the DW motion [Fig. 5(a)]. While this suggests a potential use of HfO₂ for a novel ultra-dense memory,²³ this also implies that the intrinsic polarization switching of HfO₂ films as a whole can be extremely inefficient. PFM measurements support this model, which showed about 100 times lower DW velocity compared to PZT.¹³⁵ According to this model, however, DW motion becomes practically impossible in HfO₂ FEs. The absence of DW motion within a grain would translate to an ultra-slow switching speed even for NLS mechanism, which would impose limitations on the applicability of HfO₂ in the emerging FE devices, including FeFETs and negative capacitance field-effect transistors (NCFETs). Meanwhile, Choe *et al.* pointed out that the high switching barrier in the proposed model is attributed to the structural change that reverses the quasi-chirality of the domains.⁵⁰ To find a low-barrier switching mechanism, they devised a tetragonal phase-like DW composed of 2-half-unit cells [two consecutive ivory-colored boxes in Fig. 5(b)], which leads to the same quasi-chiral symmetry within the neighboring domains. Such DW could significantly reduce the switching barrier, allowing for a rapid DW propagation in HfO₂. Moreover, as illustrated in Fig. 5(b), it can be created by a new type of domain nucleation model involving 3-half-unit cells,⁵⁰ which is calculated to be energetically preferred over the seemingly plausible half-unit cell nucleation. Together, these findings demonstrate that the fast nucleation and growth within a grain can be feasible through topological DWs in HfO₂, as has been hinted by indirect evidence in experiments.^{51,136–140} Lattice mode analysis by Qi and Zhao has revealed several more chirality-preserving switching mechanisms via the topological DWs.^{46,126}

It is worth mentioning that an alternative FE switching mechanism, based on the intermediate *o*-(*Pbcm*) phase, also exists.^{50,141} In addition to a 35% increase in remanent polarization, an intriguing feature of this mechanism is its counterintuitive labeling of

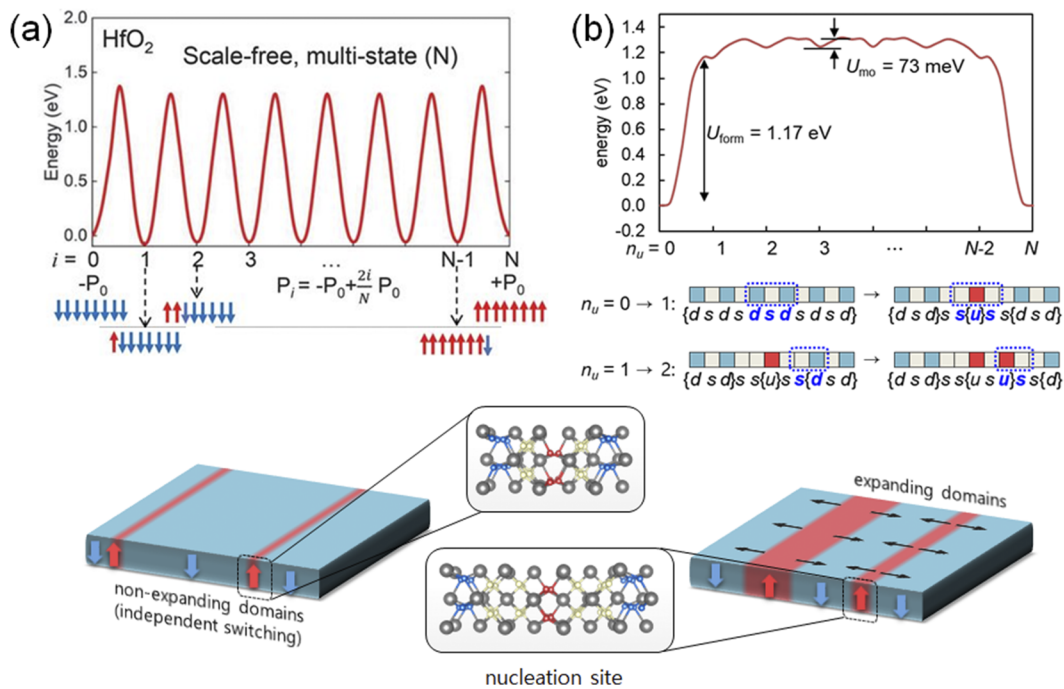


FIG. 5. Relative energies of the two different ferroelectric switching scenarios: (a) non-expanding domains (independent switching) and (b) expanding domains. Schematics of the two switching scenarios are shown. Figures adapted from Refs. 23 and 50.

the polarization orientation,⁵⁰ precisely opposite to the scenarios in Fig. 5, arising from the opposite O atom movement during FE switching. Much room remains for further studies regarding its role in the different signs of the piezoelectric coefficient,^{40,70} O migration,^{50,142,143} and DW growth.^{144,145}

4. Advances in science and engineering to meet these challenges

The key challenges in DW physics of HfO₂ can be divided into theoretical and experimental challenges. Until now, theoretical investigations are limited to neutral DWs having 180° and 90° DW angles. Considering the existence of complicated DWs in FE HfO₂, including tilted DWs⁶² and charged DWs¹³⁴ in experiments, the family of topological DWs in HfO₂ is expected to be much richer than what is currently known. In addition, due to the high computational cost, previous first-principles calculations are mostly relying on small systems no larger than eight unit cells ($\sim 1 \text{ nm}^3$). While such calculations can provide fundamental insights into DW physics, they cannot capture the realistic DW dynamics that involve collective and complex processes. A critical shortcoming, for example, is that the currently estimated E_c from first principles is generally an order of magnitude higher than the experimental values.^{52,141} There is no reliable first-principles estimate for the DW velocity in HfO₂ as well. The E_c and DW velocity of HfO₂ should be quantitatively understood using large enough supercells ($>64 \text{ nm}^3$) as they are among the most important features affecting the performance of FE devices. In addition, understanding the effect of surfaces,¹⁴⁶ interfaces,¹⁴⁷ and defects¹⁴⁸ on the DW

stability and dynamics is required. Utilization of large-scale density functional theory (DFT),^{149,150} machine-learned force field (MLFF),^{55,151} and effective lattice Hamiltonian approach⁸⁰ in FE HfO₂ is desired to gain deeper first-principles insights into the DW dynamics and E_c . This will also help set up macroscopic models for device-scale simulations, such as phase-field simulations^{120,152} and technology computer-aided design (TCAD), which require many fitting parameters that are generally not accessible to experiments.

Experimental access to the DW structure and their dynamics at the atomic level is difficult. In HfO₂-based FEs, their highly polycrystalline nature¹⁵³ with the $<20 \text{ nm}$ crystallite size and the mixed competing phases^{24,26} add additional layers of complexity.¹²³ One of the most important requirements for accurate identification of DWs is the reliable imaging of oxygen atoms in doped HfO₂ along specific crystallographic orientations.^{50,63,134} Given a range of theoretically discovered DWs,^{49,50,126} and with only a handful of observations,^{62,63,119,134} a further experimental study with advanced microscopy is needed. Unfortunately, direct observation of DW dynamics in FE HfO₂ poses even greater challenges. For example, piezoelectric force microscopy (PFM), the most widely used scanning probe microscopy (SPM) for dynamical studies, cannot provide real-time information on the DW motion at the atomic resolution.¹⁵⁴ Alternatively, *in situ* TEM typically requires special processing techniques, and it often does not represent the actual operating environment. Advances in the atomic-scale *in situ*/operando electron microscopy,^{142,155} together with *in situ* SPM,¹⁵⁶ could enable the experimental confirmation of the unique functional properties

of DWs in HfO_2 and further inspire the exploration of new DW physics.

5. Concluding remarks

The discovery of ferroelectricity in HfO_2 has not only triggered a resurgence of interest in FE devices, but it is stimulating the quest for a deeper fundamental understanding of their unconventional FE behavior. We are beginning to recognize the diversity and functionality of DWs in the $Pca2_1$ phase of HfO_2 . We anticipate that new types of functional DWs and/or intriguing topological morphologies will be experimentally revealed in the near future. Other competing FE phases, including recently suggested $\text{o-}(Pnm2_1)$ ²⁶ and rhombohedral ($R3$ or $R3m$)²⁷ phases, may also possess distinct types of DWs with various DW angles, where their DW structures remain largely unexplored. The fundamental insights obtained into the nature of DWs and their dynamics will offer a more rational design and engineering of emerging FE devices, further accelerating their development.

IV. BULK GROWTH

Xianghan Xu, Fei-Ting Huang, and Sang-Wook Cheong

A. Status

The challenge of quantum materials innovation comes with fabricating stable micro-devices with physics dominated by quantum mechanism, which has led to world-wide research efforts on functional properties of quantum materials. Likely, film forms will be used for those quantum material devices, but it is necessary to have bulk crystals to study intrinsic physical properties. In addition, there can also be applications using bulk crystals; for example, FE bulk crystals of BaTiO_3 , LiNbO_3 , and PMN-PT have been used for rectifiers, oscillators, and piezoelectric actuators. For the new generation of quantum materials, investigating a workable bulk crystal growth technique is a fundamental step to push them from laboratories into the realm of massive industrial production and applications, and HfO_2 growth is one good example.

Being studied as a high- κ material that shows good compatibility with the Si-based micro-devices, the investigation of HfO_2 bulk single-crystal growth has never stopped. In 1966, Chase and Osmer reported the growth of monoclinic HfO_2 single crystals with typical size $2 \times 2 \times 1 \text{ mm}^3$ from a PbF_2 flux.¹⁵⁷ In 1970, Ruh and Corfield reported monoclinic HfO_2 crystals grown from a $\text{Li}_2\text{O}-\text{MoO}_3$ molten flux and hydrothermally from an NH_4F solution, and needle-like or plate-like crystals were obtained.¹⁵⁸ In 2016, Lozanov *et al.* reported the growth of monoclinic HfO_2 single crystals using a reactive chemical vapor deposition with CF_4 as a transport agent.¹⁵⁹ The crystal plates show a typical size of around 2 cm. In addition, people also made attempt to get HfO_2 crystals in different room temperature phases by introducing dopants. Kadlec and Simon reported the growth of yttrium-stabilized-hafnia (YSH) single crystals in the cubic phase from melting with 20 mm dimension in diameter.¹⁶⁰ Mann and Kolis reported a hydrothermal growth method of yttrium, neodymium, holmium, and erbium stabilized cubic hafnia single

crystals having a maximum size of 0.25 mm.¹⁶¹ Kurosawa *et al.* reported the skull melting growth of 20 mm size 17% Tb-doped cubic HfO_2 crystals.¹⁶² Yu *et al.* reported the growth of cubic $\text{Hf}_{0.86}\text{Y}_{0.13}\text{Eu}_{0.01}\text{O}_{1.93}$ single crystals with an optical floating zone equipped with high-power xenon lamps.¹⁶³ Kim *et al.* reported the growth of lutetium stabilized cubic HfO_2 single crystals with a typical dimension of 5 mm by using a metal-assisted indirect arc heating method.¹⁶⁴

B. Current and future challenges

The polymorphic nature is the major difficulty in the growth of bulk HfO_2 in a certain desired phase. Typically, all the bulk single-crystal growth techniques involve an equilibrium crystallization of the thermodynamically most stable phase at the growth temperature and chemical environment, which does not encourage the growth of kinetically stabilized o-HfO_2 bulk crystals. However, in HfO_2 films, the relative energy of polymorphs and transformation kinetics between them have been found strongly depending on factors such as doping,^{60,165-168} oxygen vacancies,^{36,169,170} stress/strain,¹⁷¹ cooling rate,^{172,173} and surface energy.³⁰ Therefore, the synergistic interplay of some of those factors seems the right approach to search for kinetically stabilized phases in HfO_2 bulk materials.

For undoped HfO_2 , the structure undergoes the monoclinic (m , $P2_1/c$), tetragonal (t , $P4_2/-nmc$), and cubic ($c-Fm-3m$) phases with elevated temperature. Attempting to quench undoped HfO_2 bulk crystals from the high temperature cubic phase results in the monoclinic phase at room temperature, which means that the energy of kinetically stabilized phases remains high in undoped HfO_2 . Inspired by the fact that introducing dopants such as Zr^{4+} , Si^{4+} , Al^{3+} , La^{3+} , Gd^{3+} , and Y^{3+} can facilitate the formation of kinetically stabilized phases in HfO_2 thin films, Y^{3+} seems the most desirable dopant into bulk HfO_2 to achieve the kinetically stabilized phases for the following reasons. First, Y^{3+} has a relatively closer ionic radius to Hf^{4+} than La^{3+} and Gd^{3+} , which guarantees good solubility. Second, Y^{3+} incorporation brings great structure tunability into bulk HfO_2 . According to the equilibrium phase diagram of $\text{Y}_2\text{O}_3-\text{HfO}_2$ solid solution, introducing a 20% Y atom can fully turn the room temperature phase into a fluorite-type cubic phase. In the contrary, though Zr^{4+} also has good solubility in HfO_2 , the room temperature phase of bulk $(\text{Hf}, \text{Zr})\text{O}_2$ is always monoclinic, independent of concentrations. Moreover, the heterovalence doping of Y^{3+} spontaneously introduces oxygen vacancies, which may favor the kinetically stabilized o -phase over the m -phase, which has more oxygen coordination of Hf atoms.

Since the cubic phase has the most yttrium solubility and appears at an extreme high temperature just below the melting point, to ensure the uniform yttrium distribution, a crystallization directly from $\text{HfO}_2:\text{Y}$ molten liquid would be ideal. The refractory nature of bulk HfO_2 makes its melting point extremely high (almost 3000 °C). Even an iridium crucible that is commonly used in the Czochralski method cannot survive at such a high temperature. Nevertheless, a floating zone technique has the merit of being crucible-free that can overcome this limitation. The maximum output temperature of a floating zone furnace strongly depends on the heating elements and optics. The conventional floating zone furnace typically adopts a “halogen lamps + concave mirrors” setup, and the maximum temperature of around 2200 °C is insufficient to melt bulk

HfO_2 . Remarkably, the laser floating zone model commercialized in 2011 adopts focused high-power diode-based laser beams as heating elements, which enhances the maximum heating temperature.¹⁷⁴ Moreover, the well-focused laser beams create a large temperature gradient of around $150\text{ }^\circ\text{C/mm}$ at the solidification interface, which is ~ 5 times larger than that of a conventional floating zone furnace. For the growth of bulk HfO_2 in kinetically stabilized phases, this sharp temperature gradient facilitates rapid cooling after crystallization, which prevents undesirable yttrium diffusion and phase separation.

C. Advances in science and engineering to meet these challenges

In 2021, Xu *et al.* reported the growth of $\text{HfO}_2:\text{Y}$ bulk crystals with various Y dopant concentrations by using a laser floating zone method.³² The XRD pattern of ground crystals indicates the existence of kinetically stabilized *o*-phases, which are not found in the equilibrium Y_2O_3 - HfO_2 phase diagram. A clear hysteresis *P*-*E* loop obtained on polished 12% $\text{HfO}_2:\text{Y}$ crystals confirms that the bulk ferroelectricity and electron diffraction study unveils the non-centrosymmetric Pbc_{21} (*o*-FE) space group as the origin of FE polarization in 12% $\text{HfO}_2:\text{Y}$ single crystals. The existence of a

Pbca (*o*-AP) *o*-phase with an antipolar structure is also evidenced in 8%–11% $\text{HfO}_2:\text{Y}$ crystals. Interestingly, FE and antipolar *o*-phases only exist in as-grown crystals, which endure a relatively rapid cooling from the laser floating zone growth. Both *o*-structures remain stable at room temperature and can be transformed into a mixture of thermodynamically stabilized cubic and monoclinic phases after being annealed at $1600\text{ }^\circ\text{C}$ for days, as displayed in Figs. 6(a) and 6(b). The DFT calculation result implies that, instead of the lowest thermodynamic energy, the smallest energy barrier of the transition from cubic into *o*-FE structure plays a critical role in the stabilization of the ferroelectric *o*-phase, which explains why the formation of *o*-phases is preferred by rapid cooling.

Since the bulk single crystal gets rid of the influence of substrate materials, it provides great opportunities for investigating the intrinsic optical properties. In 2022, Fan *et al.* performed the Raman and infrared spectra on the $\text{HfO}_2:\text{Y}$ bulk single crystals in cubic and polar *o*-, antipolar *o*-, and *m*-phases.⁶¹ The experimental data are highly consistent with the theoretical calculations, which introduces the phonon mode analysis into the HfO_2 -based system. Moreover, some of HfO_2 polymorphs show significant structure similarity, adding difficulty in distinguishing them by conventional diffraction methods, but this work proves that the phonon spectra could work as a supplementary method in characterizing the polymorphs

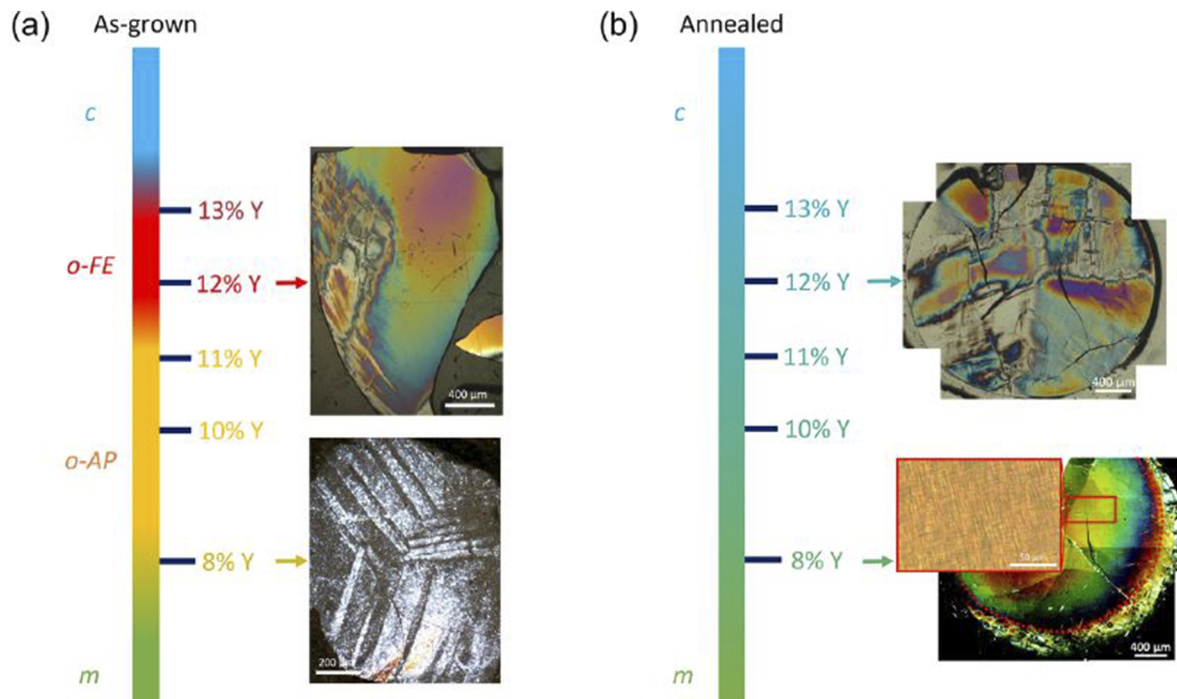


FIG. 6. The phase diagram of $\text{HfO}_2:\text{Y}$ bulk single crystals with different Y concentrations and thermal histories identifies four main phases, including the room temperature monoclinic (*m*) $\text{P}2_1/\text{c}$ phase, the high-temperature cubic (*c*) $\text{Fm}-3\text{m}$ phases, and the antipolar orthorhombic Pbca (*o*-AP) and the ferroelectric orthorhombic Pbc_{21} (*o*-FE) phases. The insets show the corresponding transmission polarized-light microscope images taken on polished cross-sectional disks of the crystal rods. (a) The as-grown (rapidly cooled) single crystals, and (b) the $1600\text{ }^\circ\text{C}$ annealed single crystals. As-grown 12% $\text{HfO}_2:\text{Y}$ belongs to the pure *o*-FE phase. The color contrasts, and fine features correspond to distinct crisscrosses of tweed domains at the outer part and a single orthorhombic domain at the center of the crystal boule. As-grown 8% $\text{HfO}_2:\text{Y}$ consists of the majority *o*-AP phase, showing large 120° -type twin features due to the presence of different choices of cell-doubling. The mixed phases contribute to the complex color contrasts and local features in crystals after annealing.

in HfO_2 -based materials by establishing a spectroscopic fingerprint for several different phases of HfO_2 .

D. Concluding remarks

The successful growth of $\text{HfO}_2:\text{Y}$ single crystals in kinetically stabilized α -phases also opens up various new experimental directions in the understanding of exotic ferroelectricity in this material. In 2020, Lee *et al.* proposed a localized polarization model in ferroelectric HfO_2 based on their calculations.²³ Therefore, experimental investigation of the possible flat phonon band is highly desired. The ferroelectric $\text{HfO}_2:\text{Y}$ single crystals with a typical mass around several grams make the inelastic neutron scattering study of the phonon dispersion achievable. Considering the reported ferroelectric $\text{Y}:\text{HfO}_2$ bulk crystal and thickness-independent ferroelectricity in $\text{Y}:\text{HfO}_2$ films,¹⁷⁵ a natural question would be why yttrium? Compared to other popular dopants in ferroelectric HfO_2 films, such as Si^{4+} and Al^{3+} , the radius of Y^{3+} is much closer to Hf^{4+} , which ensures good solubility in the bulk limit. That could be the reason why Y -doped ferroelectric HfO_2 samples tend to show minimized size dependence. On the other hand, this radius similarity may also bring a side effect, which is a

relatively smaller orthorhombic distortion magnitude in $\text{Y}:\text{HfO}_2$. Consequentially, the reported ferroelectric polarization of bulk $\text{Y}:\text{HfO}_2$ and 1 μm -thick $\text{Y}:\text{HfO}_2$ films is 6 and 15 $\mu\text{C}/\text{cm}^2$, respectively, which is smaller than the reported value in ferroelectric HfO_2 films with rare earth dopants having a larger radius, for example, 40 $\mu\text{C}/\text{cm}^2$ in $\text{La}:\text{HfO}_2$.¹⁷⁶ In the future investigation of size-independent ferroelectricity in HfO_2 -based materials, refinements of growth and annealing techniques and parameters to achieve a higher polarization in $\text{Y}:\text{HfO}_2$ are desired. Moreover, based on the discussion above, rare earth ions with a similar radius with Hf^{4+} , such as Ho^{3+} – Lu^{3+} , are also promising dopants in the stabilization of size-independence ferroelectricity in HfO_2 -based materials.

Last but not least, Yttrium-stabilized Zirconia (YSZ) is known to be a famous ionic conductor material due to the excellent yttrium mobility at high temperature, and it has been widely used as thermal barrier coating layer materials for gas turbine engines and the lining materials for high-temperature furnaces.¹⁷⁷ A similar study of the ionic conducting performance of bulk Yttrium-stabilized Hafnia (YSH) in the high-temperature regime may extend the industrial application of HfO_2 -based materials into new realms.

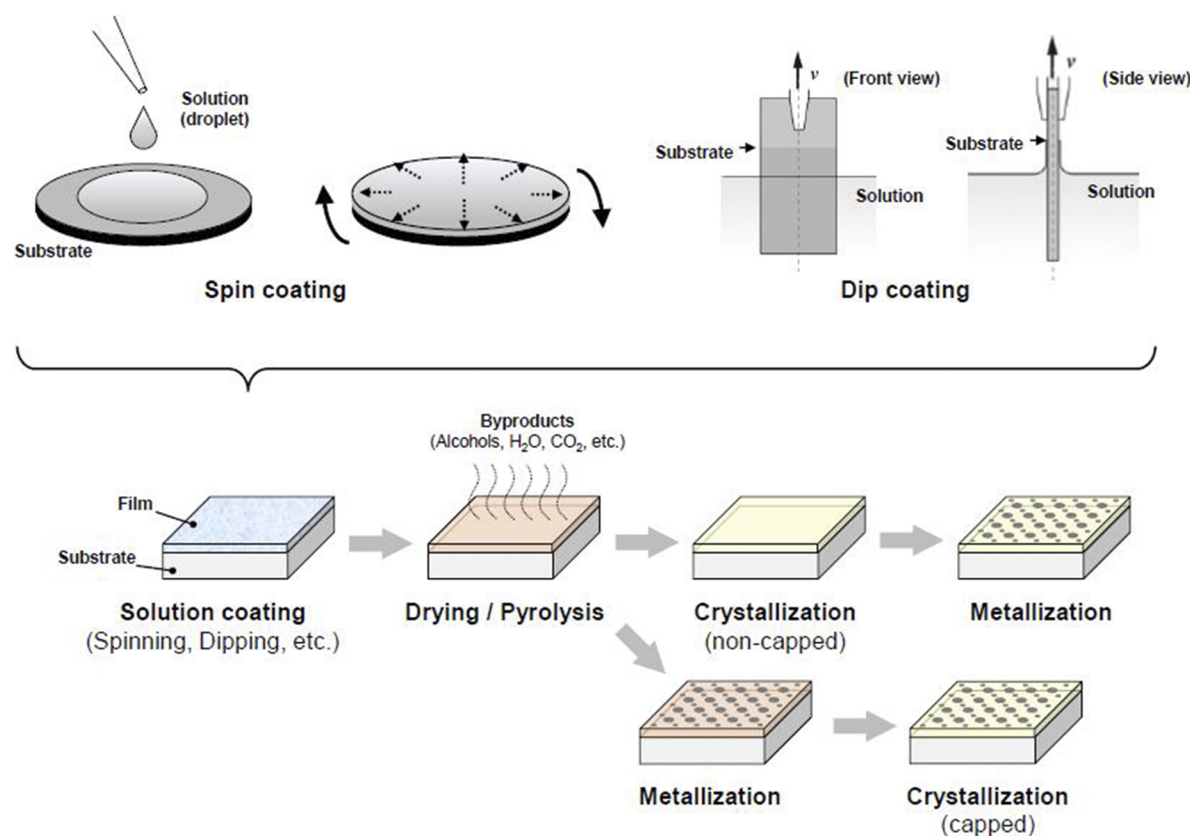


FIG. 7. Schematic image of chemical solution deposition. Process flows with non-capped (i.e., metallization after crystallization) and capped (i.e., metallization before crystallization) manners are shown, respectively.

E. Acknowledgments

This work was supported by the center for Quantum Materials Synthesis (cQMS), funded by the Gordon and Betty Moore Foundation's EPiQS initiative through Grant No. GBMF10104, and by Rutgers University.

V. THIN FILM GROWTH

A. Metal-organic chemical vapor deposition

Takahisa Shiraishi

1. Status

The crystalline phase-controlled HfO_2 - and ZrO_2 -based films are known to exhibit excellent ferroelectricity/antiferroelectricity even at a nanometer scale thickness and have been actively studied as potential candidates for applications to next-generation FE/AFE devices, such as FeRAMs, FeFETs, ferroelectric tunnel junctions (FTJs), and supercapacitors. Many research studies revealed that the origin of FE and AFE behaviors is several metastable phases with o -, t -, or r -symmetries. In addition, it was demonstrated that the stability of this crystalline phase strongly depends on the chemical compositions (doping concentration, ionic radius, valence state, and oxygen vacancy) and the structural characterizations (thickness, grain size, thermal and epitaxial strains, film/substrate interface, crystallographic orientation, and layered structure) of the films. Research has also been done to address several challenges in electrical properties, such as high E_c , low fatigue cycles, and weak P_r . Most efforts have been pursued on the materials side. On the other hand, given the continued miniaturization of FE/AFE devices and the current trend toward nanoscale electronics, it is necessary to develop deposition techniques that can adequately control the above factors affecting phase stability in the nanoscale film thickness range.

Metal-organic chemical vapor deposition (MOCVD) is still used today to produce high- k dielectric ultrathin films based on HfO_2 and ZrO_2 . This is due to the good controllability of film composition and film thickness. In addition, MOCVD is suitable for uniform deposition not only on large-area Si wafer but also on substrates with three-dimensional shapes, such as deep trench. This feature is very advantageous from the viewpoint of manufacturing next-generation FE/AFE devices. MOCVD is one of the effective approaches for designing HfO_2 - and ZrO_2 -based FEs/AFEs in the ultrathin region,^{178,179} but the understanding of the crystal growth science for realizing these films in MOCVD is still an open question. In addition, the deposition process must be thoroughly studied to exploit the advantage of MOCVD. This section focuses on techniques for controlling the structural properties of HfO_2 - and ZrO_2 -based FEs/AFEs via MOCVD, and some related research challenges are discussed below.

2. Current and future challenges

a. Epitaxial growth. Since the polarization axis differs for each metastable phase, it is critically important to control the crystallographic orientation of the HfO_2 - and ZrO_2 -based films in order to fully exhibit ferroelectricity and antiferroelectricity. In particular,

an epitaxial growth technique, so-called metal-organic vapor phase epitaxy (MOVPE), is preferred for developing a fundamental understanding of growth mechanism, phase stability, doping and strain effects, domain structure and its switching behavior, electrical properties, etc. However, a comprehensive understanding of the growth phase diagram and the process window for each metastable phase is lacking. In addition, the effects of organometallic precursors and deposition conditions on the crystal growth of HfO_2 - and ZrO_2 -based FEs/AFEs remain to be studied in detail. Moreover, lowering the thermal budget required for film formation is also an important challenge, enabling the reduction of thermal damage during device manufacturing. Therefore, an understanding of the epitaxial growth process is required at the fundamental level throughout detailed studies of precursor adsorption, diffusion on the underlying electrode layer, nucleation, and growth rate as a function of deposition conditions via theoretical and experimental approaches focusing on the metastable phase. Another key to achieving orientation control is the selection of an underlying electrode layer, which promotes the oriented growth of the metastable phase. For example, indium tin oxide and lanthanum strontium manganite have been paid attention as epitaxial electrode layers to support the formation of orthorhombic and rhombohedral phases, respectively. The deposition of these epilayers by MOVPE is an interesting topic for the simplification of manufacturing processes of FE/AFE capacitors.

b. Pulsed-MOCVD. Layered structures (e.g., bilayer, multi-layer, and superlattice) composed of HfO_2 - and ZrO_2 -based nanolayers are one of the unique approaches to improve dielectric, FE, and AFE properties, which can significantly enhance various device performances, such as endurance, fatigue recovery ability, and storage capacity. It is also possible to design the functions by combining multiple electrical characteristics. In the case of MOCVD, the layered structures can be achieved by introducing a pulsed deposition system. This system allows for alternate delivery of each precursor onto the substrate, and the cycle is repeated to form layered structures. At that time, it is necessary to precisely control the composition of each layer. Until now, $\text{HfO}_2/\text{ZrO}_2$, HfO_2 -based/ ZrO_2 -based, and FE-(Hf , Zr) O_2 /AFE-(Hf , Zr) O_2 have been studied. The next challenge of pulsed-MOCVD is multicomponentization, such as $\text{HfO}_2/\text{ZrO}_2/\text{CeO}_2$. The interesting topic is the control of constituent phases and electrical properties by utilizing the strain induced at the interface between layers. It is known that the piezoelectric response of superlattice structure is larger than that of the film form. Since there has not been much research aimed at piezoelectric applications of HfO_2 - and ZrO_2 -based ferroelectrics, the development of layered structures opens up new possibilities for these materials. However, an understanding of the synergistic effect of each layer on phase stability and electrical properties is not fully available. In addition, this effect is highly dependent on the layer thickness, which is controlled by the supply time of each precursor. Tuning of the layered structure as a function of pulsed deposition system parameters is, therefore, essential for elucidating synergistic effects through microstructural analyses focused on interface conditions, polarization states, and defects.

c. High step coverage. Three-dimensional capacitors based on deep trench structures are widely used in ferroelectric memory

devices. Adaptation of HfO_2 -based FE ultrathin films to this capacitor could make a breakthrough in the miniaturization of trench patterns and high aspect ratio. Polakowski *et al.* reported a P_r value per projected area of $152 \mu\text{C}/\text{cm}^2$ in $\text{TiN}/\text{Al}:\text{HfO}_2/\text{TiN}$ trench-type capacitors.¹⁸⁰ Recently, FinFET with HfO_2 -based FEs has also been paid attention to as a three-dimensional capacitor. In the case of the fin field-effect transistor (FinFET), it is required to uniformly cover the elongated fin patterns with an ultrathin film. So far, the three-dimensional capacitors with HfO_2 -based FEs have been achieved only by ALD. Although MOCVD has great potential as a manufacturing technique for such capacitors, several challenges remain to be addressed. One is the formation of metastable phases on the substrate with three-dimensional shape. This challenge requires an exploration of chemical composition to intrinsically improve the stability of the metastable phases. Another is the realization of high step coverage of the HfO_2 -based ultrathin films and top/bottom electrodes. Precise control of the deposition conditions (e.g., the supply rate of sources, deposition temperature, and pulse sequence) is required to uniformly cover the trenches and fins. Understanding the convection of source gas within the chamber via fluid analysis helps establish the process window. The future challenge is the deposition on the metal substrate with various shapes. Since metal substrates are excellent in workability, they are easy to apply to FE devices with a three-dimensional structure. It is also expected to develop into devices that take advantage of the flexibility of metal substrates.

3. Concluding remarks

MOCVD is an important deposition technique impacting the field of ever-developing HfO_2 - and ZrO_2 -based FEs/AFEs. This is because it yields unique results, such as excellent controllability of film thickness and chemical composition, design of the layered structure and electrical properties, and high step coverage. In particular, MOVPE helps us to better understand the effects of doping, film thickness, strain, and crystallographic orientation on phase stability, enabling full exploitation of ferroelectric/antiferroelectric properties. However, the current situation is that the use in this material field has not progressed yet. With a detailed understanding of the fundamental factors, such as deposition mechanism, growth phase diagram, process window, and pulsed system effect, MOCVD will give new avenues for next-generation FE/AFE devices equipped with HfO_2 - and ZrO_2 -based ultrathin films.

B. Chemical solution deposition

Hiroshi Uchida

1. Status

Solution-based techniques have been used for several years for manufacturing FE thin films because of their technical advantages in designing simple and versatile film-deposition processes. The term “chemical solution deposition (CSD)” includes some different types of solution-based processes for thin film deposition, such as sol-gel utilizing hydrolysis and polycondensation of metal alkoxides, metal-organic decomposition (MOD) using resources of

organic-acid salts, and other solution-based processes using various chemicals (β -diketonates, carbonylates, inorganic salts, etc.) as starting materials. These processes generally involve several simple steps, i.e., coating the precursor solution on a substrate, drying or pyrolyzing the solution to form a precursor gel film (amorphous), and annealing the gel film for crystallization. We argue that the process flow of CSD (Fig. 7) is compatible with chemical engineering and, thus, favorable for industrial mass production, such as a large-area film deposition on flat panel substrates.

The CSD process for FE thin films has been used for almost 40 years, mainly for perovskite-type ferroelectric materials, such as $\text{Pb}(\text{Zr}, \text{Ti})\text{O}_3$,^{181,182} BiFeO_3 ,^{183,184} and layered-perovskites.^{185,186} The research and development (R&D) of CSD-derived ferroelectric films has been diverse, i.e., for processing routes and material properties of film as well as for the circuit integration in miniaturized components (such as FE capacitors and FeFETs) and their circuit performances. The main targets of such research are non-volatile memory devices, piezoelectric sensors/actuators, and their advanced combinations, i.e., piezoMEMS, for commercial use. Due to this R&D, several FE devices have been commercialized and are available in our daily life. The research has also yielded commercial-grade equipment and precursor solutions for the CSD of perovskite-type FE materials.

Research on CSD-derived FE films has recently shifted to non-perovskite fluorite-type films since the finding of ferroelectricity in HfO_2 -based solid solution systems.^{60,166} The first report by Starschich *et al.*¹⁸⁷ on Y-doped HfO_2 films prepared by the hybrid-type CSD route presented the film’s ferroelectricity (with remanent polarization of $>13 \mu\text{C}/\text{cm}^2$) together with their “wake-up” behavior and piezoelectric response. This research was extended to doped HfO_2 with various dopant elements (e.g., lanthanides, transition metals, and alkaline metals), as well as solid solution systems, such as HZO ^{79,188,189} and $\text{HfO}_2:\text{CeO}_2$ (HCO).¹⁹⁰ The CSD process supports the research on HfO_2 -based FE films significantly because it is compatible with multi-component materials, enabling systematic survey on solid solution systems in the manner of combinatorial chemistry. The process mechanism of CSD has also been extensively investigated because solution-derived precursor films (amorphous) exhibit unique crystallization behavior to form the FE α -phase, which is somewhat different from the precursor films obtained from vapor deposition processes, such as ALD, pulsed laser deposition (PLD), and sputtering.^{79,188} CSD processes have been used to fabricate FE circuits, such as FeFETs or ferroelectric gate transistors (FGTs) in which FE HfO_2 -based films are used as gate insulators.^{191,192}

2. Current and future challenges

Combinatorial research on doped HfO_2 has involved a variety of dopant elements (Y^{3+} , La^{3+} , Nd^{3+} , Sm^{3+} , Er^{3+} , Yb^{3+} , Al^{3+} , Ga^{3+} , In^{3+} , Mg^{2+} , Sr^{2+} , Ba^{2+} , Co^{2+} , Ni^{2+} , and Ca^{2+} ¹⁹³⁻¹⁹⁶) to systematically organize the effect of dopant species on phase-formation behavior and FE properties. CSD be a good candidate as a combinatorial process based on chemical solution for material research on doped HfO_2 to survey the optimized composition of multi-component films in which the chemical composition of the resulting films can be easily controlled by regulating the species and concentrations of solutes in the precursor solution. Research on doped HfO_2 will be extended to “co-doped” systems that include two or more dopant species, such

as Y-doped HZO,¹⁹⁷ for addressing future challenges, i.e., stabilizing the FE HfO_2 phase, enhancing P_r or P_s , and controlling their wake-up (or fatigue) behavior.

The crystallization mechanism of CSD-derived HfO_2 films has been extensively investigated because they can be subjected to the effects of any process factor (e.g., residual stress caused by by-product removal and organic or carbon impurities included in the precursor gel films) compared with vapor deposition processes. For example, reports indicated that CSD-derived HfO_2 – ZrO_2 films tend to exhibit optimum composition with the ZrO_2 -rich region,^{79,188} which is somewhat different from HfO_2 : $\text{ZrO}_2 = 0.5$: 0.5 for ALD-derived films;¹⁶⁶ it can occur due to in-plane tensile stress generated by the pyrolysis or crystallization process. The mechanism of phase formation in CSD-derived HfO_2 – ZrO_2 films is also controlled due to the conditions of pyrolysis and crystallization (i.e., temperature, atmosphere, and pressure^{188,189,197}), which can be more significant than vapor deposition processes because of the presence of hydrocarbon impurities. In addition, systematic data for the crystallization mechanism of doped HfO_2 films are reported in recent works,^{193,196} which discussed the thermal decomposition behavior of the precursor solutions to form final products based on thermal analysis. Comprehensive approaches will be considered for solving the problems related to process factors, i.e., designing starting chemicals (alkoxides, β -diketonates, organic acid salts, etc.) and solvents that enable complete removal or by-products from the precursor films without residual stress.

The microfabrication process of FeFETs would be one issue of great importance for R&D of ferroelectric thin films. In the most recent studies, CSD is related to process flows of FeFETs in which the CSD-derived films of FEs Y-doped HZO¹⁹⁷ and HCO ¹⁹² and ITO were used as the ferroelectric gate and oxide channel layers, respectively. They exhibited on/off current ratios of 10^6 – 10^7 and memory windows with hysteresis loops of I_{DS} – V_{GS} curves. The HfO_2 -based FeFETs were also integrated with paraelectric capacitors to form ferroelectric-gate controlled variable capacitors (Fe–V cap). For advancement to FeFETs with high-density or large-scale integration, the degree of integration and reliability of gate operation will be critical issues for these applications, which can be achieved using the process mechanism of CSD as mentioned above.

3. Advances in science and engineering to meet these challenges

CSD will be used continuously for material research on HfO_2 -based FE films in the future, especially for combinatorial surveys on multicomponent systems, such as “co-doped HfO_2 ,” owing to its flexible tunability during chemical composition. Almost all metals of alkaline, alkaline-earth, transition, and lanthanoid will be commercially available for such research as starting chemicals of these elements have been delivered for commercial use. One critical issue with the survey research is the concept of material models, i.e., how to choose the species of dopant elements for the research targets (e.g., phase stability and polarization). Combination with any sophisticated approaches through theoretical calculation (such as a DFT calculation) or statistical analysis (such as a mechanical learning algorithm)^{35,36,55} will assist greatly in preparing material models.

In addition, to establish the position of CSD processes for commercial use, their essential problems related to by-products or

impurities must be overcome to maintain the reliability of circuit operation on fully integrated ferroelectric capacitors or FeFETs. The process design for the complete removal of organic species from precursor films (preferably before the crystallization step) without residual stress will be necessary, furthermore, for developing commercial-grade CSD processes. Although optimizing the process parameters for pyrolysis or crystallization is rightly an important approach for them, as clarified in previous research, other innovative actions, e.g., using designed chemicals (alkoxides or coordinate compounds with dissociable functional groups or ligands, etc.) and solvents (liquid media suitable for by-product extraction, including supercritical alcohol or CO_2 fluids¹⁹⁸) for preparing the precursor solution of CSD, are also expected strongly.

4. Concluding remarks

CSD has high compatibility with various situations of material synthesis, e.g., from lab-scale sample preparation for combinatorial surveys to the manufacturing process of FE components or devices for commercial use. It will be used differently compared with its technological counterparts, i.e., vapor deposition techniques, such as ALD, PLD, and sputtering, because it has unique advantages (tunability of chemical composition, large-area deposition, process simplicity, cost, etc.) and problems (impurity, residual stress, step coverage, etc.), which are obviously different from those of the vapor deposition. In particular, R&D for multi-component HfO_2 systems, such as co-doped HfO_2 ferroelectric films, is one important role of the CSD process because it extends to other fluorite systems, such as multicomponent ZrO_2 or CeO_2 systems, which will contribute greatly to clarifying the essential mechanism of ferroelectricity in fluorite systems.

C. Pulsed laser deposition

Florencio Sánchez and Ignasi Fina

1. Status

Research of FE HfO_2 pivots around CMOS-compatible polycrystalline films. Pulsed laser deposition (PLD) is scarcely used to grow doped HfO_2 polycrystalline films^{199,200} even though the FE phase can be obtained with a low thermal budget.²⁰¹ Commercial PLD setups allow for large-area deposition on several inches wafers, but PLD is not suitable for 3D integration and thus does not compete with ALD. Instead, PLD is well suited for growing epitaxial films, which can be model systems for a better understanding of properties and prototyping devices.

Epitaxial growth of FE HfO_2 by PLD is generally performed at a substrate temperature around 700–800 °C and an oxygen pressure around 0.01–0.1 mbar without an annealing process.^{20,27,202–205} PLD is characterized by a very high instantaneous supersaturation and extremely fast crystallization after each laser pulse. This reduces the probability of chemical segregation and formation of secondary phases compared to other techniques.

Yttria-stabilized zirconia (YSZ) fluorite single crystals were first used as a substrate for epitaxial stabilization of the α -phase, usually on indium-tin oxide (ITO) electrodes. The doped HfO_2 films replicate the orientation of the YSZ substrate, (001), (110),

or (111).^{202,206,207} Perovskite substrates, in particular SrTiO_3 (001) buffered with $\text{La}_{0.67}\text{Sr}_{0.33}\text{MnO}_3$ (LSMO) electrodes, are also used to grow doped HfO_2 (111) epitaxial films.^{20,27,203-210} The FE phase stabilized epitaxially on LSMO is claimed to be rhombohedral²⁷ or orthorhombic.^{20,203} In-plane and out-of-plane orientation can be modified by using other substrate orientations.^{67,211-213} Stress engineering allows for the control of the phase formed, and films on LSMO buffered scandate substrates are almost pure orthorhombic and have high P_r of around $25 \mu\text{C}/\text{cm}^2$.²¹⁴ Furthermore, HfO_2 films can be epitaxially integrated on $\text{Si}(001)$ using buffer layers.²¹⁵⁻²¹⁸ E_c of epitaxial films, unlike polycrystalline films, generally scales with thickness (t) according to the $E_c \propto t^{-2/3}$ dependence.^{20,204} PLD-grown epitaxial films rarely exhibit a wake-up effect, and some films present an endurance of up to 10^{11} cycles.^{20,219} Retention is generally very high, and the retention-endurance dilemma that polycrystalline films show is not present.²¹⁹

Polycrystalline or epitaxial doped HfO_2 films have also been grown at room temperature by PLD or sputtering, and the FE phase is formed by annealing.¹⁷⁵ Remarkably, polarization is high in films up to $1 \mu\text{m}$ thick, while polarization generally vanishes in other polycrystalline or epitaxial films thicker than a few tens of nanometers.¹⁷⁵ In this case, E_c does not show thickness dependence.

The PLD plasma under low pressure is extremely energetic and can degrade crystal growth. Deposition in a mixed atmosphere of Ar and O_2 has made it possible to decouple plasma energy and oxidation conditions, and a great improvement of the polarization is obtained in low oxidation conditions (Fig. 8).²²⁰ On the other hand, lattice strain seems to be less relevant than in conventional FEs. Free-standing epitaxial membranes have been obtained by chemical etching of the LSMO electrode.²²¹ After etching, strain relaxes, and the (111) out-of-plane spacing of the initial rhombohedral unit cell reduces, resulting in an o -unit cell. Membrane bending does not affect the polarization, consistent with measurements of polycrystalline HfO_2 -based membranes.

2. Current and future challenges

As mentioned, the polarization is improved in films grown by PLD under low oxidation conditions. However, the impact of the

expected oxygen vacancies on the microstructure and important properties, such as reliability and switching mechanisms, remains to be determined. On the other hand, the balance between thermodynamics and kinetics, critical in the synthesis of polycrystalline films,²²² is almost unexplored in PLD films, and only the variation of the deposition temperature has been explored.²⁰⁴ Very high polarization of about $50 \mu\text{C}/\text{cm}^2$ has been measured in epitaxial $\text{Y}:\text{HfO}_2$ (111) films on LSMO/STO(110),⁶⁷ which is much higher than $30-32 \mu\text{C}/\text{cm}^2$ expected for pure orthorhombic films (111) oriented. It has been argued²²³ that the measured polarization could contain extrinsic contributions related to oxygen migration as visualized by STEM characterization.¹⁴² On the other hand, epitaxial HZO (111) films on STO(110)²¹² or scandate²¹⁴ substrates or on STO(001) using low oxidation deposition conditions²²⁰ are almost free of parasitic phases, and its polarization is around $30 \mu\text{C}/\text{cm}^2$.

Lattice strain greatly affects the polarization of perovskite ferroelectrics, but its impact on the ferroelectric properties of HfO_2 is unclear. It is difficult to separate the effects of lattice strain from other factors, particularly the o -phase fraction. P_r of epitaxial films increases with the presence of the o -phase, which is controlled by varying the oxygen pressure during the growth, the thickness, or the substrate. In addition, P_r of epitaxial films on LSMO tends to increase with decreasing out-of-plane lattice parameters, which might indicate the presence of strain effects.²⁰ However, P_r does not change with bending in flexible epitaxial HfO_2 membranes,²²¹ although this latter result is not conclusive due to the limited explored strain range.

It is unknown why the o -phase is stable in films hundreds of nanometer thick, prepared at room temperature by PLD or sputtering and crystallized by annealing.¹⁷⁵ The contribution of surface energy is greater in films with small grains and non-columnar growth. Indeed, E_c of films prepared by solid-phase epitaxy or polycrystalline films prepared by other methods shows little thickness dependence,¹⁷⁵ while it decreases with thickness in epitaxial films prepared by conventional PLD.^{20,204} It is also suggested¹⁷⁵ that the use of Y or another rare earth as a dopant is essential, but the exact mechanism remains to be understood.

Wake-up in polycrystalline HfO_2 films is believed to be caused by redistribution of oxygen vacancies and/or t - to o -phase transformation. It is dependent on doping (atom and concentration), but there is a scattering of results for a particular composition. Wake-up in HfO_2 is not yet well understood, and epitaxial films could be a convenient model system to investigate it. However, epitaxial films prepared by PLD show little or no wake-up effect. It would be of interest to introduce oxygen vacancies or use alternative electrodes with the aim of generating wake-up to obtain information through the correlation with a well-controlled microstructure.

Fatigue is recurrently observed in epitaxial HfO_2 films, and minimizing it is a primary objective. In ferroelectric perovskites, the replacement of metallic electrodes by conducting oxides allowed for a large reduction of fatigue.²²⁴ HfO_2 -based full epitaxial oxide capacitors have not yet been investigated. On the other hand, (111) oriented $\text{Hf}_{0.5}\text{Zr}_{0.5}\text{O}_2$ epitaxial films show less fatigue²²⁵ and faster switching²²⁶ with the presence of a m -phase than almost pure o -films. It would be of interest to evaluate fatigue and other functional properties of epitaxial films that have other orientations, as well as monocrystalline films (without crystal variants).

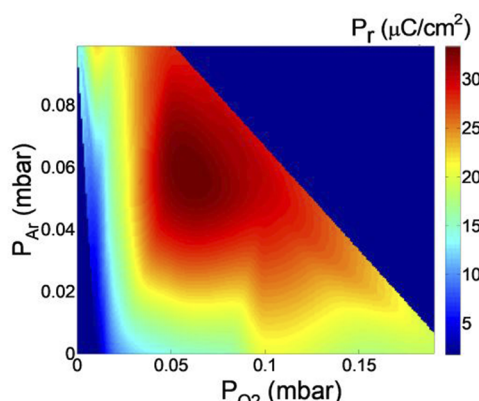


FIG. 8. Color map of P_r as a function of argon (P_{Ar}) and oxygen (P_{O_2}) pressure for $\text{Hf}_{0.5}\text{Zr}_{0.5}\text{O}_2$ (111) films deposited under a mixed Ar/O₂ atmosphere. Adapted from Ref. 220.

Ultra-thin layers are used in tunnel junctions and nanolaminates. The thickness must be ideally homogeneous and controlled with atomic precision. These requirements cannot be met with polycrystalline samples. Epitaxial films may be flatter, but control of thickness at the sub-unit cell scale and over large areas is not yet achieved. In addition, the sharper interfaces produced by epitaxial films can be advantageous to understand device response in ferroelectric capacitors or transistors.

3. Advances in science and engineering to meet these challenges

PLD chambers in clusters that include an x-ray photoelectron spectroscopy chamber for characterization without air exposure are available. These can be useful to analyze the formation and distribution of oxygen vacancies and redox processes occurring when a top electrode is deposited. On the other hand, the control of oxygen vacancies in a film prepared by PLD under mixed Ar/O₂ atmosphere²²⁰ can help us to determine the impact of vacancies on wake-up and fatigue. Epitaxial growth of LSMO or other conductive oxides, including ITO or other oxides with diverse functionality (ferroelectricity, ferromagnetism, etc.) on HfO₂, can also be of great interest to determine the possibility of improving endurance or investigating multifunctional properties in full epitaxial capacitors.

The growth rate directly affects the ratio between thermodynamics and kinetics, but its influence on *o*-phase stabilization in PLD-grown films has not been investigated. Furthermore, PLD growth is pulsed, and both the instantaneous (thickness/laser pulse) and average (thickness/second) growth rate can introduce kinetic limitations.

Strain effects on polarization are not observed in epitaxial HZO(111) membranes upon bending. Another membrane orientation, particularly (001), could perhaps be more sensitive to bending. On the other hand, stabilization of the *o*-phase in epitaxial HfO₂/LSMO bilayers on Pb(Mg, Nb)O₃–PbTiO₃ (PMN-PT) or other piezo-substrates would allow for active control of strain. PMN-PT, with a lattice parameter similar to that of some scandate substrates, is expected to be a suitable substrate. The impact of crystalline orientation determined by substrate orientation on functional properties beyond ferroelectric polarization should also help for the better understanding of properties. On the other hand, comprehensive electrical measurements could get insights into the possible coexistence of intrinsic polarization and extrinsic polarization related to oxygen migration.^{67,142}

Whether the robust ferroelectricity in films around 1 μm thick is caused by the dopant atom or by the particular microstructure of the films needs to be determined. Determining the thickness effects in HfO₂ films grown by conventional epitaxy and doped with Y and other rare earth elements would be relevant to discern whether the orthorhombic phase is, indeed, much more stable with a rare earth dopant. On the other hand, detailed microstructural characterization of a series of films with varied dependence of polarization with thickness could provide clues on the causes and suggest new growth strategies to achieve ferroelectricity in thick films prepared by other deposition techniques.

One virtue of FE HfO₂ is its robustness at the ultrathin limit, but precise control at such low thicknesses is difficult. PLD can be combined with reflection high-energy electron diffraction (RHEED) to monitor crystallinity, roughness, and formed phases and even

control the thickness with sub-unit cell accuracy in the case that epitaxial growth mode is layer-by-layer. Some HZO epitaxial films exhibit the streaky RHEED pattern.²²⁷ RHEED intensity oscillations, not yet reported, would allow for the unprecedented thickness control for ultrathin HfO₂ layers.

4. Concluding remarks

PLD has been demonstrated to be a highly effective technique for the epitaxial growth of ferroelectric HfO₂ with high homogeneity, flat surfaces, and interfaces and excellent functional properties (Fig. 9). Almost FE phase pure films can be obtained by epitaxial stress engineering or by deposition under a mixture of inert Ar and O₂ to induce oxygen vacancies. Wake-up is very low or null, and the endurance up to 10¹¹ cycles is limited by fatigue. Fatigue in full-oxide epitaxial capacitors remains to be investigated. Films hundreds of nanometers thick, grown at room temperature and crystallized by annealing, show high polarization.

The causes of this robustness are not determined. Strain effects on the polarization of HfO₂ are neither obvious nor discriminated from other factors. Advances in the fabrication of epitaxial membranes and stabilization of the ferroelectric phase on piezoelectric substrates could provide relevant information. RHEED-assisted PLD growth, rarely used to date for ferroelectric HfO₂, could be used to grow highly homogeneous epitaxial orthorhombic films with the precise control of thickness needed in tunnel junctions and nanolaminates.

5. Acknowledgments

Financial support from the Spanish Ministry of Science and Innovation (Grant No. 10.13039/501100011033), through the Severo Ochoa FUNFUTURE (Project No. CEX2019-000917-S funded by MCIN/AEI), Project No. TED2021-130453B-C21 funded by MCIN/AEI and European Union NextGenerationEU/PRTR, and Project Nos. PID2020-112548RB-I00 and PID2019-107727RB-I00 funded by MCIN/AEI, and from Generalitat de Catalunya (Grant No. 2021 SGR 00804) is acknowledged.

D. Atomic layer deposition

Min Hyuk Park, Taegyu Kwon, and Younghwan Lee

1. Status

The discovery of ferroelectricity in Si:HfO₂ has attracted massive interest from researchers and industries to solve the longstanding challenges in FE-based memory applications, such as the 130 nm size limit in technology nodes and poor complementary metal-oxide-semiconductor (CMOS) compatibility.²¹ With this discovery, 28 nm technology node FeFET,²²⁸ 22 nm technology node ferroelectric fully depleted silicon-on-insulator (FDSOI),²²⁹ and 64 kbit FeRAM were demonstrated.²³⁰ Such rapid advances in FE HfO₂ are based on ALD. Notably, more than 85% (up to 2019) of the total publications focused on ferroelectric HfO₂ are made by ALD.²³¹ ALD is a deposition technique that is based on sequential, surface chemisorption reactions between substrates, metal precursors, and reactants, as shown in Fig. 10(a).²³² Owing to its self-limiting nature and surface-saturated reaction, ALD provides numerous advantages,

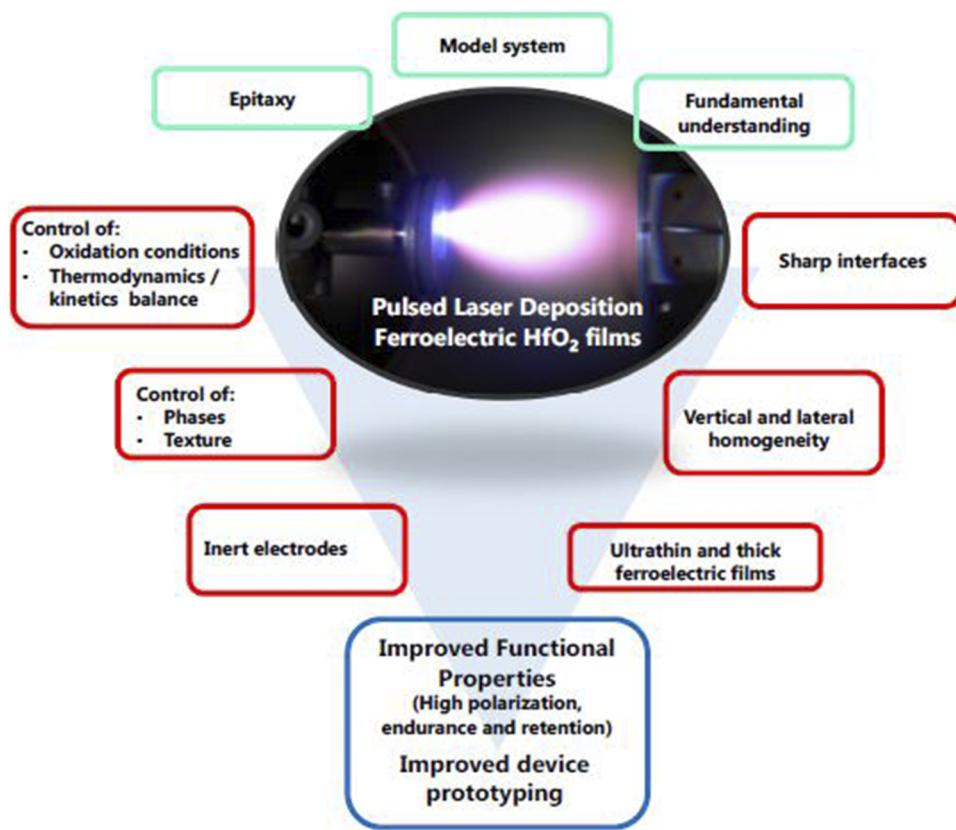


FIG. 9. Summary of current research and future challenges on the investigation of ferroelectric HfO_2 films grown by pulsed laser deposition.

such as precise control of the thickness of film within the atomic level, excellent film uniformity, conformality, step coverage, and process compatibility, which makes it useful in the semiconductor industry.²³³ Due to these advantages, ALD has been successfully implemented into the semiconductor industry mainly to deposit high- k materials (e.g., HfO_2) as a gate dielectric.²³⁴ Furthermore, to scale down the technology node to a few nanometers, depositing materials on a complex 3D structure, such as FinFET²³⁵ and gate-all-around (GAA) FET,²³⁶ homogeneously, uniformly, and conformally becomes even more important. Under such circumstances, appropriately employing the ALD in semiconductor processing is a viable option to meet the aforementioned requirements.

2. Current and future challenges

To be practically applicable, it is important for FE HfO_2 -based devices to have reliable and uniform properties. Hence, for good reliability of FE HfO_2 , properties such as less wake-up effect, high endurance, long retention, low leakage current, and high switching speed become important. It is known that the reliability of FE HfO_2 depends on the chemical, crystallographic-structural, and microstructural properties of HfO_2 (e.g., crystallographic phase, grain size, defect, and orientation), which are significantly affected by the ALD conditions. The uniformity in microstructural properties is even more important when the technology node reaches down

to an atomic scale. It should be noted that in a 5 nm-thick HfO_2 film, only ten unit cells of the HfO_2 crystal are stacked vertically. Thus, inhomogeneous film properties (e.g., high surface roughness and broad orientation distribution) throughout the surface would be a critical problem and lead to poor reliability.

The first challenge in ALD-deposited ferroelectric HfO_2 is to accurately control the chemical composition of the FE HfO_2 . In ALD, the doping concentration is controlled by the relative ratio between the injection cycles of Hf and dopant precursors. The frequently reported number of dopant injection cycles for 10 nm-thick doped HfO_2 (except in the case of Zr-doping) is less than 5, suggesting that the FE properties are strongly affected by minute changes in growth per cycle (GPC). Moreover, based on the physical scaling trends, sub-5 nm films will be required in the near future, which implies that accurate composition control will become more challenging. The unintended doping effect arising from residual impurities or oxygen vacancies is another critical issue.^{238,239} It should be noted that the majority of the ALD-deposited FE HfO_2 employs organometallic precursors in which the metallic Hf is bonded with an organic ligand. The incomplete reaction during ALD is known to increase residual impurities (such as C, N, and H concentration). The residual impurities can act as trap sites in the electrical bandgap or pinning sites for DWs, which could deteriorate device performance.

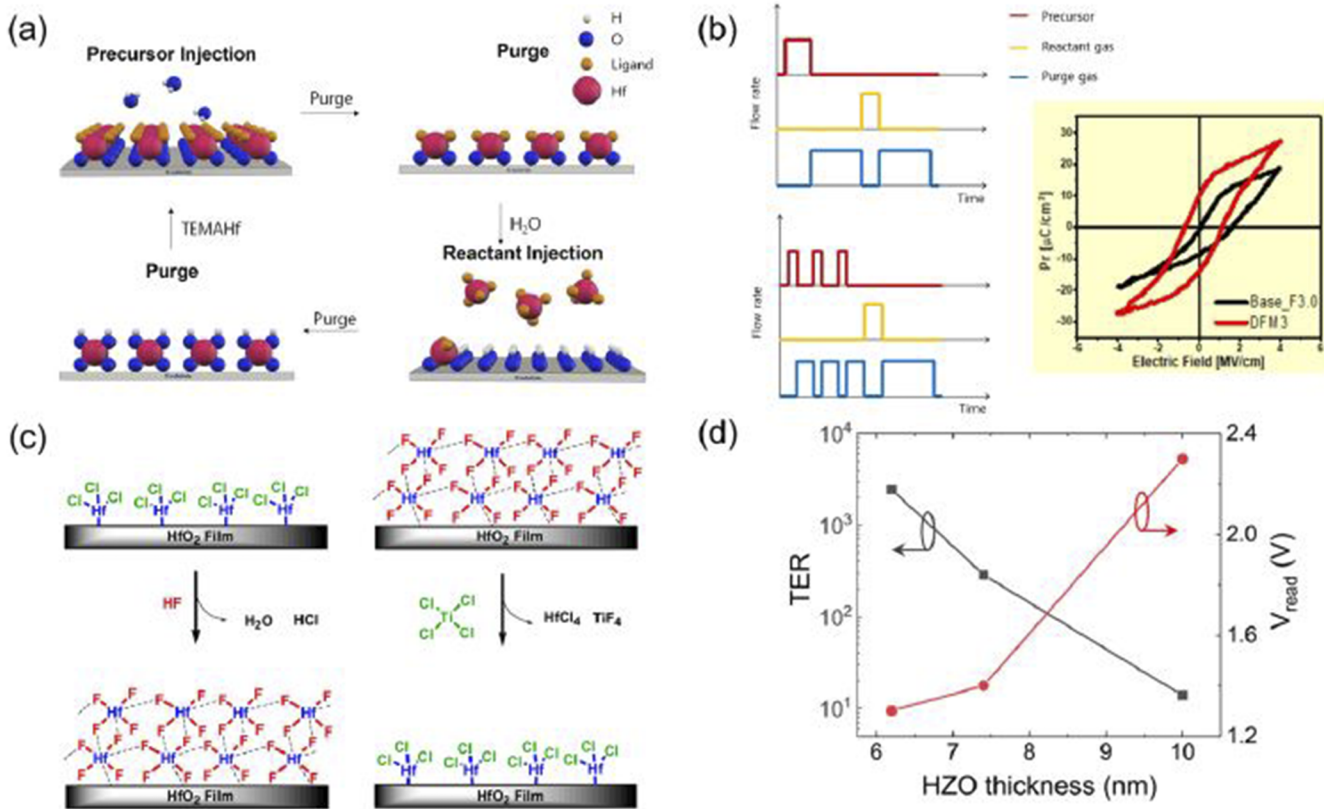


FIG. 10. (a) A general scheme of the atomic layer deposition (ALD) process for HfO₂ using HfN(CH₃)₂C₂H₅)₄ (TEMAHf) as the Hf precursor and H₂O as the reactant. Ligand refers to N(CH₃)C₂H₅. (b) Comparison of the conventional ALD process and discrete feeding (DF)-ALD process scheme (left) and the polarization-electric field hysteresis (right) of a 6 nm thick Hf_{0.5}Zr_{0.5}O₂ film sandwiched by TiN top and bottom electrodes, where the Hf_{0.5}Zr_{0.5}O₂ films were deposited using conventional ALD (black curve) and DF-ALD (red curve). The hysteresis curve is reproduced with permission from H. H. Kim, “Enhanced electrical characteristics of Hf_{1-x}Zr_xO₂ film utilizing discrete feeding method,” M.S. thesis, ■■■, 2020. Copyright 2020 Author(s), licensed under a Creative Commons Attribution 4.0 License. (c) A process scheme of atomic layer etching consisting of fluorination (left) and ligand exchange (right) steps. Reproduced with permission from Y. Lee and S. M. George, J. Vac. Sci. Technol. A **36**, 061504 (2018). Copyright 2022 American Vacuum Society.²³⁷ (d) Giant tunneling electroresistance and lowered read voltage are observed for the atomic layer etched Hf_{0.5}Zr_{0.5}O₂ film with 6.2 nm thickness. Reproduced with permission from Hoffmann *et al.*, Appl. Phys. Lett. **120**, 122901 (2022). Copyright 2022 American Institute of Physics.

30 August 2023 14:15:40

The second challenge is to deposit a uniform film with a homogeneous orientation distribution to minimize the device-to-device variation in integrated circuits with FE memories and to improve compatibility with back-end-of-line (BEOL) processes. For the case of 1T-1C FeRAM, one solution is a strategic choice of bottom electrode considering lattice mismatch. For the case of FeFETs where FE HfO₂ is directly grown on a Si substrate, there seems to be no clear solution. Although the report on ferroelectric HfO₂ with a preferred orientation thinner than 2 nm can be important progress,⁶⁹ there is no clear solution for physically scaling up its preferred orientation to the practical thickness range (~10 nm) with a suppressed leakage current. Achieving uniformity and homogeneous orientation distribution will become more difficult when FE HfO₂ films are adopted for more complicated 3D nanostructures, such as gate insulators of FinFETs or GAA FETs, 3D capacitors in FeRAMs, and 3D vertical FeFET arrays for post-NAND. Furthermore, it is not certain whether the preliminary results of the Si substrate can be applicable to poly-Si channels. Additionally, to be compatible with the BEOL

processes, the entire process, including thermal treatment, should be conducted at a temperature lower than 400 °C. Although there have been reports on FE HfO₂-ZrO₂ films crystallized at <400 °C,²⁴⁰⁻²⁴² given that the crystallization temperature generally increases with a decrease in film thickness, inducing ferroelectricity in the as-deposited film without subsequent annealing at sub-5 nm thickness regime is a promising strategy for the BEOL processes compatibility.

The third challenge is to achieve high-quality interfaces at electrodes or semiconductors because the performances of the nanoscale electronic devices are critically affected by the quality of the interfaces. In particular, in ALD-deposited FE HfO₂, an oxygen source is required to oxidize the metal precursors by removing organic ligands. The oxygen sources, such as O₃, O₂ plasma, H₂O, and H₂O₂, have been utilized for the ALD of FE HfO₂.²⁴³ These can cause chemical changes in FE HfO₂ as well as the bottom materials. For FeFETs, the interfacial or bulk traps formed at the gate stack interface have been a critical factor that limits the endurance of the device.²⁴⁴ Although inserting a high-*k* interfacial layer, such

as SiO_2 ,²⁴⁵ SiO_xN_y ,^{246,247} Al_2O_3 ,²⁴⁸ and TiO_2 ,²⁴⁹ has been suggested as a promising solution to improve the endurance of the device, adding another interfacial layer would increase the operating voltage of the devices, which is undesirable from the viewpoint of power consumption.

3. Advances in science and engineering to meet these challenges

Reducing the device size is a significant goal for the nanoelectronics industry; therefore, the production of metal oxide films with dimensions below the sub-nanometer scale is important. Recent research on sub-nanometer HfO_2 -based FEs by Cheema *et al.* in 2022 supports the importance of reducing the device size.⁶⁸ This reduction can be achieved by the newly designed ALD processes explained below. It has been reported that discrete feeding ALD (DF-ALD), which is the repetition of the precursor half-cycle procedure before the reactant half-cycle, could increase the surface coverage and lower the surface roughness by promoting monolayer-by-monolayer growth.²⁵⁰ The schemes of the conventional ALD (left top panel) and DF-ALD (left bottom panel) are compared in Fig. 10(b). Similar to replacing the second precursor half-cycle, the DF-ALD cycle from a Hf/Zr precursor to the dopant precursor enables a homogeneous distribution of a dopant across the film.^{251,252} Kim reported that adopting DF-ALD could effectively increase P_r , especially for the cases of ultra-thin films under a low thermal budget and the polarization-electric field curves of $\text{TiN}/\text{Hf}_{0.5}\text{Zr}_{0.5}\text{O}_2/\text{TiN}$ capacitors, where the $\text{Hf}_{0.5}\text{Zr}_{0.5}\text{O}_2$ films were grown using conventional ALD (black curve) and DF-ALD (red curve), are shown in the right panel of Fig. 10(b).²⁵³

Atomic layer etching (ALE) would be a potential solution to resolve the issue with the crystallization of ultra-thin HfO_2 -based ferroelectric films. A scheme of ALE of the HfO_2 film is shown in Fig. 10(c). First, a HfO_2 -based thin film can be deposited to a depth suitable for low-temperature crystallization (thickness of ~ 5 – 10 nm). Subsequently, the film can undergo atomic layer etching with accurate and uniform thickness control, which may lead to the formation of ultra-thin crystallized films with smoother surfaces. Hoffmann *et al.* reported that the device performance of FTJ with a $\text{Hf}_{0.5}\text{Zr}_{0.5}\text{O}_2$ ultra-thin film could be enhanced by adopting ALE.²⁵⁴ Figure 10(d) shows the changes in the tunneling electro-resistance ratio (TER) of the FTJ and read voltage (V_{read}) of their FTJ with varying thicknesses of the $\text{Hf}_{0.5}\text{Zr}_{0.5}\text{O}_2$ thin film. Area-selective ALD (AS-ALD) is another emerging technology that enables nanoscale patterning with reduced chemical or physical damage compared to that from a conventional dry etching process. This procedure was demonstrated for a dielectric HfO_2 film by Tao *et al.* in 2010. With regard to the improvements in 3D memory technology, such as 3D NAND, adopting the ALE and AS-ALD approaches for ferroelectric memory technology would be vital for progress in this field.

Finally, engineering the ALD process can also provide viable methods to control the interfacial properties of thin films. The recently suggested $\text{HfO}_2/\text{ZrO}_2$ nanolaminate would be an effective way to improve the electrode/ferroelectric or semiconductor/ferroelectric interfaces.^{255,256} Plasma pre-treatment of the bottom electrode or the substrate is a promising method to engineer the lower interface because the initial growth stage after ALD is strongly affected by the concentration of reactive surface functional groups, such as $-\text{OH}$.²⁵⁷ Furthermore, the fabrication of the entire MFM

stack without breaking the vacuum in a single ALD chamber, known as sequential, no-atmosphere processing (SNAP), would provide a chemically sharp interface.^{258,259} These advances can be effective solutions to achieve reliability in thin film production without inserting additional high- k interlayers.

4. Concluding remarks

The well-established ALD of HfO_2 has enabled rapid advances in HfO_2 -based ferroelectrics, and it is known that the chemical and structural properties of FE HfO_2 films are critically affected by the ALD conditions. There are several technical challenges, such as (1) accurate control of chemical composition, (2) deposition of uniform and adequately textured films with BEOL-compatible processes, and (3) high-quality interfaces at electrodes or semiconductors. Although these challenges persist even in the ~ 10 nm thickness regime, they will be more difficult due to the current trend of physical scaling-down and applications in 3D nanostructures. Thus, extensive research and development to resolve these issues are required to develop practical semiconductor devices based on ferroelectric HfO_2 . Development of new metal precursors; emerging ALD techniques, such as discrete feeding DF-ALD, SNAP ALD, and AS-ALD; and various wet/dry surface treatment techniques²⁶⁰ could be exemplary approaches.

5. Acknowledgments

This work was supported by the National Research Foundation (NRF) funded by the Korean Ministry of Science and ICT (Grant Nos. 2022M3F3A2A01073562, 2020R1C1C1008193, and 2021M3F3A2A02037889). We would like to thank Editage (www.editage.co.kr) for editing and reviewing this manuscript for English language.

E. Sputtering

Bertrand Vilquin

1. Status

A sputtering deposition is a physical vapor deposition generally carried out in a low-pressure atmosphere (pressure lower than 0.1 mbar). A cathode sputtering setup is at least a secondary vacuum chamber with a target (material to be deposited) and a substrate holder. Gas flow detectors and DC or RF generators are needed to create and control the electrical discharge of a plasma. The deposit may relate to metals or ceramics. The principle of cathode sputtering consists in generating a plasma formed mainly of high-energy ions (often ionic argon), which will sputter the target and eject atoms from it. The atoms and ions created will then be deposited on the substrate, which can be heated or not. The sputtering process will allow for controlling of the film quality by playing on the target nature (metallic, ceramic), plasma pressure and composition (reactive sputtering), and DC/RF power applied to the target.

In comparison to ALD grown FE HfO_2 , few reports on the sputtering-grown samples have been undertaken so far. Various elements can be used as dopants by sputtering to lead to ferroelectricity in HfO_2 films: Sc, Y, Nb, Al, Si, Ge, and Zr dopants.²⁶¹ We can note

that the thicker FE HfO_2 film (up to 1 μm thick) was obtained by sputtering the Y doped HfO_2 target.²⁶² Moreover, sputtering of pure HfO_2 at different target powers leads to the FE *o*-phase after appropriate annealing.²⁶³ Identically, using ion beam sputter deposition, ferroelectricity can be obtained in pure ZrO_2 with the *r*-phase^{264,265} or *o*-phase.²⁶⁶

In this present review article, we focus on the zirconium doping of HfO_2 . The sputter process shows several contributions compared to ALD, such as room temperature deposition, very low carbon contamination, non-equilibrium deposition, cost, possibility of growing the entire MFM stack inside the same system in one run, and avoiding surface and interface air contamination. In comparison to ALD, it seems that it is possible to easily get the FE *o*-phase at lower dopant concentrations.¹⁷⁰ The authors claimed that the species intermixing is improved by sputtering. For all the publications, deposition by sputtering is performed at room temperature on TiN-buffered silicon and followed by a post-deposition annealing. Room temperature deposition enabled growth on different substrates, such as 2D semiconductor MoS_2 .²⁶⁷ For the majority of articles on sputtering deposition, the post-deposition annealing temperature in order to obtain the *o*-phase is often higher than with ALD in the range 600–900 $^\circ\text{C}$.¹⁷⁰ Several explanations can be proposed: less presence of adjuvants such as carbon in order to decrease the crystallization temperature and room temperature deposition leading to a more amorphous state when the ALD process is performed around 250–300 $^\circ\text{C}$. Bouaziz *et al.*, however, were able to decrease the thermal budget to 450 $^\circ\text{C}$ with P_r rising 20 $\mu\text{C}/\text{cm}^2$ after wake-up cycles.^{11,268} Hachemi *et al.* also found an *o*-phase crystallization temperature of about 370 $^\circ\text{C}$, but the annealing was not performed in a rapid thermal annealing system but *in situ* with very low heating and cooling rates.²⁶⁹

2. Current and future challenges

Different sputter chamber configurations are used: metallic Hf/Zr single target for reactive sputtering,²⁷⁰ ceramic HZO single target,^{268,269} and co-sputtering from HfO_2 and ZrO_2 single targets, which is the most used setup.²⁷¹ Indeed, co-sputtering enables the control of more parameters, especially the zirconium dopant concentration, by tuning the ZrO_2 target power.^{263,272–274} Ferroelectricity is then found for Zr doping concentration from 0% to 50%. Single target sputtering does not allow for film composition modulation: one target for one film composition. The Zr and Hf deposition rate is target aging dependent, with the possible evolution of the Zr/Hf ratio deposition after deposition, leading to a sputtering repeatability problem. In addition, the use of the metallic Hf/Zr single target only leads to FE films with low P_r : 6 $\mu\text{C}/\text{cm}^2$ after wake-up cycling.^{14,270} This low value can be explained by the difficulty in very well controlling the film stoichiometry by reactive sputtering. On the contrary, in the case of ceramic HZO single target sputtering, sputtered and nanostructured films can reach, at a low thermal budget of 450 $^\circ\text{C}$, a remanent polarization of 20 $\mu\text{C}/\text{cm}^2$, an endurance to 1×10^7 cycles, a reducing wake-up effect, and a long-term retention.^{268,275}

Sputtering enables to perfectly control as well as engineer the interface between the ferroelectric HZO film and its electrodes by introducing a very thin metallic layer,^{276,277} leading to an increase of P_r at the lowest thickness of 6 nm by tuning the oxygen vacancies in the film.

The first important parameter to control the growth of FE HZO films is the deposition plasma pressure. Bouaziz *et al.* demonstrated the strong impact of the working pressure on the film's structural and physical properties.²⁷⁸ Indeed, the deposition pressure will modify the mean free path and scattering of sputtered species. Low-pressure deposition (5×10^{-3} mbar) led to the formation of an as-deposited *m*-phase. After post-deposition annealing, the *m*-phase proportion increased without the formation of *o*-phase whatever the annealing temperature between 400 and 600 $^\circ\text{C}$ (Fig. 11). For the as-deposited film grown at high pressure (5×10^{-2} mbar), the film is then amorphous. After annealing, the film transformed into *m*- and *o*-phases with polarization loops (Fig. 12). The microstructure, such as grains size and crystallinity, and the chemical composition in the sputtered films may be modified by the deposition pressure. Small grains induced more likely the formation of the *o*-phase.

Lee *et al.* also observed that tuning the deposition pressure can enhance the sputtered film properties.²⁷¹

The second parameter that can modify the properties of the sputtered FE HZO films is the partial oxygen pressure during the deposition. Oxygen pressure can also have a huge effect on the grains size, the deposition rate, and the film density because of the re-sputtering effect, which is more common during reactive

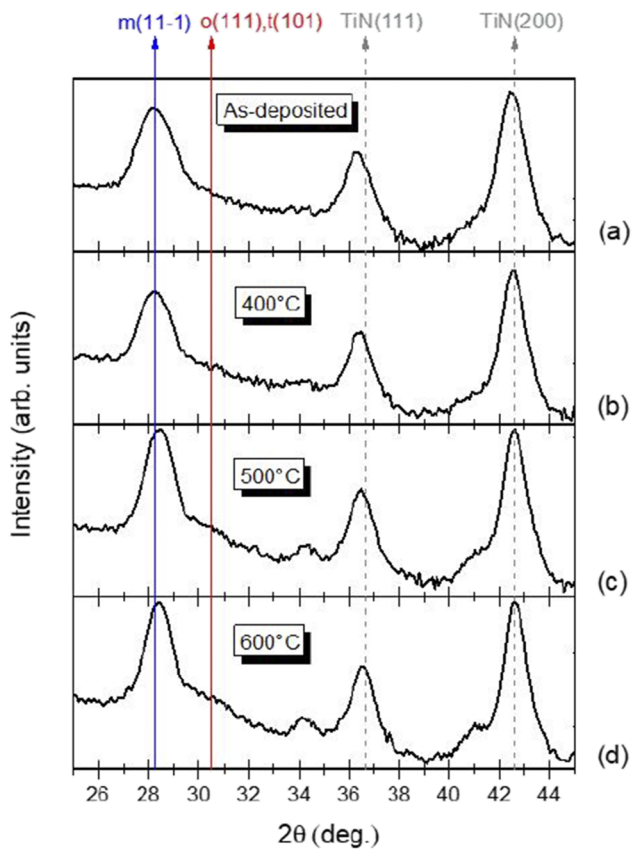


FIG. 11. (a)–(d) GIXRD of low-pressure samples grown at 5×10^{-3} mbar: as-deposited and annealed at different temperatures. Adapted from Ref. 278.

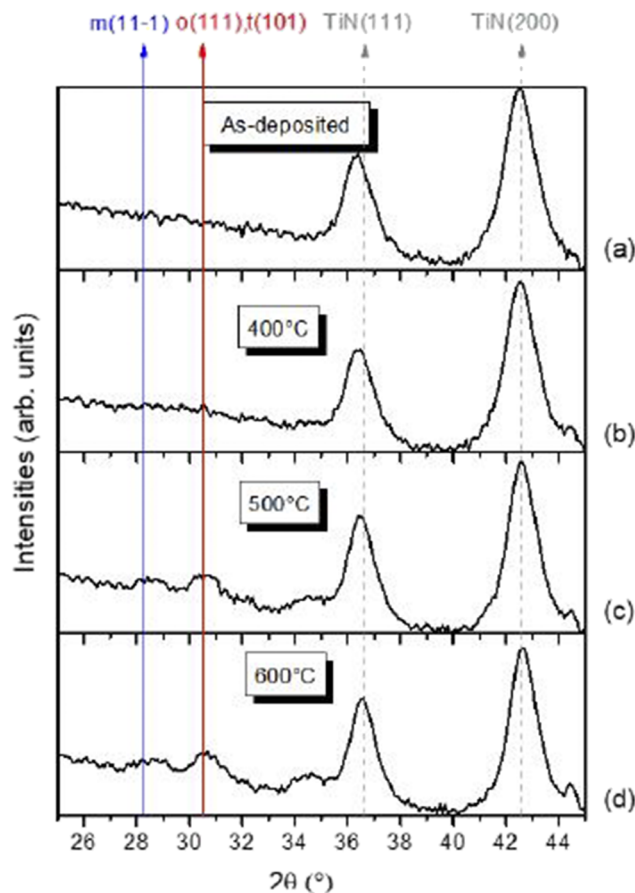


FIG. 12. (a)–(d) GIXRD of high-pressure samples grown at 5×10^{-2} mbar: as-deposited and annealed at different temperatures. Adapted from Ref. 278.

sputtering.²⁷¹ Lee *et al.* then observed a variation of the monoclinic/orthorhombic intensity ratio on their Glancing angle x-ray diffraction (GIXRD) patterns correlated with the ferroelectric properties: increasing the oxygen partial pressure led to forming more *m*-phases and decreasing P_r of the HZO film. In fact, the most favorable condition in order to optimize ferroelectricity is to sputter under pure argon, allowing for the presence of oxygen vacancies in the film.²⁷⁴

Finally, the third parameter to tune is the single HZO target applied power, which has an influence on the deposition rate but not the Hf/Zr ratio inside the film.²⁶⁹ Since the power may modify the film microstructure (strain, grain size, etc.), it will change the *o*-/*m*-phase volume ratio:²⁶³ low power favored the *m*-phase when higher pressure leads to an increase in the fraction of the *o*-phase.

The current goal is also for the ALD polycrystalline ferroelectric HfO₂ films to fix the problems of wake-up and switching endurance. One available solution will be to dope HfO₂–ZrO₂ with La, as already shown with ALD.²⁷⁹ Nevertheless, growing multi-cationic films by sputtering will need hard and complex deposition control. Another main current challenge is to produce epitaxial FEs as it is already performed by PLD, as shown in Sec. V C 1. This will require

heating the monocrystalline substrate during the deposition in order to promote the epitaxial growth.

One major future challenge is that, to date, no realization by sputtering of 1T–1C and 1T FeFET prototypes was presented in the literature, but one can note that the first articles of sputtered ferroelectric HZO films were published several years after ALD ones, and very few groups use until now this deposition process in comparison of ALD.

3. Concluding remarks

Sputtering allows us to fabricate state-of-the-art polycrystalline FE HZO films on a silicon substrate (large scale, high polarization values, composition homogeneity, low roughness surfaces, and abrupt interfaces with electrodes, interface engineering) similar to those elaborated by ALD. In addition, this room temperature growth process is CMOS compatible with a low thermal budget and allows us to control the film composition, including oxygen vacancies and device microstructuration. However, as it is impossible to realize 3D conformal depositions, advanced industrial applications, such as FinFET, will be limited.

F. Molecular beam epitaxy

Athanasis Dimoulas

1. Status

Molecular Beam Epitaxy (MBE) in ultra-high vacuum (UHV) relies on molecular flow, so it offers the possibility for thin film growth far from equilibrium, thus enabling the crystalline growth of metastable phases, which are difficult to obtain by equilibrium crystal growth (bulk or other) methodologies. As a UHV method, MBE offers excellent contamination control and *in situ* surface preparation of crystalline substrates, which enables the epitaxial growth of chemically pure thin films. Due to UHV conditions, several surface characterization techniques, such as RHEED/LEED, STM, and XPS, can be used to *in situ* monitor, in real-time, the interface and thin film surface ordering, the possible reaction at the interfaces, the stoichiometry, and the thickness with atomic precision. Being essentially a PVD methodology, MBE does not require cumbersome and time-consuming precursor development, so it stands out as a flexible technique for fast screening and exploration of new materials, including FE HfO₂.

A typical oxide MBE system consists of a UHV chamber suitable for FE HfO₂ growth, which is equipped with e-gun evaporators necessary for the co-evaporation of refractory Hf and Zr metals (Fig. 13). An important component of the growth system is a remote RF plasma source, which takes O₂ gas as input and, by creating a plasma, produces neutral atomic oxygen beam. The latter is reactive enough to oxidize Hf and Zr on the substrate at low temperature and under conditions of low partial pressure $PO_2 \sim 10^{-5}$ Torr, compatible with UHV. The RF source can also produce an atomic N beam; therefore, it is possible to grow the oxides HZO and nitrides (TiN) in sequence without breaking the vacuum. This is particularly important since TiN is considered to be the optimal top gate electrode, so the full device layer structure can be produced in one growth step.

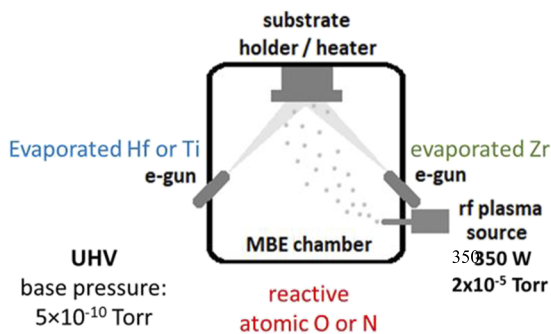


FIG. 13. Typical oxide MBE chamber used for the growth of HZO and HZO/TiN stacks.

MBE can be used, in principle, with any substrate or template. However, MBE is particularly suitable for the growth on technologically important single crystalline semiconductor substrates (Si, Ge, and GaAs) to take advantage of established *in situ* cleaning methodologies by thermal desorption of native or chemical oxides, assisted, when necessary, by ion Ar⁺ sputtering. Other crystalline metallic or semiconducting oxides (e.g., LSMO and NSTO) can be used as substrates for MBE growth. Oxide MBE is particularly suitable for the epitaxial growth of epitaxial n-STO on Si(001), which can be subsequently used for the HZO overgrowth.

While oxide molecular beam epitaxy has been extensively used for the growth of perovskite oxides, it has been rarely employed for the growth of FE HfO₂-based oxides. The main reason is that the thermodynamic/kinetic path of FE HfO₂ formation requires deposition at low temperatures in the amorphous state first, followed by annealing for the crystallization of the material in the desired orthorhombic polar phase. Therefore, most of the works are limited so far to the growth of amorphous HZO at relatively low temperature (~120 °C) by plasma-assisted molecular beam deposition (PA-MBD), rather than epitaxy.

2. Current and future challenges

PA-MBD has been employed for the growth of HZO on Ge substrates,^{280–282} which produces oxide-free interfaces. Germanates formed at the interface during deposition of HZO on Ge are unstable, and they dissociate, yielding sharp, clean interfaces as evidenced by HRTEM.²⁸⁰ PA-MBD HZO leads to thin films down to 3 nm, with exceptional thickness uniformity over the entire cm-scale wafer. HZO Ge metal–ferroelectric–semiconductor (MFS) devices made by PA-MBD^{281,282} exhibit robust hysteresis loops with high remanent polarization P_r up to 30 $\mu\text{C}/\text{cm}^2$ ^{10,280} in the pristine state with no need for wake-up when HZO is thicker than 10 nm.²⁸² However, as HZO thickness scales down, the pristine P – V loops appear to be constricted (or pinched), showing an AFE-like behavior with much reduced P_r .²⁸³

This behavior is interpreted as the effect of an enhanced depolarization field, which results in metastable ferroelectricity co-existing with a stable paraelectric phase.²⁸³ The ferroelectricity recovers with full hysteresis loops by field cycling (wake-up) attributed to the filling of pre-existing interface defect traps via charge injection from the metal electrodes.²⁸³ The woken-up metal–ferroelectric–semiconductor (MFS) devices maintain high P_r

($>20 \mu\text{C}/\text{cm}^2$) down to 5 nm HZO, which makes PA-MBD HZO useful for low voltage/low power applications.²⁸³ PA-MBD HZO presents a pure *o*-FE phase with no evidence of a monoclinic phase based on XRD and HRTEM observations. This could explain the high values of P_r obtained in MBD HZO. In addition, the use of reactive atomic oxygen and nitrogen in MBD results in efficient oxidation and nitridation, thus minimizing the oxygen vacancies at the interface, which could explain the very small imprint (Fig. 14) and very good reliability observed in TiN/HZO/Ge MFS capacitors.²⁸² While MBD has been successfully applied for the realization of HZO Ge FMS capacitors with robust FE hysteresis, the performance of Ge FTJ and FeFET memory devices is not as expected. The root cause of underperformance in Ge FeFETs²⁸⁴ is thought to be a large density of dangling bond acceptor states at the interface, which are present despite the fact that HZO/Ge is a sharp, crystalline interface. These defects strongly pin the Fermi level near the valence band, and when filled by electrons, they exert excess scattering on mobile charges in the channel. As a result, Ge *p*-channel FeFETs fabricated by MBD show a degradation of the transfer characteristics (I_d – V_g) upon programming of the ferroelectric gate, suffering from an increased subthreshold slope and reduced ON-current, which also limits the memory window to about 0.3 V.²⁸⁴ Proper passivation of the electrically active interfacial defects is necessary to improve the transistor characteristics. Since hydrogen passivation is ineffective in Ge, other methodologies, such as S passivation by immersion in sulfur-based solution, should be considered. The best passivating layer could be an ultrathin GeO₂ (<1 nm), which can be formed after thin HZO deposition by oxygen plasma post-oxidation of Ge, a methodology that is fully compatible with PA-MBD. A similar method has already been successfully applied for the passivation of Al₂O₃ high- k gate stacks on Ge for advanced CMOS.²⁸⁵

3. Advances in science and engineering to meet these challenges

While PA-MBD has already proved its strengths for the growth of FE HZO on Ge substrates, using this technique only as a deposition method of amorphous HZO does not exploit its full capacity as plasma-assisted molecular beam epitaxy (PA-MBE). The real value of the latter method is for the epitaxial growth of HZO on any substrate and, in particular, on semiconductor substrates. There are several reports of epitaxial growth by other PVD-based techniques or by PLD, which are discussed in recent review articles^{154,286,287} as well as in other sections of the present Roadmap. To the best of our knowledge, there is no report on the epitaxy of FE HfO₂ by PA-MBE. Following the successful epitaxial growth by PLD²⁷ of *r*-FE HZO on LSMO and the recent epitaxial growth of Y:HfO₂ on LSMO/STO substrate,⁶⁷ a future task is to use PA-MBE to grow high crystal quality FE HZO on oxide conductive substrates, which serve as the bottom electrodes. It is particularly interesting to grow directly on n-STO semiconductor substrates since STO has been used successfully in combination with conventional epitaxial BTO and BFO perovskite FE in high-performance FTJs with giant TER.²⁸⁸ The hope is that good epitaxial quality HZO directly grown on STO substrates by PA-MBE will improve the performance HZO-based FTJ non-volatile memory (NVM) beyond the current state of the art. The hope is that good epitaxial quality HZO directly grown on STO substrates by PA-MBE will produce high-performance HZO-based FTJ NVM, which are lacking today. Using PA-MBE, it would be

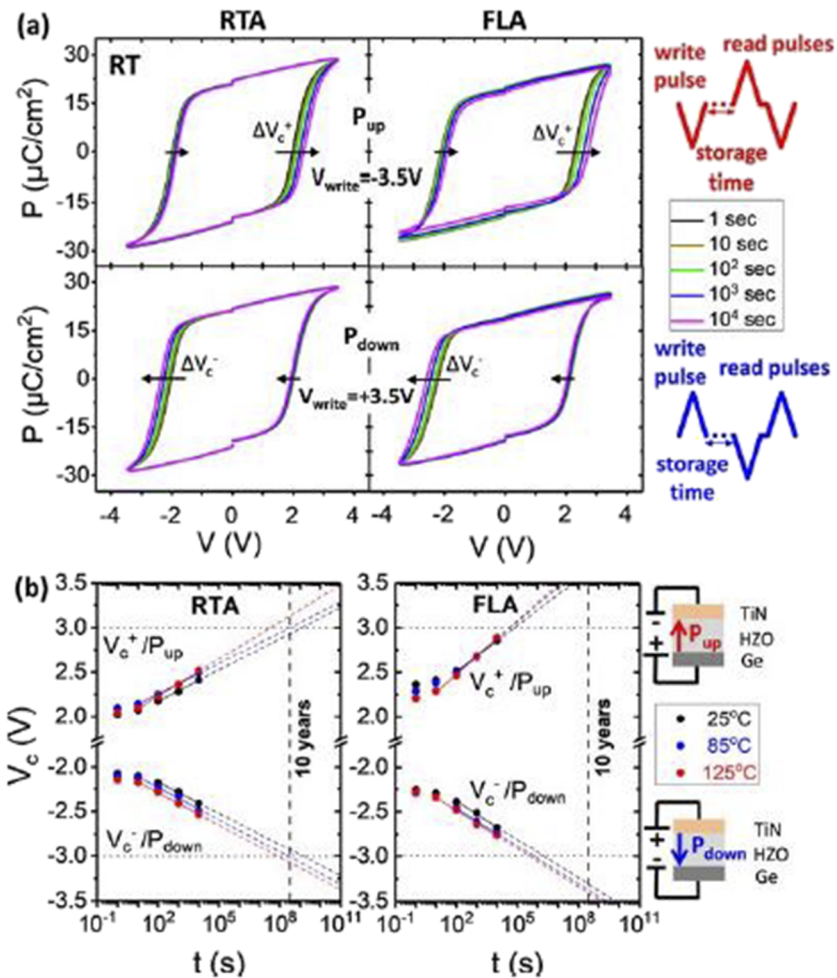


FIG. 14. TiN/HZO/Ge MFS devices fabricated by PA-MBD, showing very small imprint and good reliability.

possible to control the crystal phase, crystal orientation with respect to the growth direction, and the thickness of FE HfO_2 down to 1–2 nm, the latter being very important for the performance of FTJs. This is particularly important in light of the recent discovery of emergent ferroelectricity in ultrathin (<2 nm) $\text{Zr}:\text{HfO}_2$ ¹⁹ and ZrO_2 ⁶⁸ as a result of reduced dimensionality.⁶⁸ The most attractive feature of using STO as a substrate is that this material can be grown epitaxially on Si(001) by PA-MBE with a 45° in-plane rotation and with very good crystalline quality.²⁸⁹ Moreover, by combining O_2 partial pressure and post-growth annealing, a controlled concentration of oxygen vacancies can be created, which acts as an effective n-type doping. Therefore, it is possible to obtain in-situ, an n-type STO semiconductor bottom electrode directly on silicon and subsequently overgrow HZO and the top electrode in one growth run in the same UHV chamber by PA-MBE without breaking vacuum. However, the “holy grail” of epitaxial ferroelectrics is to achieve epitaxy directly on Silicon substrates, which facilitates the fabrication of important devices, such as FeFETs or FTJs, and their integration with Si CMOS at the

front-end-of-line (FEOL). While attempts have been made by PLD²⁹⁰ for the direct epitaxy of HZO on Si, this material may not be the best choice due to the lattice mismatch with Si, the reaction at the interface, and the complex thermodynamic phase diagram that renders it difficult to access the correct ferroelectric phase under the constrictions of epitaxy.

A good choice is stoichiometric $\text{La}_2\text{Hf}_2\text{O}_7$, which can be obtained either in the ordered fluorite phase known as pyrochlore or in the random fluorite phase, which is lattice-matched with Si. In our team, we have demonstrated²⁹¹ that this material can be grown by PA-MBE at 770 °C on Si(001) substrates, showing cube-on-cube epitaxy and clean/sharp interfaces (Fig. 15). Although the pyrochlore phase is centrosymmetric (cubic, space group symmetry $Fd\bar{3}m$), therefore non-polar, the possibility that a metastable FE phase can be accessed via strain, doping, thickness, and annealing, as in the case of FE HfO_2 , cannot be excluded. Doping $\text{La}_2\text{Hf}_2\text{O}_7$ by Zr, in analogy with doping HfO_2 with Zr, could be one way to go in the search for a possible metastable ferroelectric state. Isostructural $\text{La}_2\text{Zr}_2\text{O}_7$ is an alternative material to be investigated.

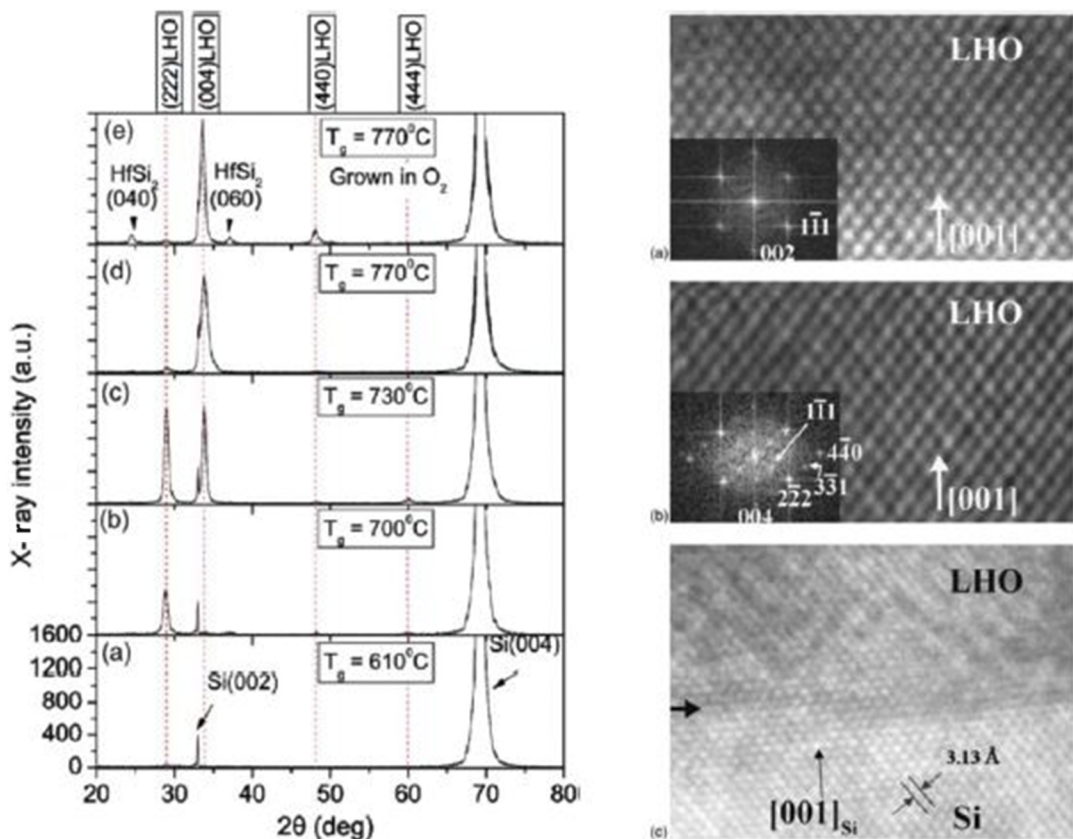


FIG. 15. Pyrochlore $\text{La}_2\text{Hf}_2\text{O}_7$ on Si(001) grown by PA-MBE, showing cube-on-cube epitaxy and sharp, clean interfaces.

In fact, ferroelectricity in frustrated $\text{La}_2\text{Zr}_2\text{O}_7$ pyrochlore grown by sol-gel on (110)-oriented STO has already been reported.²⁹² It would be a future target to grow epitaxial $\text{La}_2\text{Zr}_2\text{O}_7$ on Si or other substrates by PA-MBE with the aim to obtain the ferroelectric state. It should be noted that amorphous LaHfO_x (or La-doped HfO_2) has been adopted by key chip manufacturers to adjust the threshold voltage of nMOS in advanced CMOS. Moreover, La-doped (~9%) HZO has been developed to improve the endurance of ferroelectric capacitors and the remanent polarization.²⁹³ Therefore, La incorporation in HZO is compatible with ferroelectric HZO and Si technologies, which facilitates its entry into the research of epitaxial ferroelectric oxides in the future.

4. Concluding remarks

Most of the work so far has been performed using plasma-assisted molecular beam deposition at low temperatures to produce amorphous HZO, followed by crystallization annealing to obtain the FE *o*-phase. Very good FE material has been produced on Ge substrates with clean interfaces and pure *o*-FE phase, showing high P_r , with the minimum required wake-up in thick (10 nm) films. Ferroelectricity is maintained down to 5 nm with very good P_r , which, however, is obtained after extensive field cycling. Functional *p*-channel FeFETs on Ge substrates have been

realized. The biggest challenge at present is to use PA-MBE to produce epitaxial ferroelectrics mainly on Si substrates with expected enhanced ferroelectricity to enable integration with Si circuits. Possible metastable phases of La-containing hafnium- and zirconium-based oxides with the pyrochlore or fluorite structure are good candidates since their epitaxial growth has already been demonstrated and evidence of ferroelectricity in the Zr-based compound has been published.

VI. CHARACTERIZATION AND PROPERTIES

A. Dopants

Hiroshi Funakubo and Takao Shimizu

1. Status

Constantly obtaining the FE phase is crucial in harnessing ferroelectricity for stable device performance. The FE phase is reported to be obtained even from pure HfO_2 and ZrO_2 composition without intentionally doping. However, element doping is widely recognized to be very useful for the reproducible generation of FE phases. In fact, a huge volume of studies in terms of the ZrO_2 ceramics, used

as high-toughness ceramics and oxygen ion conductors, and high- k dielectric materials suggest that the doping element is quite effective for tuning the symmetry of fluorite oxides. A wide variety of dopant elements has been employed for the stable appearance of ferroelectricity, which is mainly induced in HfO_2 , including not only cation dopants (Mg, Sr, Ca, Ba, Al, Lu, Er, Nd, Ga, Sm, Fe, Sc, Gd, La, Y, Ce, Ge, Si, and Zr) but also an anion dopant, such as N.²⁶¹ As listed, divalent, trivalent, and tetravalent cations appear effective for forming the FE phase. In contrast, doping of higher valence dopants has hardly been reported.

$\text{HfO}_2\text{-ZrO}_2$ systems have been most widely investigated due to the stable ferroelectricity around $\text{Zr}/(\text{Hf} + \text{Zr}) = 0.5$, whose composition range is wider than other dopants in the case of around 10 nm in thickness. The wide available composition range is an advantage for the ALD process because stable ferroelectricity is obtained against composition fluctuation. However, the obtained phases are sensitive to the process conditions. In addition, the available composition range decreases with the increasing film thickness, and ferroelectricity cannot be observed above 60 nm, in general, because of the stable m -phase formation.²⁹⁴

Doping of SiO_2 or $\text{AlO}_{1.5}$ to HfO_2 is also widely investigated due to the good compatibility with the CMOS process because well-matured sources for CVD and ALD processes are available. In fact, the first demonstration of ferroelectricity was performed with Si. The composition range for ferroelectricity, which is typically several percent, is smaller than that of the ZrO_2 case.

The alkaline earth elements and rare earth elements have been extensively used for tuning the crystal symmetry of ZrO_2 ceramics. By imitating this, various elements are adapted for also FE applications. In most cases, several percent of elements are effective for ferroelectricity, similar to Si and Al. However, doping a relatively large amount of $\text{LaO}_{1.5}$ and CeO_2 (<20%) is reported to show ferroelectricity, but the available composition range is still smaller than the Zr case, which is generally over 20%.

2. Current and future challenges

There are many trials for the overall understanding of the dopant effect on the generation of FE phase from both experimental and theoretical approaches.

Due to recent progress in computational DFT studies, many researchers conducted theoretical calculations for the effect of doping. For example, Batra *et al.* calculated a doping effect of a wide variety of elements to stabilize the FE phase for HfO_2 . The formation energy of the ferroelectric o -phase is reduced by introducing the alkaline earth elements and rare earth elements that have been ascertained experimentally to obtain the FE phase. One of the fundamental issues of such a theoretical calculation approach is that the FE phase is generally not the most stable phase, namely, not the ground state. Other research groups have also reported similar results.

Interestingly, Yang *et al.* reported a significant reduction in energy difference between the most stable m -phase and the FE o -phase by Si and La doping, which have the smallest and largest ionic radii within their study.²⁹⁵ Wu *et al.* also reported the reduction of formation energy for the FE phase, together with the non-polar o -phase and the t -phase, by inducing Si.²⁹⁶ They emphasize the importance of a kinetic mechanism for forming the ferroelectric phase from the t -phase by taking into account entropy. Thus, the

dopants do not stabilize the FE phase alone, and other factors might aid it. Further development in a theoretical study is needed to understand doping effects fully.

The kinetic mechanism is also confirmed by Park *et al.*^{222,297} and Tashiro *et al.*¹⁷² The common understanding is that the FE phase is formed from the high-temperature t -phase on cooling. The dopants prevent the formation of the most stable m -phase by reducing the formation energy of metastable o - and t -phases. This kinetic mechanism mimics the formation of t -polycrystalline ZrO_2 , which is well-studied by doping Y or Ce.²⁹⁸ According to the kinetic formation mechanism, thicker films ($\sim 1 \mu\text{m}$) and even bulk single crystals have been grown by Y doping. This is in contrast to the $\text{HfO}_2\text{-ZrO}_2$ system and doping cations with small ionic radii, by which ferroelectricity can be obtained only in thin films.

Experimentally, the local environment of the dopants is also an important challenge in elucidating the doping effect. In particular, trivalent or divalent dopants favor oxygen vacancies to maintain charge neutrality. The interaction between the dopant and induced defects is quite interesting regarding the ferroelectric properties and reliability. A recent computational study proposes reducing the energy barrier for polarization switching by doping the cations with small ionic radii, such as Si and Ge.²⁹⁹ Their calculation shows that the local distortion due to reduced coordination number would decrease the energy barrier for polarization switching. This study is quite interesting because most studies on the doping effect have aimed at stabilization of the o -phase, i.e., an increase in polarization. Experimental studies concerning practical issues, enhancement in reliability, or reduction of E_c are desired.

3. Advances in science and engineering to meet these challenges

One of the challenges of doping into HfO_2 FEs is tuning and improving FE properties, particularly enhancing endurance properties and decreasing E_c . Recently, Kozodaev *et al.* have reported that La doping into $\text{Hf}_{0.5}\text{Zr}_{0.5}\text{O}_2$ improves endurance properties up to 10^{11} cycles without the involvement of fatigue and hard breakdown.³⁰⁰ Similarly, co-doping of rare earth elements (La and Y or La and Gd) into $\text{Hf}_{0.5}\text{Zr}_{0.5}\text{O}_2$ enhances the endurance property. The latter study speculates that the local structural distortion of the lattice contributes to improved endurance.³⁰¹

It is also an important challenge to clarify the local environment of dopants and also the host Hf and Zr elements in the FE phase in scientific and engineering views. However, most films with small thicknesses include tiny amounts of dopants because the volume and concentration of dopants are small. Recent advances in the thicker films ($\sim 1 \mu\text{m}$)¹⁷⁵ and bulk single crystals³² would provide a better signal-to-noise ratio. In addition, the progress in the measurements and analysis would provide informative studies.

Most studies, particularly computation-based theoretical studies, assume that dopants are incorporated into the $\text{HfO}_2\text{-ZrO}_2$ solid solution. However, rapid phase segregation has been known for doping the elements with small ionic radius, such as Si and Al, into the bulk HfO_2 or ZrO_2 . In fact, it is reported that Al tends to agglomerate during the thermal treatment process, and this agglomeration results in enhanced ferroelectricity. Such a nanoscale diffusion process would also be important for understanding the doping effect.³⁰²

It has been revealed that the simple understanding that the dopants lead the HfO_2 materials to the *o*-FE phase is difficult. Thus, modeling with kinetic dynamics is required to clarify the formation of the FE phase with dopants, including the diffusion of the elements at the nanoscale. The molecular dynamics simulation with DFT-based potential would be one of the approaches to predict the formation phase in practical conditions.³⁰³ In addition, recent progress in machine-learned potential would provide fast computing.

4. Concluding remarks

Various dopants in HfO_2 are effective in producing ferroelectricity. However, a total understanding of the doping effect has not been established yet. The kinetics during the process of forming the *o*-FE phase is crucial to clarify the doping effect. Advanced in experimental and theoretical studies, their combination is needed. In particular, thick films and single crystals provide powerful tools to investigate the local structure of dopants. Recent studies regarding reduction in E_c and enhancement in endurance are interesting next steps beyond the studies aiming at preparing the FE phase. Data scientific methods, such as machine learning and high-throughput experiments, should be adapted for optimization of the dopants elements and concentration, including co-doped systems.

5. Acknowledgments

This work was supported by the MEXT Initiative to Establish Next-generation Novel Integrated Circuits Centers (X-NICS) under Grant No. JPJ011438, MEXT Program: Data Creation and Utilization Type Material Research and Development Project under Grant No. JPMXP1122683430, and MEXT KAKENHI under Grant Nos. 19H00758, 21H01617, and 22K18307. This study was supported by the MEXT Leading Initiative for Excellent Young Researchers and a research grant from the Murata Science Foundation.

B. Defect engineering

Nick Barrett

1. Status

The successful integration of FE HfO_2 into high-performance, ultra-low power CMOS compatible memory and logic depends not only on suitable material properties but also on engineering these properties in order to optimize device performance. Key performance indicators are imprint, wake-up, fatigue, and leakage, all of which are intimately linked to the material and device responses to field cycling and, more generally, to environmental and processing conditions.

Atomic scale defects play a central role in determining not only the basic material properties but also their response to and evolution under electrical or thermal stress and field cycling. Defects can be generated during growth and by the formation of chemically and electrically distinct interface layers. Their distribution may change during cycling, presenting new challenges in terms of real device performance.

The effective processing window for reliable device operation must, therefore, take into account not only the magnitude of P_r but

also the evolution of imprint, wake-up and endurance kinetics, and leakage.

Defect control is potentially a fruitful path toward device reliability of industrial standards. Here, we will focus on engineering oxygen vacancy defects since they play a key role in both material properties and device performance³⁰⁴ although other point defects, including carbon, nitrogen, or hydrogen, as well as complex defects may also contribute³⁰⁵ and should be the subject of more complete studies.

Oxygen vacancies influence both resistive and FE switching in HfO_2 -based materials and are, therefore, of importance for two emerging non-volatile memory technologies [resistive random access memories (RRAMs) and FeRAMs].³⁰⁶ However, there is potentially a fundamental contradiction between FE memories, which depend on the insulating nature of the HfO_2 , whereas resistive memories require a low conductance state usually provided by oxygen vacancy filaments. It is, therefore, necessary to locate a sweet spot in the oxygen vacancy concentration for FE applications.

Initial oxygen vacancy distribution in as-processed hafnia layers can vary sharply over typical film thicknesses (~ 10 nm), providing a strong imprint field. This skews the polarization-field hysteresis loop and narrows the operational memory window by altering asymmetrically the threshold voltages. Uniformization of the defect distribution and defect recombination can significantly reduce the imprint during the wake-up process, as suggested by the model presented by Pešić *et al.*¹⁶⁹ [Fig. 16(a)]. Initial oxygen vacancy redistribution can give rise to a strong wake-up effect, opening the memory window. Field cycling into the fatigue regime results in a jump in oxygen vacancy density and a concomitant increase in leakage current determined by trap-assisted tunneling and closure of the memory window.³⁰⁷

Thermally stimulated depolarization current measurements have quantified activation energies for oxygen vacancy migration. The high values suggest that imprint may be due to charge trapping at defect sites rather than the charged defects themselves.³⁰⁸ The trap levels then become the important parameter. Indeed, *ab initio* simulations of defect structures and modeling of transport and FE properties have provided useful insights into the role of different defect species as charge traps and go some way to explaining the experimental fatigue and leakage current data.³⁰⁹ Thermally activated migration of oxygen vacancies at room temperature is unlikely, but mobility under a strong electric field has been reported.¹⁴² Although the kinetics are slow, the field-induced mobility may be important in determining wake-up and fatigue regimes.

First attempts at engineering the oxygen vacancy levels have been achieved by the insertion of an ultra-thin Ti layer to favor oxygen scavenging.²⁷⁶ Modest oxygen scavenging gives a higher remanent polarization by favoring *o*-phase nucleation, but too high an oxygen vacancy concentration leads to higher leakage and earlier breakdown, i.e., lower endurance.

Oxygen vacancy ordering into more complex defect structures may also contribute to the enhancement of FE properties. It has been suggested that modest vacancy concentration could be used to favor up to 80% of the *o*-phase, which could then be stabilized by subsequent re-oxidation.

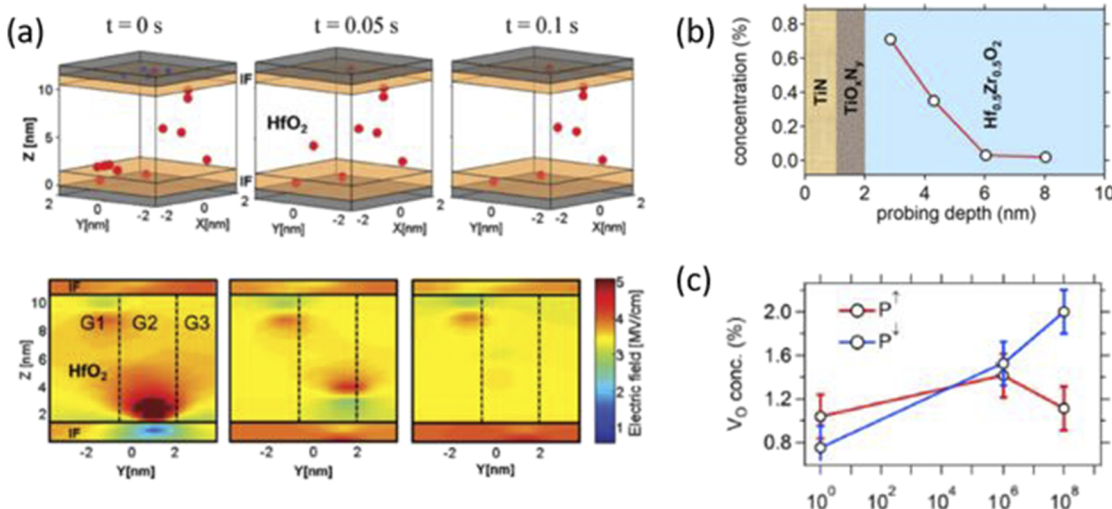


FIG. 16. (a) Simulated device wake-up and corresponding field evolution on field cycling at 4 MV cm^{-1} reproduced with permission from Pešić *et al.*, *Adv. Funct. Mater.* **26**, 4601 (2016). Copyright 2016, Wiley-VCH. (b) Oxygen vacancy profile as measured by XPS. Reproduced with permission from Hamouda *et al.*, *Appl. Phys. Lett.* **116**, 252903 (2020). Copyright 2020 AIP Publishing LLC. (c) Oxygen vacancy concentration near the top interface as a function of field cycling and polarization state. Reproduced with permission from Hamouda *et al.*, *J. Appl. Phys.* **127**, 064105 (2020). Copyright 2020, AIP Publishing LLC.

2. Current and future challenges

A major challenge is the direct measurement of the oxygen vacancy concentration. This should be as model independent as possible, although the model calculations of vacancy mobility,¹⁶⁹ charge transport,³¹⁰ and imprint, wake-up, and fatigue³⁰⁸ have provided valuable insights. Charge-based interpretations of data on oxygen vacancy concentrations are challenging since neutral defects are more difficult to identify, potentially underestimating the true defect concentration.

A second challenge is that direct measurement of the oxygen vacancy distribution in a HfO₂-based capacitor or FeFET requires both lateral and depth resolution on the scale of the devices as well as time-dependent analysis of relaxation, field cycling, and switching.

X-ray photoelectron spectroscopy (XPS) is gaining popularity based on the assumption that oxygen scavenging and the creation of oxygen vacancies give rise to the reduction of Hf cations.^{311–313} Reduced Hf carries a clear spectroscopic signal, which can be quantified in terms of vacancy concentration, as shown in Fig. 16(b). The tunable depth sensitivity of photoelectron spectroscopy, on length scales similar to the typical hafnia film thickness, provides a handle to measure the concentration profile rather than just an average measurement over the film thickness. This is crucial information to be correlated with, for example, the evolution of imprint with field cycling. Depth sensitivity can be tuned by varying the photoemission take-off angle or the photoelectron kinetic energy. Photoelectron spectroscopy in the presence of a top electrode allows for quantifying the polarization and field cycling dependence of the Schottky barrier height and hence the probability of leakage and charge injection [Fig. 16(c)]. The latter can be a further factor in determining defect concentration.³¹⁴

The disadvantage of classical XPS using standard laboratory sources is that the depth sensitivity is limited to $\sim 5 \text{ nm}$.

This precludes the use of a realistic top electrode whose thickness would extinguish the signal coming from the underlying hafnia and excludes the possibility of operando experiments to follow in-situ the oxygen vacancy evolution as a function of field cycling.

There are two ways of circumventing the top electrode obstacle. One is mechanical or chemical thinning or removal of the top electrode,³¹² allowing for the plot of the oxygen vacancy concentration profile generated by oxygen scavenging. However, this must be done carefully to avoid damaging the underlying HfO₂ by a low energy ion beam.³¹⁵

Hard x-ray photoemission (HAXPES) offers a non-destructive solution to probe through realistic electrode thicknesses thanks to the improvement in depth sensitivity by one to two orders of magnitude.^{311,312,316} HAXPES has been used to directly measure the oxygen vacancy concentration profile in the vicinity of the top TiN/HZO interface due to oxygen scavenging.³¹³ It has also provided invaluable information on the vacancy concentration near the bottom electrode as a function of oxygen-rich or oxygen-poor processing conditions, allowing for insights into the process engineering of defects.³¹⁷

3. Advances in science and engineering to meet these challenges

The increased availability of HAXPES beamlines makes such analyses more accessible; however, they remain the exception due to the six-month lead-time for experimental proposals. Typical beamtime allocations are usually not more than one week. For industrialists requiring characterization of imprint retention and endurance, this is a major obstacle.

One possibility would be a proprietary HAXPES beamline, possibly in conjunction with a Glancing angle x-ray diffraction (GIXRD) setup in order to carry out on-demand operando chemical

and structural characterization of realistic memory devices. Physical modeling to inform decisions for industrial development requires reliable and statistically significant data. Typical field cycling at 100 kHz requires one day for 10^{10} cycles without taking into account relaxation or measurement times. Several weeks are, therefore, necessary for a full *operando* characterization of the oxygen vacancy behavior as a function of polarization, switching speed, and field cycling of a single device. A comparative study integrating different processing conditions,³¹⁸ rapid thermal annealing temperatures, and solder reflow conditions in order to address packaging criteria, therefore, requires several months access. A broad consortium from academia and industry could afford such an option.

A complementary alternative would be the acquisition of recently commercialized laboratory HAXPES setups using high-energy x-ray sources, either Cr or Ga. The Ga source (delivering x rays at 9.25 keV) appears best adapted since the Ti spectra do not show interference in the core level region. The major advantage of these setups is the absence of lead-time, and their stability allows for longer acquisition times made necessary by the lower flux compared to a synchrotron beamline.³¹⁹

The second major challenge concerns the spatial resolution on the scale of real devices and, ultimately, typical domain sizes. The latter is extremely challenging, but state-of-the-art transmission electron microscopy (TEM) has demonstrated the role of electrode chemistry on the vacancy generation and kinetics.¹⁴² However, TEM cannot provide reliable information on length scales \sim 0.1–1.0 mm. Complementary techniques operating on different length scales must be developed. Photoemission electron microscopy (PEEM), providing decanometric spatial resolution in microscopic fields of view, allows, for example, characterization of \sim mm scale devices and has demonstrated the capacity to quantify oxygen vacancy concentration as a function of polarization state and cycling history.³²⁰

However, these analysis techniques are still in their infancy and require optimization in sample structuring as well as the use of higher energy photons sources to secure electrode quality.

The third challenge is the implementation of time resolution over a wide range of time-scales in order to characterize how point defect engineering can optimize switching and retention. Typical switching times targeted for HfO₂-based devices are 10–50 ns. This is well suited to pump–probe photoemission experiments synchronizing voltage generators with synchrotron radiation pulses.³²¹ Although not new, it has yet to be implemented for ferroelectric hafnia because reliable switching data also require small devices to avoid prohibitive leakage currents. Slower kinetic processes have also been reported, including defect migration, relaxation, as well as defect and dopant dependency.^{322,323} The defect concentration and profile determines the trap-assisted tunneling current, correlated with the onset of the fatigue regime and, therefore, device endurance.³⁰⁷ Determining the energy levels of the trapped electrons with respect to the conduction band will allow for refining the quantitative physical modeling.

The field is wide open and calls for considerable effort.

4. Concluding remarks

In the decade following Böschke's first paper in 2011, the understanding of the material properties of ferroelectric hafnia has

made significant progress. The increasing need for low-power digital autonomy has proposed the integration of FE HfO₂ into current electronics to the forefront of emerging technology candidates. Nevertheless, the performance metrics required to be considered as a serious technological alternative must still be met. To do so requires a demonstration of the capacity to reliably engineer and optimize the same material properties. There is no short cut, and advanced characterization platforms, including the techniques outlined here, with rapid access and throughput, are necessary.

C. Interface engineering

Jacob L. Jones, Younghwan Lee, and H. Alex Hsain

1. Status

Interfaces discussed in this section are limited to those created when two dissimilar materials are grown or placed adjacent to one another, e.g., through sequential deposition of two films. Unlike ferromagnetics, where no additional contact is needed for measuring their magnetic properties, FEs, such as HfO₂, require contacts or electrodes (at minimum) for measuring important properties, such as polarization. Thus, interfaces are inevitable in FE HfO₂ devices, and their careful design and synthesis is necessary to maximize device performance.

Interfaces of interest in HfO₂-based devices are those created between (1) the FE film and the top electrode, (2) the FE film and the substrate, and (3) additional interfaces formed within the HfO₂ film, e.g., through superlattices or layering.

FE HfO₂ is often created as a MFM structure in which metallic electrodes are in contact with FE HfO₂ at both top and bottom sides. Because most metals are strong reductants, an additional metal oxide layer at the interface of the MFM device is inevitably made, where the interfacial layer acts as an additional capacitance in series. Although this interfacial layer (or dead layer) can be detrimental to certain device properties, there can also be benefits to adding an intentional interfacial layer on the properties of the FE HfO₂-based film, i.e., creating a Metal–Ferroelectric–Insulator–Metal/Semiconductor (MFIM/S) structure. For example, adding an oxide layer, such as ZrO₂,³²⁴ Al₂O₃,³²⁵ TiO₂,³²⁶ and La_{0.67}Sr_{0.33}MnO₃ (LSMO),²¹⁴ below the FE HfO₂ introduces the ability to alter the crystallization behavior and stabilization specific phases of HfO₂ or promote texturing or epitaxial growth.

In the MFM structure, HfO₂ has been combined with many types of electrodes, including TiN,^{312,327–329} TaN,^{173,330} W,^{331,332} Pt,^{153,332,333} RuO₂,^{334–336} and IrO₂.^{337,338} Despite a wide array of electrode options, the most commonly employed electrode in combination with HfO₂ hafnia is TiN due to its oxygen-gettering nature, which yields oxygen vacancies in HfO₂. Oxygen vacancies are linked to both the stabilization of the *o*-phase of HfO₂ as well as the wake-up effect in which a redistribution of defects during cycling produces a variable P_r value.^{169,339} TiN also possesses a larger thermal expansion coefficient than HfO₂, a mismatch that may produce a tensile strain during annealing, which could facilitate stabilization of the FE HfO₂ phase. A recent study provides even more correlation between the thermal expansion coefficients, stresses, and FE properties in MFM capacitors, demonstrating that lower electrode thermal

expansion coefficients lead to higher tensile stress and enhanced ferroelectricity.³³¹

2. Current and future challenges

The propensity of TiN to act as an oxygen sink when in contact with an oxide is a primary challenge in engineering of TiN/HfO₂ interfaces. Many researchers have employed strategies such as the use of interlayers to better stabilize the HfO₂-electrode interface, i.e., creating MFIM/S structures. Recently, Zhao *et al.* have modeled FE HfO₂ interfaced with Al₂O₃, La₂O₃, SiO₂, GeO₂, and other oxides to better understand the electronic structure and the resulting asymmetric oxygen distribution-induced polarity.³⁴⁰ Yadav *et al.* investigated the use of oxygen-deficient IrO_x interlayers to reduce the interlayer formation and oxygen vacancies at the interface, which led to enhanced $2P_r$ and wake-up free behavior.³⁴¹ Mizutani *et al.* used a cerium oxide capping layer on Y-doped HfO₂ to increase the endurance limit from 10^7 to 10^{10} cycles.³⁴² Mizutani *et al.* attributed the increased cycling endurance due to CeO_x, which acts as a buffer layer that can absorb or supply O atoms during heat treatment and/or electric field cycling. Despite the potential benefits of interlayers, such as improved endurance and reduced leakage,^{343,344} a major challenge of incorporating a dielectric layer in series with a FE is the resultant loss of retention in the device. Alcala *et al.* showed that a La₂O₃ interlayer in an HZO capacitor accelerated the retention degradation process due to the depolarization fields that arise from the dielectric interlayer.³⁴⁵ Future interfacial engineering strategies are aimed at considering device properties, such as endurance, leakage, and reliability, concurrently in concert with one another.³⁴⁴

Controlling the microstructure of HfO₂-based films poses a challenge for device scaling and integration, given that the grain size and crystal structure are strongly coupled in HfO₂-based films.³⁴⁶ For example, Kim *et al.* inserted an additional 1 nm thick dielectric Al₂O₃ layer in the middle of a 40 nm thick HZO to control the grain size and obtained P_r of $10 \mu\text{C}/\text{cm}^2$, which was 11 times larger than that of single HfO₂ layer of equivalent thickness.³⁴⁷ Kim *et al.* suggested that by insertion of Al₂O₃ into the middle of HZO, it was possible to interrupt the grain growth and prevent the formation of the deleterious *m*-phase, which is favored at larger grain sizes.

Process design will also inevitably influence the HZO/TiN interface characteristics where parameters such as the selection of oxygen source and dose times or the layering sequence in HZO films have been found to alter the local chemistry and structure of films. For example, Hsain *et al.* showed that a stronger oxidizer O₂ plasma, compared to H₂O, promoted a more pronounced TiO_x interlayer between HfO₂ and the electrode, which had a beneficial impact on improving the endurance of HZO capacitors.³⁴⁸ Walters *et al.* employed the use of a sequential O₂-H₂ plasma oxidation method, which was shown to produce asymmetrical shifts in the coercive fields during retention measurements, likely due to the growth of additional interfaces of TiO_xNy.³⁴⁹ Lee *et al.* also showed how pre-deposition vacuum breaking can increase the carbon concentration within HZO films and stabilize the *t*-phase.²⁵⁸

For films containing multiple cations, such as HZO, superlattice layering within the film is another strategy to control the interfacial structure and properties. For example, Park *et al.* explored

the impact of superlattices of HfO₂ and ZrO₂ on resulting FE properties. Importantly, they reported that the starting layer could strongly influence the crystallization kinetics and subsequent phase stabilization in the FE layer.²⁵⁵ Zhao *et al.* further showed that layering superlattices of ZrO₂ and HfO₂ using 10 s dose time of O₂ plasma generated high P_r of $25.5 \mu\text{C}/\text{cm}^2$.^{10,350}

3. Advances in science and engineering to meet these challenges

One way to mitigate deleterious interfacial effects is to maintain vacuum during the deposition of the electrode and HfO₂ films. As stated earlier, the breaking of the vacuum when transferring samples between different tools causes increased carbon contamination and metal oxidation, neither of which can be well controlled. Instead, maintaining a vacuum can minimize these otherwise uncontrollable processes. In 2018, Wei *et al.*²⁷ reported the sequential deposition of LSMO and HfO₂ via PLD without breaking the vacuum. Electron microscopy and spectroscopy confirmed an excellent quality of the interface. As a more scalable process, Lee *et al.*²⁵⁸ reported the processing of electrodes and HZO in MFM capacitor geometries via ALD within the same tool without breaking the vacuum. Their process, called sequential, no-atmosphere processing (SNAP), was demonstrated on TiN/HZO/TiN stacks and resulted in devices with wake-up-free FE performance and unexpectedly high P_r ($27 \mu\text{C}/\text{cm}^2$). The improved performance was attributed to limited oxidation and carbon contamination of HZO/TiN interfaces.

Moving forward, advances in controlling atmosphere exposure between the deposition of distinct layers may prove effective at providing new ways to control interfacial characteristics. This may include, e.g., the use of SNAP in other deposition processes (e.g., physical vapor deposition) or the use of controlled gas and time exposures between the deposition of certain layers.

As the influence of defects can exacerbate the properties of interfaces, it is also critical to understand and control the source and purity of starting materials. While often overlooked in early-stage research, source purity is important in both the research environment, where variables across research labs are often unknown or not reported, and the manufacturing environment, where reproducibility is critical. Reproducibility will be a function of source purity, the specific impurities that are present, and consistency across targets, batches, and vendors. Targets for physical vapor deposition processes, e.g., could be synthesized from ~99% purity starting materials, although this may result in ~1% of unknown and inconsistent impurities that could incorporate into films and have a pronounced effect on interfacial properties. In the parallel development of ferroelectric Sc_xAl_{1-x}N, it has been recently shown that films prepared with Sc sources of nominally 99.9% vs 99.99% purity starting materials resulted in over five orders of magnitude difference in electrical leakage.³⁵¹ As FE HfO₂ matures, it will become important to either control these effects or engineer the device against their variability.

4. Concluding remarks

Although interfaces are inevitable in FE HfO₂ devices, interfacial engineering can be used to control their thickness, chemistry, structure, and properties. The major goals of interfacial engineering can be summarized as (1) mitigating deleterious interfacial

effects through controlling thickness, chemistry, etc., or (2) leveraging/engineering the interface for the specific structure and properties, e.g., through interfacial chemistry, epitaxial growth, or the growth of additional interfacial layers to influence the properties of FE films. Limitations of controlling interfacial thickness, chemistry, structure, and properties are fundamentally a function of the selected deposition technique, processing conditions, and source materials.

5. Acknowledgments

J.L.J., Y.L., and H.A.H. were supported by the U.S. National Science Foundation (NSF) under Grant Nos. IIP-1841453 and IIP-1841466 and H.A.H. further acknowledges the support from the NSF Graduate Research Fellowship Program (Grant No. DGE-1746939). J.L.J. acknowledges the support from the Laboratory Directed Research and Development program at Sandia National Laboratories, a multimission laboratory managed and operated by National Technology and Engineering Solutions of Sandia LLC, a wholly owned subsidiary of Honeywell International, Inc. for the U.S. Department of Energy's National Nuclear Security Administration under Contract No. DE-NA0003525.

D. Electrodes optimization

Mattias Borg

1. Status

To electrically interact with HfO_2 - and/or ZrO_2 -based FEs, one requires some type of electrodes. From the most basic point of view, the electrodes provide the necessary screening of the ferroelectrically induced polarization charge to stabilize P_r in the film and, in addition, create an electrical interface between the FE and the outside world. In many cases, the choice of electrodes also has a direct impact on the formation and switching properties of the FE itself, influencing the crystal phase properties, and may induce or remove defect states. For devices such as the FTJs, the electrodes' properties will also decide the device's performance, making them integral parts of the device. It is, therefore, essential to understand and control the properties of the electrodes in electronic devices based on HfO_2 - and ZrO_2 -FES. To limit the scope of the discussion, we will focus on metallic and semiconducting electrode materials that are currently compatible with Si CMOS processing, thus excluding some electrode materials, such as Au and perovskites. For brevity, we will denote the FE as HfO_2 , even though it may consist of an alloy with ZrO_2 or doped with other dopants, such as Si, Y, Gd, and La.

It is well known that the choice of metal electrodes can promote the formation of the FE Pca_21 phase by providing a beneficial in-plane tensile strain in the HfO_2 .⁶⁰ The electrodes should also be stable enough to survive the HZO crystallization process, which usually requires annealing to 400–600 °C. The electrode material needs, thus, be chosen carefully, and common materials include TiN, TaN, Pt, Ni, W, IrO_2 , and RuO_2 .^{330,337,352–355} TiN appears as the most common choice, being both thermally stable and CMOS-compatible.⁶⁰ A low electrode thermal expansion coefficient is beneficial for inducing strong tensile strain, and W was found to be particularly promising in this regard.³³¹ In addition, the electrode

deposition conditions can also matter: It has been recently discovered that deposition pressure-induced microtexture of a TiN top electrode can decide the resulting crystalline phase in HfO_2 and, thus, its FE properties.³⁵⁶ Electrode deposition by different available methods, for example, evaporation, sputtering, or ALD, therefore, cannot be expected to yield the same results, and the electrode process, thus, needs to be carefully controlled.

Second, a reactive electrode material can interact with the HfO_2 film, both during the crystallization process at high temperatures as well as during electric field cycling. Reactions can lead to oxygen scavenging, creating interfacial layers and additional oxygen vacancies in hafnia,³⁵² which can negatively affect the cycling endurance of the film. In addition, unstable electrode materials could lead to metal diffusion through hafnia during field cycling.³⁵⁷

2. Current and future challenges

A major challenge for HfO_2 -based FEs is that its large E_c (>1 MV/cm) requires the applied electric field during polarization switching to be a significant portion of the breakdown field. This promotes the creation and movement of interstitials and oxide defects, such as oxygen vacancies, in the FE film. Vacancies can accumulate at the interface to the electrodes or even move across between electrodes and the FE film, affecting the interfacial chemistry and electrode effective work function or even leading to the formation of an interfacial layer over time.

A second challenge for HfO_2 -based FE devices is the formation of interfacial layers between the electrodes and the FE film during device fabrication. Normally, a high-temperature annealing procedure (400–600 °C) is required to form the FE phase, during which the electrodes are also exposed to the high temperature. It is often observed that the common nitride electrodes TiN and TaN scavenge oxygen from the hafnia films during this process, forming interfacial metal-oxides or oxynitrides.³⁵² These interfacial layers are believed to give rise to wake-up effects as well as degrade reliability during electric field cycling.

Third, the use of semiconducting electrodes comes with additional challenges. Semiconductor electrodes are attractive for FeFETs and FTJ devices as their conductance can be strongly modulated by the polarization charge, leading to large threshold voltage shifts in FeFETs and strong tunnel barrier modulation in FTJs, resulting in large resistance state contrast. However, there is a great mismatch between the typical magnitude of polarization charge 10–30 $\mu\text{C}/\text{cm}^2$ in HfO_2 and the density of states of typical semiconductors. This leads to very large surface potentials that unequivocally activate deep trap states in the semiconductor, causing unwanted Fermi-level pinning or even irreversible damage. As an example, for Si ($N_D = 10^{15} \text{ cm}^{-3}$), the needed band bending in inversion is more than 1 V to match 20 $\mu\text{C}/\text{cm}^2$ in sheet charge. Possibly due to this effect, reports of FeFETs and FTJs with a semiconductor contact are often of gradual shifts of threshold voltage or rapidly decaying memory windows.^{354,358} Methods to overcome this mismatch will be crucial for future reliable device implementations.

3. Advances in science and engineering to meet these challenges

To meet the challenges presented above, some promising advances to be pursued will be outlined in the following. First of

all, “electrode replacement” procedures have been reported in which a top electrode is first used to achieve best possible FE properties, after which the electrode is removed, including a potential interfacial layer, and replaced by another metal suitable for the application.³⁵⁹ This method was successfully used to reliably design FTJs using a TiN/HZO/W structure during crystallization and various replacement top electrodes (W, Cr, Ni, Cr/Ni).³⁶⁰ A major benefit of this approach is to separate out the considerations of the FE synthesis from the device design considerations. So far, this method has been used only for the top electrode, which is easily accessible. If the same procedure could be used for the bottom electrode as well, it would open for even greater freedom in the device design as well as improved reliability via the complete removal of interfacial layers created during the crystallization process. Possibly, this could be realized in a 3D device process similar to that of 3D NAND Flash.

To counteract the generation of oxygen vacancy-type defects during electric field cycling, it could be beneficial to make use of electrode materials that are prone to reduction rather than oxidation. For example, metallic RuO₂ and IrO₂ have negative oxidation potentials and can therefore supply oxygen to the HfO₂. These electrode materials have been recently reported to greatly improve endurance over TaN and TiN electrodes,^{337,353} and further research in this direction appears promising to achieve reliable ferroelectric devices beyond 10¹⁰ cycles of operation.

Another option is to target inert electrodes, which are also efficient diffusion barriers. The usage of a dielectric diffusion barrier, such as Al₂O₃, has been reported to help avoid defect migration across the electrode/HfO₂ interface,^{352,361} but the inclusion of an additional dielectric leads to voltage division and added depolarization field. Instead, a similar effect could be acquired through a diffusion-resistant metal. The elemental metals Pt and Pd are excellent diffusion barriers and are chemically inert. Pt top electrodes were successfully used to achieve endurance beyond 10¹¹ cycles in capacitors with epitaxial HfO₂,²¹⁹ but whether a similar performance is possible with polycrystalline films is not clear, given the moderate improvements so far reported.³⁵⁵ Further research adding these elements after crystallization using a replacement electrode process could be of interest. Other options are transition metal nitrides other than TiN and TaN, which are also chemically stable and have good diffusion barriers. Examples of these are MoN and WN.³⁶² HfN and ZrN are also attractive options, given that they are considered the most refractive of the nitrides and share the same metal anion species as hafnium zirconate FEs.

4. Concluding remarks

In conclusion, it is important to once more point out the central role of the electrodes in both the formation of the ferroelectric phase as well as their impact on device reliability and performance. For the future, it will thus be essential to find electrodes that are stable and provide reliable interfaces to the HfO₂-based FEs. Electrode replacement methods to separate crystallization from device design, as well as electrodes with negative oxidation potential, appear as good candidates for future work, while the mismatch between the polarization charge and the low charge density in semiconductor electrodes remains an outstanding challenge.

E. Laminated structures

Konrad Seidel and Maximilian Lederer

1. Status

The stability of the FE phase of HfO₂ and ZrO₂ is strongly influenced by mechanical stress, layer thickness, chemical composition, and other parameters. Depending on the application, certain thickness requirements are present. For example, FeFETs have HfO₂ layers with a thickness in the range of 10 nm. On the other hand, piezo- and pyroelectric sensors and actuators require much thicker layers in the range of 50 nm to 1 μ m. Since the window for stabilizing the FE phase in regard to thickness is very narrow, means to transfer the properties of, e.g., a 10 nm film to thicker layers are required.

On the other hand, the layer thickness has also a major impact on the microstructure and on reliability aspects, e.g., endurance. The grain size of polycrystalline HfO₂ or ZrO₂ films will, moreover, directly affect device variability. Consequently, it is of utmost importance to control and optimize the microstructure and reliability aspects for the device application.

In order to address the aforementioned constraints, multiple groups proposed laminated structures as a solution.^{347,363} These can be grouped into two different approaches: (i) dielectric/FE heterostructures and (ii) HfO₂/ZrO₂ superlattices (see Fig. 17). The former heterostructures are usually formed by depositing ultra-thin dielectrics, such as Al₂O₃, with a thickness of less than 1 nm between layers of (doped) HfO₂ or ZrO₂ of desired thickness and layer count. In such a manner, thick FE layers are achievable, which show no increase in the *m*-phase.³⁶³ By introducing them in devices, desired properties, e.g., a large memory window, can be achieved without suffering the penalties coming from non-ideal layer thickness.³⁶⁴ Alternatively, these dielectric/FE laminates can be used to influence the grain size and endurance of devices. By introducing additional dielectric interlayers into a FE thin film of a total thickness of, e.g., 10 nm, the crystal growth is interrupted, and smaller crystallites form. In addition, the interlayer act as barriers for leakage paths, thus improving device endurance.³⁶⁵

The superlattice approach, on the other hand, stacks ultra-thin layers of alternating HfO₂ and ZrO₂. Recent works have shown that by controlling the thickness of these sublayers, the grain size and endurance can be influenced.^{259,366,367} While the exact origin of this behavior is not understood in depth at the moment, a difference in nucleation and crystal growth originating from the different physical properties of HfO₂ and ZrO₂ has been suggested as an explanation.

2. Current and future challenges

While laminated structures offer very powerful methods to overcome thickness, grain size, or reliability limitations, they also face unique challenges. For the dielectric/FE laminates, one major challenge is the interfaces introduced by the dielectric layer. Like the electrodes, these interfaces will affect the phase stabilization slightly. Especially for laminates containing more than one interlayer, it has to be ensured that the layers stabilize in the FE phase. Small changes in the doping level might, therefore, be required. Moreover, these interfaces can act as pinning sites or introduce defects and introduce parasitic capacitances, resulting in a reduced polarization response

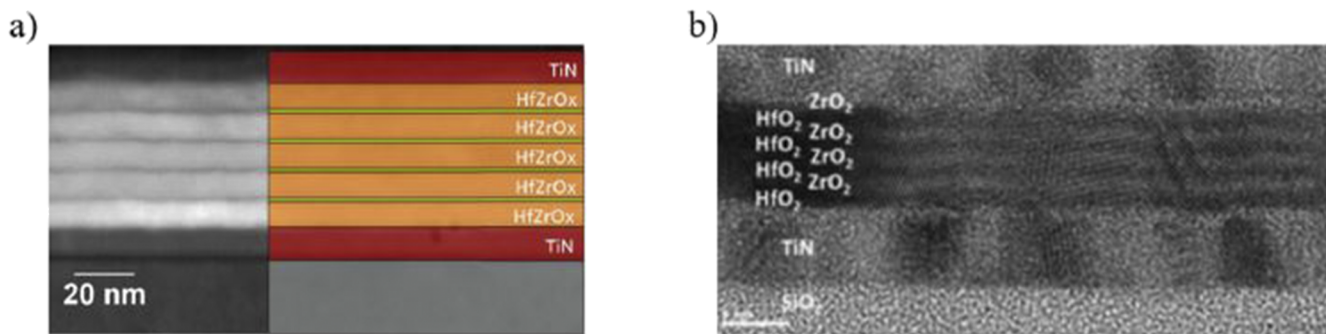


FIG. 17. Transmission electron microscopy images of laminated structures. (a) A dielectric/ferroelectric heterostructure consisting of $\text{Hf}_x\text{Zr}_{1-x}\text{O}_2$ and Al_2O_3 . In (b), a superlattice of hafnia and zirconia can be observed. Figures reproduced with permission from (a) Riedel *et al.*, AIP Adv. **6**, 095123 (2016). Copyright 2016, AIP Publishing LLC. Figures reproduced with permission from (b) Weeks *et al.*, ACS Appl. Mater. Interfaces **9**, 13440 (2017). Copyright 2017, American Chemical Society.

of the FE layer.³⁶⁵ Another challenge is the selection of the dielectric. As both materials, dielectric and FE, are oxides, interdiffusion has to be suppressed. Else, the interlayer might not be present after annealing or shifting the doping concentration of the $\text{HfO}_2/\text{ZrO}_2$ layer.

For the superlattices, on the other hand, the design freedom is constrained. While the sublayer thickness can be optimized, the total thickness is expected to be limited as the crystal growth is not stopped at the interfaces.³⁶⁷ Consequently, too thick layers are expected to transform to the *m*-phase. In addition, another challenge is the thermal budget. While $\text{HfO}_2/\text{ZrO}_2$ layers are excellently suitable for back-end-of-line applications, their application in front-end-of-line devices is strongly limited as degradation due to the high thermal budget is expected. Here, e.g., Si-doped hafnia excels due to its much higher crystallization temperature.

3. Advances in science and engineering to meet these challenges

Recent works, however, have showed possible routes to address these challenges. In the case of the dielectric/FE heterostructures, the doping level of the individual layers can be optimized in order to adapt to the changes brought forth by the interlayer interface. Similarly, combinations of differently doped HfO_2 layers have been reported and their interaction with each other via stress and mechanical stress has been discussed.⁹⁵ The models proposed herein, therefore, help us to understand how modifications of individual layers may affect the total response and allow, therefore, for optimizing and altering the ferroelectric response of dielectric/FE heterostructures.

In addition, the dielectric layer can be optimized in order to reduce defects/pinning sites at the interface while preventing interdiffusion. Therefore, recent works have explored alternative materials besides Al_2O_3 as dielectric interlayers, indicating that TiO_2 might be a suitable candidate.³⁶⁸ Nevertheless, other materials might be suitable as well, and further research will be required here.

On the other hand, the challenges for the superlattice approach can be addressed by using different compositions. Recently, it has been shown that the effects observed in the superlattice $\text{HfO}_2/\text{ZrO}_2$ structures are also present in Si-doped hafnia layers when altering the thickness of the SiO_2 -layers deposited during the atomic

layer deposition.⁹¹ Therefore, similar approaches might be suitable for enabling superlattice-optimized doped HfO_2 layers in front-end-of-line integrated devices.

Finally, the thickness limitation of superlattice structures might be overcome by combining this approach with the dielectric/FE approach, thus getting the advantages of both approaches while keeping the number of interlayers as low as possible.

4. Concluding remarks

In summary, both types of laminated structures, dielectric/FE heterostructures and superlattices, offer easy means to control the FE and reliability properties as well as the microstructure of HfO_2 and ZrO_2 layers. Moreover, heterostructures allow us to circumvent thickness limitations of the phase stabilization of the FE phase. For the future, however, further optimization of the two approaches will be required to meet current challenges. Here, optimization of doping levels in the HfO_2 and ZrO_2 layers is of importance as well as different materials should be screened for improving defect densities at interfaces or temperature stability. Nevertheless, recent results point toward promising solutions to these challenges.

F. Thickness scaling

Akira Toriumi and Shinji Migita

1. Status

The thickness scaling of FE HfO_2 will be discussed from two points of view for advanced electronic device applications. One is how the FE properties of HfO_2 are physically altered, and the other is how they are electrically affected by reducing the thickness of FE HfO_2 . FE HfO_2 was already 10 nm thick when it was discovered.⁶⁰ It is suggested that the FE origin of HfO_2 is physically different from that of other conventional FE materials and that several inherent properties of HfO_2 are involved in the appearance of the ferroelectricity. Considering the surface/volume ratio of each crystalline unit in polymorphic HfO_2 , the thickness reduction thermodynamically favors the more symmetric orthorhombic and tetragonal over

the monoclinic phase.³⁶⁹ The FE phase in HfO_2 is also theoretically expected to be more stabilized under appropriate boundary conditions, such as combined effects of strain and electric field.³¹ Furthermore, the impact of electrode interfaces on thin FE HfO_2 can be very critical, as it has been extensively studied for other FE oxides.³⁷⁰ Currently, FE properties are obtainable in MFM capacitors with 5–10 nm thick doped HfO_2 . The correlation between remanent polarization ($2P_r = P_r^+ + P_r^-$) and FE- HfO_2 thickness ($d_{\text{FE},\text{HfO}_2}$) is shown in Fig. 18.^{362,371,372} Further research was carried out for 1 nm thick HfO_2 on an oxidized Si substrate using PFM.¹⁹

The thickness scaling raises several issues depending on the application-specific requirements. The first issue to be addressed is the reduction of the operating voltage in FE devices since lower power consumption is a key requirement for the latest semiconductor devices. Under the assumption that E_c remains almost unchanged with the decrease in $d_{\text{FE},\text{HfO}_2}$,²⁷² the MFM capacitor can respond normally to the scaled voltage, and the polarization switching speed does not deteriorate, in principle. However, the tunnel leakage current significantly lowers the effective bias voltage applied to the FE layer as $d_{\text{FE},\text{HfO}_2}$ continues to decrease. To make matters worse, E_c in FE HfO_2 is relatively high compared to other FE materials, which limits the thickness scaling in MFM capacitor-type devices, although a wide energy bandgap of HfO_2 (~5.5 eV) is beneficial for suppressing the leakage current.

FeFETs and FTJs are attractive devices for advanced memory applications in addition to conventional FeRAMs. From the device designing viewpoint, a non-polar interface layer is often inserted between the FE layer and the semiconductor to avoid the degradation of FeFETs, while it is usable for achieving the higher tunnel current ratio in FTJs. Therefore, application-specific scaling scenarios that differ from the simple MFM capacitor have to be developed.

2. Current and future challenges

The maximum of $2P_r$ in Fig. 18 is in the range of 5–10 nm for all samples independent of different dopants, electrodes, or thermal treatments. Post-metallization-annealing (PMA) is better than post-deposition annealing (PDA) for obtaining improved FE properties,

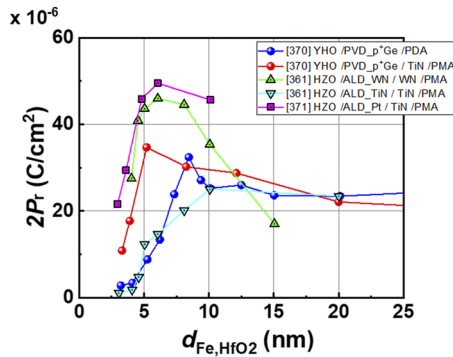


FIG. 18. $2P_r - d_{\text{FE},\text{HfO}_2}$ correlations for Y-doped HfO_2 (YHO) and $\text{Hf}_{0.5}\text{Zr}_{0.5}\text{O}_2$ (HZO) with different electrodes and thermal recipes. [x] denotes the reference number. In all cases, P_r exhibits a peak at $d_{\text{FE},\text{HfO}_2} = 5\text{--}10\text{ nm}$ and sharply decreases with the decrease in $d_{\text{FE},\text{HfO}_2}$. The polarization disappears at $d_{\text{FE},\text{HfO}_2} = 2\text{--}3\text{ nm}$.

especially in the sub-10 nm region. P_r decreases sharply with the decrease in $d_{\text{FE},\text{HfO}_2}$ below 5 nm in all cases. In contrast, it decreases gradually or remains flat with the increase in $d_{\text{FE},\text{HfO}_2}$ above 10 nm. A significant influence here is the interaction of the FE layer with the electrodes, in addition to the intrinsic effects involved in the FE layer thickness reduction. The electrode controls oxygen in and out-diffusion of the HfO_2 layer and forms non-polar and polar layers or leads to a diffusion of electrode material into the FE layer.

At present, it is difficult to experimentally observe a sufficient polarization switching signal in MFM capacitors with 2 nm thick doped HfO_2 . Structurally, non-FE crystalline phases or non-crystalline portions are more likely to be detected in XRD patterns and TEM images in the sub-5 nm thickness region. Therefore, a thorough and detailed optimization of the thermal treatments of HfO_2 with different dopant species and concentrations is required to explore the possibility of a sufficient P_r down to 2 nm. Otherwise, the application of ultra-thin FE HfO_2 films with scattered polarized regions will be limited in the microelectronics industry.

Interactions at the FE/electrode interfaces have been studied from various aspects, including a depolarization field and/or a non-switchable dipole formation at the interface.³⁷³ Since these effects generally destabilize the ferroelectricity at the interface, except in special cases,^{19,31} it is crucial to elucidate what happens physically at the FE HfO_2 interfaces.

From the viewpoint of ultra-thin FE film applications, the reduction of the effective bias voltage applied to the FE film due to the tunnel leakage current is related to the external impedance outside the MFM capacitor, which degrades the polarization switching speed as well as affects the dynamics of the polarization charge screening.

Currently, ALD is the most promising method for uniformly growing ultra-thin films. However, it is challenging to deposit doped HfO_2 films in an atomically uniform manner even after the thermal annealing because HfO_2 and dopant layers are deposited alternately or by using a cocktail of precursors. This can be a fundamental concern to the device-to-device variations in scaled FE integrated circuits because the ferroelectricity in doped HfO_2 originates from the metastable *o*-phase formation, which is likely to be affected by the variability in dopant position, particularly in ultra-thin FE HfO_2 films.

3. Advances in science and engineering to meet these challenges

A recent theoretical analysis predicts that ferroelectric switching is possible in one unit cell because a non-FE spacer separates the polarization within the unit cell, and the inter-cell interaction is expected to be very weak laterally.²³ If each unit cell can respond to the electric field independently, then the thinning limit could be one unit cell of the FE HfO_2 . However, if the FE phase metastability of the polycrystalline doped HfO_2 layer is considered, two or three unit cells without direct contact with electrodes are a reasonable estimate for the minimum $d_{\text{FE},\text{HfO}_2}$ (1–1.5 nm). Furthermore, the interface layers contacting the top and bottom electrodes tend to be non-FE because the metastable state must be sensitive to small structural and/or electronic perturbations. Therefore, two unit cells at the interfaces or one unit cell in the case of a harnessing-strain interface^{19,31} may be added, resulting in a total thickness of 1.5–2.5 nm. The oxide electrode may be advantageous for a more

intimate interface. Nevertheless, a charge redistribution at the interface may form a new interfacial dipole, destabilizing or weakening the ferroelectricity.

A small P_r (around $1 \mu\text{C}/\text{cm}^2$) can currently be detected even in sub-2 nm thick HfO_2 ³⁷⁴ because only a small fraction of the α -phase is viable in the ultra-thin HfO_2 films. Meanwhile, it has been reported that ferroelectricity has been detected in 1 nm thick ZrO_2 on SiO_2 ³⁷⁵ and that ultra-thin ZrO_2 on SiO_2 exhibits the thickness-dependent in-plane AFE-FE transition.⁶⁸ Although this is not included in the present discussion in terms of the practical applications, it is thermodynamically conceivable that the structural transformation between multiple non-monoclinic phases may occur more readily in ZrO_2 than in HfO_2 .³⁶⁹

Based on the theoretical inference and the current state of experimental achievements, the key to the successful thickness scaling of FE-doped HfO_2 will be to elucidate the interface-driven kinetics of FE phase stabilization. Even if further scaling of $d_{\text{Fe},\text{HfO}_2}$ is possible, it becomes difficult to reverse the polarization due to the effective bias reduction. The insertion of paraelectric layers to suppress the leakage current and to effectively lower E_c by exploring the depolarization field may be a technical challenge for the use of ultra-thin FE HfO_2 .

4. Concluding remarks

The minimum thickness capable of exhibiting FE properties in doped HfO_2 is ideally expected to be 1–1.5 nm. Considering possible interactions with electrodes, it will inherently be above 2 nm to exhibit sufficient polarization in the MFM capacitor. Of course, electrode materials and thermal annealing recipes will need to be rigorously scrutinized. In addition, the tunnel leakage current in ultra-thin doped HfO_2 hinders the application of a sufficiently high electric field on FE layers, which electrically limits the scaling of $d_{\text{Fe},\text{HfO}_2}$ in FE doped HfO_2 . These challenges need to be addressed together with the area scaling and operating frequency. Finally, it is worth mentioning that statistical variations in the performance of each FE device may inevitably accompany semiconductor chips equipped with high-density FE devices using ultra-thin FE-doped HfO_2 .

VII. DEVICES

A. Ferroelectric random access memories

Ruben Alcala and Uwe Schroeder

1. Status

The concept of a FeRAM is not new among emerging memory devices. In fact, the first iterations of this technology reached the market around the 1990s and employed perovskite structured PZT or layered perovskite $\text{SrBi}_2\text{Ta}_2\text{O}_9$ (SBT) FE materials.³⁷⁶ Unfortunately, the high thermal budget, hydrogen sensitivity, and unavailability of advanced deposition techniques for the complex perovskite materials resulted in this technology reaching a dead-end at the 130 nm process generation.^{376,377} Ultimately, this drove the technology toward limited niche applications. That said, the discovery and development of ferroelectric doped HfO_2 and HZO have brought a

new wave of FeRAM developments that surpass the previous limits encountered with PZT and SBT and, therefore, have re-attracted attention among emerging memory devices.³⁷⁶

The basic implementation of FeRAM technology consists in replacing the dielectric layer of the capacitor in a modified one transistor-one capacitor dynamic random-access memory (1T-1C DRAM) structure with a FE material and introducing a pulsed plate line, as shown in Fig. 21. The main goal is to have a similar performance and cell size to traditional DRAMs yet also be non-volatile and therefore finally realize a competitive nonvolatile RAM (NVRAM) technology. Regarding HZO, in particular, most major memory companies are currently assumed to have some sort of HZO-based FeRAM development program. As shown in Table I, development has not yet reached DRAM levels with respect to certain operation parameters, but significant progress has been achieved in the last few years. Even more so, FeRAM memory cells have been integrated into Mbit and Gbit arrays using standard BEOL integration flows.² Due to an ultra-low power read/write operation ($<5 \text{ nJ}/\text{pulse}$),³⁷⁸ the power consumption of FeRAM is similar to that of DRAM and static random access memory (SRAM) and several orders of magnitude lower than that of flash memory.³⁷⁹ Furthermore, a non-volatile FeRAM does not need to be refreshed after 16–64 ms as a DRAM.

For HZO-based FeRAM to contend in a broader range of applications, certain technological challenges still need to be addressed. Although not independent, these challenges or limitations can be divided into component-level and structure-level issues.

2. Current and future challenges

At the component level, the HZO-based ferroelectric capacitor of the 1T-1C structure is the most critical component since it is responsible for data storage, and the rest of the structure is a derivative of the already mature 1T-1C DRAM technology. Extensive literature regarding the optimization of the said component indicates that the state of the art of such a device is a capacitor with a roughly 8–10 nm thick HZO FE layer that has E_c of about $\pm 1.5 \text{ MV}/\text{cm}$, can obtain $2P_r$ of around $40 \mu\text{C}/\text{cm}^2$, has a switching latency in the ns range (comparable to DRAM cells), and has a reduced wake-up effect.⁸ Notwithstanding, it is important to consider what voltages can be supplied to the CMOS circuitry outside the memory array. E_c of $\pm 1.5 \text{ MV}/\text{cm}$ requires even higher fields to switch all domains. Here, companies are interested in reducing the switching voltage to 1 V with narrow switching characteristics to keep voltages in the CMOS circuitry as low as possible.

When discussing the reliability of a FE capacitor, there are two main metrics: field cycling endurance and polarization retention. Ideally, a breakdown-free device with no retention degradation in a 10-year time-frame is desired. Unfortunately, from an operational point of view, opposing paths improve each metric, that is, a lower applied voltage to switch the FE capacitor allows for an improved endurance but leads to worse retention and vice versa.^{8,380} A lower applied voltage could be compensated by increasing the pulse length up to a certain point, but this would slow down the operation speed.³⁸¹ Hence, a time-voltage trade-off exists, and a compromise is required. From a material perspective, improvement of the capacitor stack, such as reducing the defect density at the electrode-FE interface, can minimize charge injection or charge

movement in the FE layer, leading to a retention and endurance enhancement. This would be of particular interest for solving the prevailing imprint problem that these FE capacitors exhibit regarding retention.^{7,8} Improving P_r is no longer an objective since most values reported in literature can be sufficient. In fact, a second compromise is needed here, regarding sufficiently high P_r for memory performance and not too high of P_r for improved reliability, since larger P_r values enhance both aforementioned charge degradation effects.

When looking at the complete memory array and the read-out circuit, additional factors must be considered for an optimized operation. A proper read-out will depend on the potential difference between a “1” programmed state and a “0” programmed state in relation to a reference voltage (provided either as a fixed voltage or from a reference cell) at the sense amplifier. Therefore, it is not necessary to have the largest possible $2^* P_r$ but rather only one large enough for a desired capacitor area to maintain a stable memory window. On the other hand, the bit line (BL) capacitance, unfortunately, adds a lower threshold to the acceptable $2^* P_r$ values.⁷ Furthermore, larger arrays will have a larger BL capacitance; therefore, alternative design layouts may be required for optimal sensing. Additionally, in order to assure high yields, high uniformity during semiconductor processing and packaging, as well as stability during thermal processing steps and later soldering during package mounting, must be assured.²

In order for FeRAM to increase its market relevance, not only does a large memory capacity need to be possible but also memory density, in other words, the cell size, has to be improved since this is the main contributor to the cost of the memory device. Most current literature focuses on 2D structures not stepping beyond the 130 nm technology node. For more advanced technology nodes, a more aggressive capacitor scaling in the 3D direction must be implemented, as has been done for other memory technologies, such as DRAM. In this regard, first results for Gbit-sized arrays have already been published.¹

3. Advances in science and engineering to meet these challenges

On the capacitor side, it is still necessary to improve reliability. As discussed, charge injection and movement need to be reduced to enhance endurance and retention. Here, a lower switching voltage; a stable P_r , which is not too large; and a low defect density at the electrode interface and within the bulk of the FE layer are required.⁸

Regardless of what is yet to come in the development of the 1T-1C FeRAM structure, significant advancements have already been reported, mostly in the 16 to 64 kbit range,^{2,5-7} but also reaching capacities of up to 8 GB.¹ Considering this and the fact that not as large aspect ratios are necessary for similar architectures to DRAM,⁸ it may be the case that the cost-effectiveness of this technology could eventually reach or surpass DRAM values and even have a simpler path toward further down-scaling.

Alternatively, additional structures to the 1T-1C FeRAM have been proposed as emerging technologies. Some seek to improve the 1T-1C FeRAM structure, and others aim to provide an alternative operation but maintain the familiar structure. Regarding the former case, one can mention, first, the 2T-1C FeRAM structure, which implements an additional transistor for pre-charging the BL node and allows for an easier read-out of smaller structures but has

the disadvantage of higher variability,³⁸² and, second, the use of an AFE behaved material instead of a traditional FE for an improved endurance of the capacitor and apparent reduction of the coercive field.³⁸³ In the latter case, a more complex 2T-2C FeRAM structure has been proposed for local logic operations at the memory cell level.³⁸⁴ Regardless of the optimization path, the development of HZO-based FeRAM technology shows promising results for the coming years.

4. Concluding remarks

From the current standpoint of this technology, it would be unsurprising if a new generation of HZO-based FeRAMs start popping-up on the market in the next couple of years. The remaining optimization may come as a second- or third-generation iteration of this new wave of memories. Similar to other already commercialized memory technologies, in the end, the market success of this technology will be dictated by its cost-performance relation compared to alternative technologies and solutions. For instance, perhaps the first products may use a 2T-2C configuration to overcome reliability issues at the expense of a higher real-estate, and therefore cost, but subsequent generations could be finally achieved using the 1T-1C variant for a high-density nonvolatile RAM technology, a memory technology, which is still heavily sought after today.

5. Acknowledgments

R.A. was funded by the German Research Foundation (DFG)—Project Nos. 430054035 and 433647091.

B. Ferroelectric field-effect transistors

Sayeef Salahuddin and Michael Hoffmann

1. Status

In its simplest form, a FeFET is essentially an ordinary field effect transistor where the gate oxide is replaced by a FE material, as shown in Fig. 21. When the polarization inside the ferroelectric gate oxide is switched with a voltage, it shifts the threshold voltage of the transistor. In an appropriately designed transistor, this shift in the threshold voltage could lead to orders of magnitude change in the drain current. In this way, two different states of the polarization translate to two different current levels for the transistor. The potential benefits of such a device are game-changing.³⁸⁵ Unlike the other prominent memory devices, such as resistive random access memory (RRAM), phase change random access memory (PCRAM), or Magnetic Random Access Memory (MRAM), the memory element is not connected to the drain of the transistor—a combination that impedes the drain current due to added resistance. This means that READ speed is only determined by the performance of the transistor action and potentially the same READ speed as an SRAM could be possible. The ferroelectric switching speed of HfO_2 - and ZrO_2 -based materials is determined by reverse domain nucleation and growth dynamics, which have been shown to be faster than 300 ps, suggesting that even single digit picosecond switching speed is possible.¹⁴⁰ The footprint of the device is also just that of a single transistor, which is substantially smaller

than a standard SRAM cell that needs six transistors. Furthermore, the device needs minimal changes to the transistor fabrication flow—just a single additional mask is sufficient—indicating that any additional cost of manufacturing would be minimal.³⁸⁶ In addition, the FeFET enables memory cell constructs that offer new ways of doing in-memory-computing in both the digital and analog domains.^{387,388} However, critical challenges remain in terms of material optimization and device design that need to be overcome to materialize the potential benefits of FeFET technology.³⁸⁶ In the following, we provide a brief discussion of these challenges and present a roadmap of advances that are necessary to address them.

2. Current and future challenges

A key consideration for FeFETs is the fact that they are much more than the ferroelectric material itself—in fact, the ferroelectric film, together with an appropriate design for the transistor device, dictates the ultimate performance of the device. If one considers a simple MFM capacitor, one would like to optimize the material for the smallest E_c and smallest thickness (t_{FE}) to scale down the switching voltage as much as possible. However, in the FeFET device, this cannot be done. The semiconductor channel and any interfacial layer beneath the FE act as a dielectric material in series. This introduces a depolarization field (E_d),³⁸⁹ which, if larger than E_c , could completely diminish the memory behavior. E_d is inversely proportional to t_{FE} , meaning that t_{FE} cannot be scaled down arbitrarily. This means that the operating voltage (V) will be limited by these considerations. Another important parameter is the polarization (P). The shift in the threshold voltage of the transistor is proportional to P —indicating that large P is desirable. On the other hand, large P generates a large electric field in the interfacial layer, breaking it down and leading the transistor to stop working.²⁴⁵ In this case, even if the FE film is working fine, the endurance of the FeFET is limited substantially. Finally, the speed of the ferroelectric switching, in its simplest form, is dictated by an activation process—meaning that the larger the applied field compared to E_c , the exponentially faster the speed of switching.¹⁴⁰ However, applying a large electric field comes at the expense of a large operating voltage and faster oxide breakdown, which impacts endurance. These competing considerations show that a very carefully designed device and material is necessary to obtain the desired memory behavior.

Continuing along the same lines, non-ideality in the devices, unfortunately, plays a dominant role in the device behavior. Most debilitating among them is charge trapping.³⁹⁰ Band offsets between the FE and the semiconductor or interfacial layer are conducive to charge trapping. In addition, if the chemical compatibility between these dissimilar materials is weak, the dangling bonds act as a charge-trapping center. Moreover, if the electric field in the interfacial layer is too strong, as mentioned above, new bonds break every time the FE polarization is switched, increasing the number of trapped charges. The trapping and de-trapping lead to its own hysteresis, in direct analogy to today's FLASH memory devices, whose handedness is opposite to the FE hysteresis. This diminishes the FE memory action. In addition, trapped charges can screen out the polarization, further reducing memory performance.

3. Advances in science and engineering to meet these challenges

It is known from high-metal-gate studies that an oxide thickness <4 nm can effectively eliminate charge trapping in the oxide by substantially speeding up trapping/detrapping processes. This advocates for thinning down the FE oxide as much as possible. Scaling down the thickness is also necessary to scale down the channel length of FeFET devices. For FeFET with $L_G < 20$ nm, an effective oxide thickness (including the FE oxide and interfacial oxide) needs to be ~ 1 nm so that good I_{ON} , I_{OFF} characteristics can be obtained. Hafnium Oxide (HfO_2)-based FE films are, therefore, most appropriately suited for scaled FeFET applications as they retain a high enough E_c to overcome an increased depolarization field even when thinned down to very small thickness.³⁹¹ Indeed, ferroelectricity has been demonstrated in HfO_2 films as thin as 1 nm.¹⁹ On the other hand, thickness scaling increases the capacitance of the FE layer, thus shifting the share of the applied voltage from the FE layer to the underlying MOSFET. Therefore, scaling of the thickness has to be balanced by increasing the effective capacitance of the MOSFET (without the FE) itself. In this regard, it has been shown that increasing the permittivity of the interfacial layer helps lower the operating voltage.²⁴⁷ As an added benefit, it reduces the total electric field in the dielectric layer,²⁴⁵ which reduces oxide breakdown, in turn exponentially increasing the endurance. Endurance of $\sim 10^{12}$ cycles has been demonstrated.²⁴⁷ However, changing the interfacial layer brings the question of chemical compatibility of the interface. The overall effect would be negative if a higher permittivity interfacial layer introduces significantly more dangling bonds.

In recent days, several reports have demonstrated FeFET structures without using any interfacial layer, especially on oxide semiconductor channels in the context of monolithic 3D integration of FeFET technology.³⁹²⁻³⁹⁴ If these efforts are successful, the operating voltage could substantially reduce as any voltage drop associated with the interfacial layer is now eliminated. However, chemical compatibility of the FE layer with various oxide semiconductor channels needs further investigation. Interface defects could cause substantial polarization screening as mentioned before. This structure could also be more prone to READ disturb as hot electrons could easily get injected into the FE layer since no interfacial dielectric impedes their momentum. Overall, Si/SiO_2 and SiO_2/HfO_2 interfaces are the most well-studied and most optimized interfaces for transistors. Therefore, controlled modification of these interfaces could lead to the most optimized FeFET performance. FeFETs based on other interfaces will need similar optimization efforts that have gone into $Si/SiO_2/HfO_2$. There is always a place for new FE materials. However, as discussed above, any new FE material needs to be scalable to very small thicknesses, requiring high E_c . In addition, if the background permittivity can be made small, it will help the FE layer to get the lion's share of the applied voltage in the capacitance divider. Another desired property will be the abruptness of switching. A very abrupt switching will reduce the amount of field needed beyond E_c for fast switching.³⁹⁵ Finally, a large band-offset with the semiconductor channel is necessary to reduce the injection of carriers into the oxide.

4. Concluding remarks

While challenges remain in obtaining the most desirable characteristics from a FeFET device, we note here that the FeFET

uniquely combines high speed, low power, and small footprint, which makes it attractive for applications at various levels of the memory hierarchy. Additionally, in recent years, many demonstrations have shown their use for various unconventional compute paradigms, such as content addressable memory (CAM), non-volatile logic, and analog in-memory computing. Even in their current state, FeFETs provide a very efficient on-chip memory for edge artificial intelligence (AI) applications where frequent READS and non-volatile storage of the weights are primary requirements. FeFETs with FE HfO_2 layers are already available in highly scaled, 22FDX technology.³⁹⁵ If the remaining challenges of endurance and operating voltage can be overcome, FeFETs will usher in a completely new era in computing.

C. Ferroelectric tunnel junctions

Beatriz Noheda

1. Status

Arguably, ferroelectric tunnel junctions (FTJs) are the devices that can benefit the most from the advantages that HfO_2 -based ferroelectrics present with respect to other ferroelectrics. FTJs rely on ultra-thin layers, with thicknesses below 5 nm (in fact, well below this value for large bandgap materials, such as HfO_2), such as to allow for sufficient electron tunneling between the two electrodes, as shown in Fig. 21. At the same time, a robust polarization, and its imperfect screening at the asymmetric electrodes, is required to modify the average barrier height upon switching, modulating the transmission of electrons and achieving the *so-called* Tunneling Electroresistance (TER) effect.^{396–398} The appearance of polarization at the nanoscale in HfO_2 FEs, resisting depolarization, makes these materials the best candidates for FTJs. First demonstrations of Hf-based FTJs report TER values of 20 for a 2.8 nm tunnel barrier using the standard method of probing the conductance with the tip of an atomic force microscope.³⁹⁹ However, the large bandgap energies (~ 6 eV) of these materials have allowed for fabricating stand-alone FTJ devices detached from the atomic probe microscope.^{400,401} These devices, made out of 1.5–2 nm tunnel barriers of $\text{Hf}_{0.5}\text{Zr}_{0.5}\text{O}_2$ operate even with electrodes as large as $30 \times 30 \mu\text{m}^2$ without suffering from significant leakage, which is unprecedented, and show on/off ratios as large as 50. Thus, the advent of HfO_2 -based FEs represents a milestone toward the utilization of FTJs in integrated devices. The implications of this development are vast because FTJs are not only able to map the equilibrium polarization states into two-level resistance states of the device (TER effect) but can also display non-volatile multi-level resistance arising from the partial switching of FE domains, giving rise to a ferroelectric memristor.⁴⁰²

2. Current and future challenges

The thickness of the ferroelectric layer can be decreased further down to 1 nm, even on Si substrates, using ALD deposition, and these devices have shown TER values above 200 and tunneling currents above 1 A cm^{-2} .³⁵⁴ In general, HfO_2 -based devices present very good device-to-device reproducibility, even for those

that use growth techniques for which fine control is more challenging, such as PLD. However, the devices display cyclability issues. This has to do with the relatively large switching fields that approach the breakdown fields in these materials, moving oxygen vacancies across the layer, similar to resistive switching memory devices. Therefore, a robust effect is often found only at low driving voltages, for which ion migration is unimportant.^{142,223,306,401–405} However, under these conditions, reported TER values are reduced to about 5.⁴⁰⁰

Therefore, the great challenge is to design HfO_2 -based nanoscale FEs with smaller switching fields. For that, our understanding of the nature of the switching needs to be improved. The scarcity of observations of domain growth during the application of an electric field,⁵¹ as well as the dependence of the switched polarization with the magnitude and duration of the electric pulses, points to a switching mechanism whose dynamics is determined by the nucleation of domains,^{406,407} which could be a manifestation of intrinsic (non-cooperative) dipole switching. This would be consistent with the accessibility of the double-well energy landscape in these materials³⁸ and with the very particular features of the polar *o*-phase in HfO_2 : the structure is composed of polar and non-polar atomic layers parallel to the polarization direction, reducing dipole–dipole interactions and increasing the energy barrier for switching at the domain wall,²³ therefore promoting independent switching events.

Interestingly, some of the works mentioned above reporting epitaxial layers on LaSrMnO_3 -buffered perovskite substrates have shown that the ferroelectric layer is oriented along the (111) direction and has *r*-symmetry in $\text{Hf}_{0.5}\text{Zr}_{0.5}\text{O}_2$,²⁷ ZrO_2 ,^{264,408} and Y-doped HfO_2 .⁶⁷ These materials present large polarization values and no wake-up effect. Even though interpretations on the nature of this rhombohedrally distorted phase differ,^{26,27} they point to the absence of non-polar sublayers, which are expected to increase dipole–dipole interactions and lower the coercive field with respect to the *o*-phase. However, the experimental switching fields are still large (actually larger, probably due to the clamping of the layer due to the epitaxy). Therefore, understanding the structural relationship between the differently observed polar phases is still a challenge in the field.

3. Advances in science and engineering to meet these challenges

It is interesting to note that amorphous HfO_2 was reported long ago as a promising tunnel barrier for magnetic tunnel junctions using Co and Fe as magnetic electrodes, with changes of tunneling magnetoresistance (TMR) up to 30%.⁴⁰⁹ The addition of ferroelectricity in crystalline HfO_2 , thus, opens an interesting avenue for multiferroic tunnel junctions (MFTJs).^{410,411} Moreover, the large spin–orbit coupling in HfO_2 can lead to measurable values of the tunneling anomalous Hall conductivity (TAHC),⁴¹² which may lead to new functionalities.

We mentioned above the prospect of using FTJs as memristive devices. Synaptic behavior, such as potentiation/depression of the conductance upon increasing the number of electric pulses and spike-timing dependent plasticity (STDP), has also been demonstrated in epitaxial tunnel junctions.^{407,413,414} Great progress has recently been achieved toward device integration, and memristive FTJs with a back-end-of-line compatible process have been fabricated using 3.5 nm $\text{Hf}_{0.5}\text{Zr}_{0.5}\text{O}_2$ thin films, obtaining current

densities of 10 mA/cm^2 for driving voltages around 0.5 V (orders of magnitude larger than previous reports), on/off ratios of 7 (excellent for pure ferroelectric switching) at reading voltages of 10 mV , and superb retention and endurance.⁴¹⁵ A simulated neural network with the synaptic characteristics of these devices has shown a recognition accuracy of 92% (in 36 epochs) for the MNIST database.

Due to the large bandgap of these materials, layers of three nm or thicker are not suitable for direct tunneling in FTJs. However, interesting synaptic behavior can be obtained with somewhat thicker layers, based on Fowler–Nordheim tunneling or thermionic emission, depending on the electric field range.⁴¹⁶ Another example is the use of a heterostructure formed by a 12 nm thick $\text{Hf}_{0.5}\text{Zr}_{0.5}\text{O}_2$ layer and a 2 nm Al_2O_3 layer placed between two electrodes. In this case, the $\text{Hf}_{0.5}\text{Zr}_{0.5}\text{O}_2$ layer is not the tunnel barrier. In addition, in this configuration, AlO_x could also play the role of blocking ion transport across grain boundaries and/or provide an oxygen source/drain, increasing the endurance of the FTJ junctions.⁴¹⁷

It is also possible to use a layer of HfO_2 thick enough that it cannot support direct tunneling, but it can become conducting thanks to doping. This is the case of the recently reported epitaxial Y-doped HfO_2 with a thickness of 4.5 nm .⁴¹⁸ In this case, a polarization-modulated transition from Schottky-barrier-controlled charge transport to Ohmic conduction is observed with an on/off ratio of up to 540. Extending the concept of tunnel junction to these other more complex structures (even if direct tunneling is not the mechanism in place) opens a large number of possibilities for device design and optimization in the near future.

Finally, recent technological improvements allow for engineering the top electrode independently of the rest of the device, leading to a much better understanding of the bottlenecks in device performance.³⁶⁰ A very interesting line of research may come from combining 2D semiconductors with HfO_2 -based FE films. TER up to 10^3 for biases below 1 V in $\text{Hf}_{0.5}\text{Zr}_{0.5}\text{O}_2$ FTJs has been reported with MoS_2 as the electrode.^{419,420} The future looks bright for FTJs.

4. Concluding remarks

Despite existing challenges concerning reliability, thanks to the advent of hafnia-based ferroelectrics and their unprecedented polarization retention behavior upon extreme miniaturization, FTJs that use $1\text{--}2 \text{ nm}$ thick layers as the tunnel barrier are, finally, a realistic option in the memory roadmap, both for the development of digital RAM as well as for memristive devices for brain-inspired information processing.

5. Acknowledgments

This publication is part of the project TRICOLOR (with Project No. OCENW.M20.005), which is financed by the Dutch Research Council (NWO).

D. Energy storage capacitors

José P. B. Silva

1. Status

The demand for reducing both CO_2 emission and the consumption of fossil fuels requires the long-term pursuit of renewable

and sustainable energy sources, such as solar, wind, hydroelectric, and tide energy. However, these energy sources are intermittent, and thus, there is a pressing need to develop high-power-density, efficient, low-cost, and environmentally friendly energy storage (ES) devices. The major advantages of the ES in dielectric capacitors are high ES efficiency, temperature, and cycling stability, as well as high power densities. On the other hand, regular dielectric capacitors cannot compete with the orders of magnitude higher ES of batteries or fuel cells. However, the so-called supercapacitors, which combine the high power density of capacitors with much higher energy storage density (ESD), are ideal for applications where a large amount of energy has to be stored and released in a relatively short time. Currently, high ESD electrochemical supercapacitors, which are mostly based on the double-layer capacitance and pseudocapacitance effects, are used, e.g., to stabilize the power grid, recover braking energy in electric vehicles, or provide a backup power supply for critical electrical systems. Recently, there has been increasing interest in purely electrostatic solid-state supercapacitors based on highly polarizable materials that can be used for powering electronics.¹¹⁰

In this context, FE HfO_2 - and ZrO_2 -based capacitors are promising candidates despite being scarcely investigated yet.⁴²¹ Figure 19 represents the best-performing ES parameters for different FE HfO_2 - and ZrO_2 -based thin film capacitors.

For instance, a 1.0 mol. %-doped La-doped $\text{Hf}_{0.5}\text{Zr}_{0.5}\text{O}_2$ -based capacitor shows ESD values of 30 J cm^{-3} , with an efficiency of 55%.⁴²² $\text{Hf}_{0.5}\text{Zr}_{0.5}\text{O}_2$ exhibits a stable FE behavior of up to 175°C with an ESD of 55 J cm^{-3} and an efficiency of 57%.²³⁸ Silva *et al.* also demonstrated that coupling of FE ZrO_2 thin films with a dielectric $\text{HfO}_2\text{:Al}_2\text{O}_3$ layer could enhance the ESD up to 54.3 J cm^{-3} with an efficiency of 51.3%.⁴²³ Das *et al.* showed that $\text{TiN/Hf}_{0.33}\text{Zr}_{0.66}\text{O}_2/\text{TiN}$ capacitors exhibit an ESD and efficiency of $\sim 31 \text{ J cm}^{-3}$ and $\sim 38\%$, respectively.⁴²⁴ Recently, FE- $\text{Hf}_{0.5}\text{Zr}_{0.5}\text{O}_2$ (1 nm)/AFE- $\text{Hf}_{0.25}\text{Zr}_{0.75}\text{O}_2$ (9 nm) bilayered capacitors have showed an ESD as high as 71.95 J cm^{-3} , with an efficiency of 57.8%. The capacitors also showed a stable operation of up to 150°C and 10^6 cycles.⁴²⁵ In addition, a giant ESD of 109 J cm^{-3} with an efficiency $> 95\%$ was obtained with a new concept of negative-capacitance, in which $\text{Hf}_{0.5}\text{Zr}_{0.5}\text{O}_2$ and a Ta_2O_5 layer are combined.¹¹⁰ Moreover, a stable operation of up to 150°C and 10^8 charging/discharging cycles was demonstrated.

2. Current and future challenges

Biaxially oriented polypropylene (BOPP) is one of the most commonly used commercial capacitor films.^{426,427} It is bulky, has an ESD of $< 7 \text{ J cm}^{-3}$ and a charge/discharge time in the μs range,^{428,429} and has a low maximum operating temperature of 105°C .⁴²¹ In order to achieve desirable ESD, a large capacitor bank with many rolls of the polymer film is usually employed. Besides that, ESD is obtained at high voltages, unfortunately bringing new challenges to the miniaturization and reliability of advanced electronics and electrical power systems.⁴³⁰ Therefore, improving the ESD and working temperature of these capacitors is of utmost importance. Moreover, there is a need to reduce the size, weight, and cost of the capacitor structures for cutting-edge pulse power technologies.

Other polymeric materials than BOPP, glass dielectrics, and perovskite materials are being investigated for ES capacitors, which show superior ESD than BOPP.^{429,431,432} Polymers and glasses can

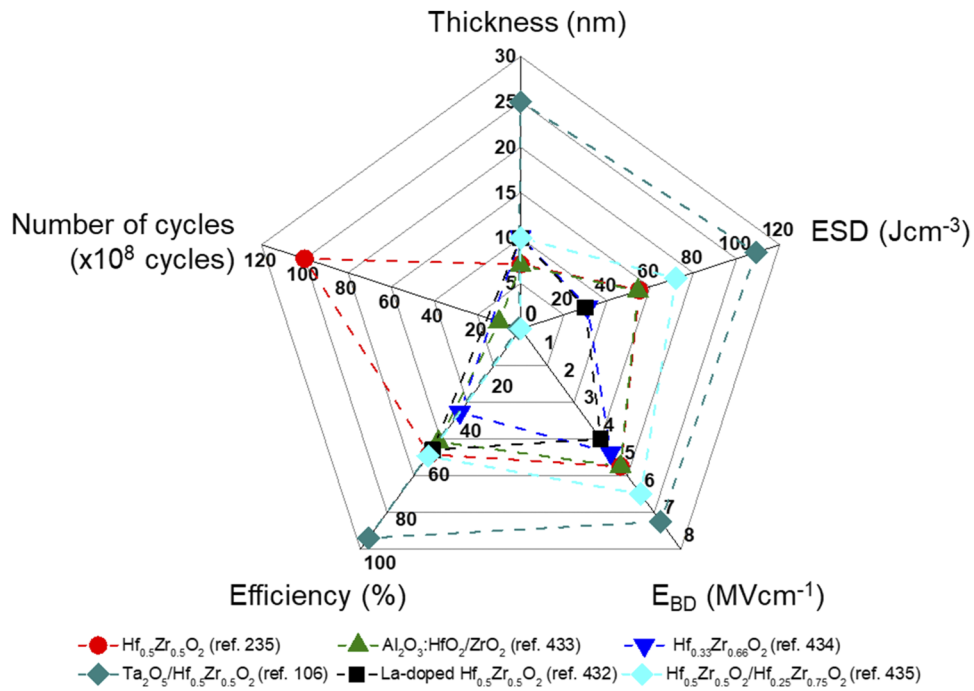


FIG. 19. Comparison of the energy storage performance obtained in FE HfO₂- and ZrO₂-based thin film capacitors. ESD = energy storage density; E_{BD} = dielectric breakdown field.

exhibit a very high E_{BD} (typically in the range of 1–10 MV/cm), but their low ϵ_r (typically <10) limits the ESD (<30 J/cm³).⁴³³ On the contrary, relaxor ferroelectrics (RFEs) and antiferroelectrics (AFEs) can display large ϵ_r values on the order of 100–1000, but they often suffer from relatively low E_{BD}, typically <500 kV/cm.⁴³³ Nevertheless, this results in a high ESD (>110 J/cm³), which is higher than the one observed in HfO₂- and ZrO₂-based capacitors.⁴²¹ However, HfO₂- and ZrO₂-based capacitors show promising physical properties that make them relevant for ES applications. Due to the large bandgaps of >5 eV and large conduction band offset when contacting nitride-based electrodes, FE HfO₂- and ZrO₂-based thin films exhibit low leakage current.³⁵⁸ This results in a very high dielectric breakdown field (E_{BD}) of up to ~5 MV cm⁻¹, which is desirable for ES applications. In addition, these materials can exhibit a high maximum polarization (P_m) of ~50 μ C cm⁻², while P_r can be adjusted from ~5 up to ~30 μ C cm⁻².²¹⁹ Another positive characteristic of HfO₂ and ZrO₂ films is their fast switching times, in the nanosecond range,⁴³⁴ and their robust FE polarization even at thicknesses as low as ~1 nm.¹⁹ This allows for the design of nanocapacitors for applications in miniaturized energy-autonomous systems. However, the ESD and efficiency are compromised by the large hysteresis loss and also by the higher E_c typical in the range of 1–5 MV cm⁻¹ in these materials.^{434,435} To compete with other promising materials, such as RFEs, it will be necessary to increase the ESD by ~50% to ~150–200 J cm⁻³, while keeping an efficiency of ~95%. To enhance ES performance, different strategies must be investigated. Moreover, to explore the full potential of the HfO₂- and ZrO₂-based capacitors for ES, the statistical breakdown strengths

E_{BD} via Weibull distribution fitting must be studied, which was not done yet.

In addition, it is important to optimize the ES properties of the FE HfO₂- and ZrO₂-based thin films; it is also important to mention that for the final application, the thickness of the substrate needs to be taken into consideration, which can significantly decrease the ES performance. Moreover, to meet the ES requirements of the automotive, power transmission, aerospace, oil, and gas industries, the temperature stability of the ES performance needs to be increased up to 250 °C,⁴³⁶ as shown for RFE ceramics and films.⁴²⁹ In addition, the performance of the capacitors should be investigated with continuous cycling and at high frequencies since most of the applications (e.g., high-frequency inverters) work at this regime.

3. Advances in science and engineering to meet these challenges

The FE properties in HfO₂- and ZrO₂-based thin films are widely being investigated. Different strategies are employed to enhance the FE polarization and reduce E_c in these films. For instance, defect engineering through ion bombardment proved to be an efficient way to improve ferroelectricity in HfO₂-based films.⁴³⁷ However, there is still no practical evidence on how much P_m can be enhanced and how this would enhance the ES performance of the devices. On the other hand, low E_c could be obtained via topological domain walls and phase boundaries, which leads to a significantly low intrinsic energy barrier for domain reversal and so allows for

rapid nucleation and growth of FE domains.^{50,144} This theoretical result still needs experimental validation, which should affect the ES performance of the capacitors.

Other strategies, such as strain, multilayer, and dead-layer engineering through deposition control, are proposed to also improve the ES performance of the capacitors and still need to be investigated in more detail.

The design of 3D nanostructures capacitors instead of the 2D ones should be investigated since they allow for much higher polarization and ESD. For example, in AFE ZrO₂-based capacitors, an enhancement of the ESD from 37 up to 937 J cm⁻³ has been obtained.³⁸³ Moreover, by integrating the FE-Hf_{0.5}Zr_{0.5}O₂ (1 nm)/AFE-Hf_{0.25}Zr_{0.75}O₂ (9 nm) bilayered capacitor into deep silicon trenches, an enhancement of the ESD from 71.95 up to 364.1 J cm⁻³ was achieved.⁴²⁵ In addition, from the Weibull distributions of the extracted maximum ESD and efficiency, it is possible to conclude that while the planar capacitors display excellent electrical uniformity, the 3D capacitors have a narrow distribution of maximum ESD. On the other hand, both the planar and 3D capacitors exhibit very close efficiencies, corresponding to 57.8% and 56.5%, respectively. Recently, negative-capacitance AFE-HZO superlattice films integrated into 3D Si capacitors have established record-high ESD (80 mJ cm⁻²) and power density (300 kW cm⁻²).¹⁹ However, there are no studies about 3D ES capacitors based on FE HfO₂- and ZrO₂-based thin films.

HfO₂- and ZrO₂-based thin films have also demonstrated in-plane polarization,^{68,210} and in the case of ZrO₂ films,⁶⁸ it would allow for the application of a high voltage (~60 V), which could be beneficial for some applications where high voltages are needed. However, the active capacitor area is reduced, and the material under the electrodes has nearly zero electric field, which can be detrimental for ES applications. Therefore, in-plane devices can also be investigated for ES applications.

Shaping the size of ferroelectric nanodomains is also envisaged to impact the ES performance of the devices, as observed in the case of RFEs where a superparaelectric state is achieved.⁴³⁸ In this state, the nanodomains are scaled down to polar clusters of several unit cells so that polarization switching hysteresis is nearly eliminated while relatively high polarization is maintained. In this case, Pan *et al.* showed an ESD of 152 J cm⁻³ with improved efficiency (>90% at an electric field of 3.5 MV cm⁻¹) in samarium-doped bismuth ferrite–barium titanate films.⁴³⁸ Moreover, a high Weibull modulus β of 14.9 is achieved, indicating narrowed distributions of E_{BD} data and improved film uniformity. The strong relaxor features in the superparaelectric films lead to temperature-insensitive dielectric properties. Therefore, the ES performance is stable over a wide temperature range (173–423 K), with an energy density variation of <6% and an efficiency variation of <13%. A similar strategy was already used in Hf_{0.2}Zr_{0.8}O₂/Al₂O₃/Hf_{0.2}Zr_{0.8}O₂ capacitors.⁴³⁹ A high ESD of 87.66 J cm⁻³ and efficiency of 68.6% together with large breakdown strength of 5.5 MV cm⁻¹ were achieved in the Hf_{0.2}Zr_{0.8}O₂/Al₂O₃/Hf_{0.2}Zr_{0.8}O₂ capacitors.⁴³⁹ However, using this strategy, the ESD and efficiency are still far from those observed in samarium-doped bismuth ferrite–barium titanate films. More investigations need to be done to further enhance the ES performance of HfO₂- and ZrO₂-based capacitors.

4. Concluding remarks

In summary, while much progress has been made over the past 10 years with regard to an understanding of the FE properties in HfO₂- and ZrO₂-based thin films, significant work remains to be done, despite these materials exhibiting fascinating properties, regarding the possibility of application of these materials in ES.

HfO₂- and ZrO₂-based capacitors enable next-generation pulsed power systems due to their superior material properties, allowing for improved ES performance compared to commercial dielectric BOPP capacitors. Multiple strategies, such as composition, doping, dead-layer engineering, and the use of negative-capacitance effects, among others, have successfully improved the ES performance of the devices. It is anticipated that a combination of these strategies will lead to further improvement in performance. To compete with other materials, such as RFE thin films, the ESD and efficiency need to be improved in terms of ES performance. Moreover, a better understanding of the ES performance at high frequencies and temperatures as well as the statistical breakdown strengths E_{BD} via Weibull distribution fitting is needed to evaluate the potential impact of the HfO₂- and ZrO₂-based capacitors in the ES sector. Finally, novel strategies are proposed to enhance the ES performance of the devices.

5. Acknowledgments

This work was supported by (i) the Portuguese Foundation for Science and Technology (FCT) in the framework of the Strategic Funding under Contract No. UIDB/04650/2020; (ii) the exploratory project, Project No. 2022.01740.PDTC; (iii) the Scientific and Technological Cooperation Program between Portugal (FCT) and France (CNRS)-2022/2023, and (iv) the European Union's Horizon 2020 Research and Innovation Program under Grant Agreement No. 958174 (M-ERA-NET3/0003/2021-NanOx4EStor). J.P.B.S. also acknowledges FCT for the contract under the Institutional Call to Scientific Employment Stimulus–2021 Call (Grant No. CECINST/00018/2021).

E. Beyond memory application and neuromorphic

Stefan Slesazeck

1. Status

Recently, it has become apparent that the conventional von-Neumann architecture has reached its limits in terms of performance and energy consumption due to the need for increasing data movement. Relief is found by combining computing and storage functionality locally within one structure. In this context, the three basic FE memory device concepts that utilize one of the most energy-efficient storage mechanisms—FE polarization switching—exhibit superior properties in terms of area and energy efficiency. The three-terminal FeFET with separate write and read terminals exhibit a tunable threshold voltage. It is programmed via its gate terminal, and the polarization state is read as drain–source current. Integrated together with conventional CMOS⁴⁴⁰ FeFETs are the most versatile FE devices that add memory functionality in analog and digital circuits. The two-terminal ferroelectric tunneling junction (FTJ) features a polarization-dependent resistance. However, in these devices,

both programming and read paths are combined. Thus, FTJs are less flexible for circuit implementation. FTJs are very interesting for massive parallel operation due to their typical high impedance.⁴⁴¹ In both device concepts, a read operation is ideally performed without affecting the polarization state. This is not the case for the third device: the FE capacitor (FeCAP). Read and write operations are combined by applying a switching pulse and measuring the resulting switching current. This makes them good candidates in regular array-like structures but restricts their application scenarios in neuromorphic circuits. In all three device concepts, the write operation is performed by applying an electric field to the ferroelectric layer that exceeds the coercive field. In a first-order approximation, the required switching energy linearly depends on switched polarization charge P_s (and thus linearly on device area) and the applied switching voltage v_s : $E \sim P_s v_s$. Thus, the switching energy of small-scaled FeFETs in the 10 nm regime is smallest with typical values in the ~ 10 pJ range on the device level, while the device area scaling of FeCAP and FTJ is limited by the required reading charge or current, respectively, thus leading to typical switching energies in the range of ~ 1 –100 fJ. The energy consumption of read operation for FeFET and FTJ strongly depends on the sensing concept, but for FeCAP equals the corresponding write energy.

Obviously, the strong differences in the read operation have a major impact on the usability in various architectural concepts. Artificial neural networks (ANNs) link input and output nodes via digital computing layers that perform matrix-vector multiplication (MVM) or multiply and accumulate (MAC) operation. Many hidden layers form deep neural networks (DNNs). The digital “synaptic weight” storage and multiplication can be realized locally in near-memory-computing (NMC) or in-memory-computing (IMC) approaches to realize the combined logic and memory functionality in FeCAP- or FeFET-based arrays.⁴⁴² Device characteristics are similar to NVMs, such as high cycling endurance, long data retention, and low switching voltages are targeted at. For analog weight storage and MAC operation, however, FeFET- and FTJ-based circuit designs take advantage of Ohm’s and Kirchhoff’s law. Thus, additional device requirements, such as linearity in weight update and IV-characteristics, high impedance, large dynamic range, and low variability, are key. Finally, spiking neural networks (SNNs) benefit from the accumulative switching properties of the ferroelectric devices.⁴⁴³ Common to all these architectures is their data-centric approach to overcome the von-Neumann bottleneck. Thus, the research on ferroelectric device applications beyond pure memory has recently gained much traction.

2. Current and future challenges

For the specific application, both readout and programming dynamics are key and strongly linked to the circuit design for the implemented learning algorithms. For FE HfO_2 , there is a trade-off between switching field and switching time.⁴⁴⁴ It is possible to obtain both digital weight update by strong programming pulses or more gradual weight update by varying programming pulse times or amplitudes or a mixture of both like in spike-time-dependent-plasticity (STDP).⁴⁴⁵ In this context, the largest challenge is seen in overcoming the typical non-linear weight update of FE devices. Moreover, caused by the poly-crystalline nature of the FE layer, there is a direct trade-off between multi-level switching and device scalability. Thus, the scalability of HfO_2 -based FE devices for

digital storage is limited to about $0.2 \mu\text{m}^2$ cell size,⁴⁴⁶ and for analog weight storage, it gets even more challenging to deal with the device-to-device variability. Target programming schemes can help at the cost of increased complexity of the programming circuit, which is detrimental for non-array like designs.

On the other hand, small-scaled FeFETs with just a small number of single FE domains exhibit versatile interesting switching dynamics. Besides digital, gradual, and cumulative switching, accumulative switching⁴⁴³ and stochastic switching⁴⁴⁷ allow for a huge variety of application cases beyond synaptic weight storage. Spike accumulation in neurons,⁴⁴⁸ the realization of physical unclonable functions (PUFs) and random number generators are some examples. However, the controllability of the single-domain switching kinetics and the distribution of coercive fields among different domains within one device are limited. Thus, a proper programming circuit design and limitation of the dynamic range are key.

For analog MAC operation, typically, a linear I – V characteristic is required. However, in FTJs, the conduction mechanisms are generally non-linear, thus limiting their suitability in this respect. A different input data representation, for example, by using pulse-width coding at constant read voltage instead of pulse amplitude coding might be one way to mitigate this issue. The non-linearity is easily circumvented in three-terminal synaptic elements or FeFETs, where the current during the reading does not flow through the ferroelectric layer but through a channel material. Excellent I_{DS} – V_{DS} linearity was obtained using conducting oxides, for example, WO_x ⁴⁴⁹ as channel materials.

For FeCAPs, up to 10^{18} switching cycles have been predicted.⁴⁴⁹ In contrast, Si-based FeFET endurance is typically limited to $\sim 10^5$ cycles, mainly due to degradation of the channel interface. FTJs suffer from similar effects, making these devices more suitable for inference applications and un-frequent weight updates. In this case, longer retention times are required, which has been demonstrated for digital storage in FeCAP⁵ and FeFET devices. However, high internal electric fields cause imprint, resulting in a low opposite state retention⁴⁵⁰ that still needs to be resolved especially for analog weight storage in FeCAPs. The same-state retention becomes more critical in FeFET and FTJ double-layer devices featuring larger depolarization fields. The situation might be relaxed for online training of neural networks because the weights are continuously updated. Hence, from an application point of view, there is a trade-off between the endurance and data retention requirements.

3. Advances in science and engineering to meet the challenges

The specific weight update characteristics of the ferroelectric devices depend on the ferroelectric film, its microstructure and the formation of domain walls, and the resulting energy barriers between the different polarization states. Thus, material optimization toward small grain sizes targeting at gradual switching of many small domains featuring a certain distribution of the E_c will be key to success of FE devices as analog synapses. In contrast, a sharp E_c distribution is mandatory for digital switches.

Besides the FE layer properties itself, the switching dynamics and device reliability are further influenced by the whole material

stack, including electrodes and their work function, interlayers or interfaces, the device structure, and size. Moreover, other physical and chemical effects, such as ion migration, oxidation of electrodes, or reduction of the metal oxide films as well as charge trapping effects,⁴⁵¹ can have a strong impact on the device's electrical characteristics. Thus, the optimization of a desired weight update characteristic has to consider not only the FE material itself but also the whole layer stack and, consequently, the device design and is subject of intense research.

For front-end-of-line (FEOL) Si-based FeFET optimization, the main focus will be on the improvement of the devices reliability in terms of cycling endurance and device-to-device variability since the FeFET size directly influences the silicon cost. FeMFETs featuring an internal electrode can benefit from the freedom to optimize the ratio between FE capacitor and gate capacitor in the trade-off between memory window and depolarization field and from the better reliability of the FeCAPs.⁴⁵² However, for this concept, any leakage current toward the floating internal node has to be prevented to avoid compensation of the polarization charge. Thus, material stack optimization toward ultra-low leakage and reliability in terms of stress-induced-leakage-current (SILC) will be of utmost importance.

The focus of FTJ development will further be driven by the need for increasing the on-current density and the optimization of the device reliability. The adoption of multiple functional layers, electrode and interface optimization, and band engineering will be a key for success.

Incorporated in circuits, the operation voltages of the FE devices ideally should not exceed 3–5 V. A reduction of the FE layer thickness might be targeted, which, however, causes increased annealing temperatures, thus affecting the BEOL compatibility. Another approach is stack engineering, e.g., combining FE HZO and AFE ZrO₂.⁹⁵

Besides the device optimization measures, also the electrical operation conditions must be adapted to the specific device design.^{445,453} Thus, a thorough design-technology-co-optimization (DTCO) will be mandatory key to success.

4. Concluding remarks

The growing interest in AI-hardware development and the need for non-volatile storage devices that are to be co-integrated with conventional CMOS devices reflect itself in a significant growth in the research on ferroelectric devices for application in beyond von-Neumann architectures during the past five years. Compared to other storage concepts, the FE devices benefit mainly from a low-power program operation, a defined and well understood physical process, and a great flexibility in device design. This gives rise to a large variety of potential application cases as digital or analog synaptic weighting elements, as spike accumulators, or as routing memory in SNNs using address-event representation (AER) of spikes. However, there are still several technological issues to be solved, and at the present, there are no clear winning usage scenarios. When looking at the current research activities in the field of neuromorphic computation, there is still a large potential for the scientific and engineering communities in terms of algorithm development and DTCO, which will finally lead to a commercial application of the “ferro-neuromorphic” devices.

VIII. OVERARCHING CHALLENGES

A. Measurement protocol

Veeresh Deshpande, Catherine Dubourdieu, and Suzanne Lancaster

1. Status

A standard measurement protocol is critical in order to accurately compare between HfO₂-based films. Typically, in order to obtain polarization–voltage (*P*–*V*) curves, the current through the capacitor during switching is integrated. Measurement techniques include the Sawyer–Tower⁴⁵⁴ or virtual ground method,⁴⁵⁵ with most commercial FE testers using the latter. When a voltage pulse is applied to a FE, the current response will consist of the switching current, leakage through the FE, and dielectric displacement current. Leakage contributions can be removed using dynamic leakage current compensation via measurement at different adjacent frequencies.⁴⁵⁶ If non-switching contributions are large, the positive-up negative-down (PUND) method⁴⁵⁷ can be applied to avoid remanent polarization overestimation. Here, two consecutive voltage pulses are applied in each polarity. The current (or charge) in the second pulse is subtracted from the first in order to remove the leakage and dielectric components, which in the ideal case yields only the remanent polarization. From this basic measurement, different pulse trains can be established, which characterize various aspects of FE device operation.⁴⁴⁵

Complementary to *P*–*V* or *I*–*V* measurements, small-signal capacitance–voltage (C–V) measurements can be used to observe the FE response, yielding a characteristic “butterfly-shape” with peaks corresponding to increased capacitances during switching.⁴⁵⁸ Finally, as FE hafnia films are dielectrics, which suffer from defect generation due to electric field stress, capacitor leakage is an important figure of merit that gives information on film and interface quality.¹⁶⁹

Measurement protocols vary based on the intended device type. The three major device types for HfO₂-based FEs are FeCAP, FTJ, and FeFET. Measurement of these devices depends on the device performance parameters to be estimated and their intended applications. The general protocols for each type, as summarized in Fig. 20, are as follows:

- FeCAP: The remanent charge, its dependence over multiple switching cycles (endurance), and its ability to retain the charge (retention) at different temperatures are the main characteristics to be determined. The remanent charge is measured via the PUND sequence. The leakage current can be determined by quasi-static (voltage sweeping) or DC *I*–*V* (voltage sampling) measurements. The remanent charge is measured with cycling to assess the endurance. Retention is ideally measured by first switching the polarization to one state and then estimating the switched charge into the new same state or opposite state after various delay times at both room temperature and elevated temperatures.⁴⁵⁹ Besides measuring the loss in stored polarization charge, retention can also be investigated via imprint, which plays a strong role in reading of the state in FeCAP.⁴⁶⁰

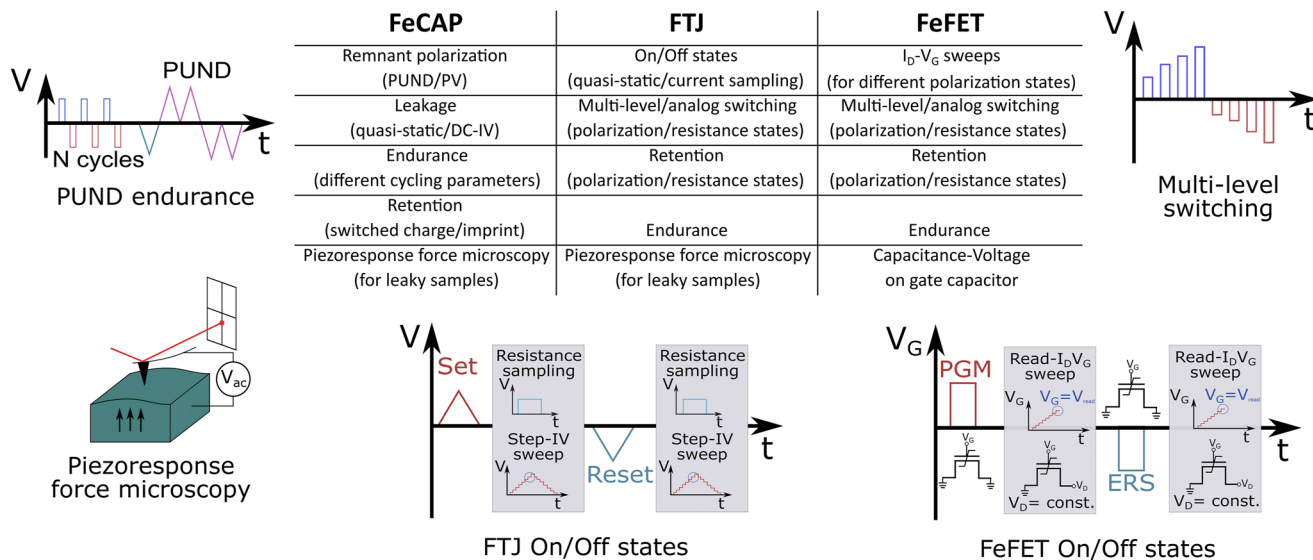


FIG. 20. Overview of standard electrical measurements for the three main ferroelectric device types (FeCAP, FTJ, and FeFET).

(b) **FTJ:** As a non-volatile memory device, the important parameters to be measured in a FTJ are the ON and OFF currents, retention of these states, and endurance. The FTJ device architecture can be a single ultra-thin layer, a bilayer, or a multilayer stack sandwiched between two electrodes. PV or piezoresponse force microscopy (PFM) measurements are performed to assess the FE switching. ON and OFF currents can be determined in different ways, discussed later. For neuromorphic applications, multiple resistance states are characterized by reading the current levels after partial switching operations performed by progressively increasing (or decreasing) the switching voltage, varying the switching pulse width, or applying several pulses of fixed amplitude and width.⁴⁶¹

(c) **FeFET:** Polarization switching measurements are performed by grounding the source and drain, while applying the switching voltage to the gate. Drain current (I_D) vs gate voltage (V_G) sweeps (up to read voltage on the gate) under applied drain voltage determine the change in threshold voltage after switching. The ON and OFF currents are estimated at fixed V_G . Retention and endurance can be measured for each state. While performing a switching IV or PV measurement is neither typical nor straightforward, ferroelectric switching can be ascertained by performing CV measurements of the gate capacitor. Multiple current states are estimated through partial switching as for FTJs. A useful technique is plotting V_G against the time it takes to close half the memory window for each state, from which the retention of each state, minimum switching time, and optimal operating parameters can be estimated.³²²

2. Current and future challenges

Certain challenges arise when the film is leaky, which is usually the case when reducing the thickness of FEs below 5 nm. Since FE materials are also piezoelectric, an alternative method to measure

the FE response is by determining the sample deformation under an AC bias through piezoresponse force microscopy (PFM). In ultra-thin films, the high leakage during switching necessitates the use of PFM for observing hysteresis.⁴⁶² At the same time, PFM must be carefully performed since other electromechanical responses, in particular charge injection, can mimic ferroelectricity⁴⁶³ and complementary methods should be applied in order to confirm the observed ferroelectricity.

Recent work has again highlighted the limitations in current FE characterization techniques for evaluating devices in the presence of a large depolarization field,⁴⁶⁴ such as in ultrathin FEs or in FEs integrated with a dielectric layer. It was shown that PUND analysis underestimates both the irreversible and remanent polarizations in the presence of depolarization fields. In the case of FeFET, parasitic charge trapping effects can obscure the memory window on short time scales while improving retention and degrading endurance.³⁹⁰ This means that reported figures of merit may sensitively depend on the exact measurement routine applied. Charge injection has been shown to play a significant role in the switching of any film integrated with a dielectric layer, for example, FTJs or negative capacitance devices.⁴⁶⁵

In FeFETs, the read and write paths are fully decoupled so that ON and OFF states can be measured independently of the switching current. Conversely, for FTJs, it is important to distinguish current components in order to properly characterize the device resistance levels. Quasi-static IV curves are reported, which cover either the whole switching range⁴⁶⁶ or only up to a defined read voltage chosen to exclude switching contributions.⁴⁶⁷ In the former case, there is a risk if trying to extract the resistance states that the tunneling current is conflated with the switching current even at low sweeping rates. Another method would be measuring the resistance state directly at the read voltage, where applying a long bias time enables the separation of the read current from background components.⁴⁶⁸ When moving to on-chip operation and characterization, a pulsed

read scheme is required where the desired device behavior can no longer be decoupled from the background currents, necessitating new measurement schemes.

The wake-up effect seen in HfO_2 -based FEs raises challenges for devices. While the FeCAPs may have nominally similar electrodes on either side of the FE, FTJs and FeFETs typically have different electrodes or interfaces, leading to an asymmetric field distribution. As such, the wake-up will depend both on the built-in imprint field and particularly on the electrical cycling parameters (waveform type, frequency, amplitude, etc.).⁴⁶⁹ Thus, the wake-up behavior needs to be characterized, well-reported, and optimized for individual device stacks.

3. Advances in science and engineering to meet these challenges

As HfO_2 -based FE technologies mature, a shift from macroscopic characterization to on-chip measurements is necessary. Characterization of on-chip FeCAP devices has already allowed for the observation of switching speeds down to the nanoseconds.⁷ A 120 dB pulse generator has been demonstrated that meets the requirements for on-chip testing of FE devices, where pulse widths can be precisely controlled across six orders of magnitude.⁴⁷⁰ This allows read, write, switching kinetics and multilevel programming operations to be performed on-chip with the same circuitry.

For lab-based characterization, the device layout also needs to be optimized to allow for the application of short pulses to avoid pad and connection parasitics from influencing the read and switching currents. For example, the use of active voltage probes for connecting devices has been recently demonstrated in order to measure FE HfO_2 without parasitic cable capacitances, enabling direct measurement of devices with areas below $1 \mu\text{m}^2$.⁴⁷¹

Due to the typically small thicknesses of $\text{HfO}_2/\text{ZrO}_2$ FEs, interfaces play a dominant role in their behavior. Recently, a pulsed measurement scheme has been proposed to quantify interface charge traps.⁴⁷² Additionally, small-signal CV measurements to quantify interface traps can be better understood by new models in combination with experiments.⁴⁷³ This demonstrates how both new measurement schemes and device modeling can contribute to a better understanding of FE device behavior.

4. Concluding remarks

Accurate measurements of the properties of HfO_2 -based FEs are pivotal in ensuring that these materials reach their potential in the field of memory devices and other applications. Proper measurements and detailed reporting of measurement schemes allow for benchmarking between different technologies and processes. However, HfO_2 FEs still suffer from reliability issues and large depolarization fields, which can obscure measurement results. Therefore, the question of how to properly characterize HfO_2 films can be broken down into two parts: the first is how to determine the fundamental properties of the FE and the second is how to correctly compare between devices and technologies.

5. Acknowledgments

The authors acknowledge funding by European Union's Horizon 2020 Research and Innovation Program under Grant Agreement No. 871737 (BeFerroSynaptic).

B. Switching voltages/retention

Simon Martin, Laurent Grenouillet, and Jean Coignus

1. Status

Since the discovery of ferroelectricity in $\text{HfO}_2/\text{ZrO}_2$ materials, FE memory paradigm has changed, in particular for FeRAM, thanks to CMOS compatibility and scalability compared to perovskite-based FeRAM. Switching voltage/time and data retention are key parameters since they dictate the performance and reliability of the memory.

The switching speed governs the latency of the memory, whereas low switching voltages allow for better scalability and lower programming energy. Endurance performances are then a mixed consequence of the optimized voltage/time programming scheme. FEs are intrinsically fast in terms of switching, with a trade-off observed between switching speed and voltage. Tagantsev *et al.* physically described this trade-off in the NLS model,⁴⁷⁴ which overcame the KAI model⁴⁷⁵ in polycrystalline ferroelectrics. Fast switching is at the expense of higher voltages: e.g., Lyu *et al.* demonstrated ultra-fast sub-ns switching on 15 nm HZO but with 9 V pulses.⁴⁷⁶ This trade-off has recently been measured in 10 nm HZO- and HSO-based single-scaled capacitors⁴⁷⁷ in the form of switching efficiency maps demonstrating 2.5 V-operation capability at the ns scale.

An important reliability feature for marketing a product is data retention. The reliability targets for 10 years data retention are 85, 125, and 165 °C for general purpose, industrial, and automotive applications, respectively. The physical understanding of retention loss is key for practical applications and future technology developments to improve those metrics. Both memory polarization states' P_{down} and P_{up} (encoding 0's and 1's) retention need to be clearly understood as different phenomena can occur and degrade the state stored in the FE capacitor. The same-state (SS) represents the non-switching state in FeRAM during read operation, and the switching state, called opposite-state (OS), is the preferred metrics for evaluating data retention in FeRAM.⁴⁷⁸ Thermal depolarization (TD) and imprint are the two main mechanisms identified for the retention degradation. The TD is an intrinsic property of the ferroelectric material: the P_r drops as the temperature rises up to the Curie temperature. This transition temperature, where ferroelectric material becomes non-polar (paraelectric phase), is high for HfO_2 -based films and bulk, typically >350 °C,^{206,416,479} favoring stable operation for memory applications. However, this temperature can be reduced with film thickness, dopants, and strain^{92,206} and, thus, strengthen the TD phenomenon. The thermal depolarization can also be due to the depolarization field induced by an incomplete polarization compensation at the electrode interfaces.⁴⁸⁰ The imprint provokes a decrease in the OS polarization and increases E_c required to switch in OS. Excellent retention has been observed on single FE capacitors 10 nm HSO at 125 °C during 1000 h⁴⁵⁹ and at 85 °C during 10 years (extrapolated).⁴⁶⁰ At the array level, Lin *et al.* exhibited an extrapolation at 10 years at 85 °C (10 nm HZO 1 kbit FeRAM) with P_r at 76% of the initial value (OS retention).⁴⁸¹ Recently, 16 kbit FeRAM HSO-based arrays have demonstrated their immunity to solder the reflow process with no bit failures after three repeated sequences up

to 260 °C (30 s).² In terms of switching time/voltage, a compelling result was demonstrated in 2020²³⁰ with the first demonstration of 64 kbit 1T-1C FeRAM arrays with 100% bit functionality, 10 ns write speed, and 2.5 V operating voltage using a 130 nm node.

2. Current and future challenges

Despite these recent advances in the field, major challenges remain to improve performance and reliability, especially at the material/stack level.

Indeed, dopants, oxygen vacancies, and charge trapping play essential roles in device functioning,³⁰⁸ affecting phase formation, FE properties, and electric conductivity. In particular, HfO₂/ZrO₂ films require oxygen vacancies to stabilize the *o*-FE phase, while a reduction in oxygen vacancy content directly leads to an unwanted increase in the non-polar monoclinic phase formation. Concentration of oxygen vacancies is difficult to control and can evolve within the films during electric field cycling. Moreover, low thermodynamic barriers between the polar *o*-phase and the non-polar *t*- and *m*-phases reflect the high degree of polymorphism in hafnia,⁴⁸² highlighting the need for careful phase engineering in thin ferroelectric films.

The electric fields experienced by FeRAM can attract charges from the electrodes and induce drift of free charges and charged defects within the layer.⁴⁸⁰ It contributes to imprint and accordingly limits data retention. The electrostatic drift associated with imprint may eventually cause sub-cycling behavior because of an incomplete switching: as a result, spontaneous back-switching of the polarization is expected to occur, resulting in retention loss. Finally, local depolarization of FE domains can also limit data retention if non-polar phases are present in the FE layer.

Assessing the aforementioned challenges is mandatory to push further the introduction of HfO₂/ZrO₂-based ferroelectrics into advanced technological nodes, which requires to lower the operating voltage below 2.5 V. Due to the switching voltage/time trade-off, this would imply longer switching times in order to avoid partial switching of the layer, the latter having a detrimental impact on the memory window (MW). To overcome this, FE films thinner than 10 nm are required to decrease to coercive voltages while keeping a complete bit cell switching. Using 8 nm HZO, Okuno *et al.* successfully demonstrated functional FeRAM memory operation down to 2 V at 16 ns.⁵ However, reducing film thickness requires higher crystallization temperatures, which can hamper BEOL integration.⁴⁸³ In addition, reducing FE film thickness increases the depolarization field,⁴⁸⁴ which in turn has a detrimental on data retention. This illustrates the need to engineer the FE stack to overcome those current and future challenges. This engineering work necessitates significant theoretical simulations, coupled with advanced experimental growth and characterization works, in order to provide a robust understanding of HfO₂/ZrO₂ films.

3. Advances in science and engineering to meet these challenges

Tahara *et al.* reported 4 nm-thick FE HZO in MFM structures with excellent FE properties,⁴⁸³ a low voltage operation of 1.0 V is reported with coercive voltages below 0.5 V while keeping a satisfactory $2P_r$ value superior to 20 $\mu\text{C}/\text{cm}^2$. Excellent OS data retention requirement of 10 years at 85 °C is also demonstrated. For 10 nm-thick HZO, crystallization is achievable at 400 °C anneal,

while 4 nm HZO requires around 500 °C to crystallize in the *o*-phase. The increase in crystallization temperature with the decreasing film thickness could be overcome in BEOL integration thanks to the nanosecond laser anneal (NLA), which is a promising way to locally rise the anneal temperature to reach *o*-phase crystallization while preserving BEOL integrity.⁴⁸⁵ As previously discussed, the oxygen content in Hf/Zr-based films is crucial to get better reliability and performance. Mittmann *et al.* have recently performed oxygen content engineering in HZO films, highlighting that not enough oxygen favors the *t*-phase while too much oxygen content takes advantage of the *m*-phase formation during the film deposition. The optimization of this parameter is key to maximize the *o*-phase formation and to improve the reliability.⁴⁸⁶

Increasing the MW would also help to minimize the OS retention loss in FeRAM. 3D FE capacitor integration seems highly suitable for advanced nodes as it favors the storage density thanks to the increase of the FE capacitor electrical surface. Lin *et al.* reported the technological potential of a BEOL 3D FeRAM, which can be integrated in a 3X nm technology node.⁴⁸⁷ 3D FE capacitors exhibit good performances with an endurance of 10^9 cycles, $2P_r$ around 18–20 $\mu\text{C}/\text{cm}^2$, and field operation at 2.2 MV/cm. P_r reaches in 1C-3D is 78% of equivalent P_r measured on a planar capacitor. Good reliability is also achieved with 10 years retention at 85 °C with 60% of the initial P_r . At the circuit level, the bit line capacitance (C_{BL}) reduction is another lever for improving MW since it affects the capacitive divider within the bit cell.² This reduction is achievable in advanced technology nodes and/or with proper design optimization.³⁷⁷

4. Concluding remarks

In conclusion, improvements in switching voltages/times and data retention are in constant progress. These key parameters are important milestones for the future integration of HfO₂- and/or ZrO₂-based FE materials in advanced technology nodes. The enhancements in terms of integration have been recently made with the fabrication of the 3D FE capacitor instead of a planar capacitor to maximize the MW and the storage density. Another integration improvement is the thickness slimming of the FE films to reduce coercive voltages keeping ferroelectric properties with crystallization temperature compatible with BEOL. Moreover, the control of the oxygen content during the deposition of hafnia/zirconia films to limit the oxygen vacancies formation and stabilize the orthorhombic polar phase is a key parameter to improve the performances and the reliability in hafnia/zirconia-based FeRAM. All these technological progresses pave the way toward an integration of hafnia/zirconia-based FeRAM in advanced technology nodes.

C. Endurance

Laura Bégon-Lours

1. Status

Remarkable efforts have been recently achieved for outperforming the endurance of HfO₂-based FE devices. On the one hand, the exploration of various materials and stacks led to the demonstration of devices pushing the maximal endurance limit from 10^4

back in 2012 to 10^{11} nowadays. Area scaling to small production-type capacitor structures could even enhance the endurance limit beyond 10^{14} cycles.⁸ Such metrics were demonstrated in both two- and three-terminal configurations. They show that FE devices are serious candidates for non-volatile memory application: in comparison, flash memories have an endurance of $\sim 10^6$ cycles, phase change materials memories have an endurance of 10^{10} , valence change resistive memories can reach 10^{12} cycles, and spin-transfer-torque magnetic memories can reach up to 10^{15} write/erase cycles.

On the other hand, studies combining materials sciences and electrical characterizations brought valuable knowledge on the control of endurance properties. Number of devices contain (on purpose or not) a dielectric layer at an interface with the FE, for example, SiO_2 at the interface between an HfO_2 gate and a Si channel. In the last decade, a number of experimental and theoretical works detailed the role of such layers in the functionality and reliability of such devices.⁴⁸⁸ Earlier, the breakdown of the dielectric gate was identified as the main cause of the device failure. This led to the emergence of interlayer free stacks, for example, using germanium²⁸² or metal oxide semi-conductors as the channel⁴⁸⁹ or electrode material. Later, the presence of defects within the HZO layer upon cycling was also studied.⁴⁹⁰ Temperature-dependent transport experiments showed that upon cycling, the energy barrier seen by electrons in the bulk of an HZO film was lowered,⁴⁹¹ indicating a redistribution of defects in the later.

Several studies confront x-ray spectroscopy analysis to electrical characterization, shedding light on the key role of contaminants in hafnia. Varying the chemistries (gas, precursors) during the ALD or during the annealing showed that dopants such as carbon or hydrogen are detrimental to endurance.⁴⁹² It was experimentally observed that MFM stacks deposited *in situ* show improved endurance compared to stacks exposed to air.⁴⁹³ The number of works combining x-ray analysis, eventually scanning transmission electron microscopy, and electrical characterization correlate the increase of the endurance to a decrease in the fraction of the *m*-phase. In general, for comparable thicknesses, a larger endurance is also observed, together with a reduced leakage current.

2. Current and future challenges

Today, the most significant trade-off in terms of endurance is the dynamic range of the device. The number of cycles a given device can endure increases as the applied electric field decreases, and the endurance figure is generally reported for “full” switching operation, i.e., reaching the maximal P_r . The corresponding electric field for HfO_2 -based FE is around 2–2.5 MV/cm. Operating the device in sub-polarization loops has proven an efficient way of increasing the endurance and eventually working with polarization states that are more stable regarding temporal drift. However, for applications such as synaptic weights for artificial neural networks, an ideal On/Off ratio of 100 is required. Today, many technologies of ferroelectric synapses do not yet meet these requirements, and making compromises on the dynamic range to guarantee a large endurance is not always possible.

The most mature HfO_2 devices (FeFET and FTJ) are based on a dielectric interlayer. The parasitic charge trapping during writing was identified as the most detrimental phenomena to the endurance. The injection of electrons or holes in the gate, promoted by large fields, leads to the creation of defects both in the interlayer and in the

hafnia. Moreover, these charges screen the ferroelectric polarization charges, reducing the ferroelectric field-effect and, thus, the device performance.

Understanding the role of oxygen vacancies is a critical aspect of solving reliability issues in FE devices. On the one hand, improvements in reliability were obtained by interfacing HZO with a metal oxide electrode, such as WO_x , VO_x , TaO_x , RuO_x , or CeO_x . Some evidence points to a supply of oxygen atoms from the electrode to HZO during the crystallization, resulting in a FE film with less interfacial oxygen vacancies and improved reliability.³⁵³ On the other hand, doping hafnia with three-valent atoms such as La increases not only the oxygen vacancy content⁴⁹⁴ but also the energy barrier for the creation of additional oxygen vacancies during cycling. Similarly, controlling the optimal fraction of FE, the *o*-phase is not trivial. A slight increase in the tetragonal phase can be beneficial to endurance, as it tends to reduce the coercive field of the thin film.²⁵⁶ It is the approach explored by the fabrication of superlattices or nanolaminates.^{350,495} It is also the mechanism behind the use of La-doping, which limits the crystallization in the *m*-phase but favors the non-polar *t*-phase. However, La-doping of HZO also leads to an enhancement of the wake-up behavior. A diminution of the coercive field was also obtained by quenching an epitaxial thin film in a tetragonal phase without any degradation of the remanent polarisation.⁴⁹⁶

Wake-up is the increase in P_r during field cycling, which can change hysteresis shape. In most cases, a pinched hysteresis loop in the pristine case opens to an unpinched loop during field cycling. Several reasons are given in the literature: There could be charges in the layer that pin the domains and inhibit their switching.¹³⁵ These charges can be redistributed by the applied external field, unpinning the domains. Furthermore, there may be a field-driven phase transition from a non-polar *t*-phase to a polar *o*-phase.^{332,497} During field cycling, strain and stress relaxation can be caused by electronic or ionic charge redistribution or injection. In addition, ferroelastic switching has been described to cause a 90° domain reorientation from an in-plane polar axis to an out-of-plane polar axis of the polar *o*-phase.^{498,499} Furthermore, a reversible transition between the polar and antipolar phases has been reported.⁶³ Wake-up effects can be drastically reduced by optimizing dopant and oxygen vacancy content,³³ stabilizing the tetragonal phase in the film. From this discussion, it is clear that each materials system possesses an optimal composition, and their control will require increasing support from first-principle simulations^{148,500} and experimental work.

3. Advances in science and engineering to meet these challenges

Regarding the dynamic-range vs endurance trade-off, combining the doping of HZO with $\sim 1\%-2\%$ mol of group III atoms with a full stack growth in one batch is a promising route. For example, La-HZO thin films show a record endurance of 10^{11} cycles³⁰⁰ at 2.5 MV/cm, while maintaining a remanent polarization as high as $28 \mu\text{C}/\text{cm}^2$, 75% of the maximal remanent polarization obtained at 3.5 MV/cm. Skopin *et al.* Gd-doped hafnia 8.8 nm films⁵⁰¹ reached 10^{10} cycles at 4 V, for a remanent polarization reaching $33 \mu\text{C}/\text{cm}^2$.

The question of parasitic charge trapping is addressed in various ways. Both on stacks with or without oxide interlayers, the reliability of films grown or crystallized with different annealing techniques is studied; see, for example, a comparison for HZO/Ge films

prepared with rapid thermal annealing vs millisecond flash lamp annealing.²⁸² Dutta *et al.* have recently demonstrated a low voltage, high-speed memory operation with high write endurance using an interlayer-free back-end-of-line (BEOL) compatible FeFET.³⁹³ By gating an amorphous indium tungsten oxide semiconductor channel with a 5 nm HZO film, they report a write voltage of only ± 1.6 V with 20 ns pulses, read-after-write latency of only 300 ns (the absence of interlayer allows for a faster de-trapping of charges), and a record high write endurance exceeding 10^{11} cycles. In TiN/HZO/TiN capacitors, the bottom TiN interface is strongly oxidized during the growth of the hafnia layer. By combining it with a metal oxide bottom interlayer, robust synaptic weights with even thinner (<4 nm) HZO films can also be fabricated in BEOL-compatible conditions, further reducing the electric field required to switch the polarization and reaching endurances above 10^{10} cycles.⁴¹⁵

Tan *et al.* also reported an endurance exceeding 10^{10} cycles in HZO films²⁴⁷ by incorporating a high- k SiN_x layer between the Si substrate and the FE. Thanks to the higher permittivity of SiN_x compared to an SiO₂ interface, a reduced electric field is required to switch the FE polarization. As discussed above, introducing a small fraction of the *t*-phase in the film can efficiently reduce the electric field required to switch the polarization without degrading P_r . In this direction, an approach for obtaining mixed-phase thin films is to minimize the phase transition from tetragonal to orthorhombic during the wake-up. Such a route will favor materials with a high remanent polarization in the pristine state, for example, by optimizing simultaneously Zr and the oxygen content.³³ Apart from the group III doping, recent work proposes introducing *t*-phase spacers (ZrO₂) within HZO in nanolaminate films,⁴⁹⁵ creating topological domain walls. Finally, the parasitic charges can be eliminated after writing by an electrical pulse: the waveform is then tailored to de-trap the charges.

4. Concluding remarks

In the last decade, the systematic benchmarking of novel stacks, geometries, and fabrications processes allowed to correlate

the endurance properties to materials and electrical properties. These correlations drove the understanding of the device's physics and, consequently, the understanding of the device's reliability. In a feedback loop, this knowledge guided the optimization of existing concepts and the creation of novel ones. As summarized in Fig. 21, the knobs for improving reliability today rely on materials engineering, the growth and crystallization conditions, and the electrical mode of operation. Similarly to ferromagnetic tunnel junctions, FE devices could, in principle, rely on purely electronic effects without any ion motion, oxidoreductions, or phase transitions. This exciting absence of intrinsic limitation should continue driving the quest for ever more endurant FE devices in the future.

5. Acknowledgments

This work received funding from c and from the Swiss National Science Foundation (SNSF) through the projects ALMOND (Grant No. 198612) and UNICO (Grant No. ANR-19-CHR3-0006).

IX. COMMERCIAL MARKET OPPORTUNITIES IN NON-VOLATILE MEMORIES

T. Mikolajick, Uwe Schroeder, and Stefan Slesazeck

A. Status

A non-volatile memory is defined by data retention of 10 years at elevated temperatures. For commercial applications, a reference temperature of about 55 °C is typically assumed to mimic a typical temperature use profile for a temperature specification of 85 °C. For automotive and industrial applications, even higher temperatures of up to 165 °C can be required. At the same time, a fast re-write speed is required. For random access memory applications, the re-write speed needs to be in the sub-nanoseconds to 10 ns range, while for storage applications, the re-write speed can be in the microsecond to millisecond range. Therefore, there is a difference in dynamics of 11–17 orders of magnitude between writing and storing. Today's charge-based non-volatile memories are far from delivering a random access functionality and have re-write times at the higher end of the mentioned range, limited endurance, and require high write voltages in the range of 10–20 V. FEs have a voltage-driven switching mechanism, and the energy barrier separating the two polarization states is reduced during switching. Therefore, they enable fast switching and non-volatile retention at low write voltages. As a consequence, already in the 1950s, the use of FeRAMs was proposed. Another unique aspect of FEs in non-volatile memories is the fact that three different readout schemes can be used that lead to three fundamentally different memory cell concepts, namely, a capacitor-based FeRAM, a FeFET, or a FTJ-based FeRAM.²¹ The three concepts can serve different application requirements. The FeRAM concept is inspired by DRAM, the FeFET has strong similarities with charge-based transistor memories using floating gates or charge trapping layers as used in Flash memories, and finally, the FTJ is a type of resistive switching memory.

The first and only concept that made it to market is FeRAM, which was first commercialized in 1993 based on a PZT FE

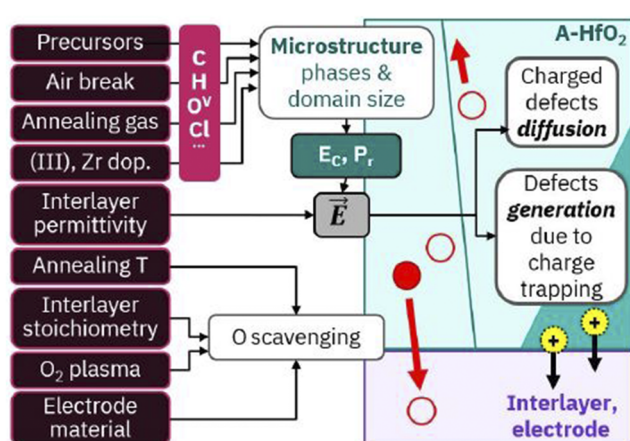


FIG. 21. Endurance: materials and process control hafnia microstructure. As the device is cycled, the existing and newly generated defects redistribute in the layer, eventually leading to the breakdown.

integrated into a CMOS base process.⁵⁰² Although big hopes were associated with this breakthrough that a non-volatile version of a DRAM would soon become available, the technology made a very slow scaling process, mainly due to the compatibility issues of PZT (and also later SBT) with CMOS processes. The FeFET development struggled from the inherent depolarization field and the low coercive as long as PZT, SBT, and related materials were used.⁵⁰³ First, FTJs were only realized mid of the first decade of the 2000s,³⁹⁸ and even today, they are still in a stage of basic research.

B. Current and future challenges

The scaling of FeRAM using PZT as a FE has stopped at the 130 nm node and is hindered by the fact that until now, the integration of PZT in scaled three-dimensional capacitors has not been mastered.⁵⁰⁴ In contrast, FE HfO₂ can easily be integrated into three-dimensional capacitors using ALD. However, the high coercive field is the biggest issue for this material system. On the one side, it requires relatively high switching voltages, and switching by sub 1 V V_{DD} available in scaled technologies is very hard to achieve. On the other side, the high field during switching limits endurance. Both issues are currently tackled by engineering the FE and the electrode materials and slow but continuous progress is visible.

For FeFET devices, the first fully integrated FeFETs based on FE HfO₂ with small dimensions were demonstrated in 2011, and continuous progress has been shown in the last years.^{385,505} Both embedded NVM³⁸⁵ and 3D integrated storage type devices⁵⁰⁵ are currently the main targets, but FeFETs are also hot candidates as primitives in in-memory and neuromorphic computing⁵⁰⁶ (see the bottom part of Fig. 22). Here, device-to-device variability is still a major issue. While realizing more homogeneous layers with respect

to domain size and orientation is the main topic that is in the focus of the material development, also smart algorithms during writing, as known from floating gate and charge trapping memories, can be used to optimize the behavior of the cells in large arrays.⁵⁰⁷ However, more sophisticated solutions tailored to the specifics of the FE switching will be required in the future.

One of the main challenges in FTJs is the very low read current. Therefore, these devices are not so much in the focus to realize pure memory applications but are mainly considered as artificial synapses in neuromorphic computing systems.⁵⁰⁶ Scaling the thickness of the FE is the natural way to increase the read current.

C. Advances in science and engineering to meet the challenges

Significant progress has been made in optimizing the material properties of FE HfO₂ in the last 10 years.²¹ For the applications in FeRAM, the technology has gone closer toward fulfilling the specification (see the section on FeRAM). However, the final goals with respect to low voltage operation and reliability have also not been achieved; impressive demonstrations, including reliability extrapolation, have been accomplished.^{8,21} The topics are mainly addressed by working on the capacitor stack. Thinner FE layers as well as different dopants can be used to reduce the voltage. At the same time, the reliability needs are tackled by optimizing both the FE material and the electrodes as well as the interface between them.²¹

For FeFET devices, the variability has been continuously reduced in large arrays.³⁸⁵ However, further improvement is required to scale the cell size to the desired region. Moreover, cell variants, such as the ferroelectric–metal–field effect transistor

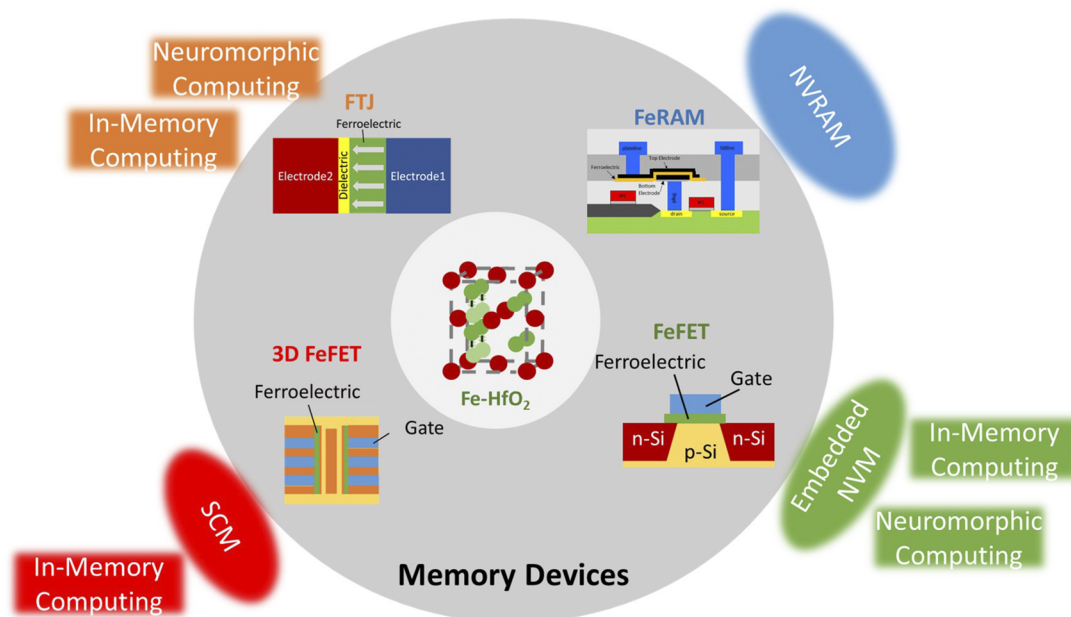


FIG. 22. Devices and possible application fields of ferroelectric devices based on hafnium oxide.

(FeMFET), can allow us to tailor the cell requirements by decoupling the FE layer optimization from optimizing the underlying field effect transistor at the price of a larger cell size and an additional floating gate.³⁵⁸ Moreover, very good progress in retention and endurance was reported.^{247,358} Since using hafnium oxide enables us to realize FeFET devices scaled to nm dimensions for the first time, new effects such as abrupt and accumulative switching have been discovered that could be explored to realize new functionalities, especially as artificial neurons in neuromorphic computing devices.⁵⁰⁶

For FTJ, many different demonstrations have been done in the last few years.⁵⁰⁷ Two paths are taken. One tries to reduce the thickness of the FE into the range of direct tunneling, while the other adds an additional dielectric tunneling layer to at least partially decouple the optimization of the FE from the requirements of achieving a high tunneling current.⁴⁶⁷ Two interesting paths have been recently shown for scaling the FE thickness. If the FE is deposited directly on silicon, also very thin films seem to show good FE properties.³⁵⁴ An alternative approach is to bring the film's optimum thickness into the FE phase and thin down the layer using atomic layer etching.²⁵⁴ In any case, as mentioned above, FTJs are still in a basic research state, and significant work is still required before such devices can be commercialized.

D. Concluding remarks

FE materials are ideally suited to realize non-volatile memory cells with very low write power. After some initial success, the field got stuck by the difficulty in integrating perovskites into a CMOS process. The discovery of ferroelectricity in CMOS-compatible HfO₂ and mixed HfO₂/ZrO₂ has revised this field in the last 10 years. Impressive demonstrations of both FeRAM and FeFET devices have shown that they can tackle different non-volatile memory use cases, such as non-volatile RAM, storage class memory, or low-cost embedded non-volatile memories, but for both technologies' reliability issues and for FeFETs, variability issues still need to be solved to commercialize the technology. Besides the applications in different memory devices, the mentioned FE devices also show great promise for in-memory and neuromorphic computing. In the last field, also FTJs are an option to realize compact synaptic functions. Figure 22 gives an overview of the possible application fields where FE devices based on HfO₂ could be seen in the future.

X. INDUSTRY PROSPECTIVE

Sou-Chi Chang, Ilya Karpov, and Uygar Avci

One of the approaches to significantly improve computing efficiency is by directly integrating high-speed and high-density memory elements closer to the high-performance computing units (cores), which are typically built by advanced logic transistors, for example, embedded DRAM (eDRAM).⁵⁰⁸ However, the scaling of conventional eDRAM has become more and more challenging due to higher transistor leakage, larger aspect ratio of capacitors, and more significant refresh power. On the other hand, FE memory, such as FeRAM, holds a great promise toward highly scalable fast embedded memory solutions because of (i) the similarity of conventional eDRAM in terms of cell structures except for replacing dielectric

capacitors with FE capacitors; (ii) better access transistor scaling due to memory bits stored in the bound charge of materials, rather than the free charge at the floating node, such as conventional DRAM; and (iii) low refresh power thanks to longer retention time from a large energy barrier between two polarization states.

It is well-known that FeRAM based on perovskite FE materials, such as PbZr_xTi_{1-x}O₃ (PZT), has been successfully commercialized since early 2000, and the thickness scaling issue due to low coercive field in PZT fundamentally prevents FeRAM from being integrated at any advanced logic technology nodes.⁵⁰⁴ Since then, not much progress is made in terms of scaling, and FeRAM is positioned only for small niche applications. However, recently, the research field of FeRAM has been re-vitalized due to the unexpected discovery on fluorite-structured HfO₂-based FEs originated from meta-stable polar *o*-phase in 2011.⁶⁰ HfO₂-based FE materials overcome the fundamental thickness scaling issues in perovskite FE materials while having low leakage due to a large bandgap. More importantly, HfO₂ is CMOS-compatible as it has been used in the gate stack of the state-of-art advanced logic transistors for more than 20 years. Among FE hafnia with different dopants, Hf_{1-x}Zr_xO₂ is particularly of interest mainly due to that (i) the thermal budget to crystallize the materials is BEOL compatible and (ii) the dominant phase can be tuned from monoclinic, tetragonal, to orthorhombic phase through different Hf and Zr ratios,¹⁶⁶ making this capacitor-based FE memory as an active research topic among other emerging memory options.

For memory options that are potentially qualified for eDRAM or last-level cache, the read and write operation times need to be less than 10 ns, the maximum operation voltage needs not to exceed 2 V with either positive or negative polarity depending on the cell designs, retention time needs to be longer than 1 ms, and read and write endurance cycles to be higher than 10¹².^{509,510} Note that these device metrics need to be satisfied at elevated temperature as the cache-level memory is close to the core computing units that are typically hot during operations. In addition, to achieve a competitive capacity, a tight distribution of variations in device metrics is required at the relevant small device dimension. To satisfy these specifications, functional FeRAM cells with scaled deep-trench AFE HZO capacitors (0.008 μm²) have been developed and demonstrated at elevated temperature to deliver the (i) operation voltage range from -1.8 to 1 V, (ii) read and write operation speed down to 2 ns, (iii) healthy retention up to 10 s, (iv) robust read and write endurance cycles up to 10¹², and (v) acceptable variations at 4σ across a 300 mm-scaled wafer.^{509,510} Note that -1.8 V is the voltage across the FE capacitor, which is defined from the inner node between FE capacitor and access transistor in a FeRAM cell and is typically implemented through voltage schemes, such as high plate line (PL) and low bit line (BL).

Even though HfO₂-based AFE capacitors close to higher-level cache memory specs have been achieved, it is of great importance to further improve read and write speed as well as reduce the operation voltage while maintaining robust retention, endurance, and variation to make HfO₂-based FeRAM a scalable memory option. More importantly, in addition to cell size scaling by making both access transistor and capacitor smaller, cost/density per bit in HfO₂-based FeRAM can be significantly improved by vertically stacking capacitors, thanks to multiple bits defined through one single lithography step.⁵⁰⁹ Note that in this stacked-capacitor architecture, all the

TABLE II. Summary of pros and remaining challenges for different types of FE devices for high-speed and high-density embedded memory applications.

Device type	FeCAP	FeFET	FTJ
Pros	High speed, low voltage, healthy retention, robust endurance, low variations, low cost vertical stack	Promising density in the form of 3D vertical stack	Promising density in the form of cross-bar array
Challenges	Continue voltage scaling, disturb immunity	High voltage, slow speed, limited write endurance, long delay between read and write, large variations in scaled dimension	Slow read, small on and off ratio

capacitors share the same bit line (BL) with individual plate line (PL) controls, and therefore, capacitors with strong read disturb immunity are the key elements to achieve such a high density with the right functionality.⁵⁰⁹

In addition to FE or AFE capacitor-based memory cells, FeFETs, where the conventional high-k dielectric is replaced by FE oxide,⁵¹¹ are also attractive as a high-density embedded memory solution since the memory cell is composed of only one transistor, potentially achieving very high-density in its three-dimensional (3D) configurations. The bits stored in FE materials are converted to high and low source-to-drain currents for fast read operations. However, to be a viable device option for high-speed and high-density embedded memory applications, there are still several challenges that need to be addressed in FeFETs, such as high operation voltage, slow write speed, limited write endurance, required long delay between initial read operation after the write operation,⁵¹² and significant degradation in variations in scaled dimension.⁵¹³

Moving toward high capacity with fast FE memory, a configuration based on a crossbar array is of great interest, as it can be easily stacked with low cost to further increase the density.⁵¹⁴ To fit into such an architecture, FTJs or diodes with a built-in selector function can be potentially served as a compact two-terminal cell structure due to (i) a large enough electric field across the junction enabling fast polarization switching with low operation voltage, (ii) robust write endurance based on polarization-dependent on and off currents, and (iii) high array scalability thanks to low write currents. Nevertheless, low read currents with a poor on/off ratio are observed for these devices and need to be further improved to make either FTJs or diodes enable this option in the fast embedded memory space.⁵¹⁵ Table II summarizes the pros and remaining challenges for different FE devices for high-speed and high-density embedded memory applications.

Except for near-memory computing, where computing occurs close to fast and high-density embedded memory elements, direct computing in memory also provides another path for breakthroughs in computing efficiency.⁵¹⁶ FE capacitors, transistors, tunnel junctions, and diodes all can be utilized as critical multi-states non-volatile memory elements for functions such as dot product due to partial polarization or domain switching in HfO_2 -based FE materials. In general, multi-state FE memory devices with a tight distribution of each state with capability for linear potentiation and

depression are desired for in-memory computing. Such functionality relies on precise controls in domain structures that remain challenging in scaled polycrystalline hafnia-based FE films prepared by industry-friendly processes, such as ALD and ALE.

The discovery of hafnia-based FE materials such as HZO opens plenty of opportunities to significantly improve future computing through integrating different types of FE memory devices into state-of-art advanced CMOS technologies. Consequently, having a comprehensive understanding of this class of materials as well as their interaction with either metals used as electrodes or the dielectrics used as at interfaces becomes vitally important to address the current challenges and to overcome the current computing bottleneck and enable the breakthroughs in computing efficiency in the future. PLD and MBE thin film fabrication technologies have been instrumental for the in-depth thin film research and characterization, while MOCVD, ALD, Sputter PVD, and CSD technologies are favorable for high-volume manufacturing. Device architectures as well as device size often put constraints on the choice for the film deposition technology. ALD hardware and technology advancements hold the most promise for 3D device stacking in bit cost scalable architectures at this time.

XI. CONCLUSIONS AND OUTLOOK

Uwe Schroeder and José P. B. Silva

Ferroelectric HfO_2 and ZrO_2 are expected to be the dominant materials in memory technologies in the short to medium term, with further promising applications in other areas, such as the energy storage. To achieve this, improvement of materials' properties is needed. There are many challenges left in all aspects of bulk growth, thin-film growth, and device processing.

With respect to bulk growth, the laser floating zone method seems to be the most convenient method to obtain α -phase $\text{HfO}_2\text{-Y}$, but it would be relevant to investigate other dopants and also yttrium-stabilized zirconia since it is a famous ionic conductor material. It was important to be able to find FE properties in bulk material and not just in small grains. Here, a solid solution with uniform Y doping in HfO_2 resulted in a centimeter-sized rod after rapid cooling of a molten liquid.

In the case of thin-film growth, there is a very large range of techniques that are being used to grow FE HfO_2 and ZrO_2 that have specific advantages and disadvantages inherent to the deposition process itself. However, fundamental research on the physical properties of these materials is important and should be conducted with the support of the academic community. In particular, a more complete understanding of the physical properties of point defects and interfacial role is highly required to fully understand the behavior of materials devices. Furthermore, we should highlight the growing interest in epitaxial films, which are now being intensively investigated, due to the reduction/elimination of some of the current issues of polycrystalline thin films, such as the wake-up effect. In this case, the PLD growth method seems to be the most used method due to the high homogeneity, flat surfaces and interfaces, and excellent functional properties.

To overcome the challenges of the wake-up effect, large switching voltages; moderate retention and endurance, imposed by FE HfO_2 - and ZrO_2 -based materials; and different strategies, such as doping, defect engineering, interface engineering, electrodes optimization, and laminated structures, are currently being investigated. Limitations of controlling structure, interfacial thickness, chemistry, and physical properties is primarily a function of the selected deposition technique, processing conditions, and source materials.

As for device improvement, it is still necessary to improve reliability of FE HfO_2 - and ZrO_2 -based capacitors. As discussed, charge injection and movement need to be reduced to enhance endurance and retention. Here, a lower switching voltage; stable P_r , which is not too large; and a low defect density at the electrode interface and within the bulk of the ferroelectric layer are required. In the case of FTJs, it is critical to reduce the switching fields, and thus, an understanding of the dynamics of polarization switching between the different phases is still needed. Interestingly, it is also possible to use a thick HfO_2 layer that does not support direct tunneling but can become conductive through doping. This should allow for the development of new devices and their optimization in the near future. On the other hand, in the case of supercapacitors, it will be necessary to increase the ESD by $\sim 50\%$, to $\sim 150 \text{ J cm}^{-3}$, while keeping an efficiency of $\sim 95\%$, and therefore, different strategies are anticipated to achieve this.

In 2021, the tenth anniversary of the revolutionary discovery of the ferroelectricity in Si-doped HfO_2 , which stimulated intensive international research on these materials, was completed. In this decade, FE HfO_2 - and ZrO_2 -based materials have attracted the interest of the scientific community, and many fundamental material and device technologies have been created. In addition, manufacturing companies started to develop their way in marketing some of these devices. However, for both FeRAM and FeFET devices, the problems of reliability and, for FeFETs, the additional problem of variability for scaled devices must be solved in order to commercialize the technology. Besides that, these materials also show potential for supercapacitors, in-memory, and neuromorphic computing.

We expect that FE HfO_2 - and ZrO_2 -based thin films reach the stage of the device's practical realization and industrialization in the following decade, providing valuable contributions to the global societal challenges.

AUTHOR DECLARATIONS

Conflict of Interest

The authors have no conflicts to disclose.

Author Contributions

José P. B. Silva: Conceptualization (lead); Investigation (equal); Writing – original draft (lead); Writing – review & editing (lead). **Ruben Alcala:** Investigation (equal); Writing – original draft (equal); Writing – review & editing (equal). **Uygar E. Avci:** Investigation (equal); Writing – original draft (equal); Writing – review & editing (equal). **Nick Barrett:** Investigation (equal); Writing – original draft (equal); Writing – review & editing (equal). **Laura Bégon-Lours:** Investigation (equal); Writing – original draft (equal); Writing – review & editing (equal). **Mattias Borg:** Investigation (equal); Writing – original draft (equal); Writing – review & editing (equal). **Seungyong Byun:** Investigation (equal); Writing – original draft (equal); Writing – review & editing (equal). **Sou-Chi Chang:** Investigation (equal); Writing – original draft (equal); Writing – review & editing (equal). **Sang-Wook Cheong:** Investigation (equal); Writing – original draft (equal); Writing – review & editing (equal). **Duk-Hyun Choe:** Investigation (equal); Writing – original draft (equal); Writing – review & editing (equal). **Jean Coignus:** Investigation (equal); Writing – original draft (equal); Writing – review & editing (equal). **Veeresh Deshpande:** Investigation (equal); Writing – original draft (equal); Writing – review & editing (equal). **Athanasis Dimoulas:** Investigation (equal); Writing – original draft (equal); Writing – review & editing (equal). **Catherine Dubourdieu:** Investigation (equal); Writing – original draft (equal); Writing – review & editing (equal). **Ignasi Fina:** Investigation (equal); Writing – original draft (equal); Writing – review & editing (equal). **Hiroshi Funakubo:** Investigation (equal); Writing – original draft (equal); Writing – review & editing (equal). **Laurent Grenouillet:** Investigation (equal); Writing – original draft (equal); Writing – review & editing (equal). **Alexei Gruverman:** Investigation (equal); Writing – original draft (equal); Writing – review & editing (equal). **Jinseong Heo:** Investigation (equal); Writing – original draft (equal); Writing – review & editing (equal). **Michael Hoffmann:** Investigation (equal); Writing – original draft (equal); Writing – review & editing (equal). **H. Alex Hsain:** Investigation (equal); Writing – original draft (equal); Writing – review & editing (equal). **Fei-Ting Huang:** Investigation (equal); Writing – original draft (equal); Writing – review & editing (equal). **Cheol Seong Hwang:** Investigation (equal); Writing – original draft (equal); Writing – review & editing (equal). **Jorge Iñiguez:** Investigation (equal); Writing – original draft (equal); Writing – review & editing (equal). **Jacob L. Jones:** Investigation (equal); Writing – original draft (equal); Writing – review & editing (equal). **Ilya V. Karpov:** Investigation (equal); Writing – original draft (equal); Writing – review & editing (equal). **Alfred Kersch:** Investigation (equal); Writing – original draft (equal); Writing – review & editing (equal). **Taegyu Kwon:** Investigation (equal); Writing – original draft (equal); Writing – review & editing (equal). **Suzanne Lancaster:** Investigation (equal); Writing – original draft (equal); Writing – review & editing (equal). **Maximilian Lederer:** Investigation (equal); Writing –

original draft (equal); Writing – review & editing (equal). **Younghwan Lee**: Investigation (equal); Writing – original draft (equal); Writing – review & editing (equal). **Patrick D. Lomenzo**: Investigation (equal); Writing – original draft (equal); Writing – review & editing (equal). **Lane W. Martin**: Investigation (equal); Writing – original draft (equal); Writing – review & editing (equal). **Simon Martin**: Investigation (equal); Writing – original draft (equal); Writing – review & editing (equal). **Shinji Migita**: Investigation (equal); Writing – original draft (equal); Writing – review & editing (equal). **Thomas Mikolajick**: Investigation (equal); Writing – original draft (equal); Writing – review & editing (equal). **Beatriz Noheda**: Investigation (equal); Writing – original draft (equal); Writing – review & editing (equal). **Min Hyuk Park**: Investigation (equal); Writing – original draft (equal); Writing – review & editing (equal). **Karin M. Rabe**: Investigation (equal); Writing – original draft (equal); Writing – review & editing (equal). **Sayeef Salahuddin**: Investigation (equal); Writing – original draft (equal); Writing – review & editing (equal). **Florencio Sánchez**: Investigation (equal); Writing – original draft (equal); Writing – review & editing (equal). **Konrad Seidel**: Investigation (equal); Writing – original draft (equal); Writing – review & editing (equal). **Takao Shimizu**: Investigation (equal); Writing – original draft (equal); Writing – review & editing (equal). **Takahisa Shiraishi**: Investigation (equal); Writing – original draft (equal); Writing – review & editing (equal). **Stefan Slesazeck**: Investigation (equal); Writing – original draft (equal); Writing – review & editing (equal). **Akira Toriumi**: Investigation (equal); Writing – original draft (equal); Writing – review & editing (equal). **Hiroshi Uchida**: Investigation (equal); Writing – original draft (equal); Writing – review & editing (equal). **Bertrand Vilquin**: Investigation (equal); Writing – original draft (equal); Writing – review & editing (equal). **Xianghan Xu**: Investigation (equal); Writing – original draft (equal); Writing – review & editing (equal). **Kun Hee Ye**: Investigation (equal); Writing – original draft (equal); Writing – review & editing (equal). **Uwe Schroeder**: Conceptualization (lead); Investigation (equal); Writing – original draft (lead); Writing – review & editing (lead).

DATA AVAILABILITY

The data that support the findings of this study are available within the article.

REFERENCES

- ¹M. Sung, K. Rho, J. Kim, J. Cheon, K. Choi, D. Kim, H. Em, G. Park, J. Woo, Y. Lee, J. Ko, M. Kim, G. Lee, S. W. Ryu, D. S. Sheen, Y. Joo, S. Kim, C. H. Cho, M.-H. Na, and J. Kim, in *2021 IEEE International Electron Devices Meeting (IEDM)* (IEEE, 2021), pp. 33.3.1–33.3.4.
- ²T. Francois, J. Coignus, A. Makosiej, B. Giraud, C. Carabasse, J. Barbot, S. Martin, N. Castellani, T. Magis, H. Grampeix, S. V. Duijn, C. Mounet, P. Chiquet, U. Schroeder, S. Slesazeck, T. Mikolajick, E. Nowak, M. Bocquet, N. Barrett, F. Andrieu, and L. Grenouillet, in *2021 IEEE International Electron Devices Meeting (IEDM)* (IEEE, 2021), pp. 33.1.1–33.1.4.
- ³AMD RyzenTM ThreadripperTM PRO 5995WX Product Specifications.
- ⁴DDR5 SDRAM MT60B2G8HB-48B Product Core Data Sheet.
- ⁵J. Okuno, T. Kunihiro, K. Konishi, H. Maemura, Y. Shuto, F. Sugaya, M. Materano, T. Ali, M. Lederer, K. Kuehnel, K. Seidel, U. Schroeder, T. Mikolajick, M. Tsukamoto, and T. Umebayashi, in *2021 IEEE International Memory Workshop (IMW)* (IEEE, 2021), pp. 1–3.
- ⁶J. Okuno, T. Kunihiro, K. Konishi, H. Maemura, Y. Shuto, F. Sugaya, M. Materano, T. Ali, K. Kuehnel, K. Seidel, U. Schroeder, T. Mikolajick, M. Tsukamoto, and T. Umebayashi, in *2020 IEEE Symposium on VLSI Technology* (IEEE, 2020), pp. 1–2.
- ⁷T. Francois, J. Coignus, A. Makosiej, B. Giraud, C. Carabasse, J. Barbot, S. Martin, N. Castellani, T. Magis, H. Grampeix, S. Van Duijn, C. Mounet, P. Chiquet, U. Schroeder, S. Slesazeck, T. Mikolajick, E. Nowak, M. Bocquet, N. Barrett, F. Andrieu, and L. Grenouillet, *IEEE Trans. Electron Devices* **69**, 2108 (2022).
- ⁸R. Alcala, M. Materano, P. D. Lomenzo, L. Grenouillet, T. Francois, J. Coignus, N. Vaxelaire, C. Carabasse, S. Chevalliez, F. Andrieu, T. Mikolajick, and U. Schroeder, *IEEE J. Electron Devices Soc.* **10**, 907 (2022).
- ⁹A. Fernandez, M. Acharya, H.-G. Lee, J. Schimpf, Y. Jiang, D. Lou, Z. Tian, and L. W. Martin, *Adv. Mater.* **34**, 2108841 (2022).
- ¹⁰M. E. Lines and A. M. Glass, *Principles and Applications of Ferroelectrics and Related Materials* (Oxford University Press, 2001).
- ¹¹S. Das, Z. Hong, M. McCarter, P. Shafer, Y.-T. Shao, D. A. Muller, L. W. Martin, and R. Ramesh, *APL Mater.* **8**, 120902 (2020).
- ¹²S. Chen, S. Yuan, Z. Hou, Y. Tang, J. Zhang, T. Wang, K. Li, W. Zhao, X. Liu, L. Chen, L. W. Martin, and Z. Chen, *Adv. Mater.* **33**, 2000857 (2020).
- ¹³A. K. Yadav, C. T. Nelson, S. L. Hsu, Z. Hong, J. D. Clarkson, C. M. Schlepütz, A. R. Damodaran, P. Shafer, E. Arenholz, L. R. Dedon, D. Chen, A. Vishwanath, A. M. Minor, L. Q. Chen, J. F. Scott, L. W. Martin, and R. Ramesh, *Nature* **530**, 198 (2016).
- ¹⁴L. Qi, S. Ruan, and Y.-J. Zeng, *Adv. Mater.* **33**, 2005098 (2021).
- ¹⁵M. Wu, *ACS Nano* **15**, 9229 (2021).
- ¹⁶J. Wu, H.-Y. Chen, N. Yang, J. Cao, X. Yan, F. Liu, Q. Sun, X. Ling, J. Guo, and H. Wang, *Nat. Electron.* **3**, 466 (2020).
- ¹⁷D. Jena, R. Page, J. Casamento, P. Dang, J. Singhal, Z. Zhang, J. Wright, G. Khalsa, Y. Cho, and H. G. Xing, *Jpn. J. Appl. Phys.* **58**, 0801 (2019).
- ¹⁸T. Mikolajick, U. Schroeder, and M. H. Park, *Appl. Phys. Lett.* **118**, 180402 (2021).
- ¹⁹S. S. Cheema, D. Kwon, N. Shanker, R. dos Reis, S. L. Hsu, J. Xiao, H. Zhang, R. Wagner, A. Datar, M. R. McCarter, C. R. Serrao, A. K. Yadav, G. Karbasian, C. H. Hsu, A. J. Tan, L. C. Wang, V. Thakare, X. Zhang, A. Mehta, E. Karapetrova, R. V. Chopdekar, P. Shafer, E. Arenholz, C. Hu, R. Proksch, R. Ramesh, J. Ciston, and S. Salahuddin, *Nature* **580**, 478 (2020).
- ²⁰I. Fina and F. Sánchez, *ACS Appl. Electron. Mater.* **3**, 1530 (2021).
- ²¹U. Schroeder, M. H. Park, T. Mikolajick, and C. S. Hwang, *Nat. Rev. Mater.* **7**, 653 (2022).
- ²²J. F. Scott, *J. Phys.: Condens. Matter* **20**, 021001 (2007).
- ²³H.-J. Lee, M. Lee, K. Lee, J. Jo, H. Yang, Y. Kim, S. C. Chae, U. Waghmare, and J. H. Lee, *Science* **369**, 1343 (2020).
- ²⁴T. D. Huan, V. Sharma, G. A. Rossetti, and R. Ramprasad, *Phys. Rev. B* **90**, 064111 (2014).
- ²⁵S. E. Reyes-Lillo, K. F. Garrity, and K. M. Rabe, *Phys. Rev. B* **90**, 140103 (2014).
- ²⁶Y. Qi, S. Singh, C. Lau, F.-T. Huang, X. Xu, F. J. Walker, C. H. Ahn, S.-W. Cheong, and K. M. Rabe, *Phys. Rev. Lett.* **125**, 257603 (2020).
- ²⁷Y. Wei, P. Nukala, M. Salverda, S. Matzen, H. J. Zhao, J. Momand, A. S. Everhardt, G. Agnus, G. R. Blake, P. Lecoer, B. J. Kooi, J. Íñiguez, B. Dkhil, and B. Noheda, *Nat. Mater.* **17**, 1095 (2018).
- ²⁸U. Schroeder, T. Mittmann, M. Materano, P. D. Lomenzo, P. Edgington, Y. H. Lee, M. Alotaibi, A. R. West, T. Mikolajick, A. Kersch, and J. L. Jones, *Adv. Electron. Mater.* **8**, 2200265 (2022).
- ²⁹L. Azevedo Antunes, R. Ganser, C. Kuenneth, and A. Kersch, *Phys. Status Solidi RRL* **16**, 2100636 (2022).
- ³⁰R. Materlik, C. Künneth, and A. Kersch, *J. Appl. Phys.* **117**, 134109 (2015).
- ³¹R. Batra, T. D. Huan, J. L. Jones, G. Rossetti, and R. Ramprasad, *J. Phys. Chem. C* **121**, 4139 (2017).
- ³²X. Xu, F.-T. Huang, Y. Qi, S. Singh, K. M. Rabe, D. Obeysekera, J. Yang, M.-W. Chu, and S.-W. Cheong, *Nat. Mater.* **20**, 826 (2021).
- ³³M. Materano, T. Mittmann, P. D. Lomenzo, C. Zhou, J. L. Jones, M. Falkowski, A. Kersch, T. Mikolajick, and U. Schroeder, *ACS Appl. Electron. Mater.* **2**, 3618 (2020).

³⁴R. Batra, T. D. Huan, G. A. Rossetti, and R. Ramprasad, *Chem. Mater.* **29**, 9102 (2017).

³⁵C. Künneth, R. Materlik, M. Falkowski, and A. Kersch, *ACS Appl. Nano Mater.* **1**, 254 (2017).

³⁶R. Materlik, C. Künneth, M. Falkowski, T. Mikolajick, and A. Kersch, *J. Appl. Phys.* **123**, 164101 (2018).

³⁷S. Dutta, H. Aramberri, T. Schenk, and J. Íñiguez, *Phys. Status Solidi RRL* **14**, 2000047 (2020).

³⁸J. Liu, S. Liu, L. H. Liu, B. Hanrahan, and S. T. Pantelides, *Phys. Rev. Appl.* **12**, 034032 (2019).

³⁹S. Dutta, P. Buraghain, S. Glinsek, C. Richter, H. Aramberri, H. Lu, U. Schroeder, E. Defay, A. Gruverman, and J. Íñiguez, *Nat. Commun.* **12**, 7301 (2021).

⁴⁰Y. Qi, S. E. Reyes-Lillo, and K. M. Rabe, [arXiv:2204.06999](https://arxiv.org/abs/2204.06999) (2022).

⁴¹S. Clima, D. J. Wouters, C. Adelmann, T. Schenk, U. Schroeder, M. Jurczak, and G. Pourtois, *Appl. Phys. Lett.* **104**, 092906 (2014).

⁴²H. Aramberri and J. Íñiguez, [arXiv:2302.00688](https://arxiv.org/abs/2302.00688) (2023).

⁴³M. Falkowski and A. Kersch, *ACS Appl. Mater. Interfaces* **12**, 32915 (2020).

⁴⁴R. Ganser, S. Bongartz, A. von Mach, L. Azevedo Antunes, and A. Kersch, *Phys. Rev. Appl.* **18**, 054066 (2022).

⁴⁵F. Delodovici, P. Barone, and S. Picozzi, *Phys. Rev. Mater.* **5**, 064405 (2021).

⁴⁶Y. Qi, S. Singh, and K. M. Rabe, [arXiv:2108.12538](https://arxiv.org/abs/2108.12538) (2022).

⁴⁷J.-H. Yuan, G.-Q. Mao, K.-H. Xue, N. Bai, C. Wang, Y. Cheng, H. Lyu, H. Sun, X. Wang, and X. Miao, *Chem. Mater.* **35**, 94 (2022).

⁴⁸M. Materano, P. D. Lomenzo, H. Mulaosmanovic, M. Hoffmann, A. Toriumi, T. Mikolajick, and U. Schroeder, *Appl. Phys. Lett.* **117**, 262904 (2020).

⁴⁹W. Ding, Y. Zhang, L. Tao, Q. Yang, and Y. Zhou, *Acta Mater.* **196**, 556 (2020).

⁵⁰D.-H. Choe, S. Kim, T. Moon, S. Jo, H. Bae, S.-G. Nam, Y. S. Lee, and J. Heo, *Mater. Today* **50**, 8 (2021).

⁵¹P. Buraghain, A. Erickson, T. Mimura, T. Shimizu, H. Funakubo, and A. Gruverman, *Adv. Funct. Mater.* **32**, 2108876 (2021).

⁵²Y. Qi and K. M. Rabe, *Phys. Rev. B* **102**, 214108 (2020).

⁵³M. Falkowski and A. Kersch, *Appl. Phys. Lett.* **118**, 032905 (2021).

⁵⁴J. Wei, L. Jiang, M. Huang, Y. Wu, and S. Chen, *Adv. Funct. Mater.* **31**, 2104913 (2021).

⁵⁵J. Wu, Y. Zhang, L. Zhang, and S. Liu, *Phys. Rev. B* **103**, 024108 (2021).

⁵⁶C. Verdi, F. Karsai, P. Liu, R. Jinnouchi, and G. Kresse, *npj Comput. Mater.* **7**, 156 (2021).

⁵⁷Q. Wu, B. He, T. Song, J. Gao, and S. Shi, *Comput. Mater. Sci.* **125**, 243 (2016).

⁵⁸M. Hoffmann, F. P. G. Fengler, M. Herzig, T. Mittmann, B. Max, U. Schroeder, R. Negrea, P. Lucian, S. Slesazeck, and T. Mikolajick, *Nature* **565**, 464 (2019).

⁵⁹J. Íñiguez, P. Zubko, I. Luk'yanchuk, and A. Cano, *Nat. Rev. Mater.* **4**, 243 (2019).

⁶⁰T. S. Böscke, J. Müller, D. Bräuhaus, U. Schröder, and U. Böttger, *Appl. Phys. Lett.* **99**, 102903 (2011).

⁶¹S. Fan, S. Singh, X. Xu, K. Park, Y. Qi, S. W. Cheong, D. Vanderbilt, K. M. Rabe, and J. L. Musfeldt, *npj Quantum Mater.* **7**, 32 (2022).

⁶²T. Kiguchi, T. Shiraishi, T. Shimizu, H. Funakubo, and T. J. Konno, *Jpn. J. Appl. Phys.* **57**, 11 (2018).

⁶³Y. Cheng, Z. Gao, K. H. Ye, H. W. Park, Y. Zheng, Y. Zheng, J. Gao, M. H. Park, J.-H. Choi, K.-H. Xue, C. S. Hwang, and H. Lyu, *Nat. Commun.* **13**, 645 (2022).

⁶⁴S. Oh, H. Kim, A. Kashir, and H. Hwang, *Appl. Phys. Lett.* **117**, 252906 (2020).

⁶⁵B. Y. Kim, H. W. Park, S. D. Hyun, Y. B. Lee, S. H. Lee, M. Oh, S. K. Ryoo, I. S. Lee, S. Byun, D. Shim, D.-Y. Cho, M. H. Park, and C. S. Hwang, *Adv. Electron. Mater.* **8**, 2100042 (2021).

⁶⁶K. Katayama, T. Shimizu, O. Sakata, T. Shiraishi, S. Nakamura, T. Kiguchi, A. Akama, T. J. Konno, H. Uchida, and H. Funakubo, *J. Appl. Phys.* **119**, 134101 (2016).

⁶⁷Y. Yun, P. Buraghain, M. Li, Z. Ahmadi, Y. Zhang, X. Li, H. Wang, J. Li, P. Lu, L. Tao, H. Wang, J. E. Shield, E. Y. Tsymbal, A. Gruverman, and X. Xu, *Nat. Mater.* **21**, 903 (2022).

⁶⁸S. S. Cheema, N. Shanker, S.-L. Hsu, Y. Rho, C.-H. Hsu, V. A. Stoica, Z. Zhang, J. W. Freeland, P. Shafer, C. P. Grigoropoulos, J. Ciston, and S. Salahuddin, *Science* **376**, 648 (2022).

⁶⁹S. S. Cheema, N. Shanker, L.-C. Wang, C.-H. Hsu, S.-L. Hsu, Y.-H. Liao, M. San Jose, J. Gomez, W. Chakraborty, W. Li, J.-H. Bae, S. K. Volkman, D. Kwon, Y. Rho, G. Pinelli, R. Rastogi, D. Pipitone, C. Stull, M. Cook, B. Tyrrell, V. A. Stoica, Z. Zhang, J. W. Freeland, C. J. Tassone, A. Mehta, G. Saheli, D. Thompson, D. I. Suh, W.-T. Koo, K.-J. Nam, D. J. Jung, W.-B. Song, C.-H. Lin, S. Nam, J. Heo, N. Parikh, C. P. Grigoropoulos, P. Shafer, P. Fay, R. Ramesh, S. Mahapatra, J. Ciston, S. Datta, M. Mohamed, C. Hu, and S. Salahuddin, *Nature* **604**, 65 (2022).

⁷⁰P. Buraghain, H. Lu, C. Richter, T. Schenk, P. Kariuki, S. Glinsek, H. Funakubo, J. Íñiguez, E. Defay, U. Schroeder, and A. Gruverman, *Adv. Mater.* **34**, 2206237 (2022).

⁷¹A. Chouprik, R. Kirtaev, E. Korostylev, V. Mikheev, M. Spiridonov, and D. Negrov, *Nanomaterials* **12**, 1483 (2022).

⁷²J. Liu, S. Liu, J.-Y. Yang, and L. Liu, *Phys. Rev. Lett.* **125**, 197601 (2020).

⁷³S. Kirbach, M. Lederer, S. Eßlinger, C. Mart, M. Czernohorsky, W. Weinreich, and T. Wallmersperger, *Appl. Phys. Lett.* **118**, 012904 (2021).

⁷⁴T. Schenk, N. Godard, A. Mahjoub, S. Girod, A. Mataz, V. Bobnar, E. Defay, and S. Glinsek, *Phys. Status Solidi RRL* **14**, 1900626 (2019).

⁷⁵L. Collins, Y. Liu, O. S. Ovchinnikova, and R. Proksch, *ACS Nano* **13**, 8055 (2019).

⁷⁶R. K. Vasudevan, N. Balke, P. Maksymovych, S. Jesse, and S. V. Kalinin, *Appl. Phys. Rev.* **4**, 021302 (2017).

⁷⁷D.-S. Park, M. Hadad, L. M. Riemer, R. Ignatans, D. Spirito, V. Esposito, V. Tileli, N. Gauquelin, D. Chezganov, D. Jannis, J. Verbeeck, S. Gorfman, N. Pryds, P. Muralt, and D. Damjanovic, *Science* **375**, 653 (2022).

⁷⁸S. Wada, H. Kakimoto, and T. Tsurumi, *Mater. Trans.* **45**, 178 (2004).

⁷⁹S. Starschich, T. Schenk, U. Schroeder, and U. Boettger, *Appl. Phys. Lett.* **110**, 182905 (2017).

⁸⁰W. Zhong, D. Vanderbilt, and K. M. Rabe, *Phys. Rev. Lett.* **73**, 1861 (1994).

⁸¹J. C. Wojdeł, P. Hermet, M. P. Ljungberg, P. Ghosez, and J. Íñiguez, *J. Phys.: Condens. Matter* **25**, 305401 (2013).

⁸²T. P. Senftle, S. Hong, M. M. Islam, S. B. Kylasa, Y. Zheng, Y. K. Shin, C. Junkermeier, R. Engel-Herbert, M. J. Janik, H. M. Aktulga, T. Verstraelen, A. Grama, and A. C. T. van Duin, *npj Comput. Mater.* **2**, 15011 (2016).

⁸³S. Tinte, M. G. Stachiootti, M. Sepliarsky, R. L. Mignoni, and C. O. Rodriguez, *J. Phys.: Condens. Matter* **11**, 9679 (1999).

⁸⁴Y.-H. Shin, V. R. Cooper, I. Grinberg, and A. M. Rappe, *Phys. Rev. B* **71**, 054104 (2005).

⁸⁵S. Jachalke, T. Schenk, M. H. Park, U. Schroeder, T. Mikolajick, H. Stöcker, E. Mehner, and D. C. Meyer, *Appl. Phys. Lett.* **112**, 142901 (2018).

⁸⁶P. D. Lomenzo, R. Alcalá, C. Richter, S. Li, T. Mikolajick, and U. Schroeder, *Appl. Phys. Lett.* **119**, 112903 (2021).

⁸⁷C. Mart, T. Kämpfe, S. Zybell, and W. Weinreich, *Appl. Phys. Lett.* **112**, 052905 (2018).

⁸⁸C. Mart, K. Kühnel, T. Kämpfe, S. Zybell, and W. Weinreich, *Appl. Phys. Lett.* **114**, 102903 (2019).

⁸⁹P. D. Lomenzo, S. Jachalke, H. Stoecker, E. Mehner, C. Richter, T. Mikolajick, and U. Schroeder, *Nano Energy* **74**, 104733 (2020).

⁹⁰C. Mart, T. Kämpfe, K. Kühnel, M. Czernohorsky, S. Kolodinski, M. Wiatr, W. Weinreich, and L. M. Eng, *APL Mater.* **9**, 051120 (2021).

⁹¹M. Neuber, M. W. Lederer, K. Mertens, T. Kämpfe, M. Czernohorsky, and K. Seidel, *Crystals* **12**, 1115 (2022).

⁹²M. Hoffmann, U. Schroeder, C. Künneth, A. Kersch, S. Starschich, U. Böttger, and T. Mikolajick, *Nano Energy* **18**, 154 (2015).

⁹³B. Ploss and S. Bauer, *Sens. Actuators, A* **26**, 407 (1991).

⁹⁴Q. Zhang and R. W. Whatmore, *J. Appl. Phys.* **94**, 5228 (2003).

⁹⁵T. Ali, D. Lehninger, M. Lederer, S. Li, K. Kühnel, C. Mart, K. Mertens, R. Hoffmann, R. Olivo, J. Emara, K. Biedermann, J. Metzger, R. Binder, M. Czernohorsky, T. Kämpfe, J. Müller, K. Seidel, and L. M. Eng, *Adv. Electron. Mater.* **8**, 2100837 (2022).

⁹⁶C. Mart, W. Weinreich, M. Czernohorsky, S. Riedel, S. Zybell, and K. Kühnel, in *2018 48th European Solid-State Device Research Conference (ESSDERC)* (IEEE, 2018), pp. 130–133.

⁹⁷R. Lehmkau, D. Mutschall, A. Kaiser, M. Ebermann, N. Neumann, M. Czernohorsky, M. Neuber, K. Hiller, J. Seiler, and T. Großmann, *Proc. SPIE* **12002**, 120020M (2022).

⁹⁸S. Jachalke, E. Mehner, H. Stöcker, J. Hanzig, M. Sonntag, T. Weigel, T. Leisegang, and D. C. Meyer, *Appl. Phys. Rev.* **4**, 021303 (2017).

⁹⁹A. K. Jonscher, *J. Chem. Soc., Faraday Trans. 2* **82**, 75 (1986).

¹⁰⁰R. Landauer, *Collect. Phenom.* **2**, 167 (1976).

¹⁰¹A. M. Bratkovsky and A. P. Levanyuk, *Appl. Phys. Lett.* **89**, 253108 (2006).

¹⁰²S. Salahuddin and S. Datta, *Nano Lett.* **8**, 405 (2007).

¹⁰³A. Islam Khan, D. Bhowmik, P. Yu, S. Joo Kim, X. Pan, R. Ramesh, and S. Salahuddin, *Appl. Phys. Lett.* **99**, 113501 (2011).

¹⁰⁴P. Zubko, J. C. Wojdel, M. Hadjimichael, S. Fernandez-Pena, A. Sené, I. Luk'yanchuk, J.-M. Triscone, and J. Iñiguez, *Nature* **534**, 524 (2016).

¹⁰⁵M. Hoffmann, S. Slesazeck, and T. Mikolajick, *APL Mater.* **9**, 020902 (2021).

¹⁰⁶M. Hoffmann and S. Salahuddin, *MRS Bull.* **46**, 930 (2021).

¹⁰⁷M. Hoffmann, M. Pešić, K. Chatterjee, A. I. Khan, S. Salahuddin, S. Slesazeck, U. Schroeder, and T. Mikolajick, *Adv. Funct. Mater.* **26**, 8643 (2016).

¹⁰⁸K. D. Kim, Y. J. Kim, M. H. Park, H. W. Park, Y. J. Kwon, Y. B. Lee, H. J. Kim, T. Moon, Y. H. Lee, S. D. Hyun, B. S. Kim, and C. S. Hwang, *Adv. Funct. Mater.* **29**, 1808228 (2019).

¹⁰⁹M. Hoffmann, Z. Wang, N. Tasneem, A. Zubair, P. V. Ravindran, M. Tian, A. A. Gaskell, D. Triyoso, S. Consiglio, K. Tapily, R. Clark, J. Hur, S. S. K. Pentapati, S. K. Lim, M. Dopita, S. Yu, W. Chern, J. Kacher, S. E. Reyes-Lillo, D. Antoniadis, J. Ravichandran, S. Slesazeck, T. Mikolajick, and A. I. Khan, *Nat. Commun.* **13**, 1228 (2022).

¹¹⁰M. Hoffmann, F. P. G. Fengler, B. Max, U. Schroeder, S. Slesazeck, and T. Mikolajick, *Adv. Energy Mater.* **9**, 1901154 (2019).

¹¹¹T. Kim, J. A. del Alamo, and D. A. Antoniadis, *IEEE Trans. Electron Devices* **69**, 4016 (2022).

¹¹²Z. Liu, H. Jiang, B. Ordway, and T. P. Ma, *IEEE Electron Device Lett.* **41**, 1492 (2020).

¹¹³M. Si, C.-J. Su, C. Jiang, N. J. Conrad, H. Zhou, K. D. Maize, G. Qiu, C.-T. Wu, A. Shakouri, M. A. Alam, and P. D. Ye, *Nat. Nanotechnol.* **13**, 24 (2017).

¹¹⁴M. A. Alam, M. Si, and P. D. Ye, *Appl. Phys. Lett.* **114**, 090401 (2019).

¹¹⁵B. Obradovic, T. Rakshit, R. Hatcher, J. A. Kittl, and M. S. Rodder, *IEEE Trans. Electron Devices* **65**, 5157 (2018).

¹¹⁶J. Van Houdt and P. Roussel, *IEEE Electron Device Lett.* **39**, 877 (2018).

¹¹⁷M. Hoffmann, S. Slesazeck, U. Schroeder, and T. Mikolajick, *Nat. Electron.* **3**, 504 (2020).

¹¹⁸A. K. Yadav, K. X. Nguyen, Z. Hong, P. García-Fernández, P. Aguado-Puente, C. T. Nelson, S. Das, B. Prasad, D. Kwon, S. Cheema, A. I. Khan, C. Hu, J. Iñiguez, J. Junquera, L.-Q. Chen, D. A. Muller, R. Ramesh, and S. Salahuddin, *Nature* **565**, 468 (2019).

¹¹⁹E. D. Grimley, T. Schenck, T. Mikolajick, U. Schroeder, and J. M. LeBeau, *Adv. Mater. Interfaces* **5**, 1701258 (2018).

¹²⁰A. K. Saha and S. K. Gupta, *Sci. Rep.* **10**, 10207 (2020).

¹²¹H. W. Park, M. Oh, and C. S. Hwang, *Adv. Funct. Mater.* **32**, 2200389 (2022).

¹²²M. Hoffmann, M. Gui, S. Slesazeck, R. Fontanini, M. Segatto, D. Esseni, and T. Mikolajick, *Adv. Funct. Mater.* **32**, 2108494 (2021).

¹²³H. Lee, D.-H. Choe, S. Jo, J.-H. Kim, H. H. Lee, H.-J. Shin, Y. Park, S. Kang, Y. Cho, S. Park, T. Moon, D. Eom, M. Leem, Y. Kim, J. Heo, E. Lee, and H. Kim, *ACS Appl. Mater. Interfaces* **13**, 36499 (2021).

¹²⁴W. Cao and K. Banerjee, *Nat. Commun.* **11**, 196 (2020).

¹²⁵M. Hoffmann, *Innovation Emerging Technol.* **9**, 2240002 (2022).

¹²⁶G.-D. Zhao, X. Liu, W. Ren, X. Zhu, and S. Yu, *Phys. Rev. B* **106**, 064104 (2022).

¹²⁷A. Kashir, M. G. Farahani, J. Lančok, H. Hwang, and S. Kamba, *Nanotechnology* **33**, 155703 (2022).

¹²⁸S. Lombardo, C. Nelson, K. Chae, S. Reyes-Lillo, M. Tian, N. Tasneem, Z. Wang, M. Hoffmann, D. Triyoso, S. Consiglio, K. Tapily, R. Clark, G. Leusink, K. Cho, A. Kummel, J. Kacher, and A. Khan, in *2020 IEEE Symposium on VLSI Technology* (IEEE, 2020), pp. 1–2.

¹²⁹M. Hoffmann, S. S. Cheema, N. Shanker, W. Li, and S. Salahuddin, in *International Electron Devices Meeting (IEDM)* (IEEE, 2022), pp. 13.2.1–13.2.4.

¹³⁰N. Zagni, P. Pavan, and M. A. Alam, *Appl. Phys. Lett.* **114**, 233102 (2019).

¹³¹I. Stolichnov, M. Cavalieri, C. Gastaldi, M. Hoffmann, U. Schroeder, T. Mikolajick, and A. M. Ionescu, *Appl. Phys. Lett.* **117**, 172902 (2020).

¹³²S. Datta, *arXiv:2112.12687* (2022).

¹³³G. Catalan, J. Seidel, R. Ramesh, and J. F. Scott, *Rev. Mod. Phys.* **84**, 119 (2012).

¹³⁴P. Zhou, B. Zeng, W. Yang, J. Liao, F. Meng, Q. Zhang, L. Gu, S. Zheng, M. Liao, and Y. Zhou, *Acta Mater.* **232**, 117920 (2022).

¹³⁵P. Buragohain, C. Richter, T. Schenk, H. Lu, T. Mikolajick, U. Schroeder, and A. Gruverman, *Appl. Phys. Lett.* **112**, 222901 (2018).

¹³⁶H. Bae, S. G. Nam, T. Moon, Y. Lee, S. Jo, D.-H. Choe, S. Kim, K.-H. Lee, and J. Heo, in *2020 IEEE International Electron Devices Meeting (IEDM)* (IEEE, 2020), pp. 31.3.1–31.3.4.

¹³⁷K. Lee, S. Kim, J.-H. Lee, B.-G. Park, and D. Kwon, *IEEE Electron Device Lett.* **42**, 323 (2021).

¹³⁸X. Lyu, P. R. Shrestha, M. Si, P. Wang, J. Li, K. P. Cheung, S. Yu, and P. D. Ye, in *2022 IEEE Symposium on VLSI Technology and Circuits* (IEEE, 2022), pp. 338–339.

¹³⁹P. Hao, S. Zheng, B. Zeng, T. Yu, Z. Yang, L. Liao, Q. Peng, Q. Yang, Y. Zhou, and M. Liao, *Adv. Funct. Mater.* **33**, 2301746 (2023).

¹⁴⁰M. M. Dahan, H. Mulaosmanovic, O. Levit, S. Dünkel, S. Beyer, and E. Yalon, *Nano Lett.* **23**, 1395 (2023).

¹⁴¹T. Maeda, B. Magyari-Kope, and Y. Nishi, in *2017 IEEE International Memory Workshop (IMW)* (IEEE, 2017).

¹⁴²P. Nukala, M. Ahmadi, Y. Wei, S. de Graaf, E. Stylianidis, T. Chakrabortty, S. Matzen, H. W. Zandbergen, A. Björling, D. Mannix, D. Carbone, B. Kooi, and B. Noheda, *Science* **372**, 630 (2021).

¹⁴³L. Chen, Z. Liang, S. Shao, Q. Huang, K. Tang, and R. Huang, *Nanoscale* **15**, 7014 (2023).

¹⁴⁴A. Silva, I. Fina, F. Sánchez, J. P. B. Silva, L. Marques, and V. Lenzi, *Mater. Today Phys.* **34**, 101064 (2023).

¹⁴⁵Y. Wu, Y. Zhang, J. Jiang, L. Jiang, M. Tang, Y. Zhou, M. Liao, Q. Yang, and E. Y. Tsymbal, “Unconventional polarization switching mechanism in (Hf, Zr)O₂ ferroelectrics,” *arXiv:2301.06248*.

¹⁴⁶D.-H. Choe, H. Bae, H. Lee, Y. Lee, T. Moon, S. G. Nam, S. Jo, H. J. Lee, E. Lee, and J. Heo, in *2021 IEEE International Electron Devices Meeting (IEDM)* (IEEE, 2021), pp. 15.1.1–15.1.4.

¹⁴⁷K. Chae, S. F. Lombardo, N. Tasneem, M. Tian, H. Kumarasubramanian, J. Hur, W. Chern, S. Yu, C. Richter, P. D. Lomenzo, M. Hoffmann, U. Schroeder, D. Triyoso, S. Consiglio, K. Tapily, R. Clark, G. Leusink, N. Bassiri-Gharb, P. Bandaru, J. Ravichandran, A. Kummel, K. Cho, J. Kacher, and A. I. Khan, *ACS Appl. Mater. Interfaces* **14**, 36771 (2022).

¹⁴⁸H. Yang, H.-J. Lee, J. Jo, C. H. Kim, and J. H. Lee, *Phys. Rev. Appl.* **14**, 064012 (2020).

¹⁴⁹A. Erba, J. Baima, I. Bush, R. Orlando, and R. Dovesi, *J. Chem. Theory Comput.* **13**, 5019 (2017).

¹⁵⁰A. Nakata, J. S. Baker, S. Y. Mujahed, J. T. L. Poulton, S. Arapan, J. Lin, Z. Raza, S. Yadav, L. Truflandier, T. Miyazaki, and D. R. Bowler, *J. Chem. Phys.* **152**, 164112 (2020).

¹⁵¹P. Liu, C. Verdi, F. Karsai, and G. Kresse, *Phys. Rev. B* **105**, 060102 (2022).

¹⁵²H. W. Park, J. Roh, Y. B. Lee, and C. S. Hwang, *Adv. Mater.* **31**, 1805266 (2019).

¹⁵³M. Hyuk Park, H. Joon Kim, Y. Jin Kim, T. Moon, and C. Seong Hwang, *Appl. Phys. Lett.* **104**, 072901 (2014).

¹⁵⁴D. H. Lee, Y. Lee, K. Yang, J. Y. Park, S. H. Kim, P. R. S. Reddy, M. Materano, H. Mulaosmanovic, T. Mikolajick, J. L. Jones, U. Schroeder, and M. H. Park, *Appl. Phys. Rev.* **8**, 021312 (2021).

¹⁵⁵K. A. Hunnestad, E. D. Roede, A. T. J. van Helvoort, and D. Meier, *J. Appl. Phys.* **128**, 191102 (2020).

¹⁵⁶Y. Liu, K. P. Kelley, H. Funakubo, S. V. Kalinin, and M. Ziatdinov, *Adv. Sci.* **9**, 2203957 (2022).

¹⁵⁷A. B. Chase and J. A. Osmer, *Am. Mineral.* **51**, 1808 (1966).

¹⁵⁸R. Ruh and P. W. R. Corfield, *J. Am. Ceram. Soc.* **53**, 126 (1970).

¹⁵⁹V. V. Lozanov, N. I. Baklanova, V. R. Shayapov, and A. S. Berezin, *Cryst. Growth Des.* **16**, 5283 (2016).

¹⁶⁰F. Kadlec and P. Simon, *Mater. Sci. Eng.: B* **72**, 56 (2000).

¹⁶¹M. Mann and J. Kolis, *J. Cryst. Growth* **312**, 461 (2010).

¹⁶²S. Kurosawa, Y. Futami, V. V. Kochurikhin, M. A. Borik, Y. Yokota, T. Yanagida, and A. Yoshikawa, *Key Eng. Mater.* **508**, 81 (2012).

¹⁶³H. Yu, C. Liu, Z. Zhang, S. Huang, Y. Yang, R. Mao, H. Feng, and J. Zhao, *Chem. Phys. Lett.* **738**, 136916 (2020).

¹⁶⁴K. J. Kim, K. Kamada, R. Murakami, T. Horiai, S. Ishikawa, V. V. Kochurikhin, M. Yoshino, A. Yamaji, Y. Shoji, S. Kurosawa, S. Toyoda, H. Sato, Y. Yokota, Y. Ohashi, and A. Yoshikawa, *Crystals* **10**, 619 (2020).

¹⁶⁵J. Müller, U. Schröder, T. S. Böscke, I. Müller, U. Böttger, L. Wilde, J. Sundqvist, M. Lemberger, P. Kücher, T. Mikolajick, and L. Frey, *J. Appl. Phys.* **110**, 114113 (2011).

¹⁶⁶J. Müller, T. S. Böscke, U. Schröder, S. Mueller, D. Bräuhaus, U. Böttger, L. Frey, and T. Mikolajick, *Nano Lett.* **12**, 4318 (2012).

¹⁶⁷S. Mueller, C. Adelmann, A. Singh, S. Van Elshocht, U. Schroeder, and T. Mikolajick, *ECS J. Solid State Sci. Technol.* **1**, 123 (2012).

¹⁶⁸S. Mueller, J. Mueller, A. Singh, S. Riedel, J. Sundqvist, U. Schroeder, and T. Mikolajick, *Adv. Funct. Mater.* **22**, 2412 (2012).

¹⁶⁹M. Pešić, F. P. G. Fengler, L. Larcher, A. Padovani, T. Schenk, E. D. Grimley, X. Sang, J. M. LeBeau, S. Slesazeck, U. Schroeder, and T. Mikolajick, *Adv. Funct. Mater.* **26**, 4601 (2016).

¹⁷⁰T. Mittmann, M. Materano, P. D. Lomenzo, M. H. Park, I. Stolichnov, M. Cavalieri, C. Zhou, C.-C. Chung, J. L. Jones, T. Szyjka, M. Müller, A. Kersch, T. Mikolajick, and U. Schroeder, *Adv. Mater. Interfaces* **6**, 1900042 (2019).

¹⁷¹Y.-C. Chiu, C.-H. Cheng, C.-Y. Chang, Y.-T. Tang, and M.-C. Chen, *Phys. Status Solidi RRL* **11**, 1600368 (2017).

¹⁷²Y. Tashiro, T. Shimizu, T. Mimura, and H. Funakubo, *ACS Appl. Electron. Mater.* **3**, 3123 (2021).

¹⁷³M. Hoffmann, U. Schroeder, T. Schenk, T. Shimizu, H. Funakubo, O. Sakata, D. Pohl, M. Drescher, C. Adelmann, R. Materlik, A. Kersch, and T. Mikolajick, *J. Appl. Phys.* **118**, 072006 (2015).

¹⁷⁴T. Ito, T. Ushiyama, Y. Yanagisawa, Y. Tomioka, I. Shindo, and A. Yanase, *J. Cryst. Growth* **363**, 264 (2013).

¹⁷⁵T. Mimura, T. Shimizu, and H. Funakubo, *Appl. Phys. Lett.* **115**, 032901 (2019).

¹⁷⁶U. Schroeder, C. Richter, M. H. Park, T. Schenk, M. Pešić, M. Hoffmann, F. P. G. Fengler, D. Pohl, B. Rellinghaus, C. Zhou, C.-C. Chung, J. L. Jones, and T. Mikolajick, *Inorg. Chem.* **57**, 2752 (2018).

¹⁷⁷A. Pimenov, J. Ullrich, P. Lunkenheimer, A. Loidl, and C. H. Rüscher, *Solid State Ionics* **109**, 111 (1998).

¹⁷⁸T. Shimizu, T. Yokouchi, T. Shiraishi, T. Oikawa, P. S. Sankara Rama Krishnan, and H. Funakubo, *Jpn. J. Appl. Phys.* **53**, 09 (2014).

¹⁷⁹T. Shiraishi, K. Katayama, T. Yokouchi, T. Shimizu, T. Oikawa, O. Sakata, H. Uchida, Y. Imai, T. Kiguchi, T. J. Konno, and H. Funakubo, *Appl. Phys. Lett.* **108**, 262904 (2016).

¹⁸⁰P. Polakowski, S. Riedel, W. Weinreich, M. Rudolf, J. Sundqvist, K. Seidel, and J. Müller, in *2014 IEEE 6th International Memory Workshop (IMW)* (IEEE, 2014).

¹⁸¹K. D. Budd, S. K. Dey, and D. A. Payne, *Br. Ceram. Proc.* **36**, 107–121 (1985).

¹⁸²S. K. Dey, K. D. Budd, and D. A. Payne, *IEEE Trans. Ultrason., Ferroelectr., Freq. Control* **35**, 80 (1988).

¹⁸³S. K. Singh, R. Ueno, H. Funakubo, H. Uchida, S. Koda, and H. Ishiwara, *Jpn. J. Appl. Phys.* **44**, 8525 (2005).

¹⁸⁴H. Uchida, R. Ueno, H. Funakubo, and S. Koda, *J. Appl. Phys.* **100**, 014106 (2006).

¹⁸⁵T. J. Boyle, C. D. Buchheit, M. A. Rodriguez, H. N. Al-Shareef, B. A. Hernandez, B. Scott, and J. W. Ziller, *J. Mater. Res.* **11**, 2274 (1996).

¹⁸⁶K. Kato, C. Zheng, J. M. Finder, S. K. Dey, and Y. Torii, *J. Am. Ceram. Soc.* **81**, 1869 (2005).

¹⁸⁷S. Starschich, D. Griesche, T. Schneller, R. Waser, and U. Böttger, *Appl. Phys. Lett.* **104**, 202903 (2014).

¹⁸⁸C. Abe, S. Nakayama, M. Shiokawa, H. Kawashima, K. Katayama, T. Shiraishi, T. Shimizu, H. Funakubo, and H. Uchida, *Ceram. Int.* **43**, 501 (2017).

¹⁸⁹S. Nakayama, H. Funakubo, and H. Uchida, *Jpn. J. Appl. Phys.* **57**, 11 (2018).

¹⁹⁰S. Zheng, Z. Zhao, Z. Liu, B. Zeng, L. Yin, Q. Peng, M. Liao, and Y. Zhou, *Appl. Phys. Lett.* **117**, 212904 (2020).

¹⁹¹Mohit, T. Miyasako, and E. Tokumitsu, *Jpn. J. Appl. Phys.* **60**, SBBM02 (2021).

¹⁹²T. Miyasako, S. Yoneda, T. Hosokura, M. Kimura, and E. Tokumitsu, *Appl. Phys. Lett.* **120**, 262901 (2022).

¹⁹³S. Starschich, D. Griesche, T. Schneller, and U. Böttger, *ECS J. Solid State Sci. Technol.* **4**, 419 (2015).

¹⁹⁴S. Starschich and U. Boettger, *J. Mater. Chem. C* **5**, 333 (2017).

¹⁹⁵Y. Yao, D. Zhou, S. Li, J. Wang, N. Sun, F. Liu, and X. Zhao, *J. Appl. Phys.* **126**, 154103 (2019).

¹⁹⁶M. Ángel Badillo-Avila, S. Taleb, T. Mokabber, J. Rieck, R. Castanedo-Pérez, G. Torres-Delgado, B. Noheda, and M. I. A. Meneses, *J. Mater. Chem. C* **11**, 1119 (2023).

¹⁹⁷Mohit, K.-i. Haga, and E. Tokumitsu, *Jpn. J. Appl. Phys.* **59**, SMMB02 (2020).

¹⁹⁸M. Shiokawa, K. Izaki, H. Funakubo, and H. Uchida, *MRS Proc.* **1729**, 99 (2015).

¹⁹⁹F. Huang, X. Chen, X. Liang, J. Qin, Y. Zhang, T. Huang, Z. Wang, B. Peng, P. Zhou, H. Lu, L. Zhang, L. Deng, M. Liu, Q. Liu, H. Tian, and L. Bi, *Phys. Chem. Chem. Phys.* **19**, 3486 (2017).

²⁰⁰Q. Shao, X. Wang, W. Jiang, Y. Chen, X. Zhang, L. Tu, T. Lin, H. Shen, X. Meng, A. Liu, and J. Wang, *Appl. Phys. Lett.* **115**, 162902 (2019).

²⁰¹M. Cavalieri, É. O'Connor, C. Gastaldi, I. Stolichnov, and A. M. Ionescu, *ACS Appl. Electron. Mater.* **2**, 1752 (2020).

²⁰²T. Shimizu, K. Katayama, T. Kiguchi, A. Akama, T. J. Konno, O. Sakata, and H. Funakubo, *Sci. Rep.* **6**, 32931 (2016).

²⁰³J. Lyu, I. Fina, R. Solanas, J. Fontcuberta, and F. Sánchez, *Appl. Phys. Lett.* **113**, 082902 (2018).

²⁰⁴J. Lyu, I. Fina, R. Solanas, J. Fontcuberta, and F. Sánchez, *ACS Appl. Electron. Mater.* **1**, 220 (2019).

²⁰⁵Z. Zhang, S.-L. Hsu, V. A. Stoica, H. Paik, E. Parsonnet, A. Qualls, J. Wang, L. Xie, M. Kumari, S. Das, Z. Leng, M. McBriarty, R. Proksch, A. Gruverman, D. G. Schlom, L.-Q. Chen, S. Salahuddin, L. W. Martin, and R. Ramesh, *Adv. Mater.* **33**, 2006089 (2021).

²⁰⁶T. Mimura, T. Shimizu, Y. Katsuya, O. Sakata, and H. Funakubo, *Jpn. J. Appl. Phys.* **59**, 04 (2020).

²⁰⁷T. Mimura, T. Shimizu, O. Sakata, and H. Funakubo, *Appl. Phys. Lett.* **118**, 112903 (2021).

²⁰⁸B. Prasad, V. Thakare, A. Kalitsov, Z. Zhang, B. Terris, and R. Ramesh, *Adv. Electron. Mater.* **7**, 2001074 (2021).

²⁰⁹Z. Shen, L. Liao, Y. Zhou, K. Xiong, J. Zeng, X. Wang, Y. Chen, J. Liu, T. Guo, S. Zhang, T. Lin, H. Shen, X. Meng, Y. Wang, Y. Cheng, J. Yang, P. Chen, L. Wang, X. Bai, J. Chu, and J. Wang, *Appl. Phys. Lett.* **120**, 162904 (2022).

²¹⁰X. Li, C. Li, Z. Xu, Y. Li, Y. Yang, H. Hu, Z. Jiang, J. Wang, J. Ren, C. Zheng, C. Lu, and Z. Wen, *Phys. Status Solidi RRL* **15**, 2000481 (2021).

²¹¹P. Jiao, J. Li, Z. Xi, X. Zhang, J. Wang, Y. Yang, Y. Deng, and D. Wu, *Appl. Phys. Lett.* **119**, 252901 (2021).

²¹²T. Song, H. Tan, S. Estandia, J. Gàzquez, M. Gich, N. Dix, I. Fina, and F. Sánchez, *Nanoscale* **14**, 2337 (2022).

²¹³T. Song, S. Estandia, N. Dix, J. Gàzquez, M. Gich, I. Fina, and F. Sánchez, *J. Mater. Chem. C* **10**, 8407 (2022).

²¹⁴S. Estandia, N. Dix, J. Gàzquez, I. Fina, J. Lyu, M. F. Chisholm, J. Fontcuberta, and F. Sánchez, *ACS Appl. Electron. Mater.* **1**, 1449 (2019).

²¹⁵T. Li, N. Zhang, Z. Sun, C. Xie, M. Ye, S. Mazumdar, L. Shu, Y. Wang, D. Wang, L. Chen, S. Ke, and H. Huang, *J. Mater. Chem. C* **6**, 9224 (2018).

²¹⁶J. Lyu, I. Fina, R. Bachelet, G. Saint-Girons, S. Estandia, J. Gàzquez, J. Fontcuberta, and F. Sánchez, *Appl. Phys. Lett.* **114**, 222901 (2019).

²¹⁷J. Lyu, I. Fina, J. Fontcuberta, and F. Sánchez, *ACS Appl. Mater. Interfaces* **11**, 6224 (2019).

²¹⁸K. Lee, T. Y. Lee, S. M. Yang, D. H. Lee, J. Park, and S. C. Chae, *Appl. Phys. Lett.* **112**, 202901 (2018).

²¹⁹J. Lyu, T. Song, I. Fina, and F. Sánchez, *Nanoscale* **12**, 11280 (2020).

²²⁰T. Song, R. Solanas, M. Qian, I. Fina, and F. Sánchez, *J. Mater. Chem. C* **10**, 1084 (2022).

²²¹H. Zhong, M. Li, Q. Zhang, L. Yang, R. He, F. Liu, Z. Liu, G. Li, Q. Sun, D. Xie, F. Meng, Q. Li, M. He, E. Guo, C. Wang, Z. Zhong, X. Wang, L. Gu, G. Yang, K. Jin, P. Gao, and C. Ge, *Adv. Mater.* **34**, 2109889 (2022).

²²²M. H. Park, Y. H. Lee, T. Mikolajick, U. Schroeder, and C. S. Hwang, *Adv. Electron. Mater.* **5**, 1800522 (2018).

²²³M. D. Glinchuk, A. N. Morozovska, A. Lukowiak, W. Stręk, M. V. Silibin, D. V. Karpinsky, Y. Kim, and S. V. Kalinin, *J. Alloys Compd.* **830**, 153628 (2020).

²²⁴M. Dawber, K. M. Rabe, and J. F. Scott, *Rev. Mod. Phys.* **77**, 1083 (2005).

²²⁵T. Song, S. Estandia, H. Tan, N. Dix, J. Gàzquez, I. Fina, and F. Sánchez, *Adv. Electron. Mater.* **8**, 2100420 (2021).

²²⁶T. Song, F. Sánchez, and I. Fina, *APL Mater.* **10**, 031108 (2022).

²²⁷L. Bégon-Lours, M. Mulder, P. Nukala, S. de Graaf, Y. A. Birkhölzer, B. Kooi, B. Noheda, G. Koster, and G. Rijnders, *Phys. Rev. Mater.* **4**, 043401 (2020).

²²⁸J. Müller, E. Yurchuk, T. Schlösser, J. Paul, R. Hoffmann, S. Müller, D. Martin, S. Slesazeck, P. Polakowski, J. Sundqvist *et al.*, in *2012 Symposium on VLSI Technology (VLSIT)* (IEEE, 2012), pp. 25–26.

²²⁹S. Dünkel, M. Treitzsch, R. Richter, P. Moll, C. Fuchs, O. Gehring, M. Majer, S. Wittek, B. Müller, T. Melde *et al.*, in *2017 IEEE International Electron Devices Meeting (IEDM)* (IEEE, 2017), pp. 19–27.

²³⁰J. Okuno, T. Kunihiro, K. Konishi, H. Maemura, Y. Shuto, F. Sugaya, M. Materano, T. Ali, K. Kuehnel, K. Seidel *et al.*, in *2020 IEEE Symposium on VLSI Technology* (IEEE, 2020), pp. 1–2.

²³¹S. J. Kim, J. Mohan, S. R. Summerfelt, and J. Kim, *JOM* **71**, 246 (2019).

²³²V. Cremers, R. L. Puurunen, and J. Dendooven, *Appl. Phys. Rev.* **6**, 021302 (2019).

²³³S. M. George, *Chem. Rev.* **110**, 111 (2010).

²³⁴K. Mistry, C. Allen, C. Auth, B. Beattie, D. Bergstrom, M. Bost, M. Brazier, M. Buehler, A. Cappellani, R. Chau *et al.*, in *2007 IEEE International Electron Devices Meeting* (IEEE, 2007), pp. 247–250.

²³⁵B. Yu, L. Chang, S. Ahmed, H. Wang, S. Bell, C.-Y. Yang, C. Tabery, C. Ho, Q. Xiang, T.-J. King *et al.*, in *Digest International Electron Devices Meeting* (IEEE, 2002), pp. 251–254.

²³⁶N. Singh, A. Agarwal, L. K. Bera, T. Y. Liow, R. Yang, S. C. Rustagi, C. H. Tung, R. Kumar, G. Q. Lo, N. Balasubramanian, and D.-L. Kwong, *IEEE Electron Device Lett.* **27**, 383 (2006).

²³⁷Y. Lee and S. M. George, *J. Vac. Sci. Technol. A* **36**, 061504 (2018).

²³⁸K. D. Kim, Y. H. Lee, T. Gwon, Y. J. Kim, H. J. Kim, T. Moon, S. D. Hyun, H. W. Park, M. H. Park, and C. S. Hwang, *Nano Energy* **39**, 390 (2017).

²³⁹K. D. Kim, M. H. Park, H. J. Kim, Y. J. Kim, T. Moon, Y. H. Lee, S. D. Hyun, T. Gwon, and C. S. Hwang, *J. Mater. Chem. C* **4**, 6864 (2016).

²⁴⁰D. Lehninger, R. Olivo, T. Ali, M. Lederer, T. Kämpfe, C. Mart, K. Biedermann, K. Kuehnel, L. Roy, M. Kalkani, and K. Seidel, *Phys. Status Solidi A* **217**, 1900840 (2020).

²⁴¹D. Lehninger, T. Ali, R. Olivo, M. Lederer, T. Kämpfe, K. Mertens, and K. Seidel, in *2020 Joint Conference of the IEEE International Frequency Control Symposium and International Symposium on Applications of Ferroelectrics (IFCS-ISAF)* (IEEE, 2020), pp. 1–3.

²⁴²H.-B. Kim, M. Jung, Y. Oh, S. W. Lee, D. Suh, and J.-H. Ahn, *Nanoscale* **13**, 8524 (2021).

²⁴³H. A. Hsain, Y. Lee, M. Materano, T. Mittmann, A. Payne, T. Mikolajick, U. Schroeder, G. N. Parsons, and J. L. Jones, *J. Vac. Sci. Technol. A* **40**, 010803 (2022).

²⁴⁴N. Gong and T.-P. Ma, *IEEE Electron Device Lett.* **39**, 15 (2017).

²⁴⁵K. Ni, P. Sharma, J. Zhang, M. Jerry, J. A. Smith, K. Tapily, R. Clark, S. Mahapatra, and S. Datta, *IEEE Trans. Electron Devices* **65**, 2461 (2018).

²⁴⁶T. Ali, P. Polakowski, S. Riedel, T. Büttner, T. Kämpfe, R. Rudolph, B. Pätzold, K. Seidel, D. Löhr, R. Hoffmann, M. Czernohorsky, K. Kuehnel, P. Steinke, J. Calvo, K. Zimmermann, and J. Müller, *IEEE Trans. Electron Devices* **65**, 3769 (2018).

²⁴⁷A. J. Tan, Y.-H. Liao, L.-C. Wang, N. Shanker, J.-H. Bae, C. Hu, and S. Salahuddin, *IEEE Electron Device Lett.* **42**, 994 (2021).

²⁴⁸C.-Y. Chan, K.-Y. Chen, H.-K. Peng, and Y.-H. Wu, in *2020 IEEE Symposium on VLSI Technology* (IEEE, 2020), pp. 1–2.

²⁴⁹S. H. Kim, G. T. Yu, G. H. Park, D. H. Lee, J. Y. Park, K. Yang, E. B. Lee, J. I. Lee, and M. H. Park, *Chem. Commun.* **57**, 12452 (2021).

²⁵⁰T. J. Park, J. H. Kim, J. H. Jang, U. K. Kim, S. Y. Lee, J. Lee, H. S. Jung, and C. S. Hwang, *Chem. Mater.* **23**, 1654 (2011).

²⁵¹H. Hernández-Arriaga, E. López-Luna, E. Martínez-Guerra, M. M. Turribiates, A. G. Rodríguez, and M. A. Vidal, *J. Appl. Phys.* **121**, 064302 (2017).

²⁵²C. Mart, K. Kuehnel, T. Kämpfe, M. Czernohorsky, M. Wiatr, S. Kolodinski, and W. Weinreich, *ACS Appl. Electron. Mater.* **1**, 2612 (2019).

²⁵³H. H. Kim, “Enhanced electrical characteristics of $Hf_{1-x}Zr_xO_2$ film utilizing discrete feeding method,” M.S. thesis, Seoul National University, 2020, <http://dcollection.snu.ac.kr/common/orgView/00000158797>.

²⁵⁴M. Hoffmann, J. A. Murdzek, S. M. George, S. Slesazeck, U. Schroeder, and T. Mikolajick, *Appl. Phys. Lett.* **120**, 122901 (2022).

²⁵⁵M. H. Park, H. J. Kim, G. Lee, J. Park, Y. H. Lee, Y. J. Kim, T. Moon, K. D. Kim, S. D. Hyun, H. W. Park *et al.*, *Appl. Phys. Rev.* **6**, 041403 (2019).

²⁵⁶J. Y. Park, D. H. Lee, K. Yang, S. H. Kim, G. T. Yu, G. H. Park, E. B. Lee, K. H. Kim, and M. H. Park, *ACS Appl. Electron. Mater.* **4**, 1369 (2021).

²⁵⁷C.-H. Chang, Y.-K. Chiou, C.-W. Hsu, and T.-B. Wu, *Electrochem. Solid-State Lett.* **10**, G5 (2007).

²⁵⁸Y. Lee, H. Alex Hsain, S. S. Fields, S. T. Jaszewski, M. D. Horgan, P. G. Edgington, J. F. Ihlefeld, G. N. Parsons, and J. L. Jones, *Appl. Phys. Lett.* **118**, 012903 (2021).

²⁵⁹Y.-K. Liang, W.-L. Li, Y.-J. Wang, L.-C. Peng, C.-C. Lu, H.-Y. Huang, S. H. Yeong, Y.-M. Lin, Y.-H. Chu, E.-Y. Chang, and C.-H. Lin, *IEEE Electron Device Lett.* **43**, 1451 (2022).

²⁶⁰H.-B. Kim, K. S. Dae, Y. Oh, S.-W. Lee, Y. Lee, S.-E. Ahn, J. H. Jang, and J.-H. Ahn, *Adv. Mater. Interfaces* **9**, 2102528 (2022).

²⁶¹L. Xu, T. Nishimura, S. Shibayama, T. Yajima, S. Migita, and A. Toriumi, *J. Appl. Phys.* **122**, 124104 (2017).

²⁶²R. Shimura, T. Mimura, T. Shimizu, Y. Tanaka, Y. Inoue, and H. Funakubo, *J. Ceram. Soc. Jpn.* **128**, 539 (2020).

²⁶³X. Wang, T. Mikolajick, and M. Grube, *Phys. Status Solidi RRL* **16**, 2100572 (2022).

²⁶⁴J. P. B. Silva, R. F. Negrea, M. C. Istrate, S. Dutta, H. Aramberri, J. Íñiguez, F. G. Figueiras, C. Ghica, K. C. Sekhar, and A. L. Khoklin, *ACS Appl. Mater. Interfaces* **13**, 51383 (2021).

²⁶⁵V. Lenzi, J. P. B. Silva, B. Šmid, V. Matolín, C. M. Istrate, C. Ghica, J. L. MacManus-Driscoll, and L. Marques, *Energy Environ. Mater.* e12500 (published online) (2022).

²⁶⁶J. P. B. Silva, M. C. Istrate, M. Hellenbrand, A. Jan, M. T. Becker, J. Symonowicz, F. G. Figueiras, V. Lenzi, M. O. Hill, C. Ghica, K. N. Romanyuk, M. J. M. Gomes, G. Di Martino, L. Marques, and J. L. MacManus-Driscoll, *Appl. Mater. Today* **30**, 101708 (2023).

²⁶⁷Y. Sun, G. Niu, W. Ren, J. Zhao, Y. Wang, H. Wu, L. Jiang, L. Dai, Y.-H. Xie, P. Rojo Romeo, J. Bouaziz, and B. Vilquin, *AIP Adv.* **11**, 065229 (2021).

²⁶⁸J. Bouaziz, P. R. Romeo, N. Baboux, and B. Vilquin, *ACS Appl. Electron. Mater.* **1**, 1740 (2019).

²⁶⁹M. B. Hachemi, B. Salem, V. Consonni, H. Roussel, A. Garraud, G. Lefevre, S. Labau, S. Basrour, and A. Bsiesy, *AIP Adv.* **11**, 085004 (2021).

²⁷⁰J. Bouaziz, P. R. Romeo, N. Baboux, R. Negrea, L. Pintilie, and B. Vilquin, *APL Mater.* **7**, 081109 (2019).

²⁷¹Y. H. Lee, H. J. Kim, T. Moon, K. D. Kim, S. D. Hyun, H. W. Park, Y. B. Lee, M. H. Park, and C. S. Hwang, *Nanotechnology* **28**, 305703 (2017).

²⁷²S. Migita, H. Ota, H. Yamada, K. Shibuya, A. Sawa, and A. Toriumi, *Jpn. J. Appl. Phys.* **57**, 04 (2018).

²⁷³Q. Luo, H. Ma, H. Su, K.-H. Xue, R. Cao, Z. Gao, J. Yu, T. Gong, X. Xu, J. Yin, P. Yuan, L. Tai, D. Dong, S. Long, Q. Liu, X.-S. Miao, H. Lv, and M. Liu, *IEEE Electron Device Lett.* **40**, 570 (2019).

²⁷⁴T. Mittmann, M. Michailow, P. D. Lomenzo, J. Gärtner, M. Falkowski, A. Kersch, T. Mikolajick, and U. Schroeder, *Nanoscale* **13**, 912 (2021).

²⁷⁵J. Bouaziz, P. Rojo Romeo, N. Baboux, and B. Vilquin, *Appl. Phys. Lett.* **118**, 082901 (2021).

²⁷⁶G. Segantini, R. Barhoumi, B. Manchon, I. Cañero Infante, P. Rojo Romeo, M. Bugnet, N. Baboux, S. Nirantar, D. Deleruyelle, S. Sriram, and B. Vilquin, *Phys. Status Solidi RRL* **16**, 2100583 (2022).

²⁷⁷B. Manchon, G. Segantini, N. Baboux, P. Rojo Romeo, R. Barhoumi, I. C. Infante, F. Alibart, D. Drouin, B. Vilquin, and D. Deleruyelle, *Phys. Status Solidi RRL* **16**, 2100585 (2022).

²⁷⁸J. Bouaziz, P. R. Romeo, N. Baboux, and B. Vilquin, *J. Vac. Sci. Technol. B* **37**, 021203 (2019).

²⁷⁹F. Mehmood, T. Mikolajick, and U. Schroeder, *Phys. Status Solidi A* **217**, 2000281 (2020).

²⁸⁰C. Zacharaki, P. Tsipas, S. Chaitoglou, S. Fragkos, M. Axiotis, A. Lagoyannis, R. Negrea, L. Pintilie, and A. Dimoulas, *Appl. Phys. Lett.* **114**, 112901 (2019).

²⁸¹C. Zacharaki, P. Tsipas, S. Chaitoglou, E. K. Evangelou, C. M. Istrate, L. Pintilie, and A. Dimoulas, *Appl. Phys. Lett.* **116**, 182904 (2020).

²⁸²C. Zacharaki, P. Tsipas, S. Chaitoglou, L. Bégon-Lours, M. Halter, and A. Dimoulas, *Appl. Phys. Lett.* **117**, 212905 (2020).

²⁸³N. Siannas, C. Zacharaki, P. Tsipas, S. Chaitoglou, L. Bégon-Lours, C. Istrate, L. Pintilie, and A. Dimoulas, *Commun. Phys.* **5**, 178 (2022).

²⁸⁴C. Zacharaki, S. Chaitoglou, N. Siannas, P. Tsipas, and A. Dimoulas, *ACS Appl. Electron. Mater.* **4**, 2815 (2022).

²⁸⁵R. Zhang, N. Taoka, P.-C. Huang, M. Takenaka, and S. Takagi, in *2011 International Electron Devices Meeting* (IEEE, 2011).

²⁸⁶J. Cao, S. Shi, Y. Zhu, and J. Chen, *Phys. Status Solidi RRL* **15**, 2100025 (2021).

²⁸⁷H. Chen, X. Zhou, L. Tang, Y. Chen, H. Luo, X. Yuan, C. R. Bowen, and D. Zhang, *Appl. Phys. Rev.* **9**, 011307 (2022).

²⁸⁸Z. Wen and D. Wu, *Adv. Mater.* **32**, 1904123 (2019).

²⁸⁹R. A. McKee, F. J. Walker, and M. F. Chisholm, *Phys. Rev. Lett.* **81**, 3014 (1998).

²⁹⁰P. Nukala, J. Antoja-Lleonart, Y. Wei, L. Yedra, B. Dkhil, and B. Noheda, *ACS Appl. Electron. Mater.* **1**, 2585 (2019).

²⁹¹A. Dimoulas, G. Vellianitis, G. Mavrou, G. Apostolopoulos, A. Travlos, C. Wiemer, M. Fanciulli, and Z. M. Rittersma, *Appl. Phys. Lett.* **85**, 3205 (2004).

²⁹²S. Saitzek, Z. Shao, A. Bayart, A. Ferri, M. Huvé, P. Roussel, and R. Desfeux, *J. Mater. Chem. C* **2**, 4037 (2014).

²⁹³A. G. Chernikova, M. G. Kozodaev, D. V. Negrov, E. V. Korostylev, M. H. Park, U. Schroeder, C. S. Hwang, and A. M. Markeev, *ACS Appl. Mater. Interfaces* **10**, 2701 (2018).

²⁹⁴M. H. Park, Y. H. Lee, H. J. Kim, Y. J. Kim, T. Moon, K. D. Kim, S. D. Hyun, and C. S. Hwang, *ACS Appl. Mater. Interfaces* **10**, 42666 (2018).

²⁹⁵H. Yang, K. Park, H.-J. Lee, J. Jo, H. Park, N. Park, J. Park, and J. H. Lee, *Inorg. Chem.* **59**, 5993 (2020).

²⁹⁶J. Wu, F. Mo, T. Saraya, T. Hiramoto, and M. Kobayashi, *Appl. Phys. Lett.* **117**, 252904 (2020).

²⁹⁷M. H. Park, C.-C. Chung, T. Schenk, C. Richter, K. Opsomer, C. Detavernier, C. Adelmann, J. L. Jones, T. Mikolajick, and U. Schroeder, *Adv. Electron. Mater.* **4**, 1800091 (2018).

²⁹⁸I. Nettleship and R. Stevens, *Int. J. High Technol. Ceram.* **3**, 1 (1987).

²⁹⁹K. Chae, A. C. Kummel, and K. Cho, *ACS Appl. Mater. Interfaces* **14**, 29007 (2022).

³⁰⁰M. G. Kozodaev, A. G. Chernikova, E. V. Korostylev, M. H. Park, R. R. Khakimov, C. S. Hwang, and A. M. Markeev, *J. Appl. Phys.* **125**, 034101 (2019).

³⁰¹M. I. Popovici, A. M. Walke, J. Bizindavyi, J. Meersschaut, K. Banerjee, G. Potoms, K. Katcko, G. Van den Bosch, R. Delhougne, G. S. Kar, and J. Van Houdt, *ACS Appl. Electron. Mater.* **4**, 1823 (2022).

³⁰²J. Lee, D. Eom, C. Lee, W. Lee, J. Oh, C. Park, J. Kim, H. Lee, S. Lee, E. Lee, and H. Kim, *Appl. Phys. Lett.* **120**, 222902 (2022).

³⁰³P. Fan, Y. K. Zhang, Q. Yang, J. Jiang, L. M. Jiang, M. Liao, and Y. C. Zhou, *J. Phys. Chem. C* **123**, 21743 (2019).

³⁰⁴M. H. Park, D. H. Lee, K. Yang, J.-Y. Park, G. T. Yu, H. W. Park, M. Materano, T. Mittmann, P. D. Lomenzo, T. Mikolajick, U. Schroeder, and C. S. Hwang, *J. Mater. Chem. C* **8**, 10526 (2020).

³⁰⁵K. Z. Rushchanskii, S. Blügel, and M. Ležaić, *Phys. Rev. Lett.* **127**, 087602 (2021).

³⁰⁶B. Max, M. Pešić, S. Slesazeck, and T. Mikolajick, *J. Appl. Phys.* **123**, 134102 (2018).

³⁰⁷D. R. Islamov, T. M. Zalyalov, O. M. Orlov, V. A. Gritsenko, and G. Y. Krasnikov, *Appl. Phys. Lett.* **117**, 162901 (2020).

³⁰⁸F. P. G. Fengler, R. Nigon, P. Muralt, E. D. Grimley, X. Sang, V. Sessi, R. Hentschel, J. M. LeBeau, T. Mikolajick, and U. Schroeder, *Adv. Electron. Mater.* **4**, 1700547 (2018).

³⁰⁹D. R. Islamov, V. A. Gritsenko, T. V. Perevalov, V. A. Pustovarov, O. M. Orlov, A. G. Chernikova, A. M. Markeev, S. Slesazeck, U. Schroeder, T. Mikolajick, and G. Y. Krasnikov, *Acta Mater.* **166**, 47 (2019).

³¹⁰V. A. Gritsenko and A. A. Gismatulin, *Appl. Phys. Lett.* **117**, 142901 (2020).

³¹¹M. Müller, P. Lömker, P. Rosenberger, M. Hussein Hamed, D. N. Mueller, R. A. Heinen, T. Szyjka, and L. Baumgarten, *J. Vac. Sci. Technol. A* **40**, 013215 (2022).

³¹²W. Hamouda, A. Pancotti, C. Lubin, L. Tortech, C. Richter, T. Mikolajick, U. Schroeder, and N. Barrett, *J. Appl. Phys.* **127**, 064105 (2020).

³¹³W. Hamouda, C. Lubin, S. Ueda, Y. Yamashita, O. Renault, F. Mehmood, T. Mikolajick, U. Schroeder, R. Negrea, and N. Barrett, *Appl. Phys. Lett.* **116**, 252903 (2020).

³¹⁴S. R. Bradley, A. L. Shluger, and G. Bersuker, *Phys. Rev. Appl.* **4**, 064008 (2015).

³¹⁵T. V. Perevalov, I. P. Prosvirin, E. A. Suprun, F. Mehmood, T. Mikolajick, U. Schroeder, and V. A. Gritsenko, *J. Sci.: Adv. Mater. Devices* **6**, 595 (2021).

³¹⁶L. Baumgarten, T. Szyjka, T. Mittmann, M. Materano, Y. Matveyev, C. Schlueter, T. Mikolajick, U. Schroeder, and M. Müller, *Appl. Phys. Lett.* **118**, 032903 (2021).

³¹⁷T. Szyjka, L. Baumgarten, T. Mittmann, Y. Matveyev, C. Schlueter, T. Mikolajick, U. Schroeder, and M. Müller, *ACS Appl. Electron. Mater.* **2**, 3152 (2020).

³¹⁸J. Lyu, I. Fina, and F. Sánchez, *Appl. Phys. Lett.* **117**, 072901 (2020).

³¹⁹T. Hashimoto, P. Amann, A. Regoutz, N. Barrett, L. F. J. Piper, W. Hamouda, O. Renault, M. Lundwall, and M. Machida, *Vac. Surf. Sci.* **64**, 493 (2021).

³²⁰W. Hamouda, F. Mehmood, T. Mikolajick, U. Schroeder, T. O. Mentes, A. Locatelli, and N. Barrett, *Appl. Phys. Lett.* **120**, 202902 (2022).

³²¹J. E. Rault, G. Agnus, T. Maroutian, V. Pillard, P. Lecoeur, G. Niu, B. Vilquin, M. G. Silly, A. Bendounan, F. Sirotti, and N. Barrett, *Phys. Rev. B* **88**, 155107 (2013).

³²²H. Mulaosmanovic, F. Muller, M. Lederer, T. Ali, R. Hoffmann, K. Seidel, H. Zhou, J. Ocker, S. Mueller, S. Dunkel, D. Kleimaier, J. Muller, M. Trentzsch, S. Beyer, E. T. Breyer, T. Mikolajick, and S. Slesazeck, *IEEE Trans. Electron Devices* **67**, 3466 (2020).

³²³T.-H. Ryu, D.-H. Min, and S.-M. Yoon, *J. Appl. Phys.* **128**, 074102 (2020).

³²⁴C. Huang, Y. Zhang, S. Zheng, Q. Yang, and M. Liao, *Phys. Rev. Appl.* **16**, 044048 (2021).

³²⁵H. Chen, L. Tang, L. Liu, Y. Chen, H. Luo, X. Yuan, and D. Zhang, *Appl. Surf. Sci.* **542**, 148737 (2021).

³²⁶Y. B. Lee, B. Y. Kim, H. W. Park, S. H. Lee, M. Oh, S. K. Ryoo, I. S. Lee, S. Byun, D. Shim, J. H. Lee, H. Kim, K. D. Kim, M. H. Park, and C. S. Hwang, *Adv. Electron. Mater.* **8**, 2200310 (2022).

³²⁷P. D. Lomenzo, P. Zhao, Q. Takmeel, S. Moghaddam, T. Nishida, M. Nelson, C. M. Fancher, E. D. Grimley, X. Sang, J. M. LeBeau, and J. L. Jones, *J. Vac. Sci. Technol. B* **32**, 03D123 (2014).

³²⁸C. Gaumer, E. Martinez, S. Lhostis, M.-J. Guittet, M. Gros-Jean, J.-P. Barnes, C. Licitra, N. Rochat, N. Barrett, F. Bertin, and A. Chabli, *Microelectron. Eng.* **88**, 72 (2011).

³²⁹D. Martin, J. Müller, T. Schenk, T. M. Arruda, A. Kumar, E. Strelcov, E. Yurchuk, S. Müller, D. Pohl, U. Schröder, S. V. Kalinin, and T. Mikolajick, *Adv. Mater.* **26**, 8198 (2014).

³³⁰P. D. Lomenzo, P. Zhao, Q. Takmeel, C. Zhou, C. M. Fancher, E. Lambers, N. G. Rudawski, J. L. Jones, S. Moghaddam, and T. Nishida, *J. Appl. Phys.* **117**, 134105 (2015).

³³¹Y. Lee, Y. Goh, J. Hwang, D. Das, and S. Jeon, *IEEE Trans. Electron Devices* **68**, 523 (2021).

³³²S. S. Fields, S. W. Smith, P. J. Ryan, S. T. Jaszewski, I. A. Brummel, A. Salanova, G. Esteves, S. L. Wolfley, M. D. Henry, P. S. Davids, and J. F. Ihlefeld, *ACS Appl. Mater. Interfaces* **12**, 26577 (2020).

³³³M. H. Park, H. J. Kim, Y. J. Kim, W. Lee, H. K. Kim, and C. S. Hwang, *Appl. Phys. Lett.* **102**, 112914 (2013).

³³⁴S. S. Fields, S. W. Smith, S. T. Jaszewski, T. Mimura, D. A. Dickie, G. Esteves, M. D. Henry, S. L. Wolfley, P. S. Davids, and J. F. Ihlefeld, *J. Appl. Phys.* **130**, 134101 (2021).

³³⁵M. H. Park, H. J. Kim, Y. J. Kim, W. Jeon, T. Moon, and C. S. Hwang, *Phys. Status Solidi RRL* **8**, 532 (2014).

³³⁶Y. Goh, S. H. Cho, S.-H. K. Park, and S. Jeon, *IEEE Trans. Electron Devices* **67**, 3431 (2020).

³³⁷T. Mittmann, T. Szyjka, H. Alex, M. C. Istrate, P. D. Lomenzo, L. Baumgarten, M. Müller, J. L. Jones, L. Pintilie, T. Mikolajick, and U. Schroeder, *Phys. Status Solidi RRL* **15**, 2100012 (2021).

³³⁸T. Szyjka, L. Baumgarten, T. Mittmann, Y. Matveyev, C. Schlueter, T. Mikolajick, U. Schroeder, and M. Müller, *Phys. Status Solidi RRL* **15**, 2100027 (2021).

³³⁹S. Starschich, S. Menzel, and U. Böttger, *Appl. Phys. Lett.* **108**, 032903 (2016).

³⁴⁰S. Zhao, B. Li, Y. Guo, and H. Li, *Appl. Phys. Lett.* **120**, 012904 (2022).

³⁴¹M. Yadav, A. Kashir, S. Oh, R. D. Nikam, H. Kim, H. Jang, and H. Hwang, *Nanotechnology* **33**, 085206 (2021).

³⁴²K. Mizutani, T. Hoshii, H. Wakabayashi, K. Tsutsui, E. Y. Chang, and K. Kakushima, *Jpn. J. Appl. Phys.* **61**, 021006 (2022).

³⁴³H. A. Hsain, Y. Lee, S. Lancaster, P. D. Lomenzo, B. Xu, T. Mikolajick, U. Schroeder, G. N. Parsons, and J. L. Jones, *Nanotechnology* **34**, 125703 (2023).

³⁴⁴F. Mehmood, R. Alcala, P. Vishnumurthy, B. Xu, R. Sachdeva, T. Mikolajick, and U. Schroeder, *Adv. Mater. Interfaces* **10**, 2202151 (2023).

³⁴⁵R. Alcala, F. Mehmood, P. Vishnumurthy, T. Mittmann, T. Mikolajick, and U. Schroeder, in *2022 IEEE International Memory Workshop (IMW)* (IEEE, 2022), pp. 1–4.

³⁴⁶M. H. Park, Y. H. Lee, H. J. Kim, T. Schenck, W. Lee, K. D. Kim, F. P. G. Fengler, T. Mikolajick, U. Schroeder, and C. S. Hwang, *Nanoscale* **9**, 9973 (2017).

³⁴⁷H. J. Kim, M. H. Park, Y. J. Kim, Y. H. Lee, W. Jeon, T. Gwon, T. Moon, K. D. Kim, and C. S. Hwang, *Appl. Phys. Lett.* **105**, 192903 (2014).

³⁴⁸H. A. Hsain, Y. Lee, S. Lancaster, M. Materano, R. Alcala, B. Xu, T. Mikolajick, U. Schroeder, G. N. Parsons, and J. L. Jones, *ACS Appl. Mater. Interfaces* **14**, 42232 (2022).

³⁴⁹G. Walters, P. Chojecki, Z. Forrester, and T. Nishida, *Appl. Phys. Lett.* **118**, 032904 (2021).

³⁵⁰Z. Zhao, Y.-R. Chen, J.-F. Wang, Y.-W. Chen, J.-R. Zou, Y. Lin, Y. Xing, C. W. Liu, and C. Hu, *IEEE Electron Device Lett.* **43**, 553 (2022).

³⁵¹J. Casamento, H. Lee, C. S. Chang, M. F. Besser, T. Maeda, D. A. Muller, H. (Grace) Xing, and D. Jena, *APL Mater.* **9**, 091106 (2021).

³⁵²B. Liu, Y. Cao, W. Zhang, and Y. Li, *Appl. Phys. Lett.* **119**, 172902 (2021).

³⁵³Y. Goh, S. H. Cho, S.-H. K. Park, and S. Jeon, *Nanoscale* **12**, 9024 (2020).

³⁵⁴S. S. Cheema, N. Shanker, C.-H. Hsu, A. Datar, J. Bae, D. Kwon, and S. Salahuddin, *Adv. Electron. Mater.* **8**, 2100499 (2021).

³⁵⁵Y.-C. Lin, F. McGuire, and A. D. Franklin, *J. Vac. Sci. Technol. B* **36**, 011204 (2018).

³⁵⁶R. Athle, A. E. O. Persson, A. Irish, H. Menon, R. Timm, and M. Borg, *ACS Appl. Mater. Interfaces* **13**, 11089 (2021).

³⁵⁷M. Saadi, P. Gonon, C. Vallée, C. Mannequin, H. Grampeix, E. Jalaguier, F. Jomni, and A. Bsiey, *J. Appl. Phys.* **119**, 114501 (2016).

³⁵⁸H. Mulaosmanovic, E. T. Breyer, S. Dünkel, S. Beyer, T. Mikolajick, and S. Slesazeck, *Nanotechnology* **32**, 502002 (2021).

³⁵⁹M. Kobayashi, Y. Tagawa, F. Mo, T. Saraya, and T. Hiramoto, *IEEE J. Electron Devices Soc.* **7**, 134 (2019).

³⁶⁰R. Athle, A. E. O. Persson, A. Troian, and M. Borg, *ACS Appl. Electron. Mater.* **4**, 1002 (2022).

³⁶¹S. Im, S.-Y. Kang, Y. Kim, J. H. Kim, J.-P. Im, S.-M. Yoon, S. E. Moon, and J. Woo, *Micromachines* **11**, 910 (2020).

³⁶²X. Lyu, M. Si, X. Sun, M. A. Capano, H. Wang, and P. D. Ye, in *2019 Symposium on VLSI Technology* (IEEE, 2019), pp. T44–T45.

³⁶³S. Riedel, P. Polakowski, and J. Müller, *AIP Adv.* **6**, 095123 (2016).

³⁶⁴T. Ali, P. Polakowski, K. Kuhnel, M. Czernohorsky, T. Kampfe, M. Rudolph, B. Patzold, D. Lehnninger, F. Müller, R. Olivo, M. Lederer, R. Hoffmann, P. Steinke, K. Zimmermann, U. Muhle, K. Seidel, and J. Müller, in *2019 IEEE International Electron Devices Meeting (IEDM)* (IEEE, 2019).

³⁶⁵M. Lederer, K. Seidel, R. Olivo, T. Kampfe, and L. M. Eng, *Front. Nanotechnol.* **4**, 900379 (2022).

³⁶⁶S. L. Weeks, A. Pal, V. K. Narasimhan, K. A. Littau, and T. Chiang, *ACS Appl. Mater. Interfaces* **9**, 13440 (2017).

³⁶⁷J. Liao, B. Zeng, Q. Sun, Q. Chen, M. Liao, C. Qiu, Z. Zhang, and Y. Zhou, *IEEE Electron Device Lett.* **40**, 1868 (2019).

³⁶⁸H. Joh, T. Jung, and S. Jeon, *IEEE Trans. Electron Devices* **68**, 2538 (2021).

³⁶⁹A. Navrotsky and S. V. Ushakov, *Materials Fundamentals of Gate Dielectrics* (Springer-Verlag, 2005), pp. 57–108.

³⁷⁰D. G. Schlom, L.-Q. Chen, C.-B. Eom, K. M. Rabe, S. K. Streiffer, and J.-M. Triscone, *Annu. Rev. Mater. Res.* **37**, 589 (2007).

³⁷¹X. Tian, S. Shibayama, T. Nishimura, T. Yajima, S. Migita, and A. Toriumi, *Appl. Phys. Lett.* **112**, 102902 (2018).

³⁷²C.-I. Wang, H.-Y. Chen, C.-Y. Wang, T.-J. Chang, Y.-S. Jiang, C.-S. Chang, and M.-J. Chen, *J. Mater. Chem. C* **9**, 12759 (2021).

³⁷³X. Liu, Y. Wang, P. V. Lukashev, J. D. Burton, and E. Y. Tsymbal, *Phys. Rev. B* **85**, 125407 (2012).

³⁷⁴Z. Gao, Y. Luo, S. Lyu, Y. Cheng, Y. Zheng, Q. Zhong, W. Zhang, and H. Lyu, *IEEE Electron Device Lett.* **42**, 1303 (2021).

³⁷⁵M. Dogan, S. Fernandez-Peña, L. Kornblum, Y. Jia, D. P. Kumah, J. W. Reiner, Z. Krivokapic, A. M. Kolpak, S. Ismail-Beigi, C. H. Ahn, and F. J. Walker, *Nano Lett.* **18**, 241 (2017).

³⁷⁶T. Mikolajick, S. Slesazeck, M. H. Park, and U. Schroeder, *MRS Bull.* **43**, 340 (2018).

³⁷⁷J. A. Rodriguez, C. Zhou, T. Graf, R. Bailey, M. Wiegand, T. Wang, M. Ball, H. C. Wen, K. R. Udayakumar, S. Summerfelt, T. San, and T. Moise, in *2016 IEEE 8th International Memory Workshop (IMW)* (IEEE, 2016), pp. 1–4.

³⁷⁸Y. Wang, C. Zhang, H. Yu, and W. Zhang, in *Proceedings of the 2012 ACM/IEEE International Symposium on Low Power Electronics and Design* (ACM, 2012), pp. 197–202.

³⁷⁹M. Trentzsch, S. Flachowsky, R. Richter, J. Paul, B. Reimer, D. Utess, S. Jansen, H. Mulaosmanovic, S. Muller, S. Slesazeck, J. Ocker, M. Noack, J. Muller, P. Polakowski, J. Schreiter, S. Beyer, T. Mikolajick, and B. Rice, in *2016 IEEE International Electron Devices Meeting (IEDM)* (IEEE, 2016), pp. 11.5.1–11.5.4.

³⁸⁰R. Alcala, P. D. Lomenzo, T. Mittman, B. Xu, R. Guido, S. Lancaster, P. Vishnumurthy, L. Grenouillet, S. Martin, J. Coignus, T. Mikolajick, and U. Schroeder, in *2022 IEEE International Electron Devices Meeting (IEDM)* (IEEE, 2022).

³⁸¹S. Lancaster, P. D. Lomenzo, M. Engl, B. Xu, T. Mikolajick, U. Schroeder, and S. Slesazeck, *Front. Nanotechnol.* **4**, 939822 (2022).

³⁸²T. Mikolajick, S. Slesazeck, U. Schroeder, P. D. Lomenzo, E. T. Breyer, H. Mulaosmanovic, M. Hoffmann, T. Mittmann, F. Mehmood, and B. Max, in *2019 IEEE International Electron Devices Meeting (IEDM)* (IEEE, 2019).

³⁸³M. Pešić, M. Hoffmann, C. Richter, T. Mikolajick, and U. Schroeder, *Adv. Funct. Mater.* **26**, 7486 (2016).

³⁸⁴T. Ravsher, H. Mulaosmanovic, E. T. Breyer, V. Havel, T. Mikolajick, and S. Slesazeck, in *2019 26th IEEE International Conference on Electronics Circuits and Systems (ICECS)* (IEEE, 2019).

³⁸⁵S. Beyer, S. Dunkel, M. Trentzsch, J. Muller, A. Hellmich, D. Utess, J. Paul, D. Kleimaier, J. Pellerin, S. Muller, J. Ocker, A. Benoit, H. Zhou, M. Mennenga, M. Schuster, F. Tassan, M. Noack, A. Pourkeramati, F. Muller, M. Lederer, T. Ali, R. Hoffmann, T. Kampfe, K. Seidel, H. Mulaosmanovic, E. T. Breyer, T. Mikolajick, and S. Slesazeck, in *2020 IEEE International Memory Workshop (IMW)* (IEEE, 2020), pp. 1–4.

³⁸⁶A. I. Khan, A. Keshavarzi, and S. Datta, *Nat. Electron.* **3**, 588 (2020).

³⁸⁷A. F. Laguna, X. Yin, D. Reis, M. Niemier, and X. S. Hu, in *Proceedings of the 2019 on Great Lakes Symposium on VLSI* (ACM, 2019), pp. 373–378.

³⁸⁸T. Soliman, F. Müller, T. Kirchner, T. Hoffmann, H. Ganem, E. Karimov, T. Ali, M. Lederer, C. Sudarshan, T. Kampfe, A. Guntoro, and N. Wehn, in *2020 IEEE International Electron Devices Meeting (IEDM)* (IEEE, 2020), pp. 29.2.1–29.2.4.

³⁸⁹M. Hoffmann, A. J. Tan, N. Shanker, Y.-H. Liao, L.-C. Wang, J.-H. Bae, C. Hu, and S. Salahuddin, *IEEE Electron Device Lett.* **43**, 717 (2022).

³⁹⁰E. Yurchuk, J. Müller, S. Muller, J. Paul, M. Petic, R. van Bentum, U. Schroeder, and T. Mikolajick, *IEEE Trans. Electron Devices* **63**, 3501 (2016).

³⁹¹N. Gong and T.-P. Ma, *IEEE Electron Device Lett.* **37**, 1123 (2016).

³⁹²A. A. Sharma, B. Doyle, H. J. Yoo, I.-C. Tung, J. Kavalieros, M. V. Metz, M. Reshotko, P. Majhi, T. Brown-Heft, Y.-J. Chen, and V. H. Le, in *2020 IEEE International Electron Devices Meeting (IEDM)* (IEEE, 2020), pp. 18.5.1–18.5.4.

³⁹³S. Dutta, H. Ye, A. A. Khandker, S. G. Kirtania, A. Khanna, K. Ni, and S. Datta, *IEEE Electron Device Lett.* **43**, 382 (2022).

³⁹⁴Z. Lin, M. Si, and P. D. Ye, in *2022 IEEE Symposium on VLSI Technology and Circuits* (IEEE, 2022), pp. 1–2.

³⁹⁵S. Dunkel, M. Trentzsch, R. Richter, P. Moll, C. Fuchs, O. Gehring, M. Majer, S. Wittek, B. Müller, T. Melde, H. Mulaosmanovic, S. Slesazeck, S. Muller, J. Ocker, M. Noack, D.-A. Lohr, P. Polakowski, J. Müller, T. Mikolajick, J. Hontschel, B. Rice, J. Pellerin, and S. Beyer, in *2017 IEEE International Electron Devices Meeting (IEDM)* (IEEE, 2017), pp. 19.7.1–19.7.4.

³⁹⁶M. Y. Zhuravlev, S. S. Jaswal, E. Y. Tsymbal, and R. F. Sabirianov, *Appl. Phys. Lett.* **87**, 222114 (2005).

³⁹⁷V. Garcia, S. Fusil, K. Bouzehouane, S. Enouz-Vedrenne, N. D. Mathur, A. Barthélémy, and M. Bibes, *Nature* **460**, 81 (2009).

³⁹⁸E. Y. Tsymbal and H. Kohlstedt, *Science* **313**, 181 (2006).

³⁹⁹F. Ambriz-Vargas, G. Kolhatkar, R. Thomas, R. Nouar, A. Sarkissian, C. Gomez-Yáñez, M. A. Gauthier, and A. Ruediger, *Appl. Phys. Lett.* **110**, 093106 (2017).

⁴⁰⁰Y. Wei, S. Matzen, T. Maroutian, G. Agnus, M. Salverda, P. Nukala, Q. Chen, J. Ye, P. Lecoeur, and B. Noheda, *Phys. Rev. Appl.* **12**, 031001 (2019).

⁴⁰¹Y. Wei, S. Matzen, C. P. Quinteros, T. Maroutian, G. Agnus, P. Lecoeur, and B. Noheda, *npj Quantum Mater.* **4**, 62 (2019).

⁴⁰²A. Chanthbouala, V. Garcia, R. O. Cherifi, K. Bouzehouane, S. Fusil, X. Moya, S. Xavier, H. Yamada, C. Deranlot, N. D. Mathur, M. Bibes, A. Barthélémy, and J. Grollier, *Nat. Mater.* **11**, 860 (2012).

⁴⁰³H. Kohlstedt, A. Petraru, K. Szot, A. Rüdiger, P. Meuffels, H. Haselier, R. Waser, and V. Nagarajan, *Appl. Phys. Lett.* **92**, 062907 (2008).

⁴⁰⁴V. Mikheev, A. Chouprik, Y. Lebedinskii, S. Zarubin, A. M. Markeev, A. V. Zenkevich, and D. Negrov, *Nanotechnology* **31**, 215205 (2020).

⁴⁰⁵M. C. Sulzbach, S. Estandia, X. Long, J. Lyu, N. Dix, J. Gázquez, M. F. Chisholm, F. Sánchez, I. Fina, and J. Fontcuberta, *Adv. Electron. Mater.* **6**, 1900852 (2019).

⁴⁰⁶N. Gong, X. Sun, H. Jiang, K. S. Chang-Liao, Q. Xia, and T. P. Ma, *Appl. Phys. Lett.* **112**, 262903 (2018).

⁴⁰⁷Y. Wei, G. Vats, and B. Noheda, *Neuromorphic Comput. Eng.* **2**, 044007 (2022).

⁴⁰⁸A. E. Boutaybi, T. Maroutian, L. Largeau, S. Matzen, and P. Lecoeur, *Phys. Rev. Mater.* **6**, 074406 (2022).

⁴⁰⁹C. L. Platt, B. Diény, and A. E. Berkowitz, *J. Appl. Phys.* **81**, 5523 (1997).

⁴¹⁰M. Y. Zhuravlev, S. Maekawa, and E. Y. Tsymbal, *Phys. Rev. B* **81**, 104419 (2010).

⁴¹¹V. Garcia, M. Bibes, L. Bocher, S. Valencia, F. Kronast, A. Crassous, X. Moya, S. Enouz-Vedrenne, A. Gloter, D. Imhoff, C. Deranlot, N. D. Mathur, S. Fusil, K. Bouzehouane, and A. Barthélémy, *Science* **327**, 1106 (2010).

⁴¹²M. Y. Zhuravlev, A. Alexandrov, L. L. Tao, and E. Y. Tsymbal, *Appl. Phys. Lett.* **113**, 172405 (2018).

⁴¹³X. Du, H. Sun, H. Wang, J. Li, Y. Yin, and X. Li, *ACS Appl. Mater. Interfaces* **14**, 1355 (2021).

⁴¹⁴M. Cervo Sulzbach, H. Tan, S. Estandia, J. Gázquez, F. Sánchez, I. Fina, and J. Fontcuberta, *ACS Appl. Electron. Mater.* **3**, 3657 (2021).

⁴¹⁵L. Bégon-Lours, M. Halter, F. M. Puglisi, L. Benatti, D. F. Falcone, Y. Popoff, D. Dávila Pineda, M. Sousa, and B. J. Offrein, *Adv. Electron. Mater.* **8**, 2101395 (2022).

⁴¹⁶Y. Wang, Q. Wang, J. Zhao, T. Niermann, Y. Liu, L. Dai, K. Zheng, Y. Sun, Y. Zhang, J. Schwarzkopf, T. Schroeder, Z. Jiang, W. Ren, and G. Niu, *Appl. Mater. Today* **29**, 101587 (2022).

⁴¹⁷M. C. Sulzbach, S. Estandia, J. Gázquez, F. Sánchez, I. Fina, and J. Fontcuberta, *Adv. Electron. Mater.* **30**, 2002638 (2020).

⁴¹⁸M. L. Müller, M. T. Becker, N. Strkalj, and J. L. MacManus-Driscoll, *Appl. Phys. Lett.* **121**, 093501 (2022).

⁴¹⁹P. Wang, C. J. Perini, A. O'Hara, H. Gong, P. Wang, E. X. Zhang, M. W. McCurdy, D. M. Fleetwood, R. D. Schrimpf, S. T. Pantelides, and E. M. Vogel, *IEEE Trans. Nucl. Sci.* **66**, 420 (2019).

⁴²⁰P. Chaudhary, P. Buragohain, M. Kozodaev, S. Zarubin, V. Mikheev, A. Chouprik, A. Lipatov, A. Sinitskii, A. Zenkevich, and A. Gruverman, *Appl. Phys. Lett.* **118**, 083106 (2021).

⁴²¹J. P. B. Silva, K. C. Sekhar, H. Pan, J. L. MacManus-Driscoll, and M. Pereira, *ACS Energy Lett.* **6**, 2208 (2021).

⁴²²M. G. Kozodaev, A. G. Chernikova, R. R. Khakimov, M. H. Park, A. M. Markeev, and C. S. Hwang, *Appl. Phys. Lett.* **113**, 123902 (2018).

⁴²³J. P. B. Silva, J. M. B. Silva, K. C. Sekhar, H. Palneedi, M. C. Istrate, R. F. Negrea, C. Ghica, A. Chahboun, M. Pereira, and M. J. M. Gomes, *J. Mater. Chem. A* **8**, 14171 (2020).

⁴²⁴D. Das, V. Gaddam, and S. Jeon, *IEEE Electron Device Lett.* **42**, 331 (2021).

⁴²⁵Y. He, G. Zheng, X. Wu, W.-J. Liu, D. W. Zhang, and S.-J. Ding, *Nanoscale Adv.* **4**, 4648 (2022).

⁴²⁶T. Zhang, X. Chen, Y. Thakur, B. Lu, Q. Zhang, J. Runt, and Q. M. Zhang, *Sci. Adv.* **6**, eaax6622 (2020).

⁴²⁷J. Sun, B. Luo, and H. Li, *Adv. Energy Sustainability Res.* **3**, 2100191 (2022).

⁴²⁸Q. Li, F. Liu, T. Yang, M. R. Gadinski, G. Zhang, L.-Q. Chen, and Q. Wang, *Proc. Natl. Acad. Sci. U. S. A.* **113**, 9995 (2016).

⁴²⁹A. R. Jayakrishnan, J. P. B. Silva, K. Kamakshi, D. Dastan, V. Annapureddy, M. Pereira, and K. C. Sekhar, *Prog. Mater. Sci.* **132**, 101046 (2023).

⁴³⁰J. Chen, Y. Wang, X. Xu, Q. Yuan, Y. Niu, Q. Wang, and H. Wang, *J. Mater. Chem. A* **7**, 3729 (2019).

⁴³¹J. Gao, D.-K. Kwon, S. Perini, J. Long, S. Zhang, and M. T. Lanagan, *J. Am. Ceram. Soc.* **99**, 4045 (2016).

⁴³²X. Wu, X. Chen, Q. M. Zhang, and D. Q. Tan, *Energy Storage Mater.* **44**, 29 (2022).

⁴³³F. Shang, J. Wei, J. Xu, G. Zhang, M. Li, K. Xu, X. Liu, B. Li, H. Huang, G. Chen, and H. Xu, *ACS Appl. Mater. Interfaces* **14**, 53081 (2022).

⁴³⁴T. Song, R. Bachelet, G. Saint-Girons, R. Solanas, I. Fina, and F. Sánchez, *ACS Appl. Electron. Mater.* **2**, 3221 (2020).

⁴³⁵A. P. S. Crema, M. C. Istrate, A. Silva, V. Lenzi, L. Domingues, M. O. Hill, V. S. Teodorescu, C. Ghica, M. J. M. Gomes, M. Pereira, L. Marques, J. L. MacManus-Driscoll, and J. P. B. Silva, *Adv. Sci.* **10**, 2207390 (2023).

⁴³⁶Y. Abdullahi Hassan and H. Hu, *Composites, Part A* **138**, 106064 (2020).

⁴³⁷S. Kang, W.-S. Jang, A. N. Morozovska, O. Kwon, Y. Jin, Y.-H. Kim, H. Bae, C. Wang, S.-H. Yang, A. Belianinov, S. Randolph, E. A. Eliseev, L. Collins, Y. Park, S. Jo, M.-H. Jung, K.-J. Go, H. W. Cho, S.-Y. Choi, J. H. Jang, S. Kim, H. Y. Jeong, J. Lee, O. S. Ovchinnikova, J. Heo, S. V. Kalinin, Y.-M. Kim, and Y. Kim, *Science* **376**, 731 (2022).

⁴³⁸H. Pan, S. Lan, S. Xu, Q. Zhang, H. Yao, Y. Liu, F. Meng, E.-J. Guo, L. Gu, D. Yi, X. Renshaw Wang, H. Huang, J. L. MacManus-Driscoll, L.-Q. Chen, K.-J. Jin, C.-W. Nan, and Y.-H. Lin, *Science* **374**, 100 (2021).

⁴³⁹H. Chen, L. Liu, Z. Yan, X. Yuan, H. Luo, and D. Zhang, *Adv. Sci.* **10**, 2300792 (2023).

⁴⁴⁰E. T. Breyer, H. Mulaosmanovic, J. Trommer, T. Melde, S. Dunkel, M. Trentzsch, S. Beyer, T. Mikolajick, and S. Slesazeck, in *ESSDERC 2019–49th European Solid-State Device Research Conference (ESSDERC)* (IEEE, 2019), pp. 118–121.

⁴⁴¹S. Lancaster, Q. T. Duong, E. Covi, T. Mikolajick, and S. Slesazeck, in *ESSCIRC 2022–IEEE 48th European Solid State Circuits Conference (ESSCIRC)* (IEEE, 2022), pp. 137–140.

⁴⁴²A. Kazemi, F. Müller, M. M. Sharifi, H. Errahmouni, G. Gerlach, T. Kämpfe, M. Imani, X. S. Hu, and M. Niemier, *Sci. Rep.* **12**, 19201 (2022).

⁴⁴³H. Mulaosmanovic, S. Dunkel, M. Trentzsch, S. Beyer, E. T. Breyer, T. Mikolajick, and S. Slesazeck, *IEEE Trans. Electron Devices* **67**, 5804 (2020).

⁴⁴⁴H. Mulaosmanovic, J. Ocker, S. Müller, U. Schroeder, J. Müller, P. Polakowski, S. Flachowsky, R. van Bentum, T. Mikolajick, and S. Slesazeck, *ACS Appl. Mater. Interfaces* **9**, 3792 (2017).

⁴⁴⁵M. Jerry, P.-Y. Chen, J. Zhang, P. Sharma, K. Ni, S. Yu, and S. Datta, in *2017 IEEE International Electron Devices Meeting (IEDM)* (IEEE, 2017), pp. 6.2.1–6.2.4.

⁴⁴⁶S. Beyer, S. Dünkel, M. Trentzsch, J. Müller, A. Hellmich, D. Utess, J. Paul, D. Kleimaier, J. Pellerin, S. Müller, J. Ocker, A. Benoit, H. Zhou, M. Mennenga, M. Schuster, F. Tassan, M. Noack, A. Pourkeramati, F. Müller, M. Lederer, T. Ali, R. Hoffmann, T. Kämpfe, K. Seidel, H. Mulaosmanovic, E. T. Breyer, T. Mikolajick, and S. Slesazeck, in *IEEE International Memory Workshop (IMW)* (IEEE, Piscataway, NJ, 2020), Vol. 1.

⁴⁴⁷H. Mulaosmanovic, T. Mikolajick, and S. Slesazeck, *IEEE Electron Device Lett.* **39**, 135 (2018).

⁴⁴⁸E. Covi, H. Mulaosmanovic, B. Max, S. Slesazeck, and T. Mikolajick, *Neuromorphic Comput. Eng.* **2**, 012002 (2022).

⁴⁴⁹M. Halter, L. Bégon-Lours, V. Bragaglia, M. Sousa, B. J. Offrein, S. Abel, M. Luisier, and J. Pompey, *ACS Appl. Mater. Interfaces* **12**, 17725 (2020).

⁴⁵⁰P. Buragohain, A. Erickson, P. Kariuki, T. Mittmann, C. Richter, P. D. Lomenzo, H. Lu, T. Schenk, T. Mikolajick, U. Schroeder, and A. Gruverman, *ACS Appl. Mater. Interfaces* **11**, 35115 (2019).

⁴⁵¹R. Fontanini, J. Barbot, M. Segatto, S. Lancaster, Q. Duong, F. Driussi, L. Grenouillet, L. Triozon, J. Coignus, T. Mikolajick, S. Slesazeck, and D. Esseni, *IEEE J. Electron Devices Soc.* **10**, 593 (2022).

⁴⁵²K. Ni, J. A. Smith, B. Grisafe, T. Rakshit, B. Obradovic, J. A. Kittl, M. Rodder, and S. Datta, in *2018 IEEE International Electron Devices Meeting (IEDM)* (IEEE, 2018), pp. 13.2.1–13.2.4.

⁴⁵³Z. Jiang, Z. Zhao, S. Deng, Y. Xiao, Y. Xu, H. Mulaosmanovic, S. Duenkel, S. Beyer, S. Meninger, M. Mohamed, R. Joshi, X. Gong, S. Kurinec, V. Narayanan, and K. Ni, *IEEE Trans. Electron Devices* **69**, 6722 (2022).

⁴⁵⁴C. B. Sawyer and C. H. Tower, *Phys. Rev.* **35**, 269 (1930).

⁴⁵⁵K. Prume, T. Schmitz, and S. Tiedke, *Polar Oxides* (Wiley, 2004), pp. 53–75.

⁴⁵⁶R. Meyer, R. Waser, K. Prume, T. Schmitz, and S. Tiedke, *Appl. Phys. Lett.* **86**, 142907 (2005).

⁴⁵⁷J. F. Scott, L. Kammerdiner, M. Parris, S. Traynor, V. Ottenbacher, A. Shawabkeh, and W. F. Oliver, *J. Appl. Phys.* **64**, 787 (1988).

⁴⁵⁸M. Massarotto, F. Driussi, A. Affanni, S. Lancaster, S. Slesazeck, T. Mikolajick, and D. Esseni, *Solid-State Electron.* **200**, 108569 (2023).

⁴⁵⁹S. Mueller, J. Muller, U. Schroeder, and T. Mikolajick, *IEEE Trans. Device Mater. Reliab.* **13**, 93 (2012).

⁴⁶⁰R. Alcala, M. Materano, P. D. Lomenzo, L. Grenouillet, T. Francois, J. Coignus, N. Vaxelaire, C. Carabasse, S. Chevalliez, F. Andrieu, T. Mikolajick, and U. Schroeder, in *2022 6th IEEE Electron Devices Technology and Manufacturing Conference (EDTM)* (IEEE, 2022).

⁴⁶¹B. Max, M. Hoffmann, H. Mulaosmanovic, S. Slesazeck, and T. Mikolajick, *ACS Appl. Electron. Mater.* **2**, 4023 (2020).

⁴⁶²F. Ambriz-Vargas, G. Kolhatkar, M. Broyer, A. Hadj-Youssef, R. Nouar, A. Sarkissian, R. Thomas, C. Gomez-Yáñez, M. A. Gauthier, and A. Ruediger, *ACS Appl. Mater. Interfaces* **9**, 13262 (2017).

⁴⁶³N. Balke, P. Maksymovych, S. Jesse, A. Herklotz, A. Tselev, C.-B. Eom, I. I. Kravchenko, P. Yu, and S. V. Kalinin, *ACS Nano* **9**, 6484 (2015).

⁴⁶⁴M. Segatto, R. Fontanini, F. Driussi, D. Lizzit, and D. Esseni, *IEEE J. Electron Devices Soc.* **10**, 324 (2022).

⁴⁶⁵M. Si, X. Lyu, and P. D. Ye, *ACS Appl. Electron. Mater.* **1**, 745 (2019).

⁴⁶⁶H.-H. Huang, T.-Y. Wu, Y.-H. Chu, M.-H. Wu, C.-H. Hsu, H.-Y. Lee, S.-S. Sheu, W.-C. Lo, and T.-H. Hou, in *2019 IEEE International Electron Devices Meeting (IEDM)* (IEEE, 2019), pp. 32.2.1–32.2.4.

⁴⁶⁷B. Max, M. Hoffmann, S. Slesazeck, and T. Mikolajick, *IEEE J. Electron Devices Soc.* **7**, 1175 (2019).

⁴⁶⁸J. Barbot, J. Coignus, F. Triozon, C. Carabasse, O. Glorieux, F. Aussenac, F. Andrieu, and L. Grenouillet, in *International Conference on Solid State Devices and Materials (SSDM)*, 2022.

⁴⁶⁹K. Nair, M. Holzer, C. Dubourdieu, and V. Deshpande, *ACS Appl. Electron. Mater.* **5**, 1478 (2023).

⁴⁷⁰S. Narayanan, E. Covi, V. Havel, C. Frenkel, S. Lancaster, Q. Duong, S. Slesazeck, T. Mikolajick, M. Payvand, and G. Indiveri, in *2022 IEEE International Symposium on Circuits and Systems (ISCAS)* (IEEE, 2022), pp. 717–721.

⁴⁷¹F. Huang, M. Passlack, S. L. Liew, Z. Yu, Q. Lin, A. Babadi, V. D.-H. Hou, P. C. McIntyre, and S. Simon Wong, *IEEE Electron Device Lett.* **43**, 212 (2022).

⁴⁷²J. Li, M. Si, Y. Qu, X. Lyu, and P. D. Ye, *IEEE Trans. Electron Devices* **68**, 1214 (2021).

⁴⁷³L. Benatti and F. M. Puglisi, in *2021 IEEE International Integrated Reliability Workshop (IIRW)* (IEEE, 2021), pp. 1–6.

⁴⁷⁴A. K. Tagantsev, I. Stolichnov, N. Setter, J. S. Cross, and M. Tsukada, *Phys. Rev. B* **66**, 214109 (2002).

⁴⁷⁵Y. Ishibashi and Y. Takagi, *J. Phys. Soc. Jpn.* **31**, 506 (1971).

⁴⁷⁶X. Lyu, M. Si, P. R. Shrestha, K. P. Cheung, and P. D. Ye, in *2019 IEEE International Electron Devices Meeting (IEDM)* (IEEE, 2019), pp. 15.2.1–15.2.4.

⁴⁷⁷T. Francois, L. Grenouillet, J. Coignus, N. Vaxelaire, C. Carabasse, F. Aussenac, S. Chevalliez, S. Slesazeck, C. Richter, P. Chiquet, M. Bocquet, U. Schroeder, T. Mikolajick, F. Gaillard, and E. Nowak, *Appl. Phys. Lett.* **118**, 062904 (2021).

⁴⁷⁸J. A. Rodriguez, K. Remack, K. Boku, K. R. Udayakumar, S. Aggarwal, S. R. Summerfelt, F. G. Celi, S. Martin, L. Hall, K. Taylor, T. Moise, H. McAdams, J. McPherson, R. Bailey, G. Fox, and M. Depner, *IEEE Trans. Device Mater. Reliab.* **4**, 436 (2004).

⁴⁷⁹T. Nishimura, L. Xu, S. Shibayama, T. Yajima, S. Migita, and A. Toriumi, *Jpn. J. Appl. Phys.* **55**, 08PB01 (2016).

⁴⁸⁰A. Chouprik, E. Kondratyuk, V. Mikheev, Y. Matveyev, M. Spiridonov, A. Chernikova, M. G. Kozodaev, A. M. Markeev, A. Zenkevich, and D. Negrov, *Acta Mater.* **204**, 116515 (2021).

⁴⁸¹Y.-D. Lin, P.-C. Yeh, Y.-T. Tang, J.-W. Su, H.-Y. Yang, Y.-H. Chen, C.-P. Lin, P.-S. Yeh, J.-C. Chen, P.-J. Tzeng, M.-H. Lee, T.-H. Hou, S.-S. Sheu, W.-C. Lo, and C.-I. Wu, in *IEEE International Electron Devices Meeting (IEDM)* (IEEE, 2021), pp. 6.4.1–6.4.4.

⁴⁸²E. D. Grimley, T. Schenk, X. Sang, M. Pešić, U. Schroeder, T. Mikolajick, and J. M. LeBeau, *Adv. Electron. Mater.* **2**, 1600173 (2016).

⁴⁸³K. Tahara, K. Toprasertpong, Y. Hikosaka, K. Nakamura, H. Saito, M. Takenaka, and S. Takagi, in *2021 Symposium on VLSI Technology* (IEEE, 2021), Vol. 1.

⁴⁸⁴P. D. Lomenzo, S. Slesazeck, M. Hoffmann, T. Mikolajick, U. Schroeder, B. Max, and T. Mikolajick, in *2019 19th Non-Volatile Memory Technology Symposium (NVMTS)* (IEEE, 2019), pp. 1–8.

⁴⁸⁵L. Grenouillet, T. Francois, J. Coignus, S. Kerdiles, N. Vaxelaire, C. Carabasse, F. Mehmood, S. Chevalliez, C. Pellissier, F. Triozon, F. Mazen, G. Rodriguez, T. Magis, V. Havel, S. Slesazeck, F. Gaillard, U. Schroeder, T. Mikolajick, and E. Nowak, in *2020 IEEE Symposium on VLSI Technology* (IEEE, 2020), pp. 1–2.

⁴⁸⁶T. Mittmann, M. Materano, S.-C. Chang, I. Karpov, T. Mikolajick, and U. Schroeder, in *2020 IEEE International Electron Devices Meeting (IEDM)* (IEEE, 2020), pp. 18.4.1–18.4.4.

⁴⁸⁷Y. D. Lin, H. Y. Lee, Y. T. Tang, P. C. Yeh, H. Y. Yang, P. S. Yeh, C. Y. Wang, J. W. Su, S. H. Li, S. S. Sheu, T. H. Hou, W. C. Lo, M. H. Lee, M. F. Chang, Y. C. King, and C. J. Lin, in *2019 IEEE International Electron Devices Meeting (IEDM)* (IEEE, 2019), Vol. 15.

⁴⁸⁸H. Mulaosmanovic, E. T. Breyer, T. Mikolajick, and S. Slesazeck, in *2020 4th IEEE Electron Devices Technology and Manufacturing Conference (EDTM)* (IEEE, 2020), pp. 1–4.

⁴⁸⁹M. Halter, L. Bégon-Lours, M. Sousa, Y. Popoff, U. Drechsler, V. Bragaglia, and B. J. Offrein, *Commun. Mater.* **4**, 14 (2023).

⁴⁹⁰P. Nukala, M. Ahmadi, Y. Wei, S. de Graaf, E. Stylianidis, T. Chakrabortty, S. Matzen, H. W. Zandbergen, A. Björling, D. Mannix, D. Carbone, B. Kooi, and B. Noheda, *Microsc. Microanal.* **28**, 2268 (2022).

⁴⁹¹L. Bégon-Lours, M. Halter, M. Sousa, Y. Popoff, D. Dávila Pineda, D. F. Falcone, Z. Yu, S. Reidt, L. Benatti, F. M. Puglisi, and B. J. Offrein, *Neuromorphic Comput. Eng.* **2**, 024001 (2022).

⁴⁹²M. Materano, P. D. Lomenzo, A. Kersch, M. H. Park, T. Mikolajick, and U. Schroeder, *Inorg. Chem. Front.* **8**, 2650 (2021).

⁴⁹³S. Belahcen, T. Francois, L. Grenouillet, A. Bsiesy, J. Coignus, and M. Bonvalot, *Appl. Phys. Lett.* **117**, 252903 (2020).

⁴⁹⁴F. Mehmood, T. Mikolajick, and U. Schroeder, *Appl. Phys. Lett.* **117**, 092902 (2020).

⁴⁹⁵H. Jang, A. Kashir, S. Oh, and H. Hwang, *Nanotechnology* **33**, 395205 (2022).

⁴⁹⁶T. Mimura, Y. Tashiro, T. Shimizu, and H. Funakubo, *ACS Appl. Electron. Mater.* **5**, 1600 (2023).

⁴⁹⁷P. D. Lomenzo, C. Richter, M. Materano, T. Mikolajick, U. Schroeder, T. Schenk, D. Spirito, and S. Gorfman, in *2020 Joint Conference of the IEEE International Frequency Control Symposium and International Symposium on Applications of Ferroelectrics (IFCS-ISAF)* (IEEE, 2020), pp. 1–4.

⁴⁹⁸T. Shimizu, T. Mimura, T. Kiguchi, T. Shiraiishi, T. Konno, Y. Katsuya, O. Sakata, and H. Funakubo, *Appl. Phys. Lett.* **113**, 212901 (2018).

⁴⁹⁹M. Lederer, T. Kämpfe, N. Vogel, D. Utess, B. Volkmann, T. Ali, R. Olivo, J. Müller, S. Beyer, M. Treitzsch, K. Seidel, and L. M. Eng, *Nanomaterials* **10**, 384 (2020).

⁵⁰⁰L.-Y. Ma and S. Liu, *Phys. Rev. Lett.* **130**, 096801 (2023).

⁵⁰¹E. V. Skopin, N. Guillaume, L. Alrifai, P. Gonon, and A. Bsiesy, *Appl. Phys. Lett.* **120**, 172901 (2022).

⁵⁰²D. Bondurant, *Ferroelectrics* **112**, 273 (1990).

⁵⁰³T. P. Ma and J.-P. Han, *IEEE Electron Device Lett.* **23**, 386 (2002).

⁵⁰⁴J.-M. Koo, J.-E. Lim, D.-C. Yoo, S.-O. Park, H.-S. Kim, H. Han, S. Baik, J.-Y. Choi, Y. J. Park, Y. Park, B.-S. Seo, S. Kim, S. Shin, J.-H. Lee, H. Baik, J.-H. Lee, J. H. Lee, and B.-J. Bae, in *IEEE International Electron Devices Meeting 2005. IEDM Technical Digest* (IEEE, 2005), pp. 340–343.

⁵⁰⁵S. Yoon, S.-I. Hong, G. Choi, D. Kim, I. Kim, S. M. Jeon, C. Kim, and K. Min, in *2022 IEEE International Memory Workshop (IMW)* (IEEE, 2022), pp. 1–4.

⁵⁰⁶T. Mikolajick, M. H. Park, L. Begon-Lours, and S. Slesazeck, *Adv. Mater.* 2206042 (published online) (2023).

⁵⁰⁷H. Zhou, J. Ocker, A. Padovani, M. Pesic, M. Trentzsch, S. Dunkel, H. Mulaosmanovic, S. Slesazeck, L. Larcher, S. Beyer, S. Muller, and T. Mikolajick, in *2020 IEEE International Electron Devices Meeting (IEDM)* (IEEE, 2020), pp. 18.6.1–18.6.4.

⁵⁰⁸F. Hamzaoglu, U. Arslan, N. Bisnik, S. Ghosh, M. B. Lal, N. Lindert, M. Meterelliyo, R. B. Osborne, J. Park, S. Tomishima, Y. Wang, and K. Zhang, in *2014 IEEE International Solid-State Circuits Conference Digest of Technical Papers (ISSCC)* (IEEE, 2014), pp. 230–231.

⁵⁰⁹S.-C. Chang, N. Haratipour, S. Shivaraman, T. L. Brown-Heft, J. Peck, C.-C. Lin, I.-C. Tung, D. R. Merrill, H. Liu, C.-Y. Lin, F. Hamzaoglu, M. V. Metz, I. A. Young, J. Kavalieratos, and U. E. Avci, in *2020 IEEE International Electron Devices Meeting (IEDM)* (IEEE, 2020), pp. 28.1.1–28.1.4.

⁵¹⁰S.-C. Chang, N. Haratipour, S. Shivaraman, C. Neumann, S. Atanasov, J. Peck, N. Kabir, I.-C. Tung, H. Liu, B. Krist, A. Oni, S. Sung, B. Doyle, G. Allen, C. Engel, A. Roy, T. Hoff, H. Li, F. Hamzaoglu, R. Bristol, M. Radosavljevic, B. Turkot, M. Metz, I. Young, J. Kavalieratos, and U. Avci, in *2021 IEEE International Electron Devices Meeting (IEDM)* (IEEE, 2021), pp. 33.2.1–33.2.4.

⁵¹¹T. S. Boscke, J. Muller, D. Brauhaus, U. Schroder, and U. Bottger, in *2011 International Electron Devices Meeting* (IEEE, 2011), pp. 24.5.1–24.5.4.

⁵¹²Z. Wang, N. Tasneem, J. Hur, H. Chen, S. Yu, W. Chern, and A. Khan, in *2021 IEEE International Electron Devices Meeting (IEDM)* (IEEE, 2021), pp. 19.3.1–19.3.4.

⁵¹³M. Kim, J. Kim, G. Park, L. Everson, H. Kim, S. Song, S. Lee, and C. H. Kim, in *2018 IEEE International Electron Devices Meeting (IEDM)* (IEEE, 2018), pp. 15.4.1–15.4.4.

⁵¹⁴G. Spadini, I. Karpov, and D. Kencke, in *2010 International Conference on Simulation of Semiconductor Processes and Devices* (IEEE, Bologna, Italy, 2010), pp. 223–226.

⁵¹⁵M. Saitoh, R. Ichihara, M. Yamaguchi, K. Suzuki, K. Takano, K. Akari, K. Takahashi, Y. Kamiya, K. Matsuo, Y. Kamimuta, K. Sakuma, K. Ota, and S. Fujii, in *2020 IEEE International Electron Devices Meeting (IEDM)* (IEEE, 2020), pp. 18.1.1–18.1.4.

⁵¹⁶K. Ishimaru, in *2019 IEEE International Electron Devices Meeting (IEDM)* (IEEE, 2019), pp. 1.3.1–1.3.6.

AFFILIATIONS

¹Physics Center of Minho and Porto Universities (CF-UM-UP), Campus de Gualtar, University of Minho, 4710-057 Braga, Portugal

²Laboratory of Physics for Materials and Emergent Technologies, LapMET, University of Minho, 4710-057 Braga, Portugal

³NaMLab gGmbH, Noethnitzer Str. 64a, 01187 Dresden, Germany

⁴Components Research, Intel Corporation, Hillsboro, Oregon 97124, USA

⁵SPEC, CEA, CNRS, CEA Saclay, Université Paris-Saclay, 91191 Gif-sur-Yvette, France

⁶IBM Research Zurich, Säumerstrasse 4, 8803 Rüschlikon, Switzerland

⁷Electrical and Information Technology, Lund University, Box 118, Lund 22 100, Sweden

⁸NanoLund, Lund University, Box 118, Lund 22 100, Sweden

⁹Department of Materials Science and Engineering and Inter-University Semiconductor Research Center, College of Engineering, Seoul National University, Seoul 08826, Republic of Korea

¹⁰Rutgers Center for Emergent Materials and Department of Physics and Astronomy, Piscataway, New Jersey 08854, USA

¹¹Device Research Center, Samsung Advanced Institute of Technology (SAIT), Suwon 16678, Republic of Korea

¹²CEA, LETI, University Grenoble Alpes, F-38000 Grenoble, France

¹³Helmholtz-Zentrum Berlin für Materialien und Energie, Hahn-Meitner-Platz 1, Berlin 14109, Germany

¹⁴National Center for Scientific Research DEMOKRITOS, 15341 Athens, Greece

¹⁵Physical Chemistry, Freie Universität Berlin, Arnimallee 22, Berlin 14195, Germany

¹⁶Institut de Ciència de Materials de Barcelona (ICMAB-CSIC), Campus UAB, Bellaterra, Barcelona 08193, Spain

¹⁷Department of Materials Science and Engineering, Tokyo Institute of Technology, 226-8502 Yokohama, Japan

¹⁸Department of Physics and Astronomy, University of Nebraska-Lincoln, Lincoln, Nebraska 68588, USA

¹⁹Department of Electrical Engineering and Computer Sciences, University of California, Berkeley, California 94720, USA

²⁰Department of Materials Science and Engineering, North Carolina State University, Raleigh, North Carolina 27695, USA

²¹Department of Physics and Materials Science, University of Luxembourg, 41 Rue du Brill, Belvaux L-4422, Luxembourg

²²Materials Research and Technology Department, Luxembourg Institute of Science and Technology, 5 Avenue des Hauts-Fourneaux, L-4362 Esch/Alzette, Luxembourg

²³Department of Applied Sciences and Mechatronics, Munich University of Applied Sciences, Lothstr. 34, D-80335 Munich, Germany

²⁴Fraunhofer Institute for Photonic Microsystems IPMS, Center Nanoelectronic Technologies (CNT), 01109 Dresden, Germany

²⁵Research Institute of Advanced Materials, Seoul National University, Seoul 08826, Republic of Korea

²⁶Department of Materials Science and Engineering, Materials Sciences Division, Lawrence Berkeley National Laboratory, University of California, Berkeley, California 94720, USA

²⁷Materials Sciences Division, Lawrence Berkeley National Laboratory, Berkeley, California 94720, USA

²⁸National Institute of Advanced Industrial Science and Technology, Kumamoto, Japan

²⁹IHM, TU Dresden, Dresden, Germany

³⁰CogniGron Center, University of Groningen, Groningen 9747 AG, The Netherlands

³¹Department of Physics and Astronomy, Rutgers University, Piscataway, New Jersey 08854, USA

³²Department of Electrical Engineering and Computer Sciences, University of California, Berkeley, California 94720, USA

³³Materials Research Center for Element Strategy, Tokyo Institute of Technology, Yokohama 226-8503, Japan

³⁴Department of Materials Science and Engineering, Tokyo Institute of Technology, Yokohama 226-8502, Japan

³⁵The University of Tokyo, Tokyo, Japan

³⁶Department of Materials and Life Sciences, Sophia University, Chiyoda, Tokyo 102-8554, Japan

³⁷Ecole Centrale de Lyon, INSA Lyon, UCBL, CPE Lyon, CNRS, INL UMR5270, Université de Lyon, 69130 Ecully, France

³⁸Department of Chemistry, Princeton University, Princeton, New Jersey 08544, USA

³⁹Electronic Materials Research Center, Korea Institute of Science and Technology, Seoul 02792, Republic of Korea

a) Author to whom correspondence should be addressed:
Uwe.Schroeder@namlab.com